VOLUME 79 MAY 22, 1975 NUMBER 11

JPCHAx

THE JOURNAL OF PHYSICAL CHEMISTRY

PUBLISHED BIWEEKLY BY THE AMERICAN CHEMICAL SOCIETY

THE JOURNAL OF

PHYSICAL CHEMISTRY

AMERICAN CHEMICAL SOCIETY, *1155 Sixteenth St., N.W., Washington, D.C. 20036*

Books and Journals Division

JOHN K CRUM *Director*
VIRGINIA E. STEWART *Assistant to the Director*

CHARLES R. BERTSCH *Head, Editorial Processing Department*
D. H. MICHAEL BOWEN *Head, Journals Department*
BACIL GUILEY *Head, Graphics and Production Department*
SELDON W. TERRANT *Head, Research and Development Department*

All manuscripts should be sent to *The Journal of Physical Chemistry*, Department of Chemistry, University of Minnesota, Minneapolis, Minn. 55455.

Additions and Corrections are published once yearly in the final issue. See Volume 78, Number 26 for the proper form.

Extensive or unusual alterations in an article after it has been set in type are made at the author's expense, and it is understood that by requesting such alterations the author agrees to defray the cost thereof.

The American Chemical Society and the Editor of *The Journal of Physical Chemistry* assume no responsibility for the statements and opinions advanced by contributors.

Correspondence regarding accepted copy, proofs, and reprints should be directed to Editorial Processing Department, American Chemical Society, 20th and Northampton Sts., Easton, Pa. 18042. Department Head: CHARLES R. BERTSCH. Associate Department Head: MARIANNE C. BROGAN. Assistant Editor: CELIA B. MCFARLAND. Editorial Assistant: JOSEPH E. YURVATI.

Advertising Office: Centcom, Ltd., 50 W. State St., Westport, Conn. 06880.

Business and Subscription Information

Send all new and renewal subscriptions *with payment* to: Office of the Controller, 1155 16th Street, N.W., Washington, D.C. 20036. Subscriptions should be renewed promptly to avoid a break in your series. All correspondence and telephone calls regarding changes of address, claims for missing issues, subscription service, the status of records, and accounts should be directed to Manager, Membership and Subscription Services, American Chemical Society, P.O. Box 3337, Columbus, Ohio 43210. Telephone (614) 421-7230. For microfiche service, contact ACS Journals Department, 1155 16th St. N.W., Washington, D.C. 20036. Telephone (202) 872-4444.

On changes of address, include both old and new addresses with ZIP code numbers, accompanied by mailing label from a recent issue. Allow four weeks for change to become effective.

Claims for missing numbers will not be allowed (1) if loss was due to failure of notice of change in address to be received before the date specified, (2) if received more than sixty days from date of issue plus time normally required for postal delivery of journal and claim, or (3) if the reason for the claim is "issue missing from files."

Subscription rates (hard copy or microfiche) in 1975: $20.00 for 1 year to ACS members; $80.00 to nonmembers. Extra postage $4.50 in Canada and PUAS, $5.00 other foreign. Supplementary material (on microfiche only) available on subscription basis, 1975 rates: $15.00 in U.S., $19.00 in Canada and PUAS, $20.00 elsewhere. All microfiche airmailed to non-U.S. addresses; air freight rates for hard-copy subscriptions available on request.

Single copies for current year: $4.00. Rates for back issues from Volume 56 to date are available from the Special Issues Sales Department, 1155 Sixteenth St., N.W., Washington, D.C. 20036.

Subscriptions to this and the other ACS periodical publications are available on microfilm. For information on microfilm write Special Issues Sales Department at the address above.

Notice to Authors last printed in the issue of January 16, 1975

THE JOURNAL OF

PHYSICAL CHEMISTRY

Volume 79, Number 11 May 22, 1975

JPCHAx 79(11) 1045–1138 (1975)

ISSN 0022-3654

COMMUNICATIONS TO THE EDITOR

There is no supplementary material for this issue.

* In papers with more than one author, the asterisk indicates the name of the author to whom inquiries about the paper should be addressed.

AUTHOR INDEX

THE JOURNAL OF
PHYSICAL CHEMISTRY

VOLUME 79, NUMBER 11 MAY 22, 1975

Dependence of the Second Explosion Limits of Hydrogen–Fluorine–Oxygen–Hydrogen Fluoride Mixtures on a Hot-Atom Effect[1]

John H. Sullivan

University of California, Los Alamos Scientific Laboratory, Los Alamos, New Mexico 87544 *(Received October 15, 1974)*

Publication costs assisted by Los Alamos Scientific Laboratory

A hot-atom effect makes the second explosion limits of H_2–F_2–O_2 mixtures (where O_2 is present in small amounts as a stabilizer) strongly dependent on composition. Although a homogeneous H_2–F_2–O_2 mixture may be stable, the gases H_2–O_2 and F_2–O_2, from which the homogeneous mixture is obtained, may be explosive during mixing. Explosion limits are given for homogeneous H_2–F_2–O_2–HF mixtures and for a system where F_2–O_2 is mixing with H_2–O_2. The possibility of a system being in an explosive concentration region during mixing can be reduced by having a larger amount of O_2 in the F_2–O_2 gas than in the H_2–O_2 gas, by mixing at high pressures above the explosion limit of F_2–O_2 mixtures that contain small amounts of H_2, or by jetting streams of F_2–O_2 into H_2–O_2.

Introduction

Investigations on the second explosion limits for H_2–F_2–O_2–M (M = He, Ar, N_2, CF_4) and H_2–F_2–O_2 systems were reported in a series of papers by Kapralova et al.[2-7] The concentrations of F_2, O_2, and M were found to be related by the empirical expression[2b]

$$(F_2) = k[(O_2)/(F_2)](M)^2 \qquad (1)$$

when (H_2) and the ratio $(O_2)/(F_2)$ were kept constant during a series of runs. A mechanism involving branching by vibrationally excited HF (here written $HF^\dagger$)

$$F + H_2 \longrightarrow HF^\dagger + H \qquad (R1)$$
$$H + F_2 \longrightarrow HF^\dagger + F \qquad (R2)$$
$$HF^\dagger + F_2 \longrightarrow HF + 2F \qquad (R3)$$
$$HF^\dagger + M \longrightarrow HF + M \qquad (R10)$$
$$H + O_2 + M \longrightarrow HO_2 + M \qquad (R11)$$

was shown to reproduce the empirical relationship (1) so that

$$(F_2) = \frac{k_{10}k_{11}}{k_2k_3}[(O_2)/(F_2)](M)^2 \qquad (2)$$

Reaction 3 is exothermic for HF ($v \geq 4$). A similar mechanism was proposed by Brokaw[8] to explain the results of Levy and Copeland.[9]

In an extensive series of runs[3] it was shown that the relationship given by eq 1 was consistent with precise experimental explosion limits obtained for H_2–F_2–O_2–M (M = He, Ar, N_2, CF_4) and H_2–F_2–O_2 systems. The dependence of the limits on the value of k_{11} (which depends on the nature of M) was also in rough agreement that given by eq 2, although precise values of k_{11} for different M's were not available. Later analysis[6] and work at low temperatures[7] (74–133 K) indicated that the major branching reaction was

$$H_2^\dagger + F_2 \longrightarrow HF + H + F \qquad (R5)$$

where $H_2^\dagger$ is a vibrationally excited molecule formed from

$$HF^\dagger + H_2 \longrightarrow H_2^\dagger + HF \qquad (R4)$$

Reaction R5 is exothermic for H_2 ($v \geq 1$). The authors showed[7] that the empirical relationship eq 1 could also be obtained from a mechanism in which branching occurred by R5 rather than by R3, and in which the major reactions were R_1, R_2, R_4, R_{10}, R_{11}, and R_{12}.

$$H_2^\dagger + M \longrightarrow H_2 + M \qquad (R12)$$

The implication of the analysis[6] and the low temperature results[7] was that the branching reaction in the experiments near room temperature was reaction R5.

A computer simulation of the reactions occurring in an H_2–F_2–O_2–HF system, when fitted to the extensive and precise data of ref 3, showed that both reactions R3 and R5 take place.[10] Moderately precise rate coefficients for both

were obtained. These rate coefficients, together with recently measured coefficients for vibrational relaxation of HF,[11-15] for vibrational relaxation of H_2,[16-18] and for recombination reactions[19-22]

$$H + O_2 + M \longrightarrow HO_2 + M$$

now allow us to calculate the explosion limits of H_2–F_2–O_2 mixtures over a large range of concentrations of H_2 and F_2.

The computer simulation[10] also showed that HF was formed in almost all H_2–F_2–O_2 mixtures within a few tenths of a second after mixing, and the reaction was then quenched; the experimental systems are then H_2–F_2–O_2–HF mixtures, and it is the explosion limits for these more inclusive systems that are of interest.

The purpose of this paper is to give the explosion limits for H_2–F_2–O_2–HF mixtures as calculated using a reaction mechanism more complete than that used by Kapralova,[3] and, more importantly, to show that these explosion limits and the explosive behavior of systems of H_2–O_2 and F_2–O_2 while mixing are very strongly dependent on a hot-atom effect. The hot-atom effect occurs in (R2), the hot H atoms having been created in (R1). Essentially we show that, if one allows for a hot-atom effect on k_2, the predicted explosive behavior is strongly influenced. This carries implications with regard to preparation of H_2–F_2–O_2 mixtures for high-powered pulsed chemical lasers by mixing of H_2–O_2 and F_2–O_2 streams.

Mechanism

The reactions that are significant in determining the explosion limits are given in Table I.

However, if we consider that only the reactions in Table I affect the explosion limits, it is then necessary to show that the many other reactions occurring in the system have only a negligible effect on the explosion limits. We consider these reactions in this section.

The rates of relaxation of HF by O_2, and of H_2 by O_2 and by HF are not included because the rates are not known. Unless the relaxation takes place by dimer formation (as in the self-relaxation of HF)[23,24] the rates of relaxation of HF and H_2 by O_2 are probably about the same as the rates of relaxation by N_2, and because the concentration of O_2 in H_2–F_2–O_2 mixtures of interest in high-powered pulsed chemical lasers is usually much smaller than that of H_2 or F_2, we shall assume for the present purposes that the rates of these relaxations can be neglected. There is no information on the rate of relaxation of H_2 by HF or other hydrogen halides, but for the rate of relaxation of H_2 by HF to be significant the rate coefficient would have to be a factor of 100 greater than the rate for H_2 self-relaxation. Also, the reactions

$$H + O_2 + M \longrightarrow HO_2 + M$$

where M = O_2, HF, are neglected. To our knowledge there is no information near room temperature for M = F_2, O_2, or HF, but if we assume the efficiencies of M = O_2 or HF for recombination are the same as the efficiency of N_2, the reactions for M = O_2 and HF can be neglected on the basis of low concentrations of these molecules.

It is necessary to show that the reactions of HO_2 and the subsequent reactions of various products do not significantly affect the explosion limit and indeed have a negligible effect compared to the hot-atom effect. The limits would be affected only by those reactions that change the concentrations of atoms.

TABLE I: Reactions that Determine the Explosion Limits of H_2–F_2–O_2–HF Systems

Reaction	Rate coefficient, cm^3/mol sec or cm^6/mol^2 sec	Note
Propagation		
R1 $F + H_2 \longrightarrow HF^\dagger + H$	$k_1 = 1.3 \times 10^{14} \times \exp(-1600/RT)$	*a*
R2 $H + F_2 \longrightarrow HF^\dagger + F$	$k_2 = 1.6 \times 10^{14} \times \exp(-2600/RT)$ see text	*b*
Branching		
R3 $HF^\dagger + F_2 \longrightarrow HF + 2F$	$k_3 = 2 \times 10^6$	*c*
R4 $HF^\dagger + H_2 \rightleftharpoons HF + H_2^\dagger$	$k_4 = 1.1 \times 10^{12} \times \exp(-570/RT)$ $k_{-4} = 1.1 \times 10^{12}$	*d*
R5 $H_2^\dagger + F_2 \longrightarrow HF + H + F$	$k_5 = 10^5$	*c*
Relaxation		
R6 $HF^\dagger + H_2 \longrightarrow HF + H_2$	$k_6 \simeq 10^{10}$	*e*
R6′ $HF^\dagger + F_2 \longrightarrow HF + F_2$	$k_{6'} \simeq 10^9$	*f*
R7 $HF^\dagger + HF \longrightarrow 2HF$	$k_7 = 8.2 \times 10^8 T + 1.2 \times 10^{17}/T^2$	*g*
R8 $H_2^\dagger + H_2 \longrightarrow 2H_2$	$k_8 = 2.85 \times 10^{10} T \times \exp(-78.89/T^{1/3})$	*h*
R8′ $H_2^\dagger + F_2 \longrightarrow H_2 + F_2$	$k_{8'} = 5.4 \times 10^9 T \times \exp(-87.34/T^{1/3})$	*i*
Termination		
R9 $H + O_2 + H_2 \longrightarrow HO_2 + H_2$	$k_9 = 5.0 \times 10^{15} \times \exp(+1500/RT)$	*j*
R9′ $H + O_2 + F_2 \longrightarrow HO_2 + F_2$	$k_{9'} \simeq 5.1 \times 10^{15} \times \exp(+990/RT)$	*k*

[a] We combined a single value of k_1 obtained near room temperature as given in ref 38 with values obtained from ref 39 to get a mean value $k_1 = 1.1 \times 10^{14} \exp(-1600/RT)$; this was increased by 20% to allow for a slight hot-atom effect. [b] For the thermal rate coefficient we used the temperature dependence of k_2 from ref 38 and the mean of the preexponential factors from ref 38 and 40. [c] Reference 10, Kapralova et al., ref 41, give a value of 1.2×10^4 cm^3/mol sec for k_5. It should be noted that the difference in the distributions of $HF^\dagger$ from (R1) and (R2) is not pertinent to our calculations. The rates of V–V transfer and V to T relaxation are so high compared to the rates of (R3) and (R5) that the distribution of HF over vibrational states is Boltzmann with a vibrational temperature somewhat higher than the translational temperature. Although (R3) takes place only for $HF^\dagger$ ($v \geq 4$) we cannot calculate the rate for these $HF^\dagger$ without knowing the fraction of $HF^\dagger$ that are in these upper states and the rate constant for these states. [d] The rate coefficient was obtained from the equilibrium constant and the measured rate coefficient (ref 11-13) for the reverse reaction. [e] An upper limit $k_6 = 1.8 \times 10^{10}$ cm^3/mol sec is given in ref 11. [f] The rate is taken to be 0.5 of that for N_2. [g] This empirical equation reproduces both the room temperature and the high temperature data for HF(1) + HF(0) → 2HF(0). See ref 15 for a summary of work on this reaction. [h] The preexponential parameter in the rate coefficient given in ref 18 was slightly adjusted to reproduce the rate at 300 K as given in ref 17. [i] The rate is assumed to be the same as that given for Ar in ref 18. [j] The rate coefficient for thermal atoms is from ref 19. [k] The rate coefficient was taken to be equal to that for M = N_2. For M = N_2 we obtained $k_9(N_2)$ from k_9 (Ar) as given in ref 19 and $k_9(N_2):k_9(Ar) = 3.4:1$ as given in ref 20. We do not include the more general reaction $H + O_2 + M \rightarrow HO_2 + M$ (R11) (used in describing Kapralova's system) because our system does not contain added inert gas.

Reactions of HO_2 that lead to inert products are

$$HO_2 \xrightarrow{wall} \qquad \text{(R13)}$$

$$2HO_2 \longrightarrow H_2O_2 + O_2 \quad \text{(R14)}$$

$$H + HO_2 \longrightarrow H_2 + O_2 \quad \text{(R15)}$$

$$F + HO_2 \longrightarrow HF + O_2 \quad \text{(R16)}$$

The amounts of H_2O_2 that are formed by (R14) during the preexplosion interval can be estimated by calculating the steady-state concentration of HO_2 that is obtained from the competition of (R13) and (R15) with (R9).[25] The concentration of H_2O_2 so calculated was small enough so that the rates of the reactions

$$H + H_2O_2 \longrightarrow H_2 + HO_2$$

$$F + H_2O_2 \longrightarrow HF + HO_2$$

which could act as additional sinks for H and F atoms, were negligible compared to the rate of (R9). The rate of

$$H_2O_2 + M \longrightarrow 2OH + M$$

is negligible at temperatures considered here.[25] The H_2 and HF formed in (R15) and (R16) are undoubtedly vibrationally excited but the number of these molecules is negligible compared to the number formed by (R1) and (R2). If the rates of (R15) and (R16) were appreciable compared to the rates of (R13) and (R14) then more than one H atom would disappear for each molecule of HO_2 formed. However, a steady-state calculation based on the production of HO_2 by (R9) and its disappearance by (R13), (R14), and (R15) indicates that the rates of (R15) and (R16) are low compared to the rates of (R13) and (R14).

The following reactions tend to make the system more explosive by negating the effect of (R9):

$$H_2 + HO_2 \longrightarrow H + H_2O_2 \quad \text{(R17)}$$

$$H + HO_2 \longrightarrow 2OH \quad \text{(R18)}$$

$$OH + H_2 \longrightarrow H_2O + H \quad \text{(R19)}$$

$$F_2 + HO_2 \longrightarrow HF + F + O_2 \quad \text{(R20)}$$

The rate of (R17) is negligible at the temperatures considered here. The effect of (R18) and (R19) can be shown to be small; the rate of (R18) relative to (R15) is $k_{18}/k_{15} \sim 1$ and the rates of (R18) and (R19) are then small compared to those of (R13) and (R14). Brokaw[26] has suggested that (R20) contributed to the results of Levy and Copeland[9] and Tal'roze[27] has suggested that (R20) may occur to produce a chain-initiated third limit at higher pressures. From an analysis of experimental data on hydrogen-rich systems Tal'roze obtained an upper limit for the rate coefficient, $k_{20} < 10^{13} \exp(-12{,}000/RT)$. The results of photochemical experiments of Levy and Copeland[28] indicate that $k_{20} < 10^5$ cm^3/mol sec and this is additional confirmation that the rate of (R20) is negligible here.

Levy and Copeland[28] also obtained evidence that in their systems the reaction

$$F + O_2 + M \longrightarrow FO_2 + M \quad \text{(R21)}$$

if it occurred, was followed by

$$FO_2 + H_2 \longrightarrow HF + O_2 + H \quad \text{(R22)}$$

and not by either of the following

$$FO_2 + H_2 \longrightarrow HF + HO_2 \quad \text{(R23)}$$

$$FO_2 + H \longrightarrow HF + O_2 \quad \text{(R24)}$$

$$FO_2 + F \longrightarrow F_2 + O_2 \quad \text{(R25)}$$

Reaction 21 would then not have any effect on the explosion limits. We therefore analyzed the explosion system by neglecting (R21) and we have shown, that for this situation, a hot-atom effect produces high-explosion limits in fluorine-rich mixtures.

However, in fluorine-rich systems the rates of (R21) and (R25) could be strongly enhanced (because of the high fluorine-atom concentration) and the possibility is present that (R21) might contribute to the explosion limit. We therefore also determined limits for the case where (R21–R25) are effective in removing atoms.

The Second Explosion Limit

A. The Case where F + O_2 + M → FO_2 + M Does Not Remove Atoms. If (R21) is not effective in removing atoms the second explosion limits for H_2–F_2–O_2–HF mixtures are then determined by reactions R1–R9′. When a steady-state approximation and the criterion for stability d(H)/d$t \leq 0$ are applied to this mechanism, the pressures at which the systems are stable are given by

$$P \geq A\left[\frac{k_4k_5\delta}{k_{-4}\gamma + k_8\delta + k_{8'}\alpha} + k_2\right] \times \left\{\frac{4}{k_6\delta + k_{6'}\alpha + k_7\gamma + [k_4\delta(k_8\delta + k_{8'}\alpha)/(k_{-4}\gamma + k_8\delta + k_{8'}\alpha)]}\right\}\frac{f}{\beta} \quad (3)$$

where α, β, γ, and δ are the fractional amounts of F_2, O_2, HF, and H_2 present, $A = 2.49 \times 10^9$ pascals mol^{-1} cm^{-3} (or 1.87×10^7 Torr mol^{-1} cm^{-3}) at 300 K, and

$$f = k_2\alpha^2/(k_8\delta + k_{8'}\alpha)$$

is a factor that is strongly dependent on the translational energy of the H atoms. In obtaining eq 3 the rates of (R3) and (R5) (as relaxation reactions for $HF^\dagger$ and $H^\dagger$) are neglected since they are negligible compared to the rates of other relaxation reactions.

The distribution of translational energies of H atoms in these systems depends on composition. The H atoms are formed hot by (R1) with initial translational energies E_i that center around the following values[29]

Fraction	E_i, kcal/mol
0.17	20
0.56	10
0.26	2

In hydrogen-rich systems, or in systems moderated by inert gas, the hydrogen atoms are moderated to a thermal translational energy distribution before colliding with F_2 molecules. The thermal rate coefficients for k_2, k_9, and $k_{9'}$, as given in Table I, are then applicable, and with $\delta \simeq 1$, $f = 2 \times 10^{12}\alpha^2/6.1 \times 10^{16} = 3 \times 10^{-5}\alpha^2$.

In fluorine-rich systems the hot hydrogen atoms collide with F_2 within one or two collisions. The rate coefficient k_2 for such atoms is, of course, much larger than the thermal rate coefficient and we estimate k_2 in fluorine-rich systems to be at least equal[30] to the collision frequency for a thermal distribution of translational energies, so that $k_2 \geq 10^{14}$ cm^3/mol sec. If we assume that in (R9′) the rate coefficient for hot atoms is about equal to that for thermal atoms[31] then at 300 K $k_{9'} \sim 2.6 \times 10^{16}$ cm^6/mol^2 sec. In fluorine rich systems $\delta = 0$, $\alpha = 1$ and $f > 10^{14}/2.6 \times 10^{16} > 0.004$.

A comparison of these two values for f indicates that the explosion limits in fluorine-rich systems are at least a factor of 130 higher than the explosion limits in hydrogen-rich or moderated systems.

While hot F atoms are produced by (R2) their effect on the rate of (R1) can be shown to be small. The distribution in the translational energies in the products of (R2) is given

by Polanyi.[32] From his results the maximum amount of translational energy in the F atoms is ca. 43 kcal/mol. Of this only $43 \times M_{H_2}/(M_{H_2} + M_F) = 4.1$ kcal/mol can act as relative translational energy for excitation during an F + H_2 collision. Blais[33] as shown that the cross section for F + $H_2(0) \rightarrow$ HF + F increases only 40% as the relative translational energy increases from 1 to 8 kcal/mol. We therefore increased the rate coefficient k_1 by 20% to allow for the hot F atoms.

The explosion limits of the extreme compositions considered above are pertinent. They determine the behavior of the system when H_2–F_2–O_2 is being prepared from H_2–O_2 and F_2–O_2. Our calculations apply to the boundary between the H_2–O_2 and F_2–O_2 gases at the time of mixing and indicate that the system will be unstable if the pressure is not greater than the explosion limit for the F_2–O_2 gas. If the system is unstable the explosion starts in the F_2–O_2 gas.

We have previously shown[10] that H_2–F_2–O_2 mixtures always react within a few tenths of a second to either explode or to produce a few percent HF which then quenches the reaction. The experimental systems whose explosions limits are of interest are then always H_2–F_2–O_2–HF systems. The explosion limit for an H_2–O_2–F_2–HF mixture should be below the limit for a fluorine-rich mixture. Such a mixture would be stable whereas the (F_2–O_2) + (H_2–O_2) system from which it is produced could be unstable toward a complete explosion during the mixing process. The rate coefficient for (R2) in an H_2–F_2–O_2–HF mixture could be obtained from a determination of the moderation function[34] and from the cross sections[30] as a function of translational energy. However, we have chosen to obtain an approximate value from the experimental explosion limit[3] as determined by Kapralova et al. for a H_2:F_2:O_2 = 3:1:0.08 mixture. We determined the value of k_2 applicable to this system by equating the right-hand side of eq 3 to the measured value of P. The values of k_9 and $k_{9'}$ were taken to the thermal rate coefficients at 300 K. The amount of HF in the experiment was unknown but was very likely less than 1%.[10] The value of k_2 was computed using $\gamma = 0.004$ and $\gamma = 0.01$ to obtain $k_2 = 1.35 \times 10^{13}$ and 1.8×10^{13} cm^3/mol sec, respectively.

It is of interest to compare the explosion limits for homogeneous H_2–F_2–O_2–HF systems to systems of F_2–O_2–HF mixing with H_2–O_2. The explosion limits for H_2:F_2:O_2:HF = 3:1:0.44:HF were calculated from eq 3 as a function of the concentration of HF. The value $k_2 \simeq 1.6 \times 10^{13}$ cm^3/mol sec, as obtained above for a H_2:F_2 = 3:1 mixture, and thermal rate coefficients for k_9 and $k_{9'}$ were used. The limits for a system of F_2–O_2–HF mixing with H_2–O_2 were also calculated but with the hot atom rate coefficient for k_2. In both the H_2–F_2–O_2–HF and the (F_2–O_2–HF) + (H_2–O_2) systems the fractional amounts of O_2 were the same at $\beta = 0.1$. The results are given in Figure 1. Because we do not know precise values of k_2, k_9, and $k_{9'}$ the curves in Figure 1 do not represent precise explosion limits. However, they do show that the dominant factor in determining the limits is the hot-atom effect. A dependence of the limits on the HF concentration, as would be expected from the relative values of k_7 and k_6 or k_7 and k_8, is also shown, but this dependence is not as strong as the dependence on the hot-atom effect.

B. The Case where F + O_2 + M → FO_2 + M Effectively Removes Atoms. When (R21–R25) are included in the mechanism, the factor that depends on the translational energy of the H atoms is

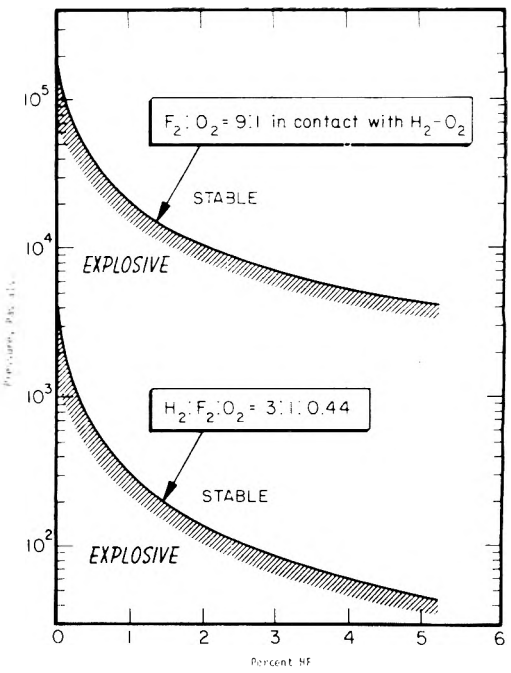

Figure 1. Explosion limits for F_2:O_2 = 9:1 in contact with H_2:O_2, and for H_2:F_2:O_2 = 3:1:0.44, as a function of amount of HF present. Limits were calculated for eq 3 with the assumption that (R21) is not effective in removing atoms.

$$f' = k_2\alpha^2 \Big/ \left(k_9\delta + k_{9'}\alpha + k_{21}\frac{k_2\alpha}{k_1\delta}\left[\frac{k_{23}(H_2) + 2k_{21}(H) + 2k_{25}(F)}{(k_{22} + k_{23})(H_2) + k_{21}(H) + k_{25}(F)}\right]\right)$$

and (R21) is effective in removing atoms when

$$k_{21}k_2\alpha/k_1\delta \geq k_9\delta + k_{9'}\alpha$$

In fluorine-rich systems, $\alpha/\beta \gg 1$, and, because the H atoms react while hot, $k_2/k_1 \gg 1$; then we may have $r \gg 1$ in the following expression

$$k_{21}k_2\alpha/k_1\delta = r(k_9\delta + k_{9'}\alpha)$$

Then

$$f' = \frac{k_1\alpha\delta}{k_{21}}\left[\frac{(k_{22} + k_{23})(H_2) + k_{21}(H) + k_{25}(F)}{k_{23}(H_2) + 2k_{21}(H) + 2k_{25}(F)}\right]$$

and $f/f' \simeq r$. The hot-atom effect that dominates the behavior of fluorine-rich mixtures in case A is then missing in case B.

In hydrogen-rich systems $f' = f$ because $k_2\alpha/k_1\delta \ll 1$.

Discussion

The preparation of stable H_2–F_2–O_2 mixtures is of practical importance in the production of powerful laser pulses,[35] and it is worth considering methods of mixing F_2–O_2 and H_2–O_2 gases to obtain stable H_2–F_2–O_2–HF mixtures. Because (R21) moderates the explosive behavior, and because there is evidence that its influence may be slight,[28] it is prudent to neglect its effect and thus estimate behavior on the basis of the most unstable or explosive mechanism, that of case A.

Our calculations on the basis of case A show that the explosion limits of H_2–F_2–O_2–HF mixtures can be estimated (eq 3 and Figure 1) if proper attention is given to the variation of k_2, k_9, and $k_{9'}$ with composition. Further, they suggest the following methods of minimizing the possibility

of explosion during the preparation of stable H_2–F_2–O_2–HF mixtures: (1) the separate H_2–O_2 and F_2–O_2 gases can be mixed at pressures greater than the explosion limit of the fluorine-rich mixture and the pressures can then be lowered; (2) some control over stability can be obtained by adding HF to the F_2–O_2 gas before mixing, and (3) because the explosion limit is proportional to $1/(O_2)$, the oxygen is more effective in stabilizing the systems when it is introduced as part of the F_2–O_2 mixture.

It may also be possible to mix H_2–O_2 and F_2–O_2 and F_2–O_2 within a time interval less than the rise time to explosion (i.e., the time for the F atom concentration or H atom concentration to attain 10^{-14} to 10^{-13} mol/cm^3 after which the system cannot be stabilized by the HF formed by the reaction[10]). In an H_2:F_2:O_2:HF = 3:1:0.08:0 mixtue at 0.05 to 0.11 atm the rise time to explosion was about 0.1 sec.[10]

Stability during the mixing process might best be obtained by flowing jets of F_2–O_2 into an H_2–O_2 mixture. As shown below, the diameter (or thickness if the jets were laminar) would have to be small enough so that diffusion of H atoms out of the jet into the H_2–O_2 system would help stabilize the F_2–O_2 side of the mixing system. The F_2–O_2 jet (containing a small amount of H_2) would be below the first explosion limit for fluorine-rich systems (although at pressures higher than the H_2–O_2 gas) and the H_2–O_2 gas (containing increasing amounts of F_2) would be above the second explosion limit for hydrogen-rich systems. Both would then be stable.

The effective rate for disappearance of an active species in a cylindrical reactor or jet, when the species is being produced throughout the whole volume and is diffusing to the wall or surface,[36] is

$$\frac{-\mathrm{d(a)}}{\mathrm{d}t} = \frac{23.2D}{d^2}\mathrm{(a)}$$

where D is the diffusion coefficient and d is the diameter of the jet. The total rate of disappearance of H atoms from such a jet of F_2–O_2 containing a small amount of H_2 would then be

$$\frac{-\mathrm{d(H)}}{\mathrm{d}t} = \frac{23.2D}{d^2}\mathrm{(H)} + k_{9'}\mathrm{(O_2)(F_2)(H)}$$

When the rate of production of H atoms by reactions 3 and 5 is included and the stability criterion $\mathrm{d(H)}/\mathrm{d}t \leq 0$ is then the critical thickness d for fluorine-rich systems at 300 K is given by

$$d \leq \left\{\left[23.2 \Big/ \left(\frac{4k_2k_3\alpha^2M}{k_6\alpha + k_7\gamma} - k_{9'}\alpha\beta M^2\right)\right]\frac{4 \times 10^{-5}D'}{M}\right\}^{1/2}$$

where M is the concentration $(F_2) + (O_2)$ in mol/cm^3, D' is the diffusion coefficient at 1 atm, and $M/4 \times 10^{-5}$ is the pressure in atm at 300 K. At 300 K, $D' \simeq 1.1$ cm^2/sec. If the value $k_2 = 10^{14}$ cm^3/mol sec (that may be appropriate for fluorine-rich systems) is used then d is given as a function of M as in Table II. For $\gamma = 0.01$, a minimum value of d, $d = 0.12$ mm, is obtained when $M = 1.7 \times 10^{-5}$ mol/cm^3.

The pressure of the F_2–O_2 jet must be greater than the pressure of H_2–O_2 gas. We consider, as an example, F_2–O_2 jetting into an H_2:F_2:O_2 = 3:1:0.44 mixture. For $\gamma = 0$, the 3:1:0.44 mixture is stable only above 3×10^3 Pa (Figure 1). The pressure of the F_2–O_2 gas must be greater than 3×10^3 Pa and maximum diameter of the jet is then about 0.28 mm. For $\gamma = 0.01$, however, an H_2:F_2:O_2 = 3:1:0.44 mixture is stable above 300 Pa (Figure 1). The maximum diameter of the jet is then greater than 1.3 mm and would allow a reasonable rate of flow.

TABLE II: Maximum Diameters of Cylindrical Jets for Flowing F_2–O_2–HF into H_2–O_2–HF (T = 300°, β = 0.1)

(M), mol cm^{-3}	P_M, Pa	γ	d, mm	γ	d, mm
10^{-4}	$2.5 \cdot 10^3$	0	0.28	0.01	1.3
10^{-5}	$2.5 \cdot 10^4$	0	0.03	0.01	0.17
10^{-4}	$2.5 \cdot 10^5$	0	0.003	0.01	Av.[a]

[a] Any value, because the pressure is above the second explosion limit for F_2–O_2 mixtures.

The maximum values of d that are allowed for stability should be much larger than those above. We used a diffusion coefficient for H atoms with a thermal distribution of translational energies at 300 K. When a correct "diffusion coefficient" for the hot H atoms is used and when proper account is taken for the production of atoms only in an annular sheath near the surface of the jet then the allowable values of d should be larger.

Acknowledgment. The reviewers' comments are gratefully acknowledged with thanks, and, in one instance, are included verbatim.

References and Notes

(1) This work was performed under the auspices of the U.S. Atomic Energy Commission.
(2) (a) G. A. Kapralova, E. M. Trofimova, L. Yu. Rusin, A. M. Chaikin, and A. E. Shilov, *Kinet. Catal.*, **4**, 567 (1963); (b) G. A. Kapralova, E. M. Trofimova, and A. E. Shilov, *ibid.*, **6**, 884 (1965).
(3) G. A. Kapralova, E. M. Margolina, and A. M. Chaikin, *Kinet. Catal.*, **10**, 23 (1969). The abscissae of Figure 2a and Figure 3 of this paper should be labeled $P^2_{H_2} \cdot 10^{-2}$ mm^2 and $P^2_{N_2} \cdot 10^{-2}$ mm^2, respectively.
(4) G. A. Kapralova and A. M. Chaikin, *Kinet. Catal.*, **10**, 195 (1969).
(5) G. A. Kapralova and A. M. Chaikin, *Combust. Flame*, **13**, 557 (1969).
(6) G. A. Kapralova, E. M. Margolina, and A. M. Chaikin, *Dokl. Akad. Nauk SSSR*, **197**, 281 (1971).
(7) G. A. Kapralova, E. M. Margolina, and A. M. Chaikin, *Dokl. Akad. Nauk SSSR*, **198**, 452 (1971).
(8) R. S. Brokaw, *J. Phys. Chem.*, **69**, 2488 (1965).
(9) J. B. Levy and B. K. W. Copeland, *J. Phys. Chem.*, **67**, 2156 (1963); **69**, 408 (1965).
(10) J. H. Sullivan, R. C. Feber, and J. W. Starner, Jr., *J. Chem. Phys.*, in press.
(11) W. H. Green and J. K. Hancock, *IEEE J. Quant. Electron.*, **QE-9**, 50 (1973).
(12) J. K. Hancock and W. H. Green, *J. Chem. Phys.*, **57**, 4515 (1972).
(13) J. J. Hinchen, *J. Chem. Phys.*, **59**, 233 (1973).
(14) J. F. Bott and N. Cohen, *J. Chem. Phys.*, **48**, 4539 (1973).
(15) L. S. Blair, W. D. Breshears, and G. L. Schott, *J. Chem. Phys.*, **59**, 1582 (1973).
(16) M. M. Audibert, C. Joffrin, and J. Ducuing, *Chem. Phys. Lett.*, **19**, 26 (1973).
(17) F. Demartini and J. Ducuing, *Phys. Rev. Lett.*, **17**, 117 (1966).
(18) J. E. Dove, D. G. Jones, and H. Teitlebaum, *Symp. (Int.) Combust., [Proc.], 14th, 1972*, (1973).
(19) D. L. Baulch, D. D. Drysdale, D. G. Horne, and A. C. Lloyd, "Evaluated Kinetic Data for High Temperature Reactions", Vol. 1, Butterworths, London, 1972.
(20) M. J. Kurylo, *J. Phys. Chem.*, **76**, 3518 (1972).
(21) A. A. Westenberg and N. deHaas, *J. Phys. Chem.*, **76**, 1586 (1972).
(22) J. J. Ahumada, J. V. Michael, and D. T. Osborne, *J. Chem. Phys.*, **57**, 3736 (1972).
(23) D. L. Thompson, *J. Chem. Phys.*, **57**, 2589 (1972).
(24) P. F. Zittel and C. B. Moore, *J. Chem. Phys.*, **59**, 6636 (1973).
(25) The rate coefficients for all reactions in the H_2–O_2 system were taken from ref 19.
(26) R. S. Brokaw, *J. Phys. Chem.*, **69**, 2808 (1965).
(27) V. L. Tal'roze, *Svobodnoradikal'nye Sostoianiya Khim.*, 165–170 (1972).
(28) J. B. Levy and B. K. W. Copeland, *J. Phys. Chem.*, **72**, 3168 (1968).
(29) J. C. Polanyi and K. B. Woodall, *J. Chem. Phys.*, **57**, 1574 (1972).
(30) Cross sections for the reaction $H + F_2 \rightarrow HF + F$ are given by N. C. Blais (Los Alamos Scientific Laboratory Report No. LA-4687) as a function of relative energy. Rate coefficients as calculated from these cross sections for 20 kcal/mol and 10 kcal/mol H atoms are much larger than 10^{14} cm^3/sec. The cross sections near 2 kcal/mol vary sharply with energy and approach zero as the energy is lowered to about 2 kcal/mol.

(31) The rate coefficients for these recombination reactions are undoubtedly smaller in a system with hot atoms than the coefficients in a thermal system. Our explosion limits in fluorine-rich systems may be underestimated.
(32) J. C. Polanyi and J. J. Sloan, *J. Chem. Phys.*, **57**, 4988 (1972).
(33) N. C. Blais, Los Alamos Scientific Laboratory Report No. LA-4603 (April 1971).
(34) R. N. Porter and S. Kunt, *J. Chem. Phys.*, **52**, 3240 (1970).
(35) N. R. Greiner, *IEEE J. Quantum Electron*, **QE-9**, No. 11, 1123 (1973); N. R. Greiner, L. S. Blair and P. F. Bird, *ibid.*, submitted for publication.
(36) V. N. Kondratiev in "Comprehensive Chemical Kinetics", Vol. 2, C. H. Bamford and C. F. H. Tipper, Ed., Elsevier, Amsterdam, 1969
(37) The diffusion coefficient for H atoms in F_2 is estimated from $D_0(H_2-N_2)$ = 0.674 cm^2/sec, "American Institute of Physics Handbook", 2nd ed, McGraw-Hill, New York, N.Y., pp 2-235. We estimate $D'(H-F_2) = 1.4D_0(H_2-N_2)(300/273)^{1.75} = 1.1$ cm^2/sec.
(38) S. W. Rabideau, H. G. Hecht, and W. B. Lewis, *J. Magn. Reson.*, **6**, 348 (1972).
(39) K. H. Homan, W. C. Solomon, J. Warnatz, H. Gg. Wagner, and C. Zetzch, *Ber. Bunsenges Phys. Chem.*, **74**, 585 (1970).
(40) A. F. Dodonov, G. K. Lavroskaya, I. I. Morozov, R. T. Albright, V. T. Tal'roze, and A. K. Lyubimova, *Kinet. Catal.*, **11**, 821 (1970). Also R. T. Albright, A. F. Dodonov, G. K. Lavroskaya, I. I. Morozov, and V. L. Tal'roze, *J. Chem. Phys.*, **50**, 3632 (1969).
(41) G. A. Kapralova, E. M. Margolina, and A. M. Chaikin, *Gorenie Vzryv, Mater. Vses, Simp., 3rd, 1971*, 634-637 (1972); *Chem. Abstr.*, **78**, 152006e (1973); G. A. Kapralova, E. M. Margolina, and A. M. Chaikin, *Dokl. Akad. Nauk SSSR*, **197**, 281 (1971).

Photolytic Decomposition of Azoethane at High Helium Pressure

S. Chervinsky[1] and I. Oref*

Department of Chemistry, Technion—Israel Institute of Technology, Haifa, Israel *(Received August 9, 1974)*

The primary quantum yield in the unimolecular decomposition of azoethane was measured in the pressure range of 6–140 atm of He. Excited azoethane was produced by a mercury lamp with wavelength of 3660 Å. The relative collision efficiencies for He were found to be in the range 0.01–0.03 depending on the model used. No systematic change occurred in the slope of the Stern–Volmer plot in the high-pressure range which was investigated. The intercept was found to be different from unity. This indicates a slight curvature in the low-pressure range. It is concluded that under the conditions used in the present experiments, no significant deviation from a statistical unimolecular theory, such as, RRKM, which is based on random lifetime assumption, was observed.

1. Introduction

The photolytic decomposition of azoethane was used as a model reaction for unimolecular decomposition in the supra-high-pressure region. Previously published experimental results agreed with statistical theories in the low- and medium-pressure regions.[2] Here we report high-pressure experimental results which complement the existing data at lower pressures.

The purpose of this high-pressure work is to test the statistical principle in unimolecular kinetic theories, such as, RRKM, which are based on the assumption that randomization of the internal energy takes place on a shorter time scale than the lifetime for decomposition of the excited parent molecule.

By using collisions between excited and deactivator molecules as means of removing energy, one can, by increasing the pressure, reduce the time scale between collisions to the time range of intramolecular randomization of the energy, thus influencing the unimolecular rate coefficient of decomposition.

Photoexcitation is a convenient technique for testing the concept of energy randomization, since a large amount of energy enters a localized region target molecule by a radiation event that occurs in a short period of time. The energy is thus introduced by a particular mechanism and in a nonrandom fashion. Any deviation from random behavior will be more apparent with the photochemical activation technique, than with thermal activation, where activation and deactivation are stepwise processes.

The literature contains varying predictions regarding the effects of increased molecular complexity and high pressure on the rate coefficient of a unimolecular reaction. In a model of thermal activation suggested by Wilson and coworkers,[3,4] a fall-off region at suprahigh pressure is predicted. Monte-Carlo calculations made by Bunker[5] indicate that the rate coefficient will rise above its "high-pressure" limit in some cases. Very little experimental information exists on the rate coefficients of unimolecular gas-phase reactions at pressures appreciably above 10 atm. The first successful experimental work on nonrandom energy distribution is the work of Rabinovitch and coworkers in chemically activated systems.[6-8,13]

In these studies, the decomposition of excited substituted cyclopropane, which is formed by the addition of a methylene radical to a double bond, was followed as a function of pressure. It was found that the apparent rate constant $\langle k_a \rangle$ increases with increase in pressure. The increase in $\langle k_a \rangle$ can be attributed to nonrandomness of the energy distribution in the excited molecule. This nonrandomness is due to the formation of an excited cyclopropyl moiety which has a large rate coefficient for unimolecular decomposition, k_N, of the order of 10^{11} sec^{-1}, and thus provides an independent channel for decomposition. There is a rate coefficient, λ,[5] of the order of 10^{12} sec^{-1}, for intramolecular energy transfer. It is the relative magnitudes of k_N, λ, and the unimolecular rate coefficient from the excited randomized molecule which determine whether nonrandom effects can be measured under given experimental conditions.[14]

The increase in $\langle k_a \rangle$ will manifest itself in photochemical systems by a systematic decrease in the slope of the Stern–Volmer plot.[15] This decrease is expected to appear in the high-pressure range and should not be confused with a curvature at low pressures which might be due to excitation of more than one electronic energy level.[2b,17] Inefficient collisions cause an increase in the slope of the Stern–Volmer plot due to a decrease in $k(E)$ as a function of pressure.[11] This effect is noticeable in theoretical calculations at low pressures when a stepladder model for energy transfer is used. The curvature is always small and within the experimental uncertainties.[18]

2. Experimental Section

Azoethane was purchased from Merck Sharp and Dohme, Canada. The azoethane was purified by fractional distillation under vacuum and kept, when not in use, in liquid air. The purity of the gas was checked by gas chromatography with 20% dioctylphthalate on a Chromosorb w column. Pure helium 99.995% was purchased from Air Precision, it was further purified by passing it over cooled molecular sieves 5A. The experimental system is composed of three parts: a light irradiation part with the reaction vessel, a detection system, and low- and high-pressure systems.

The irradiation part includes a high-pressure air-cooled mercury lamp Osram HBO 500 W/2. The 3660-Å wavelength was isolated by using a Chance-Pilkington color filter OX1.

The 200-cc reaction vessel was built from stainless steel with 1-in. quartz windows. The reaction vessel and the stainless steel tubings and connections were planned to stand pressures of up to 400 atm.

The light detection part includes two photodiodes, RCA IP39, with beam splitters which are connected differentially to a digital integrator. The difference in the electric current which is produced by the photodiodes and which is supplied to the integrator is proportional to the number of the photons absorbed by the reactant gas in the reaction vessel.

The reaction products were analyzed by an on-line Perkin-Elmer gas chromatograph. The separations of the various products were done on a molecular sieve 5A column. High helium pressure was obtained by compressing helium with a hand compressor. The gas pressure was measured with an Heise Co. gauge.

Azoethane was introduced into the reaction vessel through the vacuum system inlet. The azoethane pressure was measured with a mercury monometer and the pressure was kept constant during the whole series of runs.

The azoethane was introduced into the reaction vessel by freezing it at liquid air temperature in a cold finger which is part of the reaction vessel. At this stage final pumping was done over the sample. Azoethane was then warmed to room temperature and helium from a helium tank was compressed into the reaction vessel with a hand compressor. This procedure ensured a proper mixing of azoethane with helium. Temperature variations were never more than 0.5°.

For a given series of runs the number of absorbed photons was kept constant. This was done in order to avoid errors which are due to variations in the intensity of the lamp.

After the irradiation was completed, the azoethane was frozen out in the cold finger at liquid air temperature. The volatile products were adsorbed on a special liquid air cooled trap, which was filled with silica gel. The adsorption took place during the release of the helium from the system. This procedure separated quantitatively between the trace amount of N_2, the primary photolysis product, and the huge amount of helium. When the pressure in the system was reduced to a little over 1 atm, the trap was warmed and its volatile content was injected into a gas chromatograph.

3. Results

In order to analyze the results of the decomposition of azoethane a Stern–Volmer plot was used.

The scheme of the decomposition is

$$(CH_3CH_2)_2N_2 + h\nu \longrightarrow (CH_3CH_2)_2N_2^*$$

$$(CH_3CH_2)_2N_2^* \xrightarrow{k_a} 2CH_3CH_2\cdot + N_2$$

$$(CH_3CH_2)_2N_2^* + M \xrightarrow{\omega} (CH_3CH_2)_2N_2 + M$$

where $h\nu$ is the 3660-Å wavelength photon; k_a, the unimolecular rate coefficient for decomposition; ω, the number of collisions per second; and M, a deactivator gas molecule. In the present experiments helium was used as a deactivator. The amount of N_2 which was produced during the reaction was checked and the quantum yield for the primary photochemical reaction was calculated. The Stern–Volmer plot is

$$1/\phi(p) = 1 + a(\mathrm{M})p$$

where $\phi(p)$ is the quantum yield for decomposition as a function of the pressure, p, of the deactivator. Using data of Table I, a linear dependence of $1/\phi(p)$ on p was obtained. The slope and intercept of the line were found by using a least-squares program.

If we assume that $a(\mathrm{M})$ is proportional to the gas kinetic collision number between azoethane and helium, here M is helium, a relative collision efficiency on a collision per collision basis is defined

$$\beta^{\mathrm{HS}}(\mathrm{He}) = \frac{a(\mathrm{He})\sigma^2(\mathrm{Azo\text{–}Azo})\mu^{1/2}(\mathrm{Azo\text{–}He})}{a(\mathrm{Azo})\sigma^2(\mathrm{Azo\text{–}He})\mu^{1/2}(\mathrm{Azo\text{–}Azo})}$$

with the reduced masses μ, and σ^2 the hard-sphere cross section.

A value of $a(\mathrm{Azo}) = 3.82$ was obtained from the work of Worsham and Rice. A value of $a(\mathrm{He}) = 0.0605$ was obtained from the slope of the least-squares line. A collision diameter $\sigma = 7.7$ Å for azoethane was estimated from a model calculation. Using a Lennard-Jones, LJ, 6–12 potential, σ is replaced by $\sigma^{LJ} = \sigma(\Omega^{(2,2)*})^{1/2}$ where $\Omega^{(2,2)*}$ is determined from a table in ref 10.

By using a Lindemann model we can obtain more information. The model gives the equation:

$$\phi^{-1}(p) = 1 + \frac{k(\mathrm{deact})[\mathrm{M}]}{k(\mathrm{decomp})}$$

For simplicity we have neglected the multistep deactivation process; we used for $k(\mathrm{decomp})$ the value measured by Worsham and Rice[2a] for 3660 Å $k(\mathrm{decomp}) = 3.8 \times 10^9$ sec^{-1}. For $k(\mathrm{deact})$ we used both the gas kinetic Lennard-Jones and hard-sphere collision number $\omega^i(\mathrm{M})$ multiplied by an efficiency factor γ^i. Where i represents LJ or HS $a^i(\mathrm{M}) = \gamma^i\omega^i(\mathrm{M})/k(\mathrm{decomp})$ the reciprocal of γ^i would be a rough estimate on the number of steps necessary for the stabilization of azoethane. A comparison was made between our results and the results of Luu and Troe[9] and other works. The results are given in Table II. The details of the calculation are given in Appendix I. Table II shows that, in the present case, the helium molecule has an effi-

TABLE I: Rate of Decomposition of Photoactivated Azoethane at 298°K

p(meas), atm	p(ideal), atm	ω, 10^{-19} sec^{-1}	ϕ (quantum yield)
0	0	1	1.0
6.0	5.9	13.7	0.91
7.0	6.9	16.0	0.38
10.0	9.9	23.1	0.34
10.0	9.9	23.1	0.33
15.0	14.8	34.6	0.31
18.0	17.8	41.6	0.29
20.0	19.7	46.1	0.34
30.0	29.5	69.2	0.29
30.0	29.5	69.2	0.29
35.0	34.3	80.6	0.31
40.0	39.1	92.0	0.31
45.0	43.9	103.5	0.21
50.0	48.6	114.7	0.25
50.0	48.6	114.7	0.25
60.0	58.0	137.3	0.17
70.0	67.5	160.3	0.31
70.0	67.5	160.2	0.13
80.0	76.5	182.1	0.12
85.0	81.4	194.0	0.15
100.0	95.0	227.4	0.13
100.0	95.0	227.4	0.11
140.0	130.6	316.0	0.10

[a] Correction according to Enskog theory and Beattie-Bridgeman equation of state.

TABLE II: Comparison of the Collision Efficiencies of He between This and Other Works

Ref	β^{HS}	γ^{HS}	β^{LJ}	γ^{LJ}
This work	0.010	0.0087	0.020	0.0093
9	0.040	0.012	0.080	0.013
11	0.17		0.35	
12	0.031			

ciency factor for deactivation smaller than in chemical activation or photoactivation to vibrationally excited molecules in the electronic ground state.[9,12]

4. Discussion

The intercept of the Stern–Volmer plot, as is found by a least-squares program, is larger than unity. The deviation is larger than the standard deviation of the intercept. This is true even after the self-quenching effect is taken into consideration. It is possible that there is a slight curvature in the plot. The positive curvature is absent from the RRKM plot which is a straight line with intercept of unity. The RRKM calculations of ϕ were done according to an expression which is given by Bowers.[2b] The details of the calculations are given in Appendix II.

The absence of a positive curvature is to be expected since in the RRKM model the excitation energy is randomized throughout the whole molecule and k_a is not expected to change in the pressure range which was investigated. This is especially true for He as bath molecules since the effective collisional frequency is much lower than the nominal frequency. It is possible, however, to explain the curvature in the graph by assuming that there is some unimolecular decomposition from a nonrandom moiety in the energized molecule. It is known that the quantum yield of azomethane remains unity at fairly high pressures.[16] This means that the rate coefficient for unimolecular decomposition is fairly high. A model can be suggested in which, in the azoethane molecule, the energy is randomized in an azomethylene moiety with a nonrandom rate coefficient for decomposition, k_N, of the same order of magnitude as for azomethane decomposition. This moiety decomposes before undergoing energy randomization, or it may undergo intramolecular energy transfer, either via weak collisions, with the bath molecules, or by a spontaneous process with a rate coefficient, λ.[14,15] A computer fit to the data of such a model is shown by a dotted line in Figure 1. The details of the parameters which were used in the calculations are given in Table III. The value of the collisional efficiency is $\beta = 0.024$ and the cross section for collisional intramolecular energy transfer is found to be a factor of 4 larger than the one for collisional deactivation. If we let the collisional efficiency of the parent azoethane molecule be unity, the ratio of the calculated slope at the limit of low pressure to the slope of the line of Warsham and Rice[2a] yields $\beta_{expt} = 0.034$.

An agreement of a factor of 1.5 between these two different calculations is all one can hope for at the present, since many empirical factors still enter into the evaluation of the various parameters.

TABLE III: Parameters which Were Used in the Calculation of the Theoretical Line in Figure 1

Nonrandom rate coeff, k_N	1.3×10^{11} sec^{-1}
Nonrandom collisional deactivation rate coeff, k_{-N}	3×10^{-11} molecule^{-1} cc sec^{-1}
Intramolecular collisional energy transfer rate coeff, k_{-R}	5×10^{-10} molecule^{-1} cc sec^{-1}
Intramolecular energy transfer rate coeff, λ	4×10^{11}
Random unimolecular decomposition rate coeff, k_R	3.8×10^{9} sec^{-1}
Random collisional deactivation rate coeff, k_{-RR}	2×10^{-11} molecule^{-1} cc sec^{-1}
Collision efficiency, β	0.024

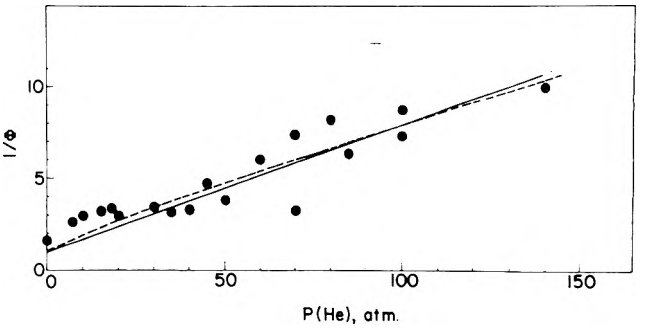

Figure 1. Quantum yield of azoethane as a function of He pressure: ϕ[RRKM] (—); ϕ from nonrandom moiety model (- - -).

5. Conclusions

It is difficult to conclude from the present results whether nonrandomization of the energy has actually occurred under the experimental conditions which were reported here. The linearity of the experimental results in the high-pressure range leads one to believe that the RRKM theory

does hold in the present case. On the other hand, the nonunit slope which indicates a positive curvature can be explained by assuming incomplete intramolecular energy transfer during the deactivation period. Increasing the effective collisional frequency by using a more efficient collider is one way of obtaining more definite information on the applicability of the RRKM theory at high pressures. We plan to use a more effective collider in order to obtain an effective collisional frequency of about 10^{13} sec^{-1}.

6. Appendix I

The correction in the high-pressure region was made by the use of the Beattie-Bridgeman equation of state[10]

$$p(\text{meas}) = \frac{RT}{\bar{V}^2}\left[\left(1 - \frac{c}{\bar{V}T^3}\right)\left(\bar{V} + B_0 - \frac{bB_0}{\bar{V}}\right) - \frac{A_0}{RT}\left(1 - \frac{a}{\bar{V}}\right)\right]$$

where A_0 = 0.0216 atm $l.^2$ mol^{-2}; a = 0.05984 M^{-1}; B_0 = 0.01400 M^{-1}; b = 0.0 M^{-1}; c = 40 °K^3 l. mol^{-1}; $\bar{V} = M^{-1}$. The correction was applied to pure helium since azoethane pressure was negligible. The dilute gas binary collision number ω for azoethane is calculated from collision theory expression

$$\omega(\text{binary}) = N(\text{He})\sigma^2(\text{Azo–He})\left[\frac{(8\bar{\eta}kT)}{\mu(\text{Azo–He})}\right]^{1/2}$$

where μ is the reduced mass of the collision partners and N(He) is the number of bath molecules per cubic centimeter. Other values are: σ(Azo) = 7.7 Å; σ(He) = 2.6 Å; σ(Azo–He) = $\frac{1}{2}(\sigma(\text{Azo}) + \sigma(\text{He}))$; $T^* = kT/\epsilon(\text{Azo–He})$; $\epsilon(\text{He})/k$ = 10.22; $\epsilon(\text{Azo})/k$ = 410 for azoethane from ref 10; ϵ(Azo–He) = $(\epsilon(\text{Azo})\epsilon(\text{He}))^{1/2}$; $\Omega^{(2,2)*}$ is tabulated as a function of T^* in ref 10. The correction to the collision diameter based on Lennard-Jones potential is $\sigma^{LJ} = \sigma^{HS}[\Omega^{(2,2)*}]^{1/2}$. Another correction for the binary collision number is the Enskog correction[10] for rigid sphere collisions. The correction factor χ is $\chi = 1 + 0.625(B/\bar{V}) + 0.287(B/\bar{V})^2 + \ldots$ where B is the second virial coefficient. Both corrections were included in the calculations of ω.

7. Appendix II

The vibrational frequencies of the azoethane molecule in the ground state were assigned according to Bowers:[2b] for the ground state, four torsional motions were treated as free rotations and the remaining 38 frequencies (cm^{-1}) were assigned as follows: 2950 (10), 1550 (1), 1450 (6), 1300 (2), 1000 (8), 900 (2), 800 (1), 600 (1), 450 (2), 315 (2), 250 (1), 150 (1).

For the excited state the stretching and twisting frequencies of the N–N bond were reduced to 50% of their ground state values.

The vibrational frequencies for the loose activated complex were taken according to Forst's[19] model for azomethane thermal decomposition. The asymmetric C–N stretching vibration was omitted. All vibrations and free internal rotations were taken to be active in the intramolecular energy exchange. There are 10 free internal rotations. The vibrational frequencies were given the following values in cm^{-1}: 2950 (10), 2000 (1), 1450 (6), 1300 (2), 1000 (4), 900 (1), 450 (2), 315 (2), 150 (3). Overall rotations were assumed to be adiabatic with unit contribution to the microscopic rate constant.

The ϕ(RRKM) was calculated from the expression

$$\phi = \int_{E_{min}}^{\infty} \frac{k_a[E^*]g[E^*]}{k_a[E^*] + \omega}\, dE$$

where $k_a[E^*]$ is the energy dependent unimolecular rate coefficient and $g[E^*]$ is the energy distribution function of the molecules in the ground state.

Neither E_{00} nor E_{min} could be assigned an a priori values. The best fit to the data was obtained with the following values: E_{00} = 54.3 kcal/mol and E_{min} = 12.6 kcal/mol compared with Bowers' E_{00} = 54.3 kcal/mol and E_{min} = 12.3 kcal/mol.

In the calculations, the light profile of the lamp and the filter-transmission characteristics were taken into account by including them in the thermal energy distribution of the ground state and using it in the equation for the calculation of the quantum yield. The density of states of the excited molecule and the number of states for the activated complex were calculated by the Whitten–Rabinovitch equation as modified by Forst.[20]

References and Notes

(1) Based on a part of a thesis to be submitted by S.C. to the senate of the Technion—I.I.T., in partial fulfillment of the requirements for the D.Sc. degree.
(2) (a) W. C. Worsham and O. K. Rice, *J. Chem. Phys.*, **46**, 2021 (1967); (b) P. G. Bowers, *J. Phys. Chem.*, **74**, 952 (1970).
(3) R. C. Baetzold and D. J. Wilson, *J. Phys. Chem.*, **68**, 3143 (1964).
(4) D. J. Wilson, *J. Phys. Chem.*, **64**, 323 (1960).
(5) D. L. Bunker, *J. Chem. Phys.*, **40**, 1946 (1964).
(6) I. Oref, D. Schuetzle, and B. S. Rabinovitch, *J. Chem. Phys.*, **54**, 575 (1971).
(7) J. D. Rynbrandt and B. S. Rabinovitch, *J. Phys. Chem.*, **75**, 2164 (1971).
(8) D. W. Placzek, B. S. Rabinovitch, and F. H. Dorer, *J. Chem. Phys.*, **44**, 279 (1966).
(9) S. H. Luu and J. Troe, *Ber. Bunsenges. Phys. Chem.*, **77**, 325 (1973).
(10) J. O. Hirschfelder, C. F. Curtis, and R. B. Bird, "Molecular Theory of Gases and Liquids", Wiley, New York, N.Y., 1954.
(11) G. H. Kohlmaier and B. S. Rabinovitch, *J. Chem. Phys.*, **38**, 1692 (1963).
(12) S. W. Orchard and B. A. Thrush, *Proc. Roy. Soc., Ser. A.*, **329**, 233 (1972).
(13) B. S. Rabinovitch, J. F. Meagher, K. J. Chao, and J. R. Barker, *J. Chem. Phys.*, **60**, 2932 (1974).
(14) For a full discussion of the conditions under which nonrandom effects can be seen, see ref 13 and a paper by I. Oref to be submitted for publication in *J. Chem. Phys.*
(15) I. Oref to be submitted for publication in *J. Chem. Phys.*
(16) See ref 2a. Also in this laboratory ϕ for azomethane remained constant at He pressures of up to 50 atm.
(17) E. C. Wu and O. K. Rice, *J. Phys. Chem.*, **72**, 542 (1968).
(18) S. H. Luu and J. Troe, *Ber. Bunsenges. Phys. Chem.*, **78**, 766 (1974).
(19) W. Forst, *J. Chem. Phys.*, **44**, 2349 (1966).
(20) W. Forst, *Chem. Rev.*, **71**, 339 (1971).

Absorption Spectra and Kinetics of Methyl and Ethyl Radicals in Water

Bernard Hickel

DRA/SRIRMa, Cen.Saclay, B.P. No 2, 91190 Gif Sur Yvette, France *(Received October 15, 1974)*

Publication costs assisted by Comissariat â l-Energie Atomique

The absorption spectra and some kinetic properties of the methyl and ethyl radicals in water were studied by pulse radiolysis. For methyl radicals the maximum of the absorption spectrum lies at 213 nm (ϵ 1600 M^{-1} cm^{-1}) while the ethyl radical spectrum shows no maximum down to 200 nm. The disappearance of methyl and ethyl radicals follows second-order kinetics. At 25°, $k_{(CH_3+CH_3)} = 1.6 \pm 0.2 \times 10^9$ M^{-1} sec^{-1} and $k_{(C_2H_5+C_2H_5)} = 1.2 \pm 0.2 \times 10^9$ M^{-1} sec^{-1}. The effect of temperature on the rate of recombination gives an apparent activation energy of 3.9 ± 0.4 kcal/mol for both methyl and ethyl radicals, and is close to the activation energy for the diffusion of the radicals in water. In the presence of oxygen a new spectrum appears centered at 250 nm with a lifetime in the millisecond range. A study of the effect of pH on this spectrum shows that the new species is not HO_2 formed by H atom transfer to the oxygen but RO_2 formed by direct addition of the radical to oxygen. For ethyl radicals the rate constant of this addition is $k_{(C_2H_5+O_2)} = 2.9 \pm 0.8 \times 10^9$ M^{-1} sec^{-1}. The reaction of the two alkyl radicals with H_2O_2 was investigated by pulse and steady-state radiolysis. The rate constant between CH_3 and C_2H_5 with H_2O_2 is comparatively slow $k \leq 10^6$ M^{-1} sec^{-1} and there is no indication that the reaction proceeds via a chain mechanism.

Introduction

During the past 10 years, the electronic absorption spectra and kinetic properties of many organic radicals in water have been reported.[1] Comparatively there are very few studies dealing with the methyl radical, one of the simplest free radicals, in water. In 1966 Thomas studied the pulse and γ radiolysis of aqueous solutions of CH_3I.[2] He showed that the solvated electron reacts with CH_3I to give I^- after a time shorter than 80 nsec, but he could not find the spectrum of CH_3 which lies too far in the uv.

Recently Stevens et al.[3] studying the pulse radiolysis of aqueous solution of methane and ethane reported broad absorption spectra without maxima between 270 and 210 nm. These were assigned to methyl and ethyl radicals formed respectively by the reaction of OH radicals with methane and ethane.

$$OH + RH \longrightarrow R\cdot + H_2O \qquad (1)$$

In the present paper we report a study of the absorption spectra and some rate constants of methyl and ethyl radicals in water by pulse and steady state radiolysis.

The range of measurements was extended further into the uv and the position of the maximum of the methyl radical spectrum in water was found and compared with the gas-phase spectrum. The effect of temperature on the rate of recombination of methyl and ethyl radicals was studied to find the activation energy of this typical radical–radical reaction in water.

Experimental Section

Irradiations. The pulse radiolysis experiments were carried out using a single 11-MeV electron pulse from the RISÖ Linac. The pulse duration can be varied in the range from 0.4 to 4 μsec with a peak current of 250 mA.

Experimental details on the pulse radiolysis system are given elsewhere.[4] The decay of the radicals was followed spectrophotometrically. A 450-W xenon lamp (Osram XBO) was used to produce the analyzing light. The intensity was increased by a factor of 30 by pulsing the lamp.[5] After a single passage through the irradiation cell the light beam is collimated on the entrance slit of a Zeiss MM12 double quartz prism monochromator. Under our experimental condition the band width of the monochromator was about 1 nm at 200 nm. An EMI 9558 Q photomultiplier was used, and the signal was displayed on a Tektronix 555 oscilloscope.

To increase the concentration of methane or ethane in solution, a pressure cell was used[4] with a pressure of gas above the solution of 30 atm. This gives concentrations of 4 $\times 10^{-2}$ and 5 $\times 10^{-2}$ M for methane and ethane, respectively, in the solution. The length of the cell was 7.1 cm.

γ radiolysis experiments were performed with a Gammacell giving a dose rate of 56 krads/hr.

Preparation of Solutions. Solutions were prepared using triply distilled water. The solutions were first deaerated by bubbling high-purity argon through them and the pressure cell was filled with argon to avoid air contamination. The cells were then pressurized with methane or ethane and shaken for 0.5 hr to ensure equilibration. Other gases, e.g., N_2O, CH_3Cl, C_2H_5Cl, and C_2H_4, were dissolved in the solution before filling the pressure cell. Their concentrations after equilibrium were estimated from the equation

$$(\text{gas})_f = (\text{gas})_i \Big/ \left(1 + \frac{V_g}{\alpha V_s}\right)$$

where V_g is the volume of gas above the solution and V_s the volume of the solution. α is the Bunsen coefficient of solubility of the gas in water. The ratio V_g/V_s is about 4. Methane and ethane were supplied by AS Dansk Ilt and Brintfabrik. Their purity was checked by mass spectrometric analysis. The other chemicals were of analytical grade and were used without purification. In some experiments H_2O_2 was made by γ irradiation of aerated triply distilled water. For a dose of 400 krads the final concentration of H_2O_2 was 1.9 $\times 10^{-4}$ M. Analysis of H_2O_2 was done using Ghormley's method.[6]

Dosimetry. The dosimetry was carried out with a solution of 10^{-3} M $K_4Fe(CN)_6$ saturated with N_2O. The ab-

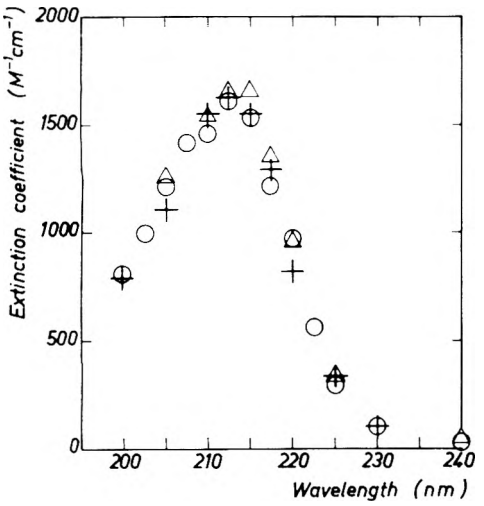

Figure 1. Absorption spectrum of the methyl radical in water at P_{CH_4} = 30 atm: (⊙) CH_4 + N_2O 3 × 10^{-3} *M*, pH 4.4, dose 1.2 krads; (△) CH_4 + CH_3Cl 1.2 × 10^{-3} *M*, dose = 0.65 krad; (+) CH_4 + $HClO_4$ 3 × 10^{-4} *M*, dose 1.2 krads.

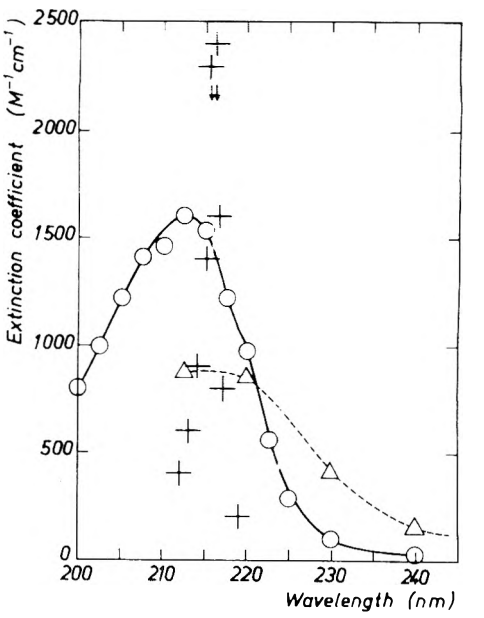

Figure 2. Spectrum of the methyl radical: (+) gas phase P_{CH_4} = 30 atm; (O) water (this work); (△) water (ref 3); (↓↓) position of the β bands of CH_3 in gas phase at low pressure (ref 12).

sorption of $Fe(CN)_6^{3-}$ was recorded at 415 nm and the dose was calculated from the following values: ε (415 nm) 1000 M^{-1} cm^{-1}, $G(Fe(CN)_6^{3-}) = g_{e_{aq}^-} + g_{OH} = 5.25$.

Results

Absorption Spectrum of CH_3. Figure 1 shows the spectrum observed in a solution of about 4 × 10^{-2} *M* of CH_4, 2 μsec after the end of a 1-μsec electron pulse. As the absorption spectrum of the hydrated electron extends into the uv we used N_2O, CH_3Cl, or H_3O^+ to scavenge electrons and prevent interference.

$$e_{aq}^- + N_2O \xrightarrow{H_2O} N_2 + OH + OH^- \quad (2)$$

$$e_{aq}^- + CH_3Cl \longrightarrow CH_3 + Cl^- \quad (3)$$

$$e_{aq}^- + H_3O^+ \longrightarrow H + H_2O \quad (4)$$

OH radicals formed by decomposition of water or by reaction with N_2O react with CH_4

$$OH + CH_4 \longrightarrow CH_3 + H_2O \quad (5)$$

The rate of reaction 5 is comparatively slow $k_5 \simeq 10^8$ M^{-1} sec^{-1},[3,7] and it is necessary to use a pressure cell to ensure complete scavenging of OH radicals. Under a pressure of 30 atm of CH_4 the halftime of reaction 5 is about 0.2 μsec. When the spectrum is recorded reactions 2–5 are complete. The hydroxyl ion formed by reaction 2 has a strong absorption at 200 nm (ε 1000) but in slightly acid solution the very fast reaction 6 takes place with a rate con-

$$H^+ + OH^- \longrightarrow H_2O \quad (6)$$

stant $k_6 = 1.4 \times 10^{11}$ M^{-1} sec^{-1}.[8] At pH 4.4 the lifetime of OH^- is about 0.2 μsec. Although CH_3Cl reacts more slowly with e_{aq}^- than does CH_3I or CH_3Br ($k_3 = 10^9$ M^{-1} sec^{-1}),[9] for our purpose it is a much better source of methyl radicals because Cl^- does not absorb at wavelengths longer than 200 nm (ε 25 at 200 nm).

The third method of scavenging e_{aq}^-, reaction 4, is not so convenient because H atoms formed by reaction 4 absorb down to 220 nm.[4] Nevertheless after subtraction of the absorption due to solvated H atoms the remaining spectrum is identical with those observed with N_2O or CH_3Cl. The H atoms formed by decomposition of water or by reaction 4 react very slowly ($k < 10^5$) with N_2O,[10] CH_4, and CH_3Cl.[11] The extinction coefficients of the methyl radical were calculated using $G(CH_3) = g_{e_{aq}^-} + g_{OH} = 5.25$ for a solution containing N_2O or CH_3Cl and $G(CH_3) = g_{OH} = 2.65$ for a solution of $HClO_4$. Figure 1 shows that the spectrum is independent of the mode of formation. The maximum lies at 213 ± 2 nm with an extinction coefficient of 1.600 ± 100 M^{-1} cm^{-1}. For wavelengths longer than 240 nm there is no absorption by CH_3 and it is possible using a normal cell to follow the decay at 250 nm of OH radicals in N_2O solution in both the absence and presence of 1.16 × 10^{-3} *M* CH_4. The difference gives $k_4 = (1.0 \pm 0.3) \times 10^8$ in good agreement with previously published values.[3,7]

Although the pulse radiolysis system was not especially well suited for gas-phase studies, it was possible to record the spectrum of CH_3 in that phase by pulsing 30 atm of CH_4. The spectrum (Figure 2) is much sharper than in water, but the position of the maximum is approximately the same: 216 nm in the gas phase compared to 213 ± 2 nm in water. As we have no dosimetry data for the gas phase the ε scale does not apply here. For comparison we have plotted on Figure 2 the position of the β bands of CH_3 radicals observed in the gas phase at low pressure by Herzberg.[12] Recently the gas-phase spectrum of CH_3 was also observed by pulse radiolysis of 1 atm of CH_4.[13]

Recombination of CH_3. The decay of the methyl radical was followed between 210 and 220 nm in solution of 4 × 10^{-2} *M* CH_4 with 2.5 × 10^{-3} *M* N_2O. The reaction follows second order kinetic and the rate constant is independent of the wavelength. The same rate constant was obtained at 215 nm in a solution containing CH_3Cl instead of N_2O (Table I).

$$CH_3 + CH_3 \longrightarrow C_2H_6 \quad (7)$$

The effect of temperature on the rate of reaction 7 was studied between 6.5 and 67°. As a first approximation the yield $g_{e_{aq}^-} + g_{OH} = G(CH_3)$ may be considered as constant in this temperature range[14] but at 213 nm, where the experiments were performed, the extinction coefficient of CH_3 decrease from 1760 at 6.5° to 1490 at 67°. A plot of log

TABLE I: Recombination of Methyl Radicals in Water at 25°

λ, nm	ε, M^{-1} cm^{-1}	k, M^{-1} sec^{-1}	System	Ref
210	1460	1.7×10^{1}	CH_3 4 × 10^{-2} M + N_2O 2.5 × 10^{-1} M	This work
213	1600	1.6×10^{1}	CH_3 4 × 10^{-2} M + N_2O 2.5 × 10^{-1} M	This work
215	1535	1.6×10^{1}	CH_3 4 × 10^{-2} M + N_2O 2.5 × 10^{-1} M	This work
220	975	1.6×10^{1}	CH_3 4 × 10^{-2} M + N_2O 2.5 × 10^{-1} M	This work
215	1535	1.65×10^{1}	CH_3 4 × 10^{-2} M + CH_3Cl 2 × 10^{-1} M	This work
220	850	1.24×10^{1}	CH_3 + N_2O	3

k_7 against $1/T$ gives approximately a straight line from which a mean apparent activation energy of 3.9 ± 0.4 kcal was derived (Figure 3). This is the order of magnitude expected for a diffusion-controlled reaction in water. (In the gas phase the recombination of CH_3 proceeds without activation energy.[15]) The activation energy of diffusion of CH_4 in water is 2.9 kcal.[16] The difference of 1 kcal may be accounted for by a stronger interaction of water with CH_3 than with CH_4. Recent determinations of diffusion coefficients of alkyl radicals in cyclohexane[17] indicate that propyl radicals diffuse more slowly than the parent hydrocarbon.

Absorption Spectrum of C_2H_5. A similar study was made with ethane to obtain the spectrum of the ethyl radical in water. Under a pressure of 30 atm of C_2H_6 the concentration of C_2H_6 in the solution is about 5×10^{-2} M.

The corresponding reactions are

$$OH + C_2H_6 \longrightarrow C_2H_5 + H_2O \quad (8)$$

$$e_{aq}^- + C_2H_5Cl \longrightarrow C_2H_5 + Cl^- \quad (9)$$

The reaction of H atoms with C_2H_6 is too slow to he important, $k_{H+C_2H_6} = 2.5 \times 10^6$ M^{-1} sec^{-1},[11] but in the presence of ethylene addition to the double bond occurs.

$$H + C_2H_4 \longrightarrow C_2H_5 \quad (10)$$

The rate constant of this reaction is fast enough, $k_{10} = 3 \times 10^9$ M^{-1} sec^{-1},[11] so that it is possible to use a low concentration of C_2H_4 and to avoid reactions with OH radicals which take place at a comparable rate.[18]

The rate constant of reaction 8 cannot be determined directly as for reaction 3 because C_2H_5 (see below) and OH absorb in the same region. k_8 was measured by competition kinetics with ferrocyanide. The decrease in absorption at 415 nm in a solution 10^{-3} M $Fe(CN)_6^{4-}$ containing millimolar concentration of N_2O in presence of ethane gives $k_{(OH+C_2H_6)}/k_{(OH+Fe(CN)_6^{4-})} = 0.17 \pm 0.3$. Taking $k_{(OH+Fe(CN)_6^{4-})} = 10^{10} \pm 0.2$ M^{-1} sec^{-1} [18] $k_{(OH+C_2H_6)} = 1.7 \pm 0.5 \times 10^9$ M^{-1} sec^{-1}.

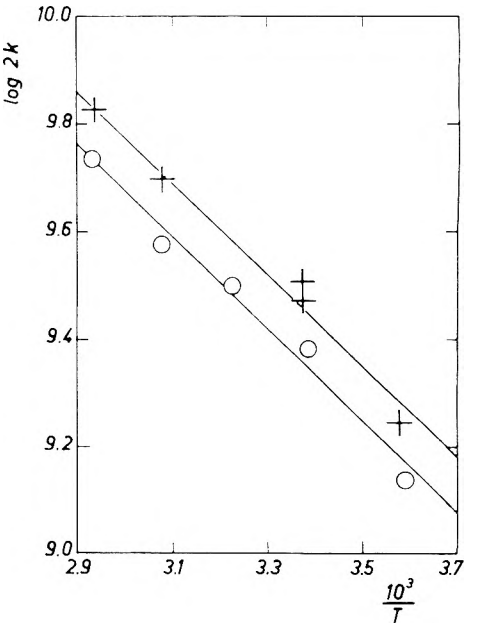

Figure 3. Arrhenius plot for the recombination of methyl and ethyl radicals in water: (+) CH_3; (⊙) C_2H_5.

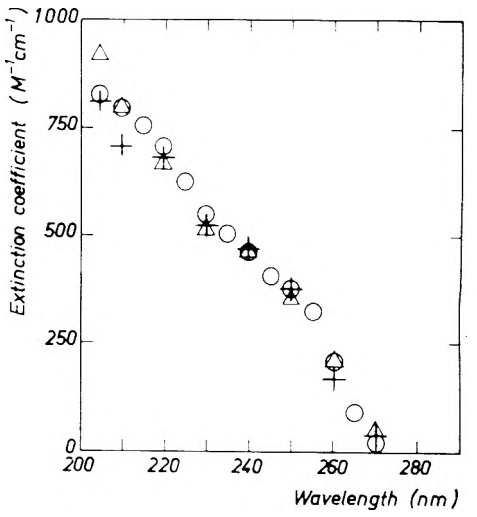

Figure 4. Absorption spectrum of the ethyl radical in water at $P_{C_2H_6}$ = 30 atm, dose = 1.6 krads: (⊙) C_2H_6 + N_2O 3 × 10^{-3} M, pH 4.4; (△) C_2H_6 + C_2H_5Cl 3 × 10^{-3} M; (+) C_2H_6 + C_2H_4 1.4 × 10^{-4} M, pH 2.8.

The spectrum of the ethyl radical in water is shown in Figure 4. The extinction coefficients were calculated taking $G(C_2H_5) = g_{e_{aq}^-} + g_{OH} = 5.25$ for solutions containing N_2O (reactions 2 and 8) and C_2H_5Cl (reactions 8 and 9). For acid solutions of ethylene $G(C_2H_5) = g_{e_{aq}^-} + g_H + g_{OH} = 5.8$ (reactions 4, 8, and 10). The spectrum shows no maximum above 200 nm and the general shape is the same as that found previously[3] but our extinction coefficients are 40% higher than in ref 3. As ethane is more reactive than methane toward OH radicals, there is the possibility that some OH was scavenged in the spurs increasing the apparent ε of C_2H_5. However, when the concentration of ethane was decreased by a factor of 7 ($C_2H_6 \simeq 7 \times 10^{-3}$ M) the same extinction coefficients were observed. It may be noticed that ε does not depend on the value used for $g_{e_{aq}^-} + g_{OH}$ because in N_2O or C_2H_5Cl solutions $G(C_2H_5) = G(Fe(CN)_6^{3-})$ and the absorption of C_2H_5 was compared directly with those of $Fe(CN)_6^{3-}$.

TABLE II: Recombination of Ethyl Radicals in Water at 25°

λ, nm	ε, M^{-1} cm^{-1}	k, M^{-1} sec^{-1}	System	Ref
210	790	1.3×10^9	C_2H_6 5×10^{-2} M + N_2O 2.5×10^{-3} M	This work
215	750	1.1×10^9	C_2H_6 5×10^{-2} M + N_2O 2.5×10^{-3} M	
220	700	1.2×10^9	C_2H_6 5×10^{-2} M + N_2O 2.5×10^{-3} M	
230	545	1.3×10^9	C_2H_6 5×10^{-2} M + N_2O 2.5×10^{-3} M	
250	375	1.0×10^9	C_2H_6 5×10^{-2} M + N_2O 2.5×10^{-3} M	
220	700	1.1×10	C_2H_6 5×10^{-2} M + C_2H_5Cl 3×10^{-3} M	
220	700	1.2×10^9	C_2H_6 5×10^{-2} M + $HClO_4$ 2×10^{-3} M + C_2H_4 1.4×10^{-4} M	
220	520	9.6×10^8	C_2H_6 + N_2O	3
250	330	9.6×10^8	C_2H_6 + N_2O	3

The decay of C_2H_5 was investigated at different wavelength from 210 to 250 nm (Table II). The decay follows second-order kinetics and identical rate constants were observed in solution of N_2O, C_2H_5Cl, and C_2H_4.

$$C_2H_5 + C_2H_5 \longrightarrow \text{products} \qquad (11)$$

$$2k_{11} = 2.3 \pm 0.3 \times 10^9\ M^{-1}\ \text{sec}^{-1}$$

The effect of temperature on the rate of recombination of ethyl radical was also studied in N_2O solutions of ethane. At 230 nm the extinction coefficient does not change with temperature between 5 and 68°. The activation energy is the same as for methyl radicals, i.e., 3.9 ± 0.3 kcal (Figure 3).

The activation energy for the diffusion of ethane in water is 2.9 kcal[16] and the same considerations apply as for the methyl radicals.

Effect of O_2 and H_2O_2. In the presence of oxygen the spectra of methyl or ethyl radicals are no longer observed and a new spectrum appears at 250 nm with a longer lifetime. This feature was observed previously by Thomas[2] and was attributed to the formation of CH_3O_2.

$$CH_3 + O_2 \longrightarrow CH_3O_2 \qquad (12)$$

$k_{12} = 4.7 \times 10^9\ M^{-1}\ \text{sec}^{-1}$. Later Stevens et al. found the same effect but with a smaller rate constant, $k_{12} = 3.2 \times 10^8\ M^{-1}\ \text{sec}^{-1}$.[3]

In the presence of N_2O to avoid the reaction of e_{aq}^- with O_2 the following reactions take place

$$e_{aq}^- + N_2O \longrightarrow OH + OH^-$$
$$OH + RH \longrightarrow R + H_2O$$
$$R + O_2 \longrightarrow RO_2$$
$$H + O_2 \longrightarrow HO_2 \rightleftharpoons H^+ + O_2^-$$

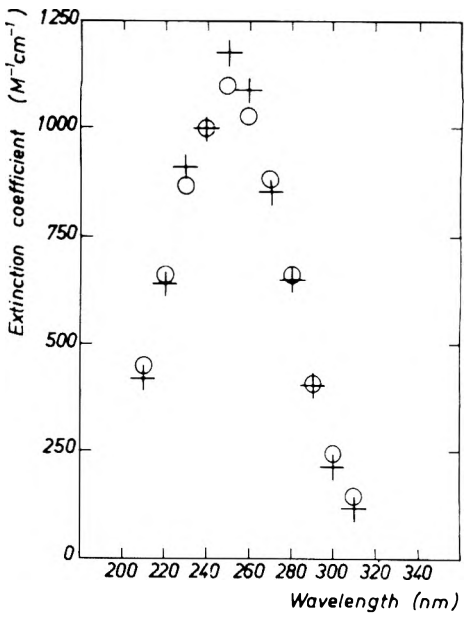

Figure 5. Absorption spectrum of CH_3O_2 at a dose 2 krads: (O) pH 4.1; (+) pH 9.9.

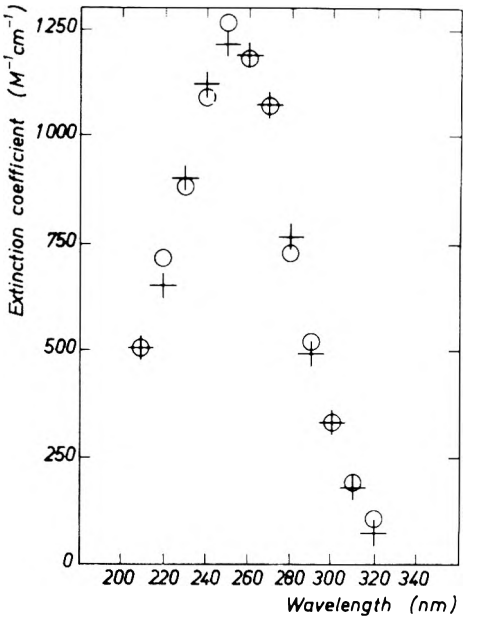

Figure 6. Absorption spectrum of $C_2H_5O_2$: (O) pH 4.1; (+) pH 9.9.

After subtraction of the spectrum of HO_2 or O_2^- coming from the reaction of H atom ($g_H = 0.55$) with oxygen, the remaining spectrum is independent of the pH of the solution between pH 4 and pH 10 (Figures 5 and 6). This rules out an additional formation of HO_2 from the reaction

$$CH_3 + O_2 \longrightarrow CH_2O + HO_2 \qquad (13)$$

$$C_2H_5 + O_2 \longrightarrow C_2H_4 + HO_2 \qquad (14)$$

The pK of HO_2 is 4.8[19,20] and if reactions 13 and 14 took place with the formation of HO_2 the spectrum would be pH dependent between pH 4 where 85% of the total HO_2 is unionized and pH 10 where the dissociation into $H^+ + O_2^-$ is almost complete.

It was found difficult to determine k_{12} owing to the problem of introducing low and well-defined concentrations of oxygen into the pressure cell, but for the reaction

$$C_2H_5 + O_2 \longrightarrow C_2H_5O_2 \qquad (15)$$

TABLE III: Decomposition of H_2O_2 under γ Radiolysis[a]

	System	$G(H_2O_2)$
a	CH_4 1.2×10^{-5} M H_2O_2 1.2×10^{-4} M N_2O 3×10^{-2} M	−0.6
b	C_2H_6 1.4×10^{-3} M H_2O_2 1.1×10^{-4} M N_2O 5×10^{-2} M	−0.17
c	C_2H_6 1.8×10^{-3} M H_2O_2 0.94×10^{-4} M	−2.5
d	C_2H_6 1.5×10^{-3} M N_2O 2.8×10^{-3} M	0.6 (initial yield)

[a] Note the difference between c and b is approximately equal to $g_{e_{aq}^-}$. In system c, e_{aq}^- is scavenged by H_2O_2 instead of N_2O.

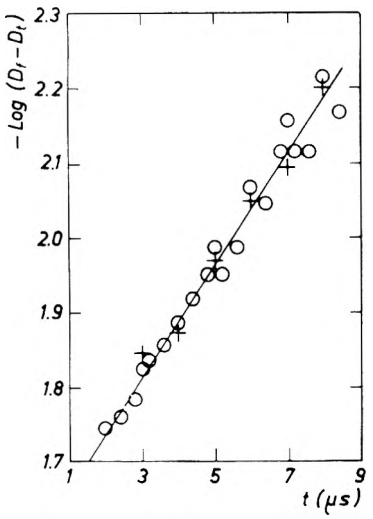

Figure 7. Kinetics of formation of $C_2H_5O_2$ at 270 nm: dose = 1.1 krads; $O_2 = 6 \times 10^{-5}$ M.

it is possible to use a normal cell and to inject into the solution a known concentration of oxygen. By following the growth of the absorption at 270 nm where C_2H_5 does not absorb appreciably it is possible to determine k_{15}. The formation of O_2^- coming from the reaction of radiolytic H atom with O_2 accounts for about 10% of the final absorption, but this reaction is 90% complete 2 μsec after the end of the pulse and a plot of $-\log (D_f - D_t)$ against time after 2 μsec gives a straight line (Figure 7). D_f is the final optical density measured 35 μsec after the end of the pulse and D_t the optical density at time t. From the slope a value of 2.9 $\pm$ 0.8 $\times$ 10^9 M^{-1} sec^{-1} was derived for k_{15} which is comparable with the value found by Thomas[2] for the corresponding reaction with CH_3.

Reaction with H_2O_2. In the presence of H_2O_2 Stevens et al. reported that the decay of CH_3 is first order[2] and they derive a rate constant of 3.5 $\times$ 10^7 M^{-1} sec^{-1} for the reaction

$$CH_3 + H_2O_2 \longrightarrow CH_3OH + OH \qquad (16)$$

We have found that 10^{-3} and 10^{-2} M H_2O_2 have no influence on the decay respectively in CH_3 and C_2H_5 which remains second order with the same rate constant. However, under our experimental conditions and for those of ref 2, OH formed by reaction 15 reacts immediately with CH_4 reforming CH_3 and the rate of disappearance of CH_3 would be the rate of chain termination, i.e.

$$CH_3 + CH_3 \longrightarrow C_2H_6$$

The same reasoning holds good for C_2H_5 and explains why there is no effect of H_2O_2. To check this explanation, the alternative being that the reaction of CH_3 or C_2H_5 with H_2O_2 is slow compared to the rate of recombination of the radicals, we have done some γ ray irradiations. If reaction 16 takes place H_2O_2 would be decomposed with a high yield. Because chain reactions are generally very sensitive to small concentrations of impurity some experiments were carried out with H_2O_2 made by γ radiolysis of aerated water. The results were identical with those obtained using analytical grade H_2O_2 and are summarized in Table III. The low yield of decomposition of H_2O_2 indicates that no chain reaction takes place between CH_3 and C_2H_5 with H_2O_2. Although very improbable the possibility exists that ROH and OH formed by reaction 16 react in the solvent cage before diffusion

$$OH + ROH \longrightarrow R'OH + H_2O \qquad (17)$$

However, the radicals formed by reaction 17 have a well-known spectrum and they absorb strongly in the uv.[21] If they were formed the optical density would increase and instead of a decay of CH_3 or C_2H_5 an apparent formation would be observed. Moreover no absorption other than those of CH_3 and C_2H_5 was observed at longer wavelength and a search for the formation of HO_2 was unsuccessful.

Nevertheless, we suggest that CH_3 and C_2H_5 react with H_2O_2 like OH by hydrogen abstraction

$$R\cdot + H_2O_2 \longrightarrow RH + HO_2 \qquad (18)$$

but this reaction is too slow ($k_{18} \leq 10^6$ M^{-1} sec^{-1}) compared to the recombination of the radicals to be observed by pulse radiolysis.

Acknowledgments. The author wishes to thank, K. Sehested and the RISÖ group for careful operation of the linear accelerator, J. Eriksen and P. Genske for invaluable technical assistance, and A. Miller for the interferometric measurement of the cell temperature. It is a pleasure to acknowledge the many stimulating discussions with P. Pagsberg and the comments of A.M. Boyd and J. Sutton during the completion of the manuscript. The author also thanks the Danish Atomic Energy Commission for financial support during the course of this work.

References and Notes

(1) A. Habersbergerova, I. Janovsky, and P. Kourim, *Radiat. Res. Rev.*, **4**, 123 (1972).
(2) J. K. Thomas, *J. Phys. Chem.*, **71**, 1919 (1967).
(3) G. C. Stevens, R. M. Clarke, and E. J. Hart, *J. Phys. Chem.*, **76**, 3863 (1972).
(4) P. Pagsberg, H. Christensen, J. Pabani, G. Nilsson, J. Fenger, and S. O. Nielsen, *J. Phys. Chem.*, **73**, 1029 (1969).
(5) T. Hviid and S. O. Nielsen, *Rev. Sci. Instrum.*, **40**, 786 (1969); **43**, 1198 (1972).
(6) A. O. Allen, C. J. Hochanadel, J. A. Ghormley, and I. W. Davies, *J. Phys Chem.*, **56**, 575 (1952).
(7) M. Anbar, D. Meyerstein, and P. Neta, *J. Chem. Soc. B*, 742 (1966).
(8) M. Eigen and L. de Maeyer, *Z. Elektrochem.*, **59**, 986 (1955); G. Ertl and H. Gerischer, *ibid.*, **65**, 629 (1961).
(9) T. I. Balkas, J. H. Fendler, and R. H. Schuler, *J. Phys. Chem.*, **74**, 4497 (1970).
(10) M. Anbar and P. Neta, *Int. J. Appl. Radiat. Isotopes*, **18**, 493 (1967).
(11) P. Neta, *Chem. Rev.*, **72**, 533 (1972).
(12) G. Herzberg and J. Shoosmith, *Can. J. Phys.*, **34**, 523 (1956).
(13) M. W. Bosnali and D. Perner, Jul 897 (1972).
(14) I. G. Draganic and Z. D. Draganic, "The Radiation Chemistry of Water", Academic Press, New York, N.Y., 1971; C. J. Hochanadel and J. A. Glormley, *Radiat. Res.*, **16**, 653 (1962).
(15) E. V. Waage and B. S. Rabinovitch, *Int. J. Chem. Kinet.*, **3**, 105 (1971).
(16) P. A. Witherspoon and D. N. Saraf, *J. Phys. Chem.*, **69**, 3752 (1965).

(17) R. D. Burkhart, R. F. Boynton, J. C. Merrill, *J. Am. Chem. Soc.*, **93**, 5013 (1971).
(18) L. F. Dorfman and G. E. Adams, *Natl. Stand. Ref. Data Ser., Natl. Bur. Stand.*, **No. 46** (1973).
(19) J. Rabani and S. O. Nielsen, *J. Phys. Chem.*, **73**, 3736 (1969).
(20) D. Behar, G. Czapski, J. Rabani, L. M. Dorfman, and H. A. Schwarz, *J. Phys. Chem.*, **74**, 3209 (1970).
(21) M. Simic, P. Neta, and E. Hayon, *J. Phys. Chem.*, **73**, 3794 (1969).

Radical Intermediates Produced from the One-Electron Reduction of Lumazine in Water

P. N. Moorthy[1] and E. Hayon*

Pioneering Research Laboratory, U.S. Army Natick Laboratories, Natick, Massachusetts 01760
(Received August 16, 1974; Revised Manuscript Received January 24, 1975)

Publication costs assisted by Natick Laboratories

The one-electron reduction of lumazine (LH_2) in aqueous solutions was brought about using e_{aq}^- and $(CH_3)_2\dot{C}OH$ radicals as the reducing agents. The fast-reaction technique of pulse radiolysis and kinetic absorption spectrophotometry was used to monitor and determine the spectral characteristics and acid–base properties of the free-radical intermediates produced. The reaction rate constants of e_{aq}^- and $(CH_3)_2\dot{C}OH$ radicals with the neutral and ionic forms LH_2, LH^-, and L^{2-} of lumazine were determined. The reactivity toward e_{aq}^- is $2–3 \times 10^{10}\ M^{-1}\ sec^{-1}$. At pH 5.2, the reaction of e_{aq}^- or $(CH_3)_2\dot{C}OH$ with LH_2 gives rise to an initial transient (T_1) which changes with time to another transient species (T_2). It is shown that proton donors lead to the change $T_1 \rightarrow T_2$. The rate constants for the reaction of T_1 with H_3O^+, LH_2, and $H_2PO_4^-$ are 1.6×10^{10}, 2.7×10^8, and $3.6 \times 10^8\ M^{-1}\ sec^{-1}$, respectively. The $-N_3H$ in lumazine is suggested to act as the proton donor for this reaction. Based on the transient spectra and ionization constants of the free radicals formed at pH 0.8, 5.2, 10.2, and 14.0, a tentative scheme of reactions is suggested for the formation of the $LH_4\cdot^+$, $(LH_2)\cdot^-$, $LH_3\cdot$, $LH_2\cdot^-$, and $LH\cdot^{2-}$ radicals.

Lumazine (I) is a substituted pteridine (II) and forms part of the skeleton of flavins, such as riboflavin (III).

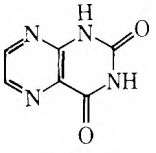

I

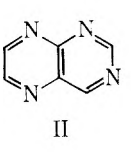

II

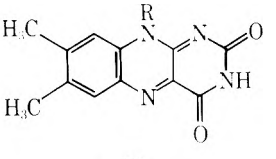

III

These molecules can be readily reduced, and the intermediate free radicals formed are considered to play a role in biochemical redox reactions. Various aspects of the physicochemical properties of these free radicals, including acid–base properties,[2] are under study. The one-electron reduction of lumazine has been examined in CF_3COOH by ESR.[3] A radical cation has been observed, with the odd electron localized on the pyrazine ring.

The radicals produced from the reduction by e_{aq}^- of the uracil[4] (U) and the pyrazine[5] (Pz) rings in lumazine have been studied, as well as the related molecules pterin,[6] folic acid,[6] quinoxaline[5] (Qx), and riboflavin[3,7] (Rb). The site of reduction and the pK_a values of the radicals produced vary considerably.

No work appears to have been carried out to determine the optical spectra, ionization constants, reactivity, and decay kinetics of the lumazine free radicals. Using the fast-reaction technique of pulse radiolysis and kinetic absorption spectrophotometry, the one-electron reduction of lumazine by e_{aq}^-, $(CH_3)_2\dot{C}OH$, and $(CH_3)_2\dot{C}O^-$ radicals in water has been studied. The results obtained are presented below.

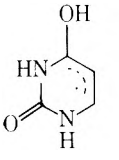

UH· (pK_a 7.3)

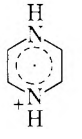

PzH_2^+ (pK_a 10.5)

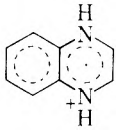

QxH_2^+ (pK_a 8.8)

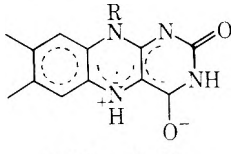

RbH· (pK_a 8.3)

Experimental Section

The pulse radiolysis experimental set-up used has been described.[8,9] Single pulses of 2.3-MeV electrons and ~30 nsec duration (Febetron 705 machine) were used.

The radiolysis of water produces e_{aq}^-, H, and OH radicals, where the numbers in parentheses are the G values (number of free radicals formed per 100 eV of energy absorbed). One-electron reduction of lumazine (LH_2) by e_{aq}^- was carried out in solutions containing ~1.0 M *tert*-butyl alcohol (to scavenge the OH radicals) and saturated with argon. One-electron reduction by $(CH_3)_2\dot{C}OH$ radicals was

$$H_2O \longrightarrow e_{aq}^-\ (2.8),\ H\ (0.6),\ \text{and}\ OH\ (2.8)$$

TABLE I: Reaction Rate Constants of e_{aq}^- and $(CH_3)_2\dot{C}OH$ Radicals with Lumazine (LH_2) in Aqueous Solution at Different pH Values

Ionic form[a]	pH	$k(e_{aq}^- + S)$, M^{-1} sec^{-1}[b]	pH	$k[(CH_3)_2\dot{C}OH + S]$, M^{-1} sec^{-1}[b]	% efficiency[c]
LH_2	6.3	2.9×10^{10}	0.8, 5.1	1.3×10^9	100
LH^-	9.9	2.1×10^{10}	9.5	1.7×10^8	70
L^{2-}	14.0	1.9×10^{10}	14.0	1.0×10^{9d}	85

[a] See text. [b] Values to ±10%. [c] Efficiency of formation of the reduced lumazine radical by one-electron reduction. [d] At this pH the donor radical is present as $(CH_3)_2CO^-$.

carried out in solutions containing 1–2 *M* isopropyl alcohol saturated with N_2O:

$$OH + (CH_3)_2CHOH \longrightarrow (CH_3)_2\dot{C}OH + H_2O \quad (1)$$

$$e_{aq}^- + N_2O \longrightarrow N_2 + OH + OH^- \quad (2)$$

$$(CH_3)_2\dot{C}OH \rightleftharpoons (CH_3)_2\dot{C}O^- + H^+ \quad pK_a = 12.2^2 \quad (3)$$

The concentrations of lumazine, *t*-BuOH, *i*-PrOH, and N_2O were chosen based on the known[10,11] rate constants for their reaction with e_{aq}^- and OH radicals in order to obtain the appropriate experimental conditions.

Extinction coefficients were derived based on the *G* values of the primary radicals from water and the KCNS dosimetry.[8] The transient absorption spectra observed were corrected for depletion of lumazine at the appropriate pH values and wavelengths.

The chemicals used were the highest purity available commercially, and were obtained from Aldrich Chemicals, Mallinckrodt, Baker and Adamson, and Eastman Chemicals. Solutions were buffered with perchloric acid, potassium hydroxide, phosphates, and borate.

Results and Discussion

Reactivity toward e_{aq}^-. The reaction rate constant of e_{aq}^- with lumazine (LH_2, $pK_a \sim -3$, 7.95, and 12.64) was determined at different pH values, by monitoring the decay kinetics of e_{aq}^- at 700 nm. At this wavelength, the electron adduct species do not absorb. From the pseudo-first-order decay at two–three concentrations of lumazine, the second-order rate constants were derived. Table I shows these values for the acid–base forms LH_2, LH^-, and L^{2-}. At pH 6.3, $k = 2.9 \times 10^{10}$ M^{-1} sec^{-1} for LH_2 and can be compared to $k = 2.3 \times 10^{10}$ M^{-1} sec^{-1} for riboflavin[10] at pH 5.9, 2.1×10^{10} M^{-1} sec^{-1} for pyrazine[5] at pH 7.0, and 2.5×10^{10} M^{-1} sec^{-1} for pterin[6] at pH 6.5.

The small decrease in the rate constant with increase in pH (Table I) may be the result of the keto–enol tautomerism of lumazine and/or to the negative charge carried by the LH^- and L^{2-} forms. At pH 14.0, the ionic strength of the solution is also affecting the observed reaction rate constant (the actual *k* values would be lower).

Reactivity toward the Acetone Ketyl Radical. The $(CH_3)_2\dot{C}OH$ radical was produced in situ and used to reduce lumazine at various pH values. Table I shows the efficiency of the electron transfer reaction 4, as well as the rate

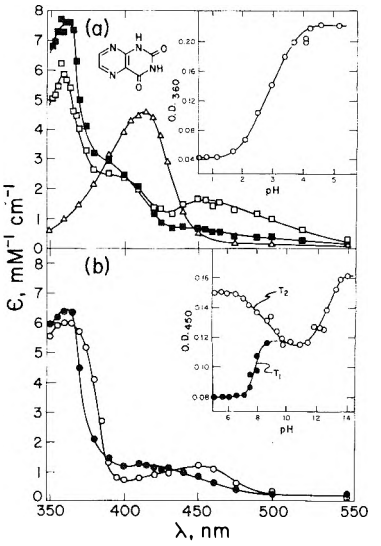

Figure 1. Optical spectra of intermediates produced from the one-electron reduction of lumazine (2.5×10^{-4} *M*) in water by (a) $(CH_3)_2\dot{C}OH$ radicals (in 1.0 *M i*-PrOH) at pH 0.8, △, and by e_{aq}^- (in 1.0 *M t*-BuOH) at pH 5.2 (T_1 species, ■, read at ~0.5 μsec after the pulse; T_2 species, □, read at ~5 μsec). Insert shows change in absorbance at 360 nm with pH; (b) e_{aq}^- at pH 10.2, ●, and pH 14.0, ○. Insert shows change in absorbance at 450 nm with pH for transient species T_1 and T_2. Total dose ~5–10 krads/pulse. The spectra have been corrected for depletion of the solute.

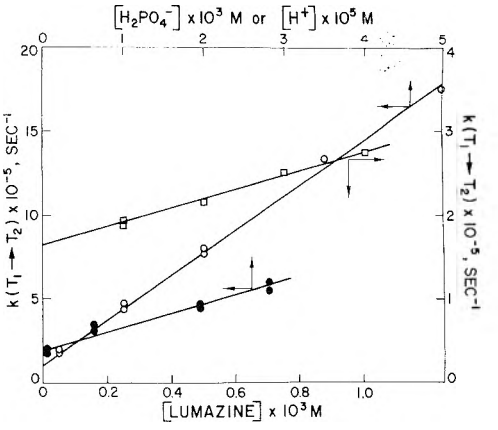

Figure 2. Dependence of the rate of protonation of the transient species T_1 and T_2 produced from the reduction of lumazine by e_{aq}^- upon the concentration of (a) lumazine, □; (b) H^+, ⊕; and (c) $H_2PO_4^-$, ○. The differences in the intercept values are due to changes in the *initial* concentrations of lumazine, H^+, or $H_2PO_4^-$ used in each case.

$$(CH_3)_2\dot{C}OH + LH_2 \longrightarrow LH_3\cdot + CH_3COCH_3 \quad (4)$$

constants for reaction 4. The values for k_4 were determined by monitoring the formation kinetics of the lumazine radicals produced at the appropriate wavelength (see below). The efficiencies were derived by comparison with the absorbance of the lumazine radicals produced directly by reaction with e_{aq}^- (*t*-BuOH system), under otherwise identical experimental conditions.

The redox potential of lumazine does not seem to have been determined. The kinetic potential[12] of the $(CH_3)_2\dot{C}OH$ radical is $E_k^{01} = -0.82$ V. The efficiency of electron transfer to LH_2 is 100% suggesting that E^{01} (LH_2) > −0.82 V. A 70% efficiency for LH^- (Table I) suggests that E^{01} (LH^-) ≤ −0.82 V. The $(CH_3)_2\dot{C}O^-$ radical has a $E_k^{01} < -1.6$ V (ref 12), and since only 85% transfer to form

TABLE II: Absorption Spectra, Extinction Coefficients, Ionization Constants, and Decay Kinetics of the Radicals Produced from the One-Electron Reduction of Lumazine in Water

pH	λ_{max}, nm	ϵ, M^{-1} cm^{-1}	$2k$, M^{-1} sec^{-1} [a]	pK_a (radical)	Suggested radical
0.8[a]	415	4.6×10^3	1.7×10^8	2.9	$LH_1^{\cdot+}$
5.2[b,c]	(T_1) 362; 450	7.8×10^3; 7.0×10^2	*d*	*e*	$(LH_2)^{\cdot-}$
	(T_2) 360; 455	5.8×10^3; 1.7×10^3	2.6×10^8		$LH_3^{\cdot}$
10.2[b]	362; ~415	6.4×10^3; 1.2×10^3	1.2×10^8	~8.6	$LH_2^{\cdot-}$
14.0[b]	365; 450	6.1×10^3; 1.2×10^3	1.1×10^8	~12.6	$LH^{\cdot 2-}$

[a] Radical produced by reaction with $(CH_3)_2\dot{C}OH$. [b] Radical produced by reaction with e_{aq}^-. [c] Transient species T_1 and T_2 observed at this pH. [d] T_1 decays by first-order kinetics to give transient T_2 (see text). [e] T_1 species has an apparent pK_a ~ 7.9 (see text).

TABLE III: Rate Constants for Protonation of the Lumazine Radical Anion (T_1 Species) by Proton Donors in Water[a]

Proton donor, HA	$k(T_1 \xrightarrow{HA} T_2)$, M^{-1} sec^{-1} [a]
H_3O^+	1.6×10^{10}
Lumazine, LH_2	2.7×10^8
$H_2PO_4^-$	3.6×10^8
H_2O	~10^5 sec^{-1} [b]

[a] See text. [b] Intercept value in plot of the multilinear regression analysis of the kinetic data, assumed to represent protonation by the solvent.

L^{2-} was observed, it follows that the redox potential of L^{2-} is very negative. These observations indicate that the dike- to form of lumazine is much more easily reduced than the monoenolate (or dienolate) form. Similar differences between the reducibilities of the keto and enol forms of other compounds have been observed.[6] The more powerful reducing agent e_{aq}^- ($E^0 \sim -2.8$ V) does not probe into such differences in reactivity.

Formation of Free Radical Intermediates

The intermediates produced from the reaction of e_{aq}^- with lumazine in aqueous solution (in the presence of 1.0 *M* *t*-BuOH) at pH 5.2 are shown in Figure 1a. The transient absorption spectrum and extinction coefficient observed at ~0.5 μsec after the electron pulse (transient T_1) changes with time to give another transient species (T_2) whose spectrum was read at ~5 μsec after the pulse (Figure 1a and Table II).

The change from T_1 to T_2 was found to require a proton, reaction 5. Various proton donors were found to bring

$$T_1 \xrightarrow{HA} T_2 \qquad (5)$$

about this reaction, albeit at different rates. Figure 2 shows the dependence of k_5 upon the concentrations of H^+, lumazine, and $H_2PO_4^-$ ions (used as buffer). The rate constants for protonation of the T_1 radical intermediate by various proton donors are given in Table III.

Protonation of T_1 by H_3O^+ is very fast, $k = 1.6 \times 10^{10}$ M^{-1} sec^{-1}, whereas lumazine and $H_2PO_4^-$ protonate T_1 with rate constant values of 2.7×10^8 and 3.6×10^8 M^{-1} sec^{-1}, respectively.

Similar intermediate species T_1 and T_2 were observed on one-electron reduction of various aromatic nitrogen heterocyclic compounds, including pyrazine,[5,13] pterin,[6] folic acid,[6] pyridoxin,[14] and pyridoxal phosphate.[14] In the case of protonation of the pterin T_1 species by pterin itself, it was clearly shown[6] that the proton comes from the $-N_3H$ position since no protonation was observed from 3-methylpterin. Based on these results, it is suggested that the protonation of the T_1 species by lumazine may also be due primarily to the $-N_3H$ group in lumazine.

At pH 0.8, the reaction of $(CH_3)_2\dot{C}OH$ radicals with LH_2 produced a completely different transient spectrum with λ_{max} 415 nm, see Figure 1a. Although there is no way of comparing this spectrum with that formed by reaction of e_{aq}^- with lumazine, the observed spectrum can nevertheless be attributed to such a species for the following reasons: such an identity was established at pH 5, and neither lumazine nor the acetone ketyl radical have a pK_a in the pH range 0.8–5.0. Since their redox potentials remain unchanged, it is reasonable to assume that one-electron reduction of lumazine by $(CH_3)_2\dot{C}OH$ at pH 0.8 occurs via an electron transfer mechanism.

On pulse radiolysis of lumazine at pH 10.2 (ionic form LH^-), a different transient absorption spectrum is formed (Figure 1b). Only one intermediate was observed (i.e., there is no change in the spectrum with time). Another transient spectrum is formed when e_{aq}^- reacts with L^{2-} at pH 14.0. The changes in absorbance of the intermediates with pH at fixed wavelengths are shown in the inserts to Figure 1 (see also Table II).

Scheme I is tentative. Other configurations for the radical intermediates are not presented. This scheme was chosen for the following reasons: (a) due to its similarity to the radicals identified[3,7] from riboflavin, (b) the strong electron affinity of the pyrazine ring and the great ease for protonation of pyrazinyl radicals,[5,13,15] and (c) similar mechanisms have been suggested[6] for pterin and folic acid.

From ESR data, Ehrenberg et al.[3] inferred the formation of the radical cation $LH_4 \cdot^+$ produced from the one-electron reduction of lumazine in acid media, with the odd electron localized on the pyrazine ring. The pK_a = 2.9 for this species (see Scheme I) appears reasonable, if one considers the base weakening effect of the benzene ring. Thus the pK_a of the lumazine cation LH_3^+ is −3 as compared to 0.65 for the pyrazine cation $PzH \cdot^+$. On this basis one can expect that the lumazine cation radical $LH_4 \cdot^+$ should have a much lower pK_a (observed value is ~2.9) than that of the pyrazine cation radical $PzH_2 \cdot^+$ (pK_a = 10.5[5]).

The subsequent ionization constants of the lumazine radicals are close enough to those of lumazine itself. What calls for comment is the assignment of the T_1 species. In this connection it may be noted that although the transformation from T_1 to T_2 is brought about by proton donors, these two species are not related to each other as conjugate

Scheme I

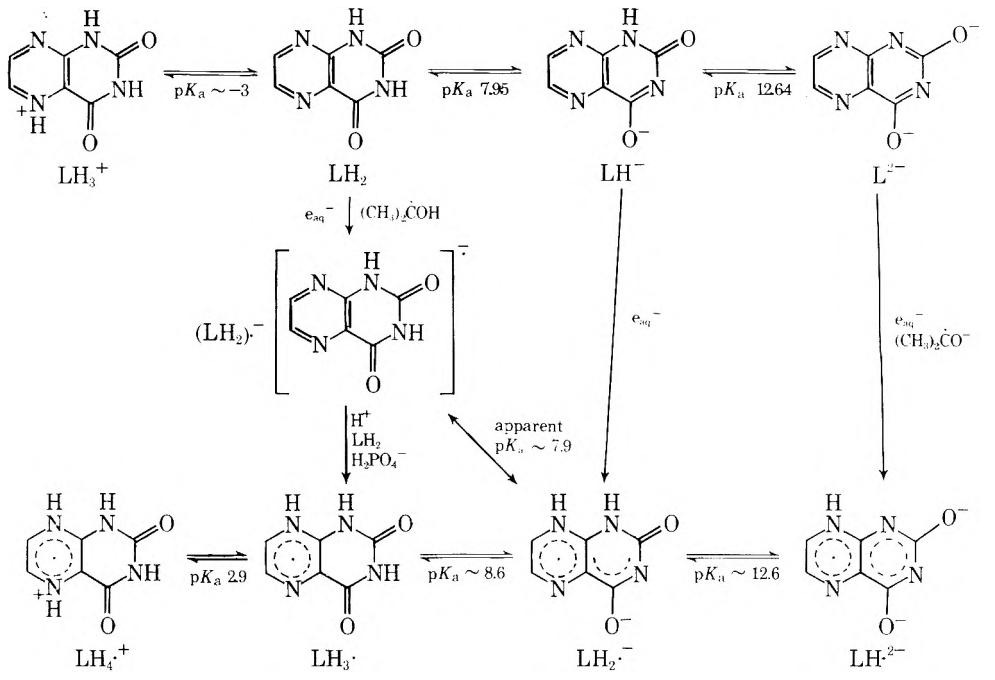

acid–base pairs. Thus the T_2 spectrum at pH 10.2 (at which pH T_2 would be present in the deprotonated basic form) is not the same as the T_1 spectrum at pH 5.2. We suggest that at, e.g., pH 5.2, T_1 is a radical anion, $(LH_2)\cdot^-$ (possibly a ketyl radical anion at the C_4 position, similar to pyrimidines[4]), which undergoes an irreversible protonation reaction to give the radical $LH_3\cdot$. This radical has a $pK_a \sim 8.6$ for the ionization of N_1H. The $pK_a \sim 7.9$ for the T_1 species is only an apparent one: with increasing pH, reaction 4 becomes progressively slower. The change in absorbance of T_1 with pH reflects the difference in the rates of protonation of N_{10} and deprotonation of N_3H.

The $LH_2\cdot^-$ and $LH\cdot^{2-}$ radicals appear to be reasonably good reducing agents. They were both able to reduce anthraquinone-2,6-disulfonate (AQ, $E^{01} = -0.184$ V) to the radical anion $\cdot AQ^-$ with ~100% efficiency and a rate constant for electron transfer of $\sim 1.2 \times 10^9\ M^{-1}\ sec^{-1}$. Acetophenone ($E^{01} = -1.3$ V) could not be reduced by either $LH_2\cdot^-$ or $LH\cdot^{2-}$ radicals.

References and Notes

(1) Visiting Scientist from the Chemistry Division, Bhabha Atomic Research Center, Trombay, Bombay.
(2) E. Hayon and M. Simic, *Acc. Chem. Res.*, **7**, 114 (1974).
(3) A. Ehrenberg, P. Hemmerich, F. Muller, and W. Pfleiderer, *Eur. J. Biochem.*, **16**, 584 (1970).
(4) E. Hayon, *J. Chem. Phys.*, **51**, 4881 (1969).
(5) P. N. Moorthy and E. Hayon, *J. Phys. Chem.*, **78**, 2615 (1974).
(6) P. N. Moorthy and E. Hayon, *J. Phys. Chem.*, submitted for publication.
(7) H. Kamin, Ed., "Flavins and Flavoproteins", University Park Press, Baltimore, Md., 1971; R. D. Draper and L. L. Ingraham, *Arch. Biochem. Biophys.*, **125**, 802 (1968); E. J. Land and A. J. Swallow, *Biochemistry*, **8**, 2117 (1969); S. P. Vaish and G. Tollin, *Bioenergetics*, **2**, 61 (1971).
(8) M. Simic, P. Neta, and E. Hayon, *J. Phys. Chem.*, **73**, 3794 (1969).
(9) J. P. Keene, E. D. Black, and E. Hayon, *Rev. Sci. Instrum.*, **40**, 1199 (1969).
(10) M. Anbar, M. Bambenek, and A. B. Ross, *Natl. Stand. Ref. Data Ser., Natl. Bur. Stand.*, **No. 43** (May 1973).
(11) L. M. Dorfman and G. E. Adams, *Natl. Stand. Ref. Data Ser., Natl. Bur. Stand.*, **No. 46** (June 1973).
(12) P. S. Rao and E. Hayon, *J. Am. Chem. Soc.*, **96**, 1287 (1974); *ibid.*, in press.
(13) D. V. Bent, E. Hayon, and P. N. Moorthy, *J. Am. Chem. Soc.*, in press.
(14) P. N. Moorthy and E. Hayon, *J. Am. Chem. Soc.*, in press.
(15) J. L. Fox, S. P. Laberge, K. Nishimoto, and L. S. Forster, *Biochim. Biophys. Acta*, **136**, 544 (1967).

Oxidation of Aromatic Amines and Diamines by OH Radicals. Formation and Ionization Constants of Amine Cation Radicals in Water

P. S. Rao and E. Hayon*

Pioneering Research Laboratory, U.S. Army Natick Laboratories, Natick, Massachusetts 01760
(Received August 16, 1974; Revised Manuscript Received February 18, 1975)

Publication costs assisted by Natick Laboratories

The one-electron oxidation by hydroxyl radicals of aromatic amines and diamines in water was studied using the fast-reaction technique of pulse radiolysis and kinetic absorption spectrophotometry. The following compounds were examined: N,N,N^1,N^1-tetramethyl-*p*-phenylenediamine (TMPD), *p*-phenylenediamine (PD), N,N-dimethyl-*p*-phenylenediamine (DMPD), N,N,N^1,N^1-tetramethylbenzidine (TMB), and diphenylamine (DPA). The main initial reaction of the OH radicals is suggested to be an addition to these compounds to give absorption spectra which absorb strongly in the visible and uv regions. These OH radical adducts decay by first-order kinetics and have lifetimes of ~5–50 μsec, dependent on the pH, buffer concentration, and the nature of the aromatic amines and diamines. They decay to give species with somewhat similar absorption spectra and extinction coefficients, which are very long lived in the absence of oxygen. The latter species are assigned to the cation radicals $TMPD^{\cdot+}$, $PD^{\cdot+}$, $DMPD^{\cdot+}$, $TMB^{\cdot+}$, and $DPA^{\cdot+}$. The OH radical adducts and the cation radicals have acid–base properties. The pK_a values of the cation radicals $TMPDH^{\cdot 2+}$, $PDH^{\cdot 2+}$, $DMPDH^{\cdot 2+}$, $TMBH^{\cdot 2+}$, and $DPAH^{\cdot 2+}$ were found to be 5.3, 5.9, 6.1, 5.1, and 4.2, respectively. The results indicate that these aromatic amines and diamines can be oxidized by free radicals to yield the corresponding cation radicals.

Introduction

The oxidation of aromatic amines in solution has been studied[1,2] by anodic electrochemistry using absorption spectrophotometry and ESR to observe and identify the intermediates produced in these organic redox systems. The ease of removal of electrons from the amino function makes it possible to study the oxidation reaction pathways of amines. The photochemistry[3] and radiation chemistry[4] of some aromatic amines, in particular N,N,N^1,N^1-tetramethyl-*p*-phenylenediamine (TMPD), have so far been studied mainly in organic solvents.

Another pathway for the oxidation of aromatic amines and diamines which has not received much attention is via their reaction with oxidizing free radicals. We report below a study of the one-electron oxidation of some aromatic amines and diamines in water by hydroxyl radicals. The fast-reaction technique of pulse radiolysis and kinetic absorption spectrophotometry was used to generate OH radicals and examine their subsequent reactions with these compounds.

The following compounds have been examined: N,N,N^1,N^1-tetramethyl-*p*-phenylenediamine (TMPD), *p*-phenylenediamine (PD), N,N-dimethyl-*p*-phenylenediamine (DMPD), N,N,N^1,N^1-tetramethylbenzidine (TMB), and diphenylamine (DPA).

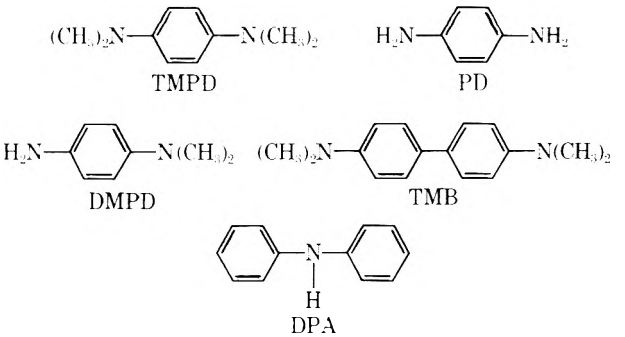

Experimental Section

The pulse radiolysis equipment and experimental conditions employed have been described.[5,6] Single pulses of 2.3-MeV electrons and ~30-nsec duration were used.

The radiolysis of water produces

$$H_2O \rightsquigarrow e_{aq}^-\ (2.8),\ OH\ (2.8),\ \text{and}\ H\ (0.6)$$

where the numbers in parentheses are the G values (number of radicals produced per 100 eV of energy absorbed).

All experiments were carried out in the presence of 1 atm of N_2O ($\sim 2.2 \times 10^{-2}$ M) in order to convert the e_{aq}^- into OH radicals:

$$e_{aq}^- + N_2O \rightarrow N_2 + OH + OH^- \qquad (1)$$

where $k_1 = 8.7 \times 10^9$ M^{-1} sec^{-1} (ref 7). The OH radicals then react with the aromatic amines, as described below. The H atoms formed in the radiation chemistry of water presumably add to the benzene ring of these compounds to produce cyclohexadienyl type radicals, which usually absorb in the 350–400-nm region.

The chemicals used were the best research grade commercially available, and were purchased from Aldrich, Eastman Chemicals, K and K Laboratories, Mallinckrodt, and Baker and Adamson. They were used without further purification. Diphenylamine (Eastman and Aldrich) was recrystallized twice from methyl alcohol. Due to their ease of oxidation in solution, special care was taken to thoroughly degass the solutions before adding the amines and diamines. Exposure to room light and to the monitoring light from the xenon lamp used in the pulse radiolysis experiments was kept to a minimum. A synchronized shutter[5] and appropriate cut-off filters were also used.

TABLE I: Reaction Rate Constants of e_{aq}^- with Aromatic Amines and Diamines in Water

Amine	pH	k, M^{-1} sec^{-1} [a]
TMPD	8.0	9.1×10^7
PD	9.0	9.6×10^7
DMPD	9.0	1.6×10^8
TMB	9.0	1.7×10^8
DPA	9.2	1.5×10^9

[a] Determined in the presence of ~0.5 M t-BuOH by monitoring the decay kinetics of e_{aq}^- at 700 nm.

Solutions were buffered using perchloric acid, potassium hydroxide, and ~1 mM phosphate and borate buffers.

The extinction coefficients presented were derived using the G values given above and KCNS dosimetry.[5]

Results and Discussion

Aliphatic[8] and aromatic[9] amines are known to react relatively fast with OH radicals. The reaction rate constants increase on ionization of the $-NH_3^+$ or $-NR_2H^+$ groups. The reaction rate constants of e_{aq}^- with the aromatic amines and diamines examined in this work were not known. These rates were determined by following the decay kinetics of e_{aq}^- at 700 nm. The values obtained are given in Table I. The $k(e_{aq}^- + \text{diphenylamine}) = 1.5 \times 10^9$ M^{-1} sec^{-1} is surprisingly high. Repurified material gave essentially the same value.

The concentrations of the amines and diamines used were chosen such that all (>95%) of the e_{aq}^- reacted with N_2O, reaction 1. All the experiments to be described below were carried out in the presence of 1 atm of N_2O.

N,N,N¹,N¹-Tetramethyl-p-phenylenediamine (TMPD). The reaction of OH radicals with TMPD (5 mM) at pH 3.2 produced, immediately after the 30-nsec pulse, intermediates which absorb strongly in the uv and visible regions, with maxima at ~335, 565, and 610 nm, see Figure 1. About 20–30 μsec later, changes in absorbance were observed at most wavelengths. The new absorption spectrum has similar maxima at ~330, 565, and 610 nm, Figure 1, but different extinction coefficients. On reaction of OH radicals with TMPD at pH 8.0, the absorption spectrum of the initial intermediate also changes with time to give another species whose bands in the visible region have higher extinction coefficients, see Figure 1 and Table II. It should be pointed out that the change in absorbance with time increases at some wavelengths and decreases at other wavelengths. This indicates the presence of at least two transient species.

The second intermediates whose spectra are fully developed ~20–30 μsec after the pulse are very stable (over periods of minutes, the time duration of the observation) so long as oxygen is not introduced in the system. These spectra resemble the spectrum of the $TMPD^{\cdot+}$ cation radical (Wurster's blue) and have similar[10] maxima and extinction coefficients in the visible region.

The following mechanism is suggested: the OH radicals add to TMPD either to the aromatic ring or to the N-amine groups. Addition to the ring can occur at either an α or β position to the amine. From the similarity of the spectra of the initial and final intermediates one cannot differentiate between the different possibilities. The addition reaction is represented by reaction 2. The initial intermediate is suggested to be mainly the OH adduct. From the similarity of the spectrum of the second intermediate with the known spectrum of $TMPD^{\cdot+}$, loss of OH^- is suggested to occur:

$$OH\text{-}TMPD \rightarrow OH + TMPD^{\cdot+} \quad (3)$$

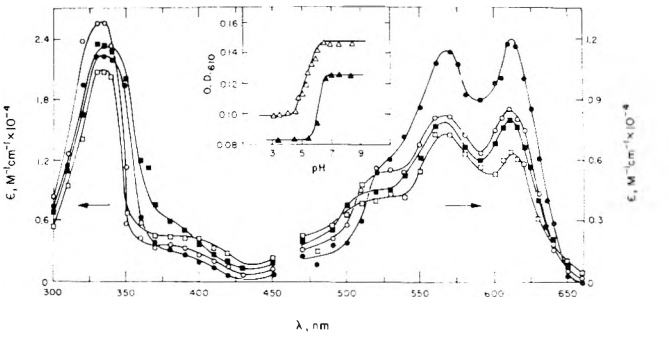

Figure 1. Optical spectra of intermediates produced from the reaction of OH radicals with tetramethyl-p-phenylenediamine (5 mM) in aqueous solution, N_2O (1 atm): (a) initial intermediate at pH 3.2 (□) and pH 8.0 (■); (b) second intermediate at pH 3.2 (○) and pH 8.0 (●). Total dose ~1.2 krads/pulse. Insert shows ΔOD at 610 nm vs. pH for OH adduct (▲) and cation radical (■).

In acid solutions, reactions 4 and 5 are suggested (protonation of one of the amines only is shown, since it is not known whether both amines are protonated under these conditions).

$$OH + TMPDH^+ \rightarrow OH\text{-}TMPDH^+ \quad (4)$$

$$OH\text{-}TMPDH^+ \rightarrow OH^- + TMPDH^{\cdot 2+} \quad (5)$$

The absorbances of the initial and the second intermediates were measured at 610 nm as a function of pH. Titration curves are observed, from which pK_a values of 6.2 and 5.3 for the OH adduct and the cation radical, respectively, can be derived (see insert Figure 1). This shows for the first time the acid–base properties of amine cation radicals:

$$OH\text{-}TMPDH^+ \rightleftharpoons OH\text{-}TMPD + H^+ \qquad pK_a = 6.2$$

$$TMPDH^{\cdot 2+} \rightleftharpoons TMPD^{\cdot+} + H^+ \qquad pK_a = 5.3$$

The rate constants of reactions 3 and 5 were determined, Table III, and are found to be $\sim 8.0 \times 10^4$ and $\sim 1.0 \times 10^5$ sec^{-1}, respectively. This small difference may not be significant, and may be dependent on the nature and concentration of the buffer used.

In support of the formation of $TMPD^{\cdot+}$ from the oxidation of TMPD by OH radicals is the similarity of the absorption spectrum of $TMPD^{\cdot+}$ and its extinction coefficients with those given in the literature.[10] For the 610–620-nm band, ε values in various organic solvents ranging from 1.3 to 2.0×10^4 M^{-1} cm^{-1} have been reported.[10] In this work, an ϵ_{612} of 1.2×10^4 M^{-1} cm^{-1} (Table II) was found in water.

p-Phenylenediamine (PD). The reaction of OH radicals with p-phenylenediamine (pK_a = 3.3 and 6.1) gave rise to intermediates which changed with time, as well as with pH (see Figure 2 and Table II). The sequence of reactions occurring are similar to those described above for TMPD:

$$OH + PD \rightarrow OH\text{-}PD \rightarrow OH^- + PD^{\cdot+} \quad (6)$$

$$OH + PDH^+ \rightarrow OH\text{-}PDH^+ \rightarrow OH^- + PDH^{\cdot 2+} \quad (7)$$

$$OH\text{-}PDH^+ \rightleftharpoons OH\text{-}PD + H^+ \qquad pK_a = 5.9$$

$$PDH^{\cdot 2+} \rightleftharpoons PD^{\cdot+} + H^+ \qquad pK_a = 5.9$$

TABLE II: Absorption Maxima, Extinction Coefficients, and Ionization Constants of the OH Radical Adducts and Radical Cations of Aromatic Amines and Diamines in Aqueous Solution

		OH adduct[b]					Cation radical[b]				
		Acid form		Base form			Acid form		Base form		
Amine[a]	pK_a (radical)	λ_{max}	ϵ	λ_{max}	ϵ	pK_a (radical)	λ_{max}	ϵ	λ_{max}	ϵ
TMPD	6.2	335	2.0×10^4	340	2.3×10^4	5.3	330	2.5×10^4	335	2.3×10^4
		565	7.4×10^3	570	8.1×10^3		565	7.8×10^3	570	1.1×10^4
		610	8.2×10^3	610	1.2×10^4		610	8.6×10^3	612	1.2×10^4
PD (3.3, 6.1)	5.9	325	1.4×10^4	325	1.7×10^4	5.9	325	1.3×10^4	325	1.6×10^4
		455	4.6×10^3	460	7.8×10^3		455	4.7×10^3	460	7.1×10^3
				480	6.4×10^3		480	4.0×10^3	480	5.8×10^3
DMPD		330	9.0×10^3			6.1	330	1.2×10^4		
		510	3.0×10^3	515	5.4×10^3		515	7.3×10^3	515	5.2×10^3
		560	3.0×10^3	560	5.2×10^3		560	6.3×10^3	560	5.5×10^3
TMB[c]						5.1	470	1.2×10^4	470	3.8×10^3
							700	1.6×10^3	700	8.0×10^2
DPA (0.8)	4.2	335	1.6×10^4	325	6.5×10^3	4.2	335	1.3×10^4	320	1.5×10^4
		670	8.0×10^3	670	6.0×10^3		675	8.0×10^3	700	1.2×10^3
				675	2.0×10^3					

[a] See text for list of compounds; values in parentheses are pK_a. [b] Wavelength given in nm units and ϵ in M^{-1} cm $^{-1}$; ϵ values derived assuming [radical] = [OH], see text. [c] Mixture of OH adduct and cation radical probably present (see text).

TABLE III: Rate of Formation of Radical Cations from the Decay of the OH Radical Adducts to Aromatic Amines and Diamines in Water

Amine[a]	pH	Wavelength monitored, nm	k, sec^{-1}
TMPD	3.2	370; 610	1.0×10^5
	8.0	610	8.0×10^4
PD	3.5	370	3.0×10^5
	9.0	370; 480	6.0×10^4
DMPD	3.2	545	6.0×10^5
	8.0	350	5.0×10^4
TMB	3.5	475	1.0×10^5
	9.2	450	2.0×10^4
DPA	3.0	320	1.0×10^5
	9.0	320	2.0×10^4

[a] See text for list of compounds.

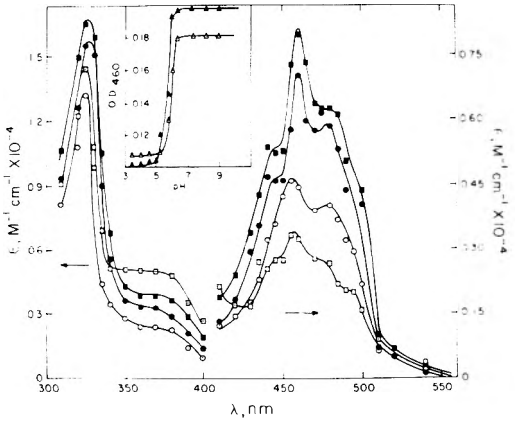

Figure 2. Optical spectra of intermediates produced from the reaction of OH radicals with *p*-phenylenediamine (2 m*M*) in aqueous solution, N_2O (1 atm): (a) initial intermediate pH 3.2 (□) and pH 8.0 (■); (b) second intermediate at pH 3.2 (○) and pH 8.0 (●). Total dose ~2.0 krads/pulse. Insert shows ΔOD at 460 nm vs. pH for OH adduct (▲) and cation radical (△).

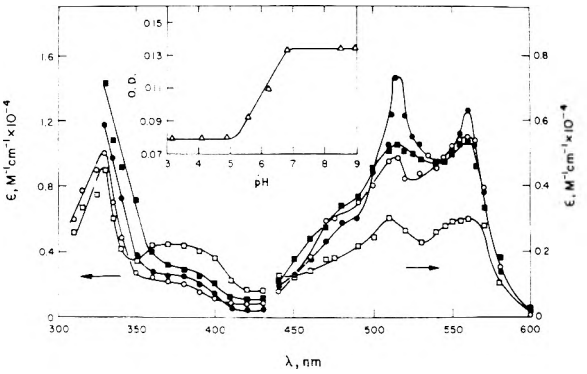

Figure 3. Optical spectra of intermediates produced from the reaction of OH radicals with *N,N*-dimethyl-*p*-phenylenediamine (2 m*M*) in aqueous solution, N_2O (1 atm): (a) initial intermediate at pH 3.2 (□) and pH 8.0 (■); (b) second intermediate at pH 3.2 (○) and pH 8.0 (●). Total dose ~1.5 krads/pulse. Insert shows ΔOD at 350 nm vs. pH for cation radical (△).

The spectrum of the $PD^{\cdot+}$ cation radical observed is quite similar to that observed in ethanol.[10] The ϵ values in the literature for the 460-nm band are, however, higher by a factor ≥3.0. No explanation can be offered at present for this difference.

The rates of decay of the initial intermediate to form the second radical are given in Table III. Values of 3.0×10^5 and 6.0×10^4 sec^{-1} at pH 3.5 and 9.0 were observed.

N,N-Dimethyl-p-phenylenediamine (DMPD). With DMPD (pK_a = 2.85), because the molecule is not symmetric the reaction of OH radicals can produce more than one isomer. The initial OH adduct spectra at pH 3.2 and 8.0, as well as the corresponding cation radical spectra, are shown in Figure 3 and Table II. The spectrum of the $DMPD^{\cdot+}$ radical cation is in general agreement with that reported in the literature.[10]

The ionization constant of the $DMPDH^{\cdot 2+}$ radical is ~6.1:

$$DMPDH^{\cdot 2+} \rightleftharpoons DMPD^{\cdot +} + H^+ \qquad pK_a \sim 6.1$$

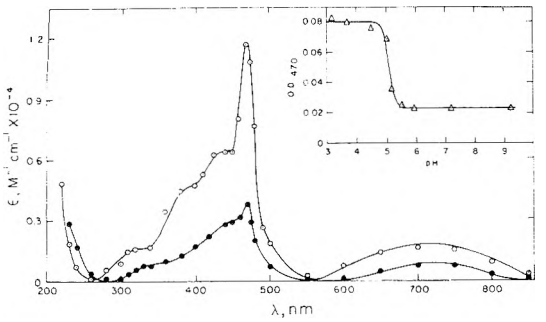

Figure 4. Optical spectra of intermediates produced from the reaction of OH radicals with *N,N,N*^{1},*N*^{1}-tetramethylbenzidine (2 × 10^{-4} *M*) in aqueous solution, N_2O (1 atm) at pH 3.5 (O) and pH 9.2 (●). Total dose ~1.5 krads/pulse. Insert shows ΔOD at 470 nm vs. pH. Extinction coefficients may be low (see text).

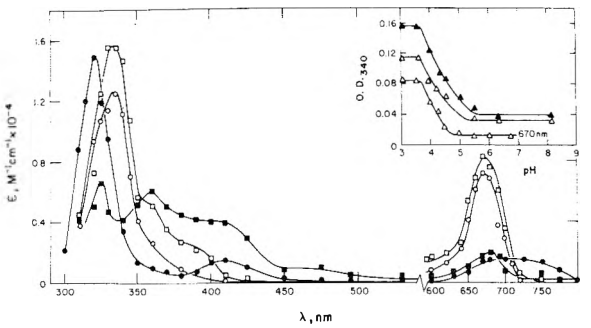

Figure 5. Optical spectra of intermediates produced from the reaction of OH radicals with diphenylamine (2 × 10^{-4} *M*) in aqueous solution, N_2O (1 atm): (a) initial intermediate at pH 3.0 (□) and pH 9.0 (■); (b) second intermediate at pH 3.0 (O) and pH 9.0 (●). Total dose ~1.5 krads/pulse. Insert shows ΔOD at 340 and 670 nm vs. pH for OH adduct (▲) and cation radical (△,△). Extinction coefficients low (see text).

N,N,N^1,*N*^{1}-*Tetramethylbenzidine (TMB).* The reaction of OH radicals with TMB can produce different OH adducts which may not all lead to the formation of the TMB·$^+$ radical cation. Hence the spectrum shown in Figure 4 may contain bands which do not represent the absorption spectrum of TMB·$^+$. The main absorption maximum at ~470 nm probably represent TMB·$^+$. It also agrees with a recently reported[11] spectrum for this cation radical. The ESR spectrum has also been examined.[12] The extinction coefficients given in Table II may be too low since a fraction of the OH radicals do not oxidize TMB to form TMB·$^+$.

A pK_a ~ 5.1 was observed for the dissociation of TMBH·$^{2+}$, see Figure 4 and Table II.

Diphenylamine (DPA). As discussed above for TMB, some of the OH radicals reacting with diphenylamine (pK_a = 0.79) produce adducts which do not probably form the DPA·$^+$ cation radical.

The spectra of the initial and second intermediates at pH 3.0 and 9.0 are shown in Figure 5 and Table II. The DPA·$^+$ radical cation is reported[10] to have bands with maxima at 350 and 660–680 nm, in reasonable agreement with the spectrum shown in Figure 5. The extinction coefficients given in Table II are considered to be too low since only a fraction of the OH radicals form DPA·$^+$.

A pK_a = 4.2 has been observed for

$$DPAH^{\cdot 2+} \rightleftharpoons DPA^{\cdot +} + H^+$$

The rates of decay of the initial intermediate to form the cation radicals are 1.0 × 10^5 and 2.0 × 10^5 sec^{-1} at pH 3.0 and 9.0, respectively, see Table III.

Conclusions

The main reaction of OH radicals with aromatic amines and diamines in water was shown to form initially an OH radical adduct. These OH adducts have a lifetime of 5–50 μsec, dependent on the nature of the amines, the pH of the experiment, and the buffer concentration. They decay by a first-order process to generate the corresponding cation radicals. These cation radicals have acid–base properties and their ionization constants have been determined. With some compound, the OH adducts do not appear to form quantitatively the corresponding cation radicals. Furthermore, due to the similarity in the absorption spectra of the initial and second intermediates formed in these systems, one cannot exclude the possibility of some direct formation of cation radicals via an electron transfer from the amines to OH radicals.

In addition to the well-known oxidation of aromatic amines and diamines in electrochemistry, photochemistry, and radiation chemistry, the above results indicate that the reaction of these compounds with certain free radicals can also lead to their oxidation.

References and Notes

(1) R. N. Adams, *Acc. Chem. Res.*, **2**, 175 (1969); "Electrochemistry at Solid Electrodes", Marcel Dekker, New York, N.Y., 1969.
(2) "Organic Electrochemistry", M. M. Baizer, Ed., Marcel Dekker, New York, N.Y., 1973.
(3) See, e.g., G. N. Lewis and D. Lipkin, *J. Am. Chem. Soc.*, **64**, 2801 (1942); L. Michaelis, *Ann. N.Y. Acad. Sci.*, **40**, 60 (1940); W. C. Meyer and A. C. Albrecht, *J. Chem. Phys.*, **66**, 1168 (1963); R. L. Hand and R. F. Nelson, *J. Am. Chem. Soc.*, **96**, 850 (1974).
(4) See, e.g., D. W. Skelly and W. H. Hamill, *J. Phys. Chem.*, **70**, 1636 (1966); R. V. Bensasson and J. K. Thomas, *Int. J. Radiat. Phys. Chem.*, **1**, 185 (1969); "Radical Ions", E. T. Kaiser and L. Kevan, Ed., Interscience, New York, N.Y., 1968.
(5) M. Simic, P. Neta, and E. Hayon, *J. Phys. Chem.*, **73**, 3794 (1969).
(6) J. P. Keene, E. D. Black, and E. Hayon, *Rev. Sci. Instrum.*, **40**, 1199 (1969).
(7) M. Anbar, M. Bambenek, and A. B. Ross, *Nat. Stand. Ref. Data Ser., Nat. Bur. Stand.*, **No. 43** (May 1973).
(8) M. Simic, P. Neta, and E. Hayon, *Int. J. Radiat. Phys. Chem.*, **3**, 309 (1971).
(9) A. Wigger, W. Grunbein, A. Henglein, and E. J. Land, *Z. Naturforsch. B*, **24**, 1262 (1969); N. Getoff and F. Schworer, *Int. J. Radiat. Phys. Chem.*, **2**, 81 (1970).
(10) A. Habersbergerová, I. Janovský, and P. Kouřim, *Radiat. Res. Rev.*, **4**, 123 (1972).
(11) J. Wheeler and R. F. Nelson, *J. Phys. Chem.*, **77**, 2490 (1973).
(12) J. M. Frisch and R. N. Adams, *J. Chem. Phys.*, **43**, 1887 (1965).

Radiation-Induced Homolytic Aromatic Substitution. III. Hydroxylation and Nitration of Benzene[1]

Manfred K. Eberhardt

Puerto Rico Nuclear Center,[2] Caparra Heights Station, San Juan, Puerto Rico 00935
(Received March 16, 1974; Revised Manuscript Received January 24, 1975)

Publication costs assisted by the Puerto Rico Nuclear Center

The radiolysis of aqueous $NaNO_3$ solutions (1 *M*) saturated with benzene has been studied under a variety of conditions. The main products are phenol, nitrobenzene, and biphenyl, whose yields are dependent on dose, dose rate, oxygen concentration, and pH. In the presence of oxygen the yield of phenol increases whereas nitrobenzene and biphenyl formation is almost completely suppressed. Low pH increases the yield of phenol and nitrobenzene and decreases the yield of biphenyl compared to neutral solutions. Contrary to previous reports only trace amounts of *o*- and *p*-nitrophenol were found in a ratio of 60% ortho:40% para. A mechanism for the formation of the products involving ·OH, NO_2·, and NO_3· radicals has been proposed.

Introduction

A number of authors[3-5] have investigated the radiolysis of aqueous $NaNO_3$ solutions containing benzene and reported the formation of *o*- and *p*-nitrophenol in relatively high yields (*G* 0.28–0.96). Unfortunately one author only reported the *G* values for o-nitrophenol[3] and another only for *p*-nitrophenol,[5] however, under different conditions. Phenol was found to be absent in all cases, whereas the absence of nitrobenzene was reported by Broszkiewiecz and unspecified amounts of nitrobenzene were reported by Sugimoto, *et al.* For the formation of nitrophenol a radiation-induced mechanism from phenol has been proposed.[5] In view of the incomplete analysis and the divergent results in previous work, we have investigated the radiation-induced hydroxylation and nitration of benzene.

Experimental Section

Materials. All solutions were prepared using deionized and subsequently double distilled water as solvent. Benzene, sodium nitrate, and sulfuric acid were reagent grade materials. Argon- and oxygen-saturated solutions were prepared by bubbling the gas through 1 l. of aqueous sodium nitrate solution for about 1 hr. The gas was introduced by means of a hypodermic needle punched through a rubber stopper. The saturation was enhanced by frequent shaking. After saturation the benzene was introduced with a graduated syringe, and dissolved by vigorous shaking.

Irradiations. Irradiations were carried out with a ^{60}Co room source. The dose rate was determined by Fricke dosimetry using a value of 15.6 for *G* (Fe^{3+}). The dose rate was 480 or 65.3 rads/min. All irradiations were carried out at a benzene concentration of 20×10^{-3} *M* (saturated solution). The experiments at low pH were in 0.1 *N* H_2SO_4.

Analytical Procedure. Immediately after irradiation the pH of the irradiated solutions was adjusted to about 4.3. Then the solutions were extracted with 200 ml of ether and seven times with 100 ml of ether. The ether solution was dried over 80 g of Na_2SO_4 and subsequently concentrated to 10 ml, and analyzed by vapor phase chromatography using a hydrogen flame detector. All product peaks were identified by their retention time on two different columns: a 6 ft × ⅛ in. stainless steel column packed with diethylene glycol succinate 5% on Chromosorb W-AW DMCS 100–120 mesh. At 150° and a flow rate of 25 ml of He/min, the product peaks appeared in the following sequence: nitrobenzene, phenol, and biphenyl. Phenol and biphenyl had the same retention time under these conditions. The nitrophenols were methylated with CH_2N_2 and analyzed as described previously.[1a] The second column was a 6 ft × ⅛ in. column packed with silicone SF-96. At 100° and a flow rate of 25 ml of He/min the product peaks appeared in the following sequence: phenol, nitrobenzene, and biphenyl. The biphenyl was analyzed on the same column at 150°.

For a quantitative determination of the products $NaNO_3$ solutions containing known amounts of product were worked up and analyzed under the same conditions as described above. *G*(biphenyl) was determined by comparison with ether solutions of biphenyl.

Results and Discussion

The results are shown in Tables I and II. Each *G* value represents the average of at least three determinations. The experiments were found to be reproducible within less than ±5%. The radiolysis of aqueous nitrate solutions has been the subject of intensive investigations.[6] Sharpatyi and Molin's investigation[7] of ESR spectra during the radiolysis of a frozen aqueous $NaNO_3$ solution showed that NO_2· was the main intermediate in the conversion of NO_3^- to NO_2^-. They also observed a radical containing quadrivalent nitrogen ($HNO_3^{\cdot -}$). Subsequently NO_2· and NO_3· radicals were discovered in concentrated (>0.5 *M*) neutral $NaNO_3$ solutions by pulse radiolysis.[8] The final products of the radiolysis of $NaNO_3$ solutions are H_2, H_2O_2, O_2, and NO_2^-. The oxygen has been shown to be a direct action product, i.e., its yield is directly proportional to the $NaNO_3$ concentration.[9] On the basis of the above mentioned evidence the following reaction mechanisms have been proposed: indirect effect[6,10,11]

$$NO_3^- + e_{aq}^- \longrightarrow NO_3^{\cdot 2-} \xrightarrow{H^+} HNO_3^{\cdot -} \quad (1)$$

$$NO_3^- + H\cdot \longrightarrow HNO_3^{\cdot -} \quad (2)$$

$$HNO_3^{\cdot -} \longrightarrow OH^- + NO_2\cdot \quad (3)$$

$$2NO_2\cdot + H_2O \longrightarrow NO_2^- + NO_3^- + 2H^+ \quad (4)$$

$$NO_2^- + \cdot OH \longrightarrow OH^- + NO_2\cdot \quad (5)$$

direct effect[9,12]

$$NO_3^- \longrightarrow NO_2^- + {}^1/_2O_2 \quad (6)$$

$$NO_3^- \longrightarrow (NO_2\cdot + O + e^-) \quad (7)$$

$$NO_2\cdot + O \longrightarrow NO_3\cdot \quad (8)$$

The OH radical has been shown[11] not to react with NO_3^- but only with NO_2^-. The homolytic nitration of aromatic hydrocarbons has been extensively studied by Titov,[13] who concluded that the initial step in the reaction between benzene and NO_2 was addition followed by disproportionation to give nitrobenzene. It has however subsequently been shown by Bunbury[14] that there is no reaction between benzene and NO_2–N_2O_4 in the liquid phase at room temperature.

The formation of nitrobenzene in our experiments therefore does not follow the normal homolytic substitution pattern: addition followed by disproportionation. This is also evident from the fact that oxygen does not increase the yield of nitrobenzene, as is generally the case in homolytic aromatic substitution,[1a,15,16] but almost completely suppresses nitrobenzene formation (see Table II). In presence of oxygen however the yield of phenol increases considerably. We propose the mechanism shown in Scheme I.

Scheme I

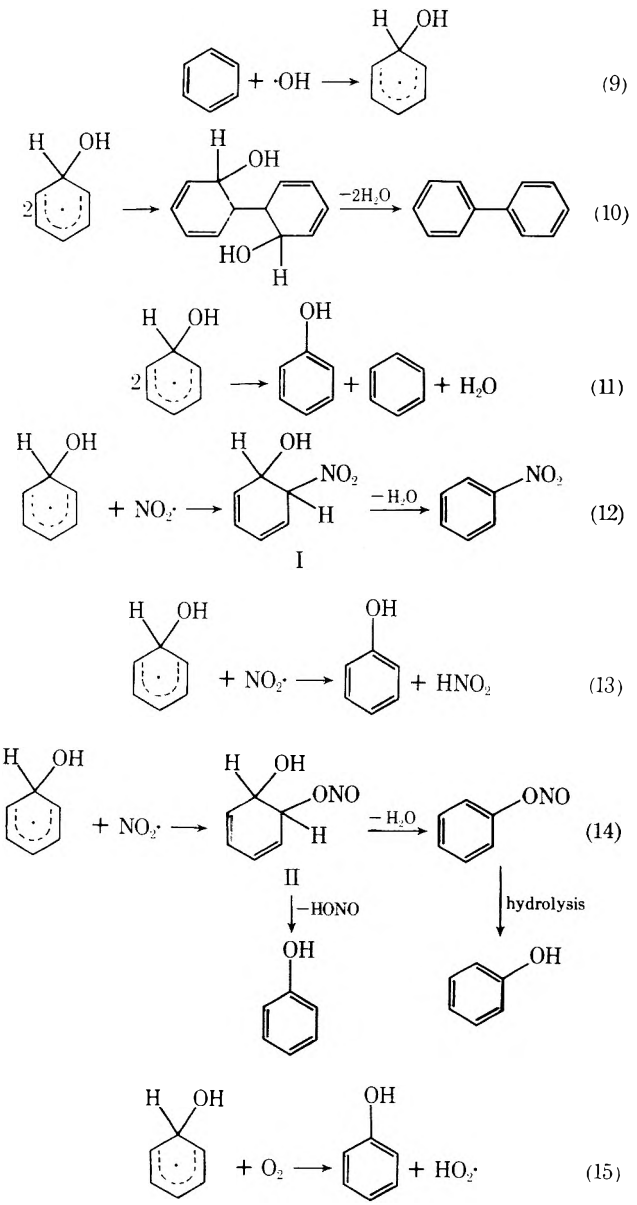

TABLE I: Effect of Dose on the Hydroxylation, Nitration, and Phenylation of Benzene[a]

Total dose, eV/l.	G(Ph-OH)	G(Ph-NO_2)	G-(Ph_2)	G(o-nitrophenol)	G(p-nitrophenol)
1.35×10^{21}	0.74	0.75	0.25		
2.7×10^{21}	0.71	0.51	0.25	0.05	0.04
5.4×10^{21}	0.73	0.38	0.28	0.03	0.02
8.1×10^{21}	0.74	0.34	0.30	0.03	0.02
10.8×10^{21}	0.77	0.32	0.30		
13.5×10^{21}	0.73	0.28	0.30		

[a] Dose rate 3.0×10^{19} eV/l. min; solutions were 1.0 M in $NaNO_3$ and 2.0×10^{-2} M in benzene and were deoxygenated by bubbling argon through 1 l. solution for 1 hr.

In absence of oxygen the hydroxycyclohexadienyl radical can either disproportionate (reaction 11), dimerize (reaction 10), or react with $NO_2\cdot$ (reactions 12–14). Reactions 9 and 12 have also been proposed in the nitration of aromatic compounds by pernitrous acid.[17] $NO_2\cdot$ can react with the hydroxycyclohexadienyl radical by recombination either at the nitrogen (reaction 12) or at the oxygen (reaction 14). Many examples of this behaviour are known.[18]

The elimination of H_2O from compounds of type I and II is supported by analogous eliminations from cyclohexadienes, such as, the room temperature elimination of HCl from 1-chloro-2-nitrocyclohexadiene to give nitrobenzene.[19]

At low pH (0.1 N H_2SO_4) the yield of phenol and nitrobenzene increases by a factor of 2 while biphenyl is decreasing (Table II). The $NO_2\cdot$ radical is produced via reaction 1–3. At low pH we have therefore a higher concentration of $NO_2\cdot$. On the basis of reactions 12–14 we expect that at low pH the G(nitrobenzene) and G(phenol) increase by the same percentage, which is indeed observed.

The elimination of H_2O from adducts, such as I and II as well as the hydrolysis of phenyl nitrate may be a slow process in neutral solution. This might explain the increase in G(phenol) and G(nitrobenzene) at low pH. To test for this possibility we irradiated a deoxygenated 1 M $NaNO_3$ solution of benzene for 1.5 hr at a dose rate of 3.0×10^{19} eV/min l. After irradiation the solution was made 0.1 N in H_2SO_4 and left standing for 1.5 hr. No significant post-irradiation change in G(phenol), G(nitrobenzene), and G(biphenyl) was observed. We therefore feel sure that the pH effect is due to an increased $NO_2\cdot$ radical concentration at low pH.

In presence of oxygen the O_2, reaction 15, will compete with reactions 10–14 and therefore suppress the formation of nitrobenzene and biphenyl and increase the yield of phenol (see Table II). In addition to reaction 15 O_2 can decrease the formation of $NO_2\cdot$ by reacting with the precursor of the $NO_2\cdot$ radical[10]

$$HNO_3^{\cdot-} + O_2 \longrightarrow NO_3^- + HO_2\cdot \quad (16)$$

Reaction 16 will compete with reaction 3. With increasing dose we get an increase in O_2 and a decrease in $NO_2\cdot$. The decrease of G(Ph–NO_2) with increasing dose (see Table I) is consistent with this mechanism.

The small amounts of O_2 formed during the radiolysis of nitrate solutions will be able to compete more favorably with the disproportionation of the hydroxycyclohexadienyl

TABLE II: Effect of Dose Rate, pH, and Oxygen on the Hydroxylation, Nitration, and Phenylation of Benzene[a]

Conditions	Dose rate, eV/l. min	Total dose, eV/l.	G(PhOH)	G($PhNO_2$)	G(Ph_2)	G(*o*-nitrophenol)	G(*p*-nitrophenol)
Ar	3.0×10^{19}	2.7×10^{21}	0.71	0.51	0.25	0.05	0.04
Ar	4.1×10^{18}	2.7×10^{21}	1.0	0.42	0.25		
Ar + 0.1 N H_2SO_4	3.0×10^{19}	2.7×10^{21}	1.40	1.15	0.10	0.025	0.016
O_2	3.0×10^{19}	2.7×10^{21}	2.0	Trace	Trace	None	None

[a] All solutions were 1.0 M $NaNO_3$ and 2.0×10^{-2} M benzene.

radical at low dose rates. We expect an increase in G(phenol) and a decrease in G(nitrobenzene) and G(biphenyl) at low dose rates. The results in Table II show that we indeed observe an increase in G(phenol) and a decrease in G(nitrobenzene), but the G(biphenyl) is unaffected.

This suggests a mechanism for biphenyl formation not involving dimerization of hydroxycyclohexadienyl radicals. The recent observation[1b] of phenylcyclohexadienes in the radiolysis of aqueous benzene solution suggested the possibility of the intermediate formation of phenyl radicals. Since we do not observe any phenylcyclohexadienes we conclude that the phenylcyclohexadienyl radicals react with $\cdot NO_2$ and with O_2 to give biphenyl. Unfortunately, one cannot distinguish phenyl radicals from hydroxycyclohexadienyl radicals by scavenging experiments. With $NO_2\cdot$ we expect to obtain nitrobenzene and phenol in both cases via reactions 12–14 and reactions[20]

$$Ph\cdot + NO_2\cdot \longrightarrow Ph\text{–}NO_2 \qquad (17)$$

$$Ph\cdot + NO_2\cdot \longrightarrow Ph\text{–}ONO \xrightarrow{\text{hydrolysis}} Ph\text{–}OH \qquad (18)$$

At the $NaNO_3$ concentration used in this work (1 M) we have to consider also reactions of benzene with $NO_3\cdot$ radical:

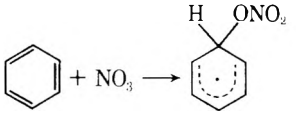

(19)

The intermediate nitroxycyclohexadienyl radical can undergo all the reactions of the hydroxycyclohexadienyl radical. The disproportionation product $Ph\text{–}ONO_2$ will readily undergo hydrolysis to give phenol.

According to our mechanism and our results in Table II we have at low pH, G(phenol) + G(nitrobenzene) + $2G$(biphenyl) = $G(\cdot OH)$ = 2.75, which means a quantitative accounting of the ·OH radicals.

In all our experiments we find only exceedingly small amounts of nitrophenols. The large amounts of *p*-nitrophenol reported previously by Sugimoto, *et al.*,[5] are due to a chemical nitration of phenol by HNO_3. The nitration of phenol with dilute nitric acid is well known[21] and is catalyzed by traces of HNO_2, which are formed in the radiolysis.

To demonstrate the formation of nitrophenols by nitration of the small amounts of phenol formed during the radiolysis we proceeded as follows: we irradiated a 1 M $NaNO_3$ solution for 1.5 hr in the absence of O_2 (same time and dose rate as our solutions containing benzene). We subsequently made the solution 0.1 N in H_2SO_4 and added a solution containing 6.8 mg of phenol. After 24 hr we adjusted the pH to about 4.3 and extracted with ether and allowed it to react with CH_2N_2 as described in the Experimental Section. We found about 4.0 mg of *o*-nitrophenol and 3.5 mg of *p*-nitrophenol (53.5% ortho and 46.7% para) as expected for an electrophilic aromatic nitration. The long irradiation time (16 hr) in acidic solution was probably mainly responsible for the large amount of *p*-nitrophenol found by the Japanese workers.

References and Notes

(1) For previous papers in this series see (a) M. K. Eberhardt and M. Yoshida, *J. Phys. Chem.*, **77**, 589 (1973); (b) M. K. Eberhardt, *ibid.*, **78**, 1795 (1974).
(2) This paper was prepared in connection with work under Contract No. AT-(40-1)-1833 with the U.S. Atomic Energy Commission.
(3) R. K. Broszkiewicz, *Nature (London)*, 1235 (1966).
(4) A. I. Chernova, V. D. Orekhov, and M. A. Proskurnin, *Trans. All-Union Conf. Radiat. Chem., 2nd*, 245 (1962).
(5) K. Sugimoto, W. Ando, and S. Oae, *Bull. Chem. Soc. Jap.*, **36**, 124 (1963).
(6) For a review of the older literature see A. K. Pikaev, *Russ. Chem. Rev.*, **29**, 235 (1960).
(7) V. A. Sharpatyi and V. N. Molin, Summaries of Reports presented at the Tashkent Conference on the Peaceful Uses of Atomic Energy, Tashkent 1959, p 74.
(8) M. Daniels, *J. Phys. Chem.*, **70**, 3022 (1966).
(9) H. A. Mahlman, *J. Chem. Phys.*, **35**, 936 (1961).
(10) V. A. Sharpatyi, V. D. Orekhov, and M. A. Proskurnin, *Izd. Akad. Nauk SSR*, 37 (1958); *Dokl. Akad. Nauk SSR*, **124**, 1279 (1959).
(11) M. Daniels and E. E. Wigg, *J. Phys. Chem.*, **71**, 1024 (1967).
(12) M. Daniels, *Adv. Chem. Ser.*, **No. 81**, 153 (1968).
(13) A. I. Titov, *Tetrahedron*, **19**, 557 (1963).
(14) D. L. Bunbury, *Can. J. Chem.*, **43**, 1714 (1965).
(15) M. K. Eberhardt and E. L. Eliel, *J. Org. Chem.*, **27**, 2289 (1962).
(16) L. M. Dorfman, I. A. Taub, and R. E. Bühler, *J. Chem. Phys.*, **36**, 3051 (1962).
(17) E. Halfpenny and P. L. Robinson, *J. Chem. Soc.*, 939 (1952).
(18) Y. Rees and G. H. Williams, *Adv. Free Radical Chem.*, **3**, 199 (1969).
(19) W. Steinkopf and M. Kühnel, *Berichte*, **75**, 1323 (1942).
(20) E. K. Fields and S. Meyerson, *J. Am. Chem. Soc.*, **89**, 3224 (1967).
(21) W. Seidenfaden and D. Pawellek in "Aromatische Nitroverbindungen", Vol. x/1, Houben-Weyl, 1971, p 559, and references cited therein.

Reactions of Trapped Electrons by Quantum Mechanical Tunneling Observed by Pulse Radiolysis of an Aqueous Glass[1]

John R. Miller

Chemistry Division, Argonne National Laboratory, Argonne, Illinois 60439

(Received August 30, 1974; Revised Manuscript Received January 24, 1975)

Publication costs assisted by Argonne National Laboratory

Reactions of trapped electrons with electron acceptors appear to involve electron transfer by quantum mechanical tunneling through tens of ångströms of inert solvent. These reactions are observed by pulse radiolysis of aqueous 6 *M* NaOH solutions frozen to a rigid glass. The observed reactions show several unusual kinetic features, including the following. (1) The reactions progress with the logarithm of time over our experimental time range, $<10^{-6}$ to 10^{3} sec. (2) The reaction rates are independent of temperature from 77 to 143°K. (3) A tenfold change in acceptor concentration decreases the lifetime of the trapped electrons by about 10^{6}. (4) Rates of reaction with different acceptors vary over a range greater than 10^{10} for acceptors whose rate constants for reaction with hydrated electrons in liquid water differ by less than 10^{2}. These observations are in good agreement with model calculations of electron tunneling. The evidence for tunneling, inferences about some mechanistic details of electron tunneling reactions, and possible alternative mechanisms to tunneling are discussed. It is concluded that Franck–Condon restrictions, which depend strongly on the difference between the electron affinity of the acceptor and the energy of the donor, may be an important cause of the very low reactivities of weak acceptors. However it may also be necessary to invoke some more complex electronic process to explain the apparently stronger dependence of reaction rate on distance for weak acceptors.

I. Introduction

A. General Introduction. Evidence that electrons trapped in rigid glassy matrices tunnel tens of ångströms to react with electron acceptors has been reported from several laboratories.[2-12] This evidence includes observation of time dependent reactions of trapped, solvated electrons in a number of glassy matrices. These matrices are known to be so rigid that highly reactive intermediates, such as solvated electrons, may be trapped indefinitely (lifetimes of days at least) and show no measurable conductivity. Observed reactions have been shown to be temperature independent between 4 and 77°K by Kieffer et al.[4] and between 4 and 120°K by Zamaraev et al.[5] Most of the reactions have only been studied on the minutes time scale, but limited data has been obtained to 0.1 sec[5] and 1 msec.[9]

The importance of tunneling in electron transfer reactions in solution was suggested several years ago.[13] However because reactants in solution diffuse together so rapidly, tunneling does not make a large contribution to the reaction cross section. It is therefore difficult to show experimentally that tunneling plays a role in reactions in solution, and it is nearly impossible to gain knowledge about details of the tunneling process. Electron tunneling apparently has a more clear role in biological electron transport, because the active components are often immobilized on membranes. Experimental evidence for tunneling in electron transfer from cytochrome c to chlorophyll has been reported.[14,15]

While there is considerable evidence that electron tunneling does occur in chemical reactions, there is little experimental information available which can illuminate the details of the tunneling reactions. This paper reports results of pulse radiolysis of rigid 6 *M* NaOH aqueous glasses. Reactions of the trapped, solvated electrons with a variety of electron acceptors have been studied to times as short as 20 nsec, but more commonly to about 1 μsec. The results are discussed in the framework of the simple, barrier-penetration model of electron tunneling, which will be seen to be adequate to understand some of the experimental data, but not all of it.

B. The Barrier Penetration Model of Electron Tunneling. This simple model for transfer of a solvated electron to an electron acceptor has been described before.[3,8] The transmission coefficient (T) for an electron impinging on a potential energy barrier is multiplied by a frequency factor approximated as the frequency of electronic motion (about 10^{15} sec^{-1}) for a localized state such as a solvated electron:

$$\text{tunneling rate} \cong 10^{15}T \tag{1}$$

The distance a solvated electron may tunnel is then[3,8]

$$a = a_0 + 2.26(15 + \log t)B^{-1/2} \tag{2}$$

where a is in ångströms, the time t is in seconds, and the binding energy, B, of the solvated electron is in electron volts. The constant a_0 is added to account for the finite radii of the solvated electron and the electron acceptor. Its value is assumed to be about 5 Å. Equation 2 may be obtained by other methods than the barrier penetration calculation (see Discussion section IVC). If at time t every solvated electron within distance a of an electron acceptor is captured, the fraction P of the solvated electrons which survive capture is[8]

$$P = \exp(-2.51 \times 10^{-3}a^{3}M) \tag{3}$$

where M is the molar concentration of electron acceptors assumed to be distributed randomly. Combining (2) and (3)

$$P = \exp(-2.51 \times 10^{-3})[a_0 + 2.26B^{-1/2}(15 + \log t)]^{3}M \tag{4}$$

II. Experimental Section

A. Materials and Sample Preparation. The following chemicals were used without further purification: NaOH, Na_2CrO_4–$4H_2O$, $NaNO_3$, picric acid (Baker Analyzed); $KMnO_4$, $NaIO_4$, $NaBrO_3$ (Baker and Adamson, reagent); $NaIO_3$ (G. F. Smith, reagent); $NaNO_2$ (Mallinckrodt, reagent); $NaClO_3$ (Fisher certified); $Co(en)_3Cl_3$ (K & K); $K_3Co(CN)_6$ (Alfa); $K_3Cr(CN)_6$, $NaReO_4$ (ROC/RIC); acrylamide (Eastman, reagent); $K_3Fe(CN)_6$, K_2OsO_4·$2H_2O$ (Fluka, puriss.); $K_2Ni(CN)_4$, $Co(NH_3)_6(ClO_4)_3$, $Na_3Fe(CN)_5NH_3$ (from our stocks, assumed to be from same sources given in ref 16).

Appropriate weights of the solid materials were dissolved in 6 *M* NaOH and placed in quartz cells similar to those used by Richards and Thomas,[17] but some had a 2 cm, rather than 1-cm optical path length. The windows were industrial grade fused silica which resists radiation darkening. The sample solutions were bubbled with helium for 3 min, and given two freeze–pump–thaw cycles prior to sealing off on the vacuum line. The exclusion of air made samples less prone to cracking when frozen, but showed no noticeable effect on solvated electrons produced in the frozen samples.

Neptunium(VII) solutions were prepared and assayed by Dr. J. C. Sullivan using methods described by Sullivan and Zielen.[18] MnO_4^- solutions were prepared in water at twice the desired concentration, bubbled with helium, and then mixed with 12 *M* NaOH which had also been bubbled with helium. The mixing was done at 0° and the sample was immersed in liquid nitrogen within 1 min after the beginning of mixing to prevent reduction of MnO_4^- by 6 *M* NaOH. A cell with a 2-mm path length was used because of the strong MnO_4^- absorption.

B. The Sample Cell. During experiments, the samples were placed in a styrofoam coffee cup filled with liquid nitrogen. The analyzing light beam entered this cup through evacuated quartz tubes about 2.5 cm in diameter and 6 cm long. The silica optical windows at the ends of these evacuated tubes pressed tightly against the windows of the sample cell. A drop of pentanol applied to the windows formed a thin (ca. 0.1 mm) film between the windows of the evacuated tubes and the sample cell. This excluded bubbling, liquid nitrogen from the light path. Thus the sample was immersed in liquid nitrogen except for the optical windows. When the styrofoam cup was filled with liquid nitrogen, enough liquid nitrogen remained to completely cover the sample for at least 10 min. Slush baths were used for temperatures above 77°K.

The Argonne linac produced 2 to 40 nsec pulses of 13-MeV electrons at 10 A or 200-nsec pulses at 0.2 to 1.0 A. The electrons passed into the cell perpendicular to the analyzing light beam and were stopped in a copper block to give a relative measure of dose. The dose per pulse was typically about 10 krads.

C. Light Detection and Signal Recording 10^{-6} to 10^2 sec. To prevent the analyzing light from affecting the sample, a monochrometer was placed between the 250-W xenon lamp and the sample, in addition to the monochrometer between the sample and photomultiplier. Further, the light was chopped at 30 Hz. The chopper wheel passed a ca. 1-msec light pulse and a shorter light pulse 3.5 msec later, decreasing the average light intensity by a factor of 20.

Measuring and recording the signal from the photomultiplier over eight or more orders of magnitude change in time was accomplished by two methods, which will be described elsewhere.[19] The first method used pulsed unblanking of an oscilloscope at a number of logarithmically spaced delays after firing of the linac. The other involved the use of a Biomation 8100 transient recorder operated under active control of the Chemistry Division's Sigma 5 computer. The only significant gap in the data is between 3.5 and 33 msec.

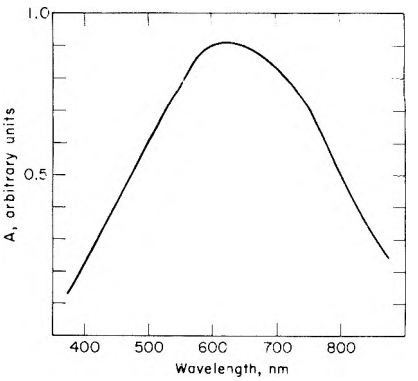

Figure 1. The absorption spectrum of trapped, solvated electrons in 6 *M* NaOH at 77°K, 0.1 sec after their production by pulse radiolysis. The spectrum shifts slightly to the blue with time (see Figure 2) as was reported earlier by Buxton.[20]

D. Reliability of the Experimental Data. The shapes of the decay curves reported below were reproducible, but the yields were subject to variations. All of the causes of these variations have not been identified and eliminated, and an uncertainty of ±10% remains.

A serious concern is the possibility of bleaching of the trapped electrons by the analyzing light. The experimental apparatus was designed to minimize this problem (see section C), which will be most serious at longer times. Tests on 0.05 *M* nitrate samples showed no detectable difference in the decay curve when the light intensity was decreased by a factor of 14 by a filter placed before the sample. The lower light intensity forced a loss in fast time response, and was not used routinely, but optical bleaching is apparently not important.

III. Results

A. The 6 M NaOH Matrix. The absorption spectrum of the trapped, solvated electron in 6 *M* NaOH aqueous glass at 77°K is shown in Figure 1. The spectrum, taken at 0.1 μsec, is red shifted from the better known spectrum taken minutes or hours after γ irradiation. Buxton has reported a similar result.[20] The way in which absorbance changes with time at four different wavelengths is shown in Figure 2. There is considerable decay near the red end of the spectrum. There is a smaller growth in the central and blue portions of the spectrum at times less than 10^{-2} sec.

The changes in the absorption spectrum are probably due to two processes: (1) relaxation to more strongly solvate the electrons, thus deepening their traps and giving rise to a blue shift; (2) loss of electrons. A loss of electrons could occur by reaction with radiation products such as O^- ions in a tunneling process.[5] Probably more growth of absorption would be seen throughout the blue side of the spectrum if loss of electrons did not occur.

Figure 3 shows the effect of increasing temperature on the trapped electron absorption at 550 nm. The effects of diffusion, probably $e_s^- + O^-$, are clear at 156°K and above. Alkaline aqueous glasses begin to soften at temperatures above 135°K.[20] Slow diffusion is probably occurring at 143°K, but reaction leading to disappearance of the elec-

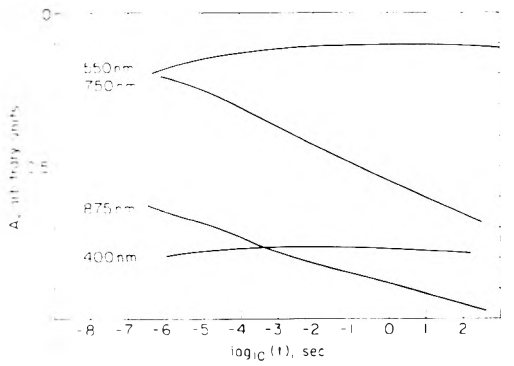

Figure 2. Changes of absorbance (A) with time at different wavelengths for trapped solvated electrons in 6 M NaOH at 77°K.

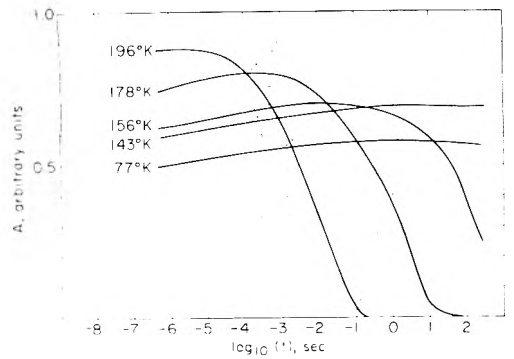

Figure 3. Effects of temperature on the changes of absorbance at 550 nm with time for trapped solvated electrons in 6 M NaOH.

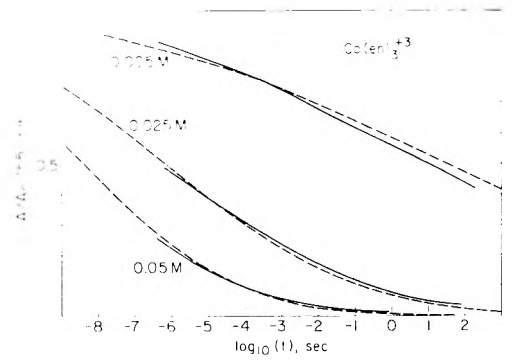

Figure 4. Decay of trapped electrons in 6 M NaOH at 77°K by reaction with $Co(en)_3^{3+}$. The absorbance (A) at each time is divided by the absorbance (A_0) in the "pure" 6 M NaOH matrix at the same time. The plot then gives the fraction of the trapped electrons not captured, thus correcting for the small absorbance changes in the pure matrix. The dashed curves are simulated decay curves for a tunneling reaction (eq 4 with B = 1.2 eV and a_0 = 4 Å).

trons is slow because the O^- concentration is less than 10^{-4} M.

B. Reactions with Acceptors at 77°K. Figure 4 shows decay of solvated electron absorption at 550 nm in the presence of $Co(en)_3^{3+}$, where en is ethylenediamine. The absorbance in each sample is plotted as a fraction of the absorbance (A_0) in 6 M NaOH taken under identical conditions. This corrects for the slight growth observed at 550 nm in the "pure" 6 M NaOH matrix. The simulated decay curves were computed according to eq 4, taking the binding energy (B) to be 1.2 eV, which is approximately equal to

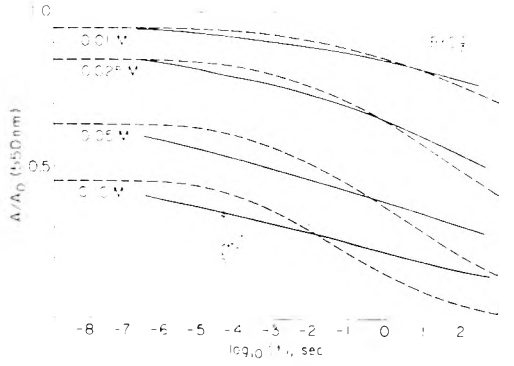

Figure 5. Reaction of trapped electrons with the weak acceptor, BrO_3^-, in 6 M NaOH at 77°K. The simulated decays (dashed curves) were calculated for B = 1.2 eV, a_0 = 4 Å, and an "inefficiency factor" of 10^{-11} (see section IIIB), and some capture of electrons prior to solvation was assumed. Still the experimental curves are "flatter" than the simulated curves.

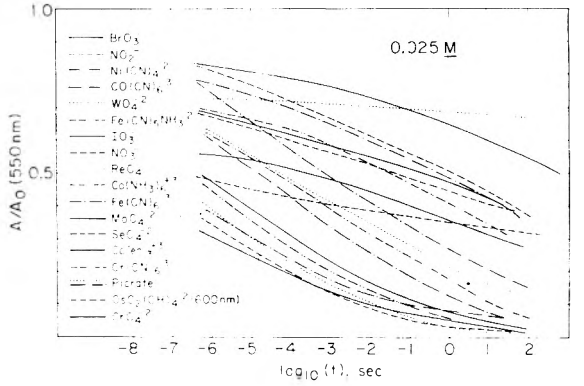

Figure 6. Reactions of trapped electrons in 6 M NaOH at 77°K with a wide variety of acceptors, present at 0.025 M in each case. One of the two curves given for picrate was corrected for a permanent absorption formed from picrate. $Fe(CN)_5NH_3^{2-}$ has changed color indicating that in 6 M NaOH, this ion is altered, and $Fe(CN)_5NH_3^{2-}$ is not the actual reactant.

the low energy onset of the solvated electrons' absorption spectrum. This selection of binding energy is consistent with the conclusion of Eisele and Kevan[21] that the absorption spectrum in 10 M NaOH glass is due to photodetachment of solvated electrons.

BrO_3^- is a much less effective electron acceptor (Figure 5), and the experimental curves show little resemblance to simulations of eq 4. The simulated curves in Figure 5 differ from those of eq 4 by the introduction of an "inefficiency factor", F, so that eq 1 becomes

$$\text{tunneling rate} = 10^{15}(T)(F) \qquad (5)$$

The introduction of the adjustable parameter, F, adds a factor log F in eq 2 and 4, and therefore simply translates the simulated curves along the log (t) axis.

The fit of the simulated curves to the experimental curves has been further improved by assuming that, at each concentration, a certain fraction of the electrons was captured before becoming solvated (capture of "dry electrons"). However the agreement between theory and experiment is still poor. The experimental decay curves are "flatter" (less steep) than the simulated curves. This "flatness" of the decay curves suggests that the tunneling rate falls off more rapidly with distance than anticipated, i.e., that elec-

TABLE I: The Relationships of "Efficiency Factors" for Reaction of Trapped, Solvated Electrons to the Absorption Onsets for Electron Acceptors, and to the Acceptor Rate Constants, k, for Reaction with Hydrated Electrons in Water

Acceptor	Inefficiency factor[a]	Absorption onset,[b] eV	$10^{-9}k$, dm^3 mol^{-1} sec^{-1}[c]
ClO_3^-	10^{-15}	5.6	0.35–0.002
$ClAc^-$	10^{-12}	5.1	0.89–2.5
WO_4^-	10^{-11}	5.1	
BrO_3^-	10^{-9}	4.7	2.1–7.8
NO_3^-	10^{-8}	(4.1), 4.9	8.2–11
MoO_4^{2-}	10^{-7}	4.4	
NO_2^-	10^{-7}	(3.5), 4.9	3.8–8.0
IO_3^-	10^{-7}	(4.4), 4.5	7.7–9.6
$Fe(CN)_5NH_3^{2-}$	10^{-7}		
$Ni(CN)_4^{2-}$	10^{-7}	3.1	4.1
ReO_4^-	10^{-4}	3.7	
$Co(CN)_6^{3-}$	10^{-4}	3.4	1.0–5.0
$Co(NH_3)_6^{3+}$	10^{-2}	(3.5, 2.8), 4.9	76–90
$Fe(CN)_6^{3-}$	10^{-1}	2.6	3.0
$Cr(CN)_6^{3-}$	10^{0}	2.5	4.2
$Co(en)_3^{3+}$	10^{0}	2.3	73–85
Picrate	10^{0}	2.3	35–39
$OsO_2(OH)_4^{2-}$	10^{0}	1.8	
MnO_4^-	$\approx 10^{0}$		22–44
Np(VII)	10^{4}	(2.0), 2.3	
SeO_4^{2-}	?	5.4	

[a] An order of magnitude correction for the difference between calculated and observed reaction rates, as introduced in eq 5. The inefficiency is presumably due to Franck-Condon restrictions, etc. Because the fit to the data is not good for weak acceptors (see Figure 5 for example), these efficiency factors are somewhat arbitrary. [b] The photon energy above which the molar, decadic extinction coefficient of the species, in water, remains greater than 100. Most species show a sudden onset to continuous high, optical absorption, but some have absorption peaks at energies lower than this onset. These peaks are indicated in parentheses. [c] Range of values given in ref 38.

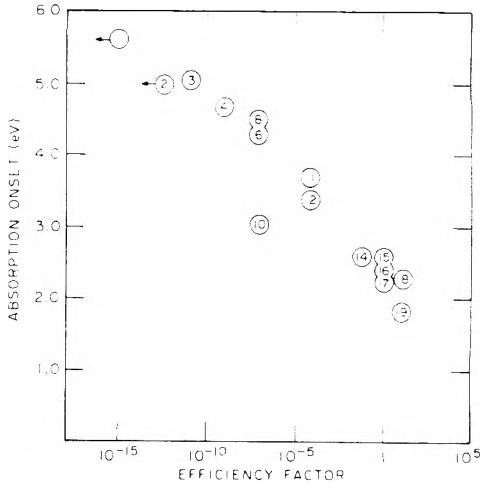

Figure 7. The correlation between "efficiency factors" for reaction of acceptors with trapped electrons and the onset for optical absorption by the acceptors in aqueous solution. The correlation implies a correlation of electron affinity with reactivity (see section IIIB). Those acceptors which had spectra with peaks, rather than a simple onset to continuous strong absorption, have been omitted from the plot.

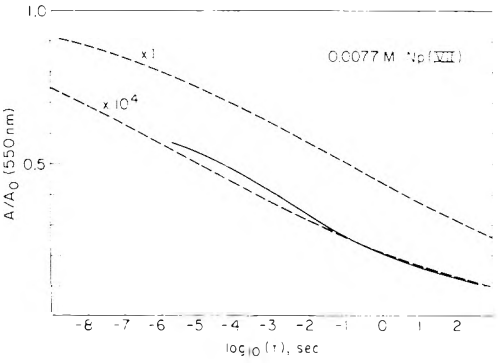

Figure 8. Reaction of trapped electrons in 6 M NaOH at 77°K with Np(VII) at 7.7×10^{-3} M. The simulated curve (dashed) does not agree with experiment unless we take an efficiency factor of 10^4; Np(VII) appears much more reactive than any other acceptor tested.

tron–acceptor pairs separated by large distances live relatively longer than expected.

Figure 6 shows decay curves for a wide variety of acceptors all at 0.025 M concentration. There seems to be an almost continuous variation from strong to weak acceptors, stronger acceptors being defined as those which give greater electron capture rates. The stronger acceptors give decay curves which agree reasonably well with simulations according to the model. The weaker acceptors give "flatter" decay curves, indicating a stronger distance dependence of the tunneling rate, as was seen for BrO_3^- in Figure 5.

The electron capture rate also seems to correlate with electron affinity of the acceptor. Although measurements of electron affinities of these acceptors have not been made, those known as good oxidizing agents give faster electron capture rates. The acceptors giving the fastest capture rates are colored, and as a general rule acceptors with longer wavelength absorption bands give faster electron capture rates. (See Table I and Figure 7.) Longer wavelength absorption bands imply lower energy unoccupied orbitals and thus greater electron affinities.

While the simple tunneling calculations describe the data well only for strong acceptors, it may still be of some use to parameterize the data by obtaining approximate "efficiency factors" (eq 5). The data of Figure 6 were used. Because the fits for the weaker acceptors were poor, the efficiency factors, given in Table I, have limited meaning. The factors are useful in comparing electron capture rates of different acceptors *at the same distance* from a solvated electron. A discussion of rationale for comparing efficiencies of electron acceptors is given in the Discussion section.

Table I contains entries for acceptors not run at 0.025 M. MnO_4^- was run at 0.01 M and at 600 nm because of its strong visible absorption. The decay curve (not shown) was similar to that for CrO_4^{2-} under the same conditions. Np^{7+} (probably present as NpO_5^{3-}) showed a remarkably high efficiency (see Figure 8).

Figure 9 shows decays trapped electrons in 6 M NaOH glass in the presence of high concentrations of very inefficient electron acceptors. The decays in the presence of 0.25 M chloroacetate and 1.0 M ClO_3^- show extreme examples of inefficient reactions. In 1.0 M ClO_3^- only about 15% of the electrons are captured, indicating, according to eq 3, a capture radius of only 4 Å. Apparently only reactions between nearest neighbors or next nearest neighbors are involved. Even if this reaction is still primarily electronic and

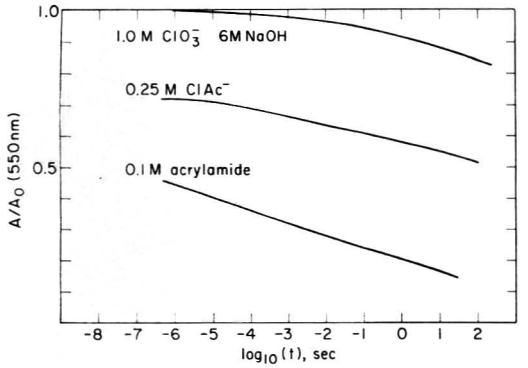

Figure 9. Reactions of trapped electrons in 6 *M* NaOH at 77°K with high concentrations of very inefficient acceptors.

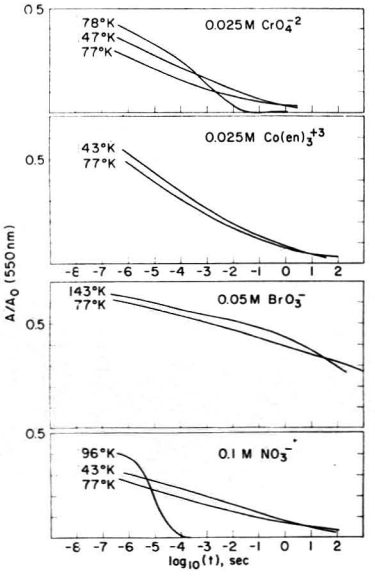

Figure 10. Effects of temperature on reactions of trapped electrons with acceptors in 6 *M* NaOH. The decays are temperature independent until times at which diffusion begins to be important. The initial yields reflect more efficient "dry electron" capture at lower temperatures.

nonadiabatic, it may not be entirely appropriate to call it a tunneling process.

C. Effects of Temperature of Reactions with Solutes. Figure 10 shows decay curves for CrO_4^{2-}, $Co(en)_3^{3+}$, BrO_3^-, and NO_3^- at different temperatures. Nearly doubling the absolute temperature causes no change in the shape of the decay curves at times shorter than 1 sec. At longer times diffusion begins to make a contribution to the reaction at 143°K. Buxton and coworkers concluded that a similar glass, 10 *M* NaOH, was "essentially rigid" at 135°K.[20] Even at 178°K the curve remains parallel to the lower temperature curves until diffusion becomes important at a few hundred microseconds.

While the decay curves from 10^{-6} to 1 sec are not changed by nearly doubling the absolute temperature, the initial yields are changed. Apparently reactions of electrons prior to solvation are more efficient at lower temperature. This is not surprising since both thermalization and solvation of the electron by the matrix may be slower at lower temperatures so that acceptors may more readily compete with the matrix for the electrons.

We also note that the difference between initial yields at 77 and 143°K is relatively small for $Co(en)_3^{3+}$. Probably the presolvation processes are relatively unimportant for $Co(en)_3^{3+}$ at both temperatures.

D. Effects of Dose. Reactions of Electrons with Irradiation Products. A sample was preirradiated to 60 Mrads, and the trapped electrons were bleached with visible light. The sample was then pulsed, and the newly created trapped electrons were observed to decay. A/A_0 was 0.65 at 0.5 μsec and decayed to 0.18 at 30 sec, where A_0 is again the absorbance in the "pure" matrix, without preirradiation.

The decay shows that trapped, solvated electrons react with radiation products created in the 60-Mrad preirradiation. This reaction can account for the decreasing e_s^- yield with increasing dose observed with γ radiation.[22] The main reactant is probably O^-, known to be present at about 0.025 *M* at 20 Mrads.[22] The O^- concentration at 60 Mrads is probably 0.05–0.075 *M*. It appears that O^- is a relatively ineffective electron acceptor, comparable, perhaps, with NO_3^-.

IV. Discussion

A. Summary of Results. The experimental results have been presented by comparison with simple model calculations of a tunneling process. We now summarize the basic features of the results, dividing them into three categories: those results *strongly supporting* the tunneling model, those results which do not clearly support or contradict the model, and those which clearly contradict at least the simple model of tunneling. Observations which strongly support the suggestion that electrons tunnel through tens of ångströms of inert solvent to react with electron acceptors are the following: (1) the very existence of reactions in a rigid matrix in which translational diffusion is virtually eliminated (Diffusion is discussed in section IVG.) (2) The reactions progress toward completion approximately with the logarithm of time. (3) The lifetimes of the trapped electrons decrease approximately exponentially with acceptor concentration, a tenfold increase in concentration typically decreasing the half-life by a factor of about 10^6. (4) The reaction rates are independent of temperature from 77°K up to the softening point of the matrix. (5) The existance of at least one acceptor (SeO_4^{2-}) which efficiently reduces the initial yield of trapped electrons, but which reacts only weakly with solvated electrons. This tends to preclude the possibility that the observed reactions involve escape of electrons from their traps to re-form mobile electrons (see section IVG). (6) The decay curves for reactions with several of the best electron acceptors are very similar, and are fitted very well by model tunneling calculations using only one adjustable parameter. Also this adjustable parameter, the binding energy of the trapped electron, was assigned in accordance with independent experimental information from photoconductivity studies (see section IIIB).

The above support for the tunneling mechanism is discussed in section IVG, which describes problems which arise from attempts to account for the data in more conventional ways.

Other features of the results can be accounted for within the framework of the simple tunneling model, but are not necessarily required by the tunneling model, and do not clearly support or contradict the model. (7) The electron acceptors investigated display a very wide range of reactivities (Table I and Figure 6), spanning more than 10 orders of magnitude. (8) The reactivity correlates with optical spectra (Figure 7) and oxidizing power suggesting that the

reactivity of an electron acceptor is strongly related to its electron affinity.

One observation is in clear disagreement with the simple model of tunneling: (9) the shape of the decay curves "flatten" for weak acceptors (section IIIB) implying that the reaction rates with weak acceptors depend more strongly on distance (between the solvated electron and the acceptor).

Modification of the model is apparently required to explain this result.

B. Considerations in Kinetics of Electron Capture Processes in Glasses. When comparing rates of reaction with different acceptors we must attempt to compare the rates for electron–acceptor pairs separated *by the same distance.* This can be done if we compare different acceptors at the same concentration and ask, "what is the time required to capture the same fraction of the trapped electrons?" A glance at Figure 6 indicates the large range of reactivities evaluated in this way.

C. Tunneling Theory. (1) *Tunneling in Systems with Simple Potential Functions.* The results were discussed in comparison with calculated rates for penetration of rectangular barriers by free particles. A more realistic model system would involve tunneling between two states, both of which are bound, and the problem should be done in three dimensions. Brocklehurst[23] has recently described such a model calculation, giving a result quite similar to the barrier penetration calculation. Brocklehurst used a "golden rule" expression to calculate the tunneling rate:

$$k = 2\pi\beta^2/\bar{n}\alpha \qquad (6)$$

where k is the tunneling rate, β is interaction energy between the initial and final states, and α is level width for the final state, determined by the rate of relaxation of the final state $\alpha/\bar{n}$.[23] This expression is one of the limiting forms described by Voltz, who recently clarified the theory for energy transfer between weakly interacting molecular systems,[24] showing that the Förster theory[25] is applicable to most cases. The work of Voltz applies also to intermolecular electron tunneling.

The most important quantity in the tunneling calculation of eq 6 is β, the energy of interaction between the initial and final states. Brocklehurst used the interaction energy for the case where the initial and final one electron states are both eigenfunctions of the Coulomb potential—the case of H_2^+ at large internuclear separation. Wilson obtained very similar results using "square well" potentials, either cubic or spherical in shape.[26] *The expression Brocklehurst obtained is identical with that of the simple barrier penetration calculation, except that Brocklehurst's preexponential factor is larger by about* 10^4. This would give tunneling distances about 8 Å greater than those of eq 2. Brocklehurst attributed the larger preexponential factor to the "resonant nature" of intermolecular electron tunneling, as opposed to penetration of a barrier by a free particle.[23]

An alternate view is that Brocklehurst's preexponential factor of about $10^{19.5}$ sec^{-1} is too high, because his 10^{11} sec^{-1} rate of relaxation of the final state is too slow. An electron newly captured by a molecule in a condensed medium will be immediately subject to large changes in electronic and vibrational polarization of the medium. The accepting level will therefore have a lifetime of only about 10^{-15} sec and will therefore be very broad—perhaps approaching 1 eV. This assumed relaxation rate of 10^{15} sec^{-1} reduces the preexponential factor to about 10^{16}, in close agreement with the simple barrier penetration calculation. Thus eq 2 will be considered to be representative of both methods of calculation.

(2) *The effect of Relaxation on Tunneling Rates. A Digression.* The effect of relaxation of the electron accepting state, as outlined by Voltz for the parallel case of energy transfer, gives an example of the way wave properties of matter often give surprising results. We might consider the process naively as occurring in two steps: (1) transfer of the electron to the acceptor, forming a state which is resonant with the electron donor, and (2) relaxation to lower the energy. Some components of this relaxation will be due to electronic and fast vibrational changes occurring in about 10^{-14} to 10^{-15} sec. Strangely enough, a faster relaxation process leads to a slower overall reaction according to eq 5. The opposite is true in the case of resonant interaction, but this case is not of interest in intermolecular electron transfer in condensed media.

This behavior is similar to the behavior of a pair of weakly coupled classical oscillators, such as masses on springs. In the classical case the transfer of energy from a free oscillator to a second, strongly damped oscillator is slowed because the damped oscillator (analogous to the relaxation) cannot easily move under the oscillatory force. In the limit of an infinite damping coefficient, the oscillator is held rigid and cannot receive any energy from the moving oscillator.

(3) *Criticisms of the Theory.* At least four criticisms of the theory should be mentioned. The first is that the model considers smooth energy barriers, while in reality a complicated, fluctuating potential separates the solvated electron and the acceptor. The second problem, closely related, is the assumption that the barrier height is equal to the energy needed to release the solvated electron to a mobile, or quasi-free state. This is questionable because there is probably considerable kinetic energy in the lowest-energy mobile electron state. This kinetic energy is analogous to zero point energy in molecular vibration. In rare gas liquids the zero point kinetic energy for a mobile electron is calculated to be larger than 1 eV.[27] It is not clear that this energy may simply be treated as an effective potential energy.

A third factor not considered is the effect of the level width. We have assumed that the electron accepting level is very broad because of fast relaxation. This may substantially decrease the interaction energy of eq 5, decreasing the tunneling rate. However there may be a compensating increase in rate due to interaction with several such broadened levels. This may be a serious weakness of the theory, which requires further theoretical work.

A careful theoretical study of tunneling might clarify these points, and would probably raise others. Additional complications, not considered theoretical in nature, are discussed in section IVE.

D. Inefficiency Due to Energy-Dependent Franck–Condon Factors. The observed reaction rates of trapped electrons with various electron acceptors appear to range over 15 orders of magnitude. This section points out that Franck–Condon factors may be expected to attenuate the reaction rates more strongly for acceptors with lower electron affinities. Even though tunneling is a resonant process between states of the same energy, the correlation between tunneling rate and electron affinity (section IIIB) is not surprising.

Figure 11 illustrates energy requirements in a tunneling

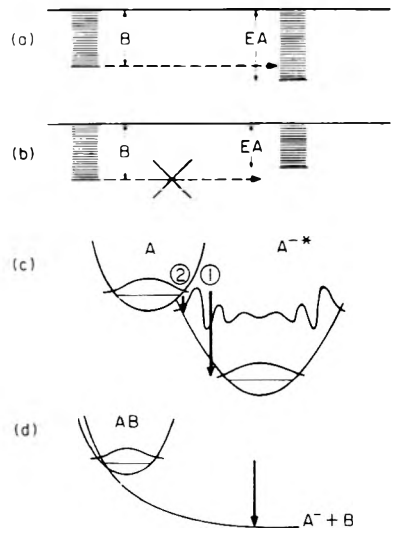

Figure 11. Schematics of tunneling energetics. (a and b) Tunneling can occur to a vibrationally excited level of the acceptor only if the electron affinity of the acceptor (EA) is greater than the binding energy (B) of the trapped electron. However Franck–Condon restrictions may make transitions utilizing all of A's electron affinity very weak, such as transition 1 in (c); whereas transition 2, to a vibrationally excited level gives good overlap of the vibrational wave functions. Such effects will also be very important for dissociative electron capture (d).

process. In Figure 11a, tunneling occurs from the ground state of the solvated electron to a vibrationally excited level of the acceptor. However in Figure 11b the electron affinity (EA) of the acceptor is less than the binding energy (B) of the solvated electron; no tunneling may occur. Figure 11a and 11b carry the suggestion that for acceptors with EA > B, tunneling occurs, but for weaker acceptors, EA < B, the tunneling rate is zero. The figure carries no suggestion that the rate should depend strongly on the difference between EA and B.

But comparing group of acceptors the decrease of reactivity is not a sudden drop to zero at EA = B; it is gradual decrease, due, at least in part, to Franck–Condon restrictions. The equilibrium nuclear configuration of the acceptor will, in general, change substantially after it accepts an electron. Therefore a transition making use of the full equilibrium (adiabatic) electron affinity is generally so seriously attenuated that it is of no importance in electron capture process which must take place on electronic time scales. There are probably several possible vertical electron capture process, with different electron affinities and different Franck–Condon factors. The closer a transition is to using the full, adiabatic, electron affinity, the weaker the transition is likely to be. If the electron affinity of the acceptor is small, capture of the electron may require most of the electron affinity of the acceptor (arrow 1 in Figure 11c). The Franck–Condon effect attenuates this transition by several orders of magnitude. When the electron affinity of the acceptor is large, only a fraction of it is required. Then the much more efficient transition to a higher vibrational level can occur (arrow 2 in Figure 11c). Such effects are also very important in dissociative electron capture processes (Figure 11d).

Thus, it is the vertical electron affinity that determines whether a tunneling reaction can or cannot occur. However in these experiments in which a tremendous range transition probabilities are observed, the vertical electron affinity is not a well-defined number. It may become larger (closer to the equilibrium electron affinity), but at the expense of a smaller Franck–Condon factor, which makes the reaction slow. It is expected that for electron affinities sufficiently larger than the binding energy of the electron, the rate will be fast and approximately independent of the electron affinity. For smaller electron affinities, the rate would go smoothly to zero as EA becomes less than B.

In conclusion, the rate of tunneling processes will be severely slowed unless the reaction is sufficiently exoergic: efficient tunneling requires a substantial amount of wasted energy, in contrast to a common picture of tunneling as an energy-conserving process. The wasted energy may be very small if the acceptor undergoes little change in nuclear configuration after accepting an electron. However additional energy waste will occur due to relaxations of the solvent in response to the displacement of an electronic charge.

Franck–Condon restrictions may account for the observed wide range of reactivities, and the apparent correlation of reactivity with electron affinity. However the Franck–Condon factors are not expected to depend on distance, and cannot explain the changes in the shapes of the decay curves for weak acceptors (the "flattening" described in section IIIB).

E. Complications not Taken into Account in the Model Calculations. The following complications probably modify the observed decay curves, and may be responsible, in part, for the disagreement with model calculations for weak acceptors. (1) All of the electrons do not have a single binding energy (trap depth). (2) The trap depths change with time. (3) There is considerable uncertainty in the average binding energy. A nonrandom distribution of trapped electrons relative to acceptors may arise because of (4) presolvation ("dry electron") reactions with acceptors, which may remove some close pairs, and (5) the nonuniform distribution of trapped electrons relative to each other in spurs and tracks, may locally deplete the acceptor concentration.

1, 2, and 3. Trap Depth Variations. Different trap depths are suggested by the shifting of the absorption spectrum in photobleaching experiments.[29-31] However only small shifts are obtained, and bleaching with monochromatic 633-nm laser light does not "burn a hole" in the spectrum; it removes the entire spectrum, giving only a slight blue shift as the bleaching progresses.[32] These facts imply that the spectrum of each individual, trapped electron is nearly as broad as entire spectrum, and that the spread in trap depths is only 20 or 30%.

The spectrum also changes with time (Figure 2) suggesting that the traps deepen with time. Both the presence of a range of trap depths, and a change of trap depth with time are expected to "flatten" the decay curves, because the more deeply trapped electrons must tunnel through a higher barrier, and would therefore decay more slowly. However this does not explain why the decay curves are flattened for weaker acceptors. The reaction rates might depend even more strongly on trap depths if Franck–Condon factors were strongly energy dependent, as suggested in section IVD. The change in shape ("flattening") of decay curves for weak acceptors (e.g., BrO_3^-, Figure 5) is probably caused, in part, by variations in trap depths.

There is also considerable uncertainty about the actual relation of the trap depth to the observed optical spectrum. While we have assumed an average trap depth of about 1.2 eV, the photocurrent in 10 M NaOH was measured only

down to 1.9 eV.[21] Some photobleaching experiments in 10 *M* KOH suggest trap depths above 2 eV. The choice of 1.2 eV is reasonable, but not uniquely determined by experiment.

4 and 5. Spatial Distribution. The distribution of the acceptors in the matrix is probably homogeneous. The samples were all transparent with no evidence of precipitation, and the shapes of the rate curves do not correlate with solubility. However the nonhomogeneous distribution of the electrons may cause some problem. Radiation creates electrons and other radicals in locally concentrated regions,[33] containing about 3–5 ion pairs. The fact that the electrons may be close enough to react with positive charge (which reacts to form the O^- radical in alkaline, aqueous systems) is not important to our results, because we observe only the fraction of the electrons which have not so reacted at any time.

The high, local concentration of electrons in the spur might locally deplete the acceptor concentration, both slowing the decays and flattening the decay curves. However this effect should be greatest on strong acceptors present at low concentrations. As noted earlier, the opposite is observed; the decay curves are "flattened" most for weak acceptors and high acceptor concentrations. Apparently local concentration effects are much less important than other factors, which probably relate to the specific electron–acceptor interaction.

F. Reactions Prior to Solvation. Dry Electrons. Electrons may react with electron acceptors prior to solvation of the electron. Hamill[34] has called these "dry electron" reactions, and evidence for such reactions has been provided by Hunt's group.[35,36]

Prior to findings of tunneling by trapped, solvated electrons, all reactions of electrons with acceptors in rigid glasses were attributed to mobile, or "dry" electrons. Now the question is, how much, if any, dry electron capture occurs. The experimental data do not extend to the solvation time of the electron and considerable reaction of solvated electrons probably occurs prior to our earliest observations. Therefore, it is difficult to say how much of the reduction in the initial yield of trapped electrons, observed at about 1 μsec, is due to presolvation reactions. The shapes of many of the decay curves do suggest that such reactions are occurring, particularly for the unusual case of SeO_4^{2-}, which strongly reduces the initial yield, but reacts only weakly with the trapped electrons.

Whatever the mechanism of presolvation, electron capture is, it must involve very fast processes during which there can be little opportunity for changes in the positions of nucleii. Therefore, the energy-dependent, Franck–Condon factors discussed in section IVD are likely to be as important in presolvation reactions as in long-range tunneling reactions. This may partially account for the relationship between solvated electron and presolvation reactions found recently by Lam and Hunt.[37]

G. Alternatives to Tunneling? Some Requirements. (1) *Diffusion.* Most of the main features of the data, listed in section IVA, are contrary to the usual behavior of diffusion reactions. This is consistent with the long lives (weeks at least) of the trapped electrons, and their lack of conductivity,[21] except when detrapped by light. A rapid diffusion process with a small activation energy is known for protons in ice. However this results from the ability of the proton to fit into the periodic structure of ice with little disruption. Disorder destroys this special mobility, as indicated by the surprising fact that the mobility of the proton is smaller in liquid water than in ice. In disordered solids such as the glasses, composed of polar molecules, protons and electrons are expected to be immobile.

(2) *Local Heating.* Transient local heating and softening of the matrix could not explain the results, because there is insufficient energy deposited by the radiation to account for reactions. Moreover, local heating should have increased the reaction more when the matrix was closer to the softening point. This is contrary to failure of increased temperature to increase the reaction rates.

H. Unresolved Questions. At least two features of the data are not adequately explained: (1) the "flattening" of the decay curves for weak acceptors, which implies a stronger dependence of tunneling rate on distance. The complications considered as contributing to this flattening (section IVE) are not, in the author's opinion, sufficient to account for all of this "flattening". (2) The very large range of reactivities for different acceptors, and the dependence of the reactivities on electron affinity have been attributed to energy-dependent Franck–Condon factors at least as small as 10^{-10}. One might then expect some thermal activation of such reactions, but none is observed.

These features of the data seem to point to a more complex electronic process for tunneling to acceptors with marginally sufficient electron affinities.

Acknowledgments. The author is grateful to Drs. M.S. Matheson, C.D. Jonah, and J.E. Martin for helpful discussions, to Don Ficht, Lee Rawson, and Ben Naderer for excellent operation of the Linac, and to Argonne National Laboratory for a postdoctoral fellowship.

References and Notes

(1) Work performed under the auspices of the U.S. Atomic Energy Commission.
(2) (a) H. Tsujikawa, K. Fueki, and Z. Kuri, *Bull. Chem. Soc. Jpn.*, **38**, 2210 (1965); (b) B. G. Ershov and E. L. Tseitlin, *Khim. Vys. Energ.*, **4**, 186 (1970).
(3) A. I. Mikhailov, *Dokl. Akad. Nauk. SSSR*, **197**, 136 (1971).
(4) F. Kieffer, C. Meyer, and J. Rigaut, *Chem. Phys. Lett.*, **11**, 359 (1971).
(5) K. I. Zamaraev, R. F. Khairuditor, A. I. Mikhailov, and V. I. Goldanskii, *Dokl. Akad. Nauk SSSR*, **199**, 640 (1971).
(6) R. F. Khairutdinov, A. I. Mikhailov, and K. I. Zamaraev, *Dokl. Akad. Nauk SSSR*, **200**, 905 (1971).
(7) E. L. Girina and B. G. Ershov, *Izv. Akad. Nauk SSSR, Ser. Khim*, 278 (1972).
(8) J. R. Miller, *J. Chem. Phys.*, **56**, 5173 (1972).
(9) J. R. Miller and J. E. Willard, *J. Phys. Chem.*, **76**, 2641 (1972).
(10) J. Kroh and Cz. Stradowski, *Intl. J. Radiat. Phys. Chem.*, **5**, 243 (1973).
(11) J. R. Miller, *Chem. Phys. Lett.*, **22**, 180 (1973).
(12) V. I. Gol'danskii, K. I. Zamaraev, A. I. Mikhailov, and R. F. Khairuditov, *Akad. Nauk SSSR*, preprinted (1972).
(13) R. J. Marcus, B. J. Zwolinski, and H. Eyring, *J. Phys. Chem.*, **58**, 432 (1954).
(14) B. Chance, D. Devault, V. Legallais, L. Mela, and T. Yonetani in "Nobel Symposium 5", S. Claesson, Ed., Almquist and Wiksell, Stockholm, 1967, p 437.
(15) D. DeVault, J. Parkes, and B. Chance, *Nature (London)*, **215**, 642 (1967).
(16) M. Anbar and E. J. Hart, *Adv. Chem. Ser.*, **No. 81**, 79 (1968).
(17) J. T. Richards and J. K. Thomas, *J. Chem. Phys.*, **53**, 218 (1970).
(18) J. C. Sullivan and A. J. Zielen, *Inorg. Nucl. Chem. Lett.*, **5**, 927 (1969).
(19) J. Miller, B. Clift, J. Hines, R. Runowski, and K. Johnson, to be submitted for publication.
(20) G. V. Buxton, F. C. R. Cattell, and F. S. Dainton, *Trans. Faraday Soc.*, **67**, 687 (1971).
(21) I. Eisele and L. Kevan, *J. Chem. Phys.*, **53**, 1867 (1970).
(22) H. Hase and L. Kevan, *J. Chem. Phys.*, **53**, 3183 (1970).
(23) B. Brocklehurst, *Chem. Phys.*, **2**, 6 (1973).
(24) R. Voltz, *Chem. Phys. Lett.*, **11**, 208 (1971).
(25) Th. Forster in "Modern Quantum Chemistry", Part 3, O. Sinanoğlu, Ed., Academic Press, New York, N.Y., 1965, p 93.
(26) C. W. Wilson, unpublished.
(27) B. E. Springett, J. Jortner, and M. H. Cohen, *J. Chem. Phys.*, **48**, 2720 (1968).

(28) D. A. Copeland and N. R. Kestner, *J. Chem. Phys.*, **53**, 1189 (1970).
(29) B. G. Ershov and A. K. Pikaev, *Dokl. Akad. Nauk SSSR* (or *Russ. J. Phys. Chem.*), **41**, 1394 (1967).
(30) B. G. Ershov, O. F. Khodzhaev, and A. K. Pikaev, *Dokl. Akad. Nauk. SSSR*, **179**, 911 (1968).
(31) G. V. Buxton, F. S. Dainton, T. Lantz, and P. Sargent, *Trans. Faraday Soc.*, **66**, 2962 (1970)
(32) K. K. Ho and L. Kevan, *Intl. J. Radiat. Phys. Chem.*, **3**, 193 (1971).
(33) A. Mozumder and J. L. Magee, *Radiat. Res.*, **28**, 203 (1966).
(34) W. D. Hamill, *J. Phys. Chem.*, **73**, 1341 (1969).
(35) R. K. Wolff, M. J. Bronskill, and J. W. Hunt, *J. Chem. Phys.*, **53**, 4211 (1970).
(36) J. E. Aldrich, M. J. Bronskill, R. K. Wolff, and J. W. Hunt, *J. Chem. Phys.*, **55**, 530 (1971).
(37) G. A. Lam and J. W. Hunt, Proceedings of the 5th International Symposium on Radiation Research, Seattle, July 1974, to be published.
(38) M. Anbar, M. Bombenek, and A. B. Ross, *Natl. Bur. Stand. Ref. Data Ser., Natl. Bur. Stand.*, **No. 43** (1973).

Thermochemistry of the Gas-Phase Reaction $CF_2{=}CF_2 + I_2 = CF_2ICF_2I$. Heat of Formation of 1,2-Diiodoperfluoroethane and of Iodoperfluoroethane[1a]

E-Chung Wu,[1b] J. M. Pickard, and A. S. Rodgers*

Thermodynamics Research Center, Department of Chemistry, Texas A&M University, College Station, Texas 77843
(Received August 19, 1974; Revised Manuscript Received February 3, 1975)

The gas-phase equilibrium $C_2F_4 + I_2 = C_2F_4I_2$ has been studied spectrophotometrically at 270 nm over the temperature range from 477 to 562 K. Side reactions occurred at low pressures of I_2 but were suppressed at higher pressures. The heat of the reaction at 298.15 K was found to be -16.6 ± 0.5 kcal mol^{-1} which led to $\Delta H_f°$ (CF_2ICF_2I,g,298) $= -159.1 \pm 0.5$ kcal mol^{-1}. From this result, the heat of formation of iodoperfluoroethane was estimated as $\Delta H_f°$ (CF_3CF_2I,g,298) $= -240.0 \pm 1$ kcal mol^{-1}.

Introduction

Benson and Amano[2] have reported on studies of gas-phase equilibrium in the CH_2ICH_2I, I_2, $CH_2{=}CH_2$ system and on similar systems with propylene and cyclopropane from which they were able to evaluate the thermodynamic properties of hydrocarbon iodides.

In the course of our investigations of the thermochemistry of fluorocarbons and fluorocarbon free radicals, we have need of the heat of formation of CF_3CF_2I. A reliable estimate of this quantity should be obtained as the mean of the heats of formation of CF_3CF_3 and CF_2ICF_2I.[3,4] The former seems firmly established[5] but the latter is unknown. To this end we have undertaken a spectrophotometric investigation of equilibrium in reaction 1, the results of which are

$$CF_2{=}CF_2 + I_2 = CF_2ICF_2I \qquad (1)$$

reported here. In addition, an independent determination of the ideal gas thermodynamic functions ($C_p°$, $S°$, $H_T° - H_0°$, and $(G_T° - H_0°)/T$) for CF_2ICF_2I has been undertaken, the details of which will be reported elsewhere.[6]

Experimental Section

Tetrafluoroethylene was obtained from the Columbia Organic Chemical Co., and was purified by vacuum distillation. Reagent grade iodine was obtained from J. T. Baker Chemical Co., it was vacuum sublimed before each use.

The experimental apparatus and procedure has been described in detail elsewhere.[7] Briefly, the apparatus consists of a Heath Model EU 701 single-beam uv–visible spectrophotometer, and a 20 × 3.8 cm quartz reaction vessel in a wire-wound aluminum oven. The temperature is controlled to ±0.1° with less than 0.5° variation along the reaction cell. Initial gas concentrations were determined manometrically with a Validyne variable reluctance pressure transducer and the progress of the reaction, to equilibrium, was followed spectrophotometrically. Preliminary experiments were performed at 496 K and 500 nm at which wavelength I_2 is the only absorbing species. With $P°_{I_2} = 3.0$ and $P°_{C_2F_4} = 50$–200 Torr, it was found that $\Delta P_{eq}/\Delta P_{I_2} = 3$–10 depending on $P°_{C_2F_4}$, the larger values of $P°_{C_2F_4}$ corresponding to higher ratios. This suggested telomerization of the C_2F_4, a common phenomena in C_2F_4 radical reactions.[8-10] However, when the partial pressure of I_2 was increased to ca. 20 Torr, then ΔP_{eq} was in the range 0.5–2 Torr and was quite stable for several hours, indicating that high partial pressures of I_2 successfully inhibited the telomerization reaction. Unfortunately, I_2 could not be spectrophotometrically measured at these high concentrations. Consequently, it was necessary to follow the course of the reaction at 270 nm, the wavelength of the maximum absorbance in the uv. At this wavelength, the absorbance of C_2F_4 is negligible, and that of I_2 is small (0.01 OD Torr^{-1}), so that the primary species accounting for the absorbance is the adduct CF_2ICF_2I. Unfortunately its absorption coefficient could not be directly determined due to its rapid decomposition to C_2F_4 and I_2. This problem can be overcome under restricted experimental conditions. Let us define the absorption coefficient, α_i^λ, such that the absorbance, A^λ, is given by

$$A^\lambda = \sum_i \alpha_i P_i \qquad (2)$$

Thus, the initial absorbance at 270 nm (where $\alpha_{C_2F_4}^{270} = 0.000$) is given by

$$A_0 = \alpha_{I_2} P°_{I_2}$$

TABLE I: Spectrophotometric Data for Equilibrium in the Reaction $C_2F_4 + I_2 = CF_2ICF_2I$ at 270 nm

Temp, K	$P^\circ_{I_2}$, Torr	$P^\circ_{C_2F_4}$, Torr	ΔA, OD	K_{ap}, 10^{-4} OD Torr^{-2}
477.2	20.4	62.7	0.655	5.12
	19.0	78.1	0.723	4.87
	15.8	84.7	0.657	4.91
	15.3	111.8	0.835	4.88
			Av	4.95 ± 0.1
496.2	21.5	294.3	1.356	2.14
	21.1	117.9	0.604	2.43
	21.1	61.9	0.335	2.56
	20.5	73.5	0.367	2.44
	20.5	43.5	0.220	2.47
	20.1	84.3	0.445	2.63
	20.1	53.4	0.290	2.70
	15.2	140.3	0.538	2.52
	15.2	45.8	0.183	2.63
	11.5	112.0	0.318	2.47
	10.2	99.3	0.250	2.47
			Av	2.50 ± 0.1
519.0	20.2	54.3	0.140	1.28
	20.0	206.0	0.487	1.18
	20.0	96.0	0.231	1.20
	19.9	117.1	0.289	1.24
	19.9	84.6	0.211	1.25
	19.8	147.9	0.372	1.27
	19.7	190.3	0.453	1.21
	19.7	108.3	0.260	1.22
	18.9	184.1	0.435	1.25
	18.9	66.6	0.160	1.27
	15.3	70.4	0.135	1.25
	10.0	122.5	0.154	1.26
	10.0	68.9	0.087	1.26
	10.0	101.0	0.126	1.25
			Av	1.24 ± 0.02
537.5	25.9	113.7	0.197	0.669
	25.9	260.2	0.440	0.653
	25.7	86.3	0.154	0.694
	25.1	68.9	0.128	0.740
	20.3	205.8	0.275	0.658
	20.1	118.2	0.158	0.665
	20.1	164.2	0.222	0.673
	19.8	55.5	0.076	0.692
	14.4	114.7	0.108	0.675
	9.9	111.2	0.077	0.699
			Av	0.680 ± 0.02
562.5	25.5	120.5	0.103	0.335
	25.2	262.8	0.218	0.329
	25.2	62.4	0.055	0.350
	25.1	87.9	0.077	0.349
	20.2	70.0	0.049	0.347
	20.0	102.1	0.071	0.348
	19.8	189.2	0.125	0.334
	19.1	147.9	0.095	0.336
			Av	0.341 ± 0.008

and at equilibrium for reaction 1

$$A_{eq} = \alpha_{C_2F_4I_2}P^e_{C_2F_4I_2} + \alpha_{I_2}P^e_{I_2}$$

therefore

$$\Delta A = A_{eq} - A_0 = \alpha_{C_2F_4I_2}P^e_{C_2F_4I_2} + \alpha_{I_2}(P^e_{I_2} - P^\circ_{I_2})$$

From stoichiometry

$$P^\circ_{I_2} - P^e_{I_2} = P_{C_2F_4I_2}$$

so that

$$\Delta A = (\alpha_{C_2F_4I_2} - \alpha_{I_2})P^e_{C_2F_4I_2} = \alpha' P^e_{C_2F_4I_2} \quad (3)$$

The equilibrium constant, K, for reaction 1 becomes

$$K = \frac{\Delta A/\alpha'}{(P^\circ_{I_2} - \Delta A/\alpha')(P^\circ_{C_2F_4} - \Delta A/\alpha')} \quad (4)$$

If conditions are chosen such that $P°_{C_2F_4} \gg P^e_{C_2F_4I_2}$ and $P°_{C_2F_4}/P°_{I_2} \leq 10$ to limit telomer formation, then eq 4 may be simplified and rearranged to yield, at 270 nm

$$\frac{P°_{I_2}}{\Delta A} = \frac{1}{\alpha' K P°_{C_2F_4}} + \frac{1}{\alpha'} \quad (5)$$

Thus a plot of $(P°_{I_2}/\Delta A)$ vs $(P°_{C_2F_4})^{-1}$ will yield both K and α'.

Results

If the partial pressure of $C_2F_4I_2$ is small, even compared to the partial pressure of iodine, then eq 4 may be further simplified to yield an apparent equilibrium constant, K_{ap}, defined by

$$K_{ap} = \Delta A / P°_{I_2} P°_{C_2F_4} \quad (6)$$

It should be noted that, while K_{ap} will be approximately equal to $\alpha' K$, as determined from eq 5, it will be smaller than this value, approaching it only as the partial pressure of $C_2F_4I_2$ becomes negligible compared with both iodine and C_2F_4.

The data for the equilibrium study of reaction 1 are summarized in Table I and the resulting values of K_{ap}, and its average, at each temperature are given in the last column of Table I. It should be noted that, at several temperatures, the partial pressure of iodine has been varied by a factor of 2, that of C_2F_4 by a factor of at least 4 and the ratio, $P°_{C_2F_4}/P°_{I_2}$ has been varied from 2 to 10; yet the values of K_{ap} are constant with an average deviation of 4% or less. This establishes the fact that equilibrium is, indeed, achieved and that $P^e_{C_2F_4I_2}$ is small compared with $P°_{I_2}$ and $P°_{C_2F_4}$.

If telomerization were occurring under the experimental conditions of Table I one would expect this to increase the concentration of organic iodides and, thereby, the experimental value of ΔA and K_{ap}. Since the extent of telomerization increases with increasing $P°_{C_2F_4}$ for a given $P°_{I_2}$ so should K_{ap}. On the other hand, in the absence of side reactions, eq 5 would predict that, for a given $P°_{I_2}$, K_{ap} should decrease with increasing $P°_{C_2F_4}$. This latter is, indeed, the observed trend in K_{ap} (see particularly the data at 496, 519, and 537 K in Table I) and provides experimental verification that side reactions, previously observed for ratios of $P°_{C_2F_4}/P°_{I_2} > 50$, are unimportant under the experimental conditions of Table I.

As these preliminary considerations have established that reaction 1 is the only process taking place to any significant extent and that equilibrium has been achieved, one may then analyze the data of Table I in terms of eq 5 to obtain values of $\alpha' K$ that take into account the small amount of iodine that has been consumed in reaching equilibrium. The values of $\alpha' K$, α', and their standard deviations obtained from a least-squares analysis of the equilibrium data at each temperature are given in Table II. As expected, the values of $\alpha' K$ are from 5 to 10% greater than the corresponding mean values of K_{ap} and the values of α' are very imprecise because of the small variation in K_{ap}.

Extinction coefficients at absorbtion maxima are nominally independent of temperature, particularly over narrow ranges such as used here. Consequently $\alpha' T$ may be taken as constant and log $(\alpha' KT)$ will have the same temperature dependence as does log K. A plot of log $(\alpha' KT)$ vs $1/T$ for the data of Table II is given in Figure 1 and a least-squares analysis of the expected linear relation yields the heat of

TABLE II: Summary of the Analysis of the Data at 270 nm for Equilibrium in the Reaction $C_2F_4 + I_2 = CF_2ICF_2I$ at Various Temperatures (See Eq 5)

Temp, K	$\alpha' K$,[a] 10^{-1} OD Torr^{-1}	α',[a] OD Torr^{-1}
477.2	5.45 ± 0.3	0.45 ± 0.3
496.2	2.67 ± 0.09	0.32 ± 0.18
519.0	1.29 ± 0.02	0.35 ± 0.12
537.5	0.729 ± 0.02	0.13 ± 0.06
562.5	0.358 ± 0.003	0.093 ± 0.02

[a] Errors are one standard deviation.

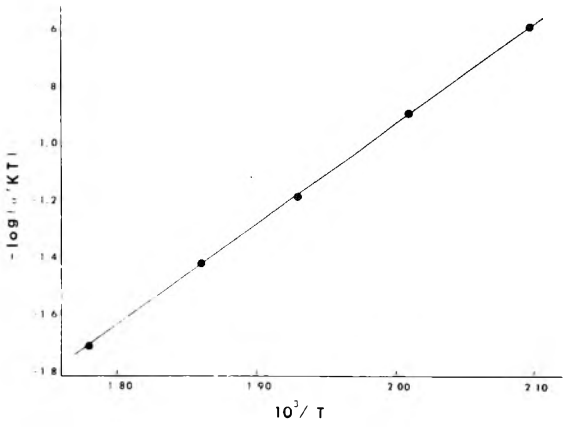

Figure 1. A plot of log $(\alpha' KT)$ vs. $1000/T$ for the reaction $CF_2{=}CF_2 + I_2 = CF_2ICF_2I$.

reaction 1 at 500 K, the mean reaction temperature; $\Delta H_r°$ (1,500) = −15.9 ± 0.1 kcal mol^{-1}.

The imprecision quoted is one standard deviation, however, due to the approximations made in the determination of $\Delta H_r°$ (1,500) an imprecision of ±0.5 kcal mol^{-1} seems more appropriate so that the preferred value becomes $\Delta H_r°$ (1,500) = −15.9 ± 0.5 kcal mol^{-1}. It may be noted that a plot of log $(K_{ap}T)$ vs $1/T$ yields results essentially indistinguishable from the above.

Discussion

(a) Heat of Formation of CF_2ICF_2I. The heat of reaction 1 may be corrected to 298.15 K using the thermodynamic data Ford and Rodgers[6] for CF_2ICF_2I and that of the JANAF Thermochemical Tables[11] for $CF_2{=}CF_2$ and I_2. This yields $\Delta H_r°$ (1,298) = −16.6 ± 0.5 kcal mol^{-1}. Further, $\Delta H_f°$ (I_2,g,298) = 14.92 and $\Delta H_f°$ (C_2F_4,g,298) = −157.4 ± 0.2 kcal mol^{-1}, consistent with the recent values of $\Delta H_f°$ (HF,aq,298).[12] When $\Delta H_r°$ (1,298) is combined with the above, one obtains $\Delta H_f°$ (CF_2ICF_2I,g,298) = −159.1 ± 0.5 kcal mol^{-1}.

(b) Heat of Formation of CF_3CF_2I. It is the fundamental basis of the method of group additivity that disproportionation reactions of type 7 have approximately zero heat of

$$RNNR + SNNS = 2RNNS \quad (7)$$

reaction[3a] and this has been verified for many classes of compounds.[3] However, it has been suggested,[3b] and recently confirmed,[4] that for groups (RN,SN) of very different polarity this approximation may not be valid. Thus, for reaction 8 $\Delta H_r°$ (8,298) = −15.6 kcal mol^{-1}.[4] However,

$$CF_3CF_3 + CH_3CH_3 = 2CF_3CH_3 \quad (8)$$

such should not be the case for reaction 9 so that one can

$$CF_3CF_3 + CF_2ICF_2I = 2CF_3CF_2I. \quad (9)$$

expect, to a very good approximation, that $\Delta H_r°$ (9,298) = 0 ± 2 kcal mol^{-1}. This is combined with $\Delta H_f°$ (CF_3CF_3,g,298) = −320.9 ± 0.8 kcal mol^{-1} [5] to yield $\Delta H_f°$ (CF_3CF_2I,g,298) = −240.0 ± 1 kcal mol^{-1}.

(c) Estimated Entropy Change for Reaction 1. The experimental results for α' at each temperature are very imprecise due, essentially, to the small partial pressures of $C_2F_4I_2$ formed at equilibrium. However, advantage can be taken of the fact that $\alpha'T$ is expected to be independent of temperature over a 100° range, so that an average of the five values of $\alpha'T$ can be used to obtain a "best" value of α' and, therefore, of the equilibrium constant. The data of Table II yield $(\alpha'T)_{av}$ = 136 ± 60 OD K Torr^{-1}. This seems a reasonable result when compared with the value $(\alpha'T)_{av}$ = 46.8 ± 0.6 OD K Torr^{-1} which was obtained for CF_3CF_2I in the same system and over the same temperature range. The individual values of $\alpha'T$ in Table II appear to decrease with increasing temperature, however, there is no reason, either theoretical or statistical, to regard this trend as real. This view is also supported by the absence of a temperature dependence in the much more precise values of $\alpha'T$ obtained for CF_3CF_2I.

Thus, at the mean reaction temperature, 519 K, α' = 0.26 ± 0.11 OD Torr^{-1} so that K_{eq} (519 K) = 0.38 ± 0.16 atm^{-1}. This result may be combined with $\Delta H_r°$ (1,519) = −15.9 ± 0.5 kcal mol^{-1} to yield $\Delta S_r°$ (1,519) = −32.6 ± 1.2 cal mol^{-1} K^{-1}.

The entropy of CF_2ICF_2I has been estimated statistically[6] and this result, combined with the entropies of C_2F_4 and I_2,[11] lead to $\Delta S_r°$ (1,500) = −35.1 ± 2 cal mol^{-1} K^{-1}. The satisfactory agreement between these two estimates further confirms the value for the enthalpy of reaction 1 reported here.

References and Notes

(1) (a) This research was supported by the Robert A. Welch Foundation. (b) Robert A. Welch Foundation Post-Doctoral Fellow.
(2) S. W. Benson and A. Amano, *J. Chem. Phys.*, **36**, 3464 (1962).
(3) (a) S. W. Benson and J. H. Buss, *J. Chem. Phys.*, **29**, 546 (1958); (b) S. W. Benson, F. R. Cruickshank, D. M. Golden, G. R. Haugen, H. E. O'Neal, A. S. Rodgers, R. Shaw, and R. Walsh, *Chem. Rev.*, **69**, 279 (1969).
(4) A. S. Rodgers and W. G. F. Ford, *Int. J. Chem. Kinet.*, **5**, 965 (1973).
(5) S. S. Chem, A. S. Rodgers, J. Chao, R. C. Wilhoit, and B. J. Zwolinski, *Nat. Stand. Ref. Data Ser., Nat. Bur. Stand.*, **No. 3-35706** (Jan 1974).
(6) W. G. F. Ford and A. S. Rodgers, unpublished results.
(7) E. C. Wu and A. S. Rodgers, *Int. J. Chem. Kinet.*, **5**, 1001 (1973).
(8) J. P. Sloan, J. M. Tedder, and J. C. Walton, *J. Chem. Soc., Faraday Trans. 1*, 1143 (1973).
(9) R. N. Haszeldine, S. Lythgoe, and P. J. Robinson, *J. Chem. Soc. B*, 1634 (1970).
(10) H. W. Sidebottom, J. M. Tedder, and J. C. Walton, *Trans. Faraday Soc.*, **66**, 2038 (1970).
(11) "JANAF Thermochemical Tables", Dan Stull, Ed., The Dow Thermal Laboratory, Dow Chemical Co., Midland, Mich., U.S. Department of Commerce, PB No. 168370 and supplements.
(12) G. K. Johnson, P. N. Smith, and W. N. Hubbard, *J. Chem. Thermodyn.*, **5**, 793 (1973).

Dipole Moment and Dimerization Equilibria of Inorganic Salts Dissolved in Weakly Polar Solvents

Danielle Ménard and Martial Chabanel*

Laboratoire de Spectrochimie Moléculaire. U.E.R. de Chimie, 44037 Nantes-Cedex, France

(Received March 27, 1974; Revised Manuscript Received January 20, 1975)

Publication costs assisted by the University of Nantes

The association of lithium and silver salts in some solvents of low dielectric constant was studied by means of dielectric measurements. The results indicate that, in most cases, ion pairs associate to form dimers. The following order of solvent associating power was found: dimethyl carbonate (DMC) < diethyl carbonate (DEC) < dimethoxymethane (DMM) < diethyl ether. The values of dipole moments of ion pairs are for LiBr, 8.1 D, for LiNCS, 10.5 D, for $LiClO_4$, 10.6 D, and for $AgClO_4$, 10.9 D. These results are interpreted by using a polarizable ion-pair model.

Introduction

An ionic crystal can be considered as a huge aggregate $M_n^+X_n^-$. If its temperature becomes sufficiently high the crystal is broken into small fragments and it vaporizes. The vapors are composed of ion pairs M^+X^- and of higher neutral aggregates $M_n^+X_n^-$ with small values of n.[1] Free ions are not present in measurable amounts because their energy is very high.

Fragmentation of the crystals is facilitated by a solvent S provided that there are strong solute–solvent interactions. In this case the dissolution of the crystal is effective at ordinary temperatures. If the solvent is very basic, M^+X^- interactions, which ensure the stability of the crystal, are entirely replaced in solution by M^+–S interactions, and S is a highly ionizing solvent.

On the other hand, in moderately or weakly basic solvents, the competition between M^+–S and M^+–X^- interactions must be taken into consideration. There is first an

equilibrium between solvated ions and ion pairs $M^+X^-S_n$. Much work has been done concerning this problem, especially using conductivity measurements.[2] If the basicity of the solvent is low, formation of higher aggregates $M_k^+X_l^-S_m$ must also be taken into account. In such solvents of low dielectric constant (e.g., $\epsilon < 5$) ionic conductivity is small, at least in dilute solutions, and it gives little information about predominant neutral species.[3] However, low-frequency dielectric measurements become feasible. They can be applied to complex formation[4] and self-association studies, as in the case of molecular associations. Few such studies have been reported because solubility and conductivity impose severe restrictions. Yet, several authors[5] have studied self-association of organic 1-1 salts to determine the dipole moment of ion pairs. A nonpolar solvent, generally benzene, has been chosen, but it dissolves no common inorganic salt except $AgClO_4$.

This lead us to choose slightly polar solvents in this work. Organic carbonates $(RO)_2CO$ have a C=O group with a dipole moment almost balanced by the two C-O-C dipoles. Thus, the total dipole and the dielectric constant are very low ($\epsilon \leq 3.1$). Aliphatic ethers ($\epsilon \leq 4.2$) and dimethoxymethane ($\epsilon = 2.7$) have similar properties. In these solvents the solubility of lithium 1-1 salts with a large anion (LiBr, $LiClO_4$, LiSCN, . . .) is high. The solubility of $AgClO_4$ is much smaller (≤ 0.1 *M*). Dioxane is a poor solvent probably because it forms stable solid solvates in which dioxane molecules are in bridging positions.[6a]

Experimental Section

Commercial dimethyl carbonate (DMC) and diethyl carbonate (DEC) contain small amounts of water and alcohol (methanol or ethanol) which form azeotropes.[7] These solvents were distilled and then stored several days on molecular sieves 4 Å (Merck LAB beads). High-purity DMC was obtained by freezing slowly the refined solvent in a cryostat at 2°. Each time approximately 80% of the solvent was retained for the subsequent crystallization. This operation was repeated three times. Some physical constants were determined concerning this compound: melting point 4.65 ± 0.05°, dielectric constant $\epsilon = 3.087 \pm 0.005$ at 25°. The variation of ϵ with temperature is represented by the formula $d\epsilon/dt = -2.0 \times 10^{-5}(t - 65)$, which corresponds to a slow parabolic variation. Dimethoxymethane (DMM) and diethyl ether (Baker Analyzed Reagents) were dried on sodium wire, then distilled, and stored on molecular sieves 4 Å.

LiBr (Prolabo pur) was dried at 150° for 48 hr. $AgClO_4$ and LiSCN (Alfa Inorganics) were dried under vacuum in a drying pistol at 110° for 8 hr. $LiClO_4$ (Fluka purum anhydrous) was dried at 300° under vacuum.

All solutions used in a series of measurements were prepared by diluting the most concentrated one. Three series of measurements were made for each system. $LiClO_4$ was weighed before preparing the solution. The solutions of other salts were titrated by Volhard's method. A weighed sample of solution was poured into water without separating the solvent and it was magnetically stirred during the titration. Pure salts were analyzed using the same method.

Dielectric constants and refractive indexes were measured at 25 ± 0.1°. A WTW DM/01 dipolmeter, using a fixed frequency of 2 MHz, was equipped with DFL 1 and DFL 2 cells. Refractive indexes of concentrated solutions were measured with an Abbe refractometer. When only dilute solutions were available ($AgClO_4$), refractive indexes were calculated from ionic polarizations.

Results

Dimerization Equilibria. Our cryoscopic measurements in DMC[8] have shown that, even in concentrated solutions, the association numbers of lithium salts are never significantly higher than two. The same result has been found by Batson and Kraus[9] for $AgClO_4$ in benzene. Although in some cases higher polymerization may occur, it is assumed that at low concentrations the only equilibrium is

$$2A \overset{K}{\rightleftharpoons} A_2$$
$$c(1 - x) \quad cx/2$$

A = ion pair A_2 = dimer

where c is the molarity of the salt and $\Delta\epsilon$ is the difference between the dielectric constants of the solution and of the solvent. If it is assumed that interactions between solute particles are negligible

$$\Delta\epsilon = \delta_1[A] + \delta_2[A_2] \tag{1}$$

From these definitions it is readily shown that

$$\Delta\epsilon/c = \delta_1 - (\delta_1 - \delta_2/2)x \tag{2}$$

and

$$x = \frac{4Kc}{1 + 4Kc + (1 + 8Kc)^{1/2}} \tag{3}$$

An approximate value of K is first calculated by using the experimental data at three concentrations. This value is obtained by a third degree equation, after elimination of δ_1 and δ_2. The result then is improved by plotting $\Delta\epsilon/c$ against x for different values of K. The selected value corresponds to the best correlation coefficient in the linear regression. $\delta_2/2 - \delta_1$ and δ_1 are the slope and the $\Delta\epsilon/c$ intercept. This method also provides the uncertainties about K, δ_1, and δ_2. The most precise extrapolation is obtained with the less associating solvent. Concerning highly associating solvents (DMM and ether), extrapolation to zero concentration is impossible. δ_1 is calculated assuming that ion pairs have the same dipole moment as in less associating solvents. The curves, $\Delta\epsilon/c$ against c, were fitted within experimental error in the studied range of concentrations as shown in Figure 1. Bauge and Smith[5] used a different linearization procedure (δ_2 is adjusted instead of K). It has been verified that their method provides the same results as ours.

For the $LiClO_4$-DMC system, ionic conductivity appears at low concentrations. Although measurements could not be quantitatively interpreted, it is obvious that $LiClO_4$ is self-associated to only a slight extent in this solvent. On the other hand, LiBr is almost completely dimerized in DMM as shown by the linearity of the plot of $\Delta\epsilon$ against c (slope 0.5 M^{-1}), and by Boule's isopiestic measurements.[10] We have shown that LiBr forms tetrameric species in diethyl ether.[11] The study of LiSCN is of particular interest because the dimer was identified by its infrared spectrum in ester solutions.[12] In ether LiSCN is completely dimerized even at low concentrations ($\Delta\epsilon/c = 0.15\ M^{-1}$).

The results are summarized in Table I. Errors in calculated values of δ_1 and δ_2 are about ±0.5. K values are given with an uncertainty of ±20%.

Dipole Moment of Ion Pairs. Several theoretical or semiempirical formulas have been proposed for dipole moment

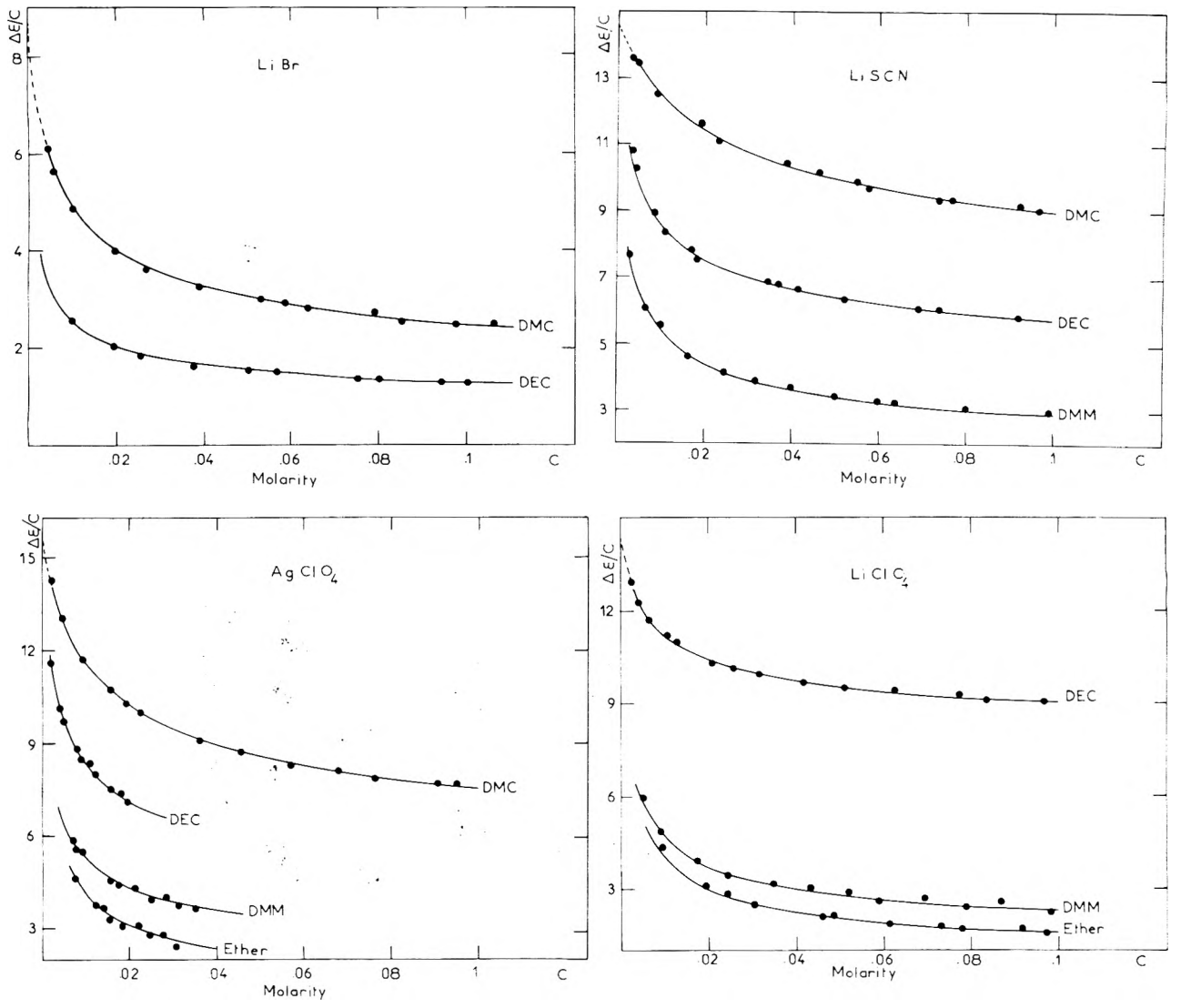

Figure 1. Dielectric constant increments of salts in various solvents.

calculations in polar solvents. Onsager's formula has been adapted for mixtures by Barriol and Weissbecker.[13]

$$\frac{N}{9kT\epsilon_0}\sum_i c_i\mu_i^2 = \frac{(\epsilon - n^2)(2\epsilon + n^2)}{\epsilon(n^2 + 2)^2} \quad (4)$$

where N is Avogadro's number, c_i and μ_i are, respectively, the concentration and the dipole moment of component i, ϵ is the dielectric constant of the solution, and n is its refractive index.

Osipov[14] have proposed a similar formula

$$\frac{N}{9kT\epsilon_0}\sum_i c_i\mu_i^2 = \frac{(\epsilon - 1)(\epsilon + 2)}{8\epsilon} - \frac{(n^2 - 1)(n^2 + 2)}{8n^2} \quad (5)$$

Equations 4 and 5 are identical when $n^2 = 2$. For that reason they yield results which are not significantly different. However, for a binary dilute solution in a nonpolar solvent, eq 4 reduces to Guggenheim's formula. When the solvent is polar, and at infinite dilution, eq 4 gives

$$\mu^2 = \frac{9kT\epsilon_0}{N}\left[A\frac{d\epsilon}{dc} + B\frac{d(n^2)}{dc} - \frac{1}{\rho}\frac{d\rho}{dc} + \frac{M}{\rho}\right]\frac{(\epsilon - n^2)(2\epsilon + n^2)}{\epsilon(n^2 + 2)^2} \quad (6)$$

where

$$A = 1/(\epsilon - n^2) + 2/(2\epsilon + n^2) - 1/\epsilon$$

$$B = -1/(\epsilon - n^2) + 1/(2\epsilon + n^2) - 2/(n^2 + 2)$$

c is the concentration of the solute, ρ is the density of the solvent, and M is the molecular weight of the solute. Increments are extrapolated to zero solute concentration. When the refractive index is measured in the visible région (n_D), Böttcher[15] recommends use of $n^2 = 1.05n_D^2$ in the formulas. This atomic polarization correction may be insufficient when solvent molecules have balanced dipoles.[16] Equation 6 was therefore tested by measuring the dipole moments of some organic molecules in DMC. The values are in good agreement with values in benzene, which are given in parentheses: acetonitrile 3.45 D (3.47); nitrobenzene 3.99 D (3.93); propylenecarbonate 5.05 D (4.98).

The same calculation was applied to ion pairs. As pointed out by Kraus,[17] atomic polarization of ion pairs is negligible. The results are listed in Table II.

Discussion

Dimerization Equilibria. X-Rays have shown that in solid organic solvates,[6] lithium ions are coordinated by four

TABLE I: Dielectric Increments and Dimerization Equilibrium Constants at 25° (M^{-1})

Salt	Solvent	δ_1	δ_2	K	Salt	Solvent	δ_1	δ_2	K
LiBr	DMC	8.7	1.8	90	LiSCN	DMC	14.6	10.8	20
	DEC	8.5[a]	1.3	650		DEC	14.3[a]	8.0	140
						DMM	13.7[a]	3.1	350
$AgClO_4$	DMC	15.7	8.6	45					
	DEC	15.1[a]	6.2	150	$LiClO_4$	DEC	14.7	15.0	90
	DMM	14.8[a]	3.4	500		DMM	14.0[a]	2.0	450
	Ether[b]	16.6[a]	0.6	700		Ether[b]	15.8[a]	0.4	650

[a] δ_1 calculated from the dipole moment of the ion pair. [b] Measurements in ether were achieved at 20°.

TABLE II: Calculated Dipole Moments of Ion Pairs

Ion pair	LiBr	LiNCS	$AgClO_4$	$LiClO_4$
Dipole moment, D	8.1 ± 0.2	10.5 ± 0.3	10.9 ± 0.3	10.6 ± 0.3

ligand molecules. In solutions the coordination numbers determined by various techniques are of the same order.[18]

The successive stages of the association process can be described by the competition between solvent and anion in the first coordination shell of the cation. The first stage is the formation of an ion pair, and the second is a dimerization equilibrium.

The value of K is a measure of the associating power of the solvent. In all investigated cases, the order of increasing K values is independent of the salt. Therefore, the associating power seems to be an intrinsic property of the solvent. It must be emphasized that this order is the same for lithium salts and for $AgClO_4$, although Ag^+ is a soft cation having a large radius. Wong and Popov[19] have made isopiestic measurements concerning salt solutions in acetone and tetrahydrofuran (THF). All these results enable us to propose the following qualitative scale of associating power: acetone < THF < DMC < DEC < DMM < diethyl ether.

Although DMC and DEC are very similar solvents, their associating powers are different. Several factors contribute to this difference: molarity of the pure liquids, dielectric constant, and especially steric hindrance. According to Gutmann,[20] "Steric considerations will become important when small ions are to be coordinated by several large and bulky ligands". Steric factors may also explain why diethyl ether is more associating than carbonates although it is slightly more basic. Respective DN_{SbCl_5} values are 19 and 15, but the basic oxygen atom is more deeply embedded in diethyl ether than in carbonyl compounds. In fact, several lithium compounds are tetrameric in ethers. In these species, each Li^+ cation is probably coordinated by one ether molecule and there is little steric hindrance arising from the solvent. DMM is a flexible molecule, and it is difficult to give any interpretation of its associating power.

In every case the order of increasing stability of salt dimers is $LiClO_4$ < LiSCN < $AgClO_4$ < LiBr. It is roughly the same order as the difference in radii between the anion and cation. When this difference is too small (e.g., LiCl) the crystal is too stable to be dissolved in these solvents. The same conclusion can be drawn from Wong and Popov's results.[19] Kertes and Markovits[21] have observed a similar trend in the stability order of tri-*n*-dodecylammonium aggregates. In this case it is noticeable that the cation is bulkier than the anion.

Dipole Moments. From the values of μ it is possible to derive approximate values of internuclear separations r. Ion pairs, except LiNCS, are considered to be constituted of spherical ions, each of which is polarized by the electrostatic field of the other. If the polarizabilities of the ions are designated α_1, α_2, then the net dipole moment of the ion pair is given by[22]

$$\mu = er\left[1 - \frac{r^3(\alpha_1 + \alpha_2) + 4\alpha_1\alpha_2}{r^6 - 4\alpha_1\alpha_2}\right]$$

Fajan's[23] values of ion polarizabilities in solution were used in the previous formula: $\alpha(Li^+) = 0.03$ Å^3; $\alpha(Br^-) = 4.85$ Å^3; $\alpha(Ag^+) = 2$ Å^3; $\alpha(ClO_4^-) = 5.3$ Å^3. For anions, they are somewhat higher than in the crystalline state.[24] Calculated internuclear separations are: r(LiBr) = 2.49 Å; r(Li-ClO_4) = 2.88 Å; r($AgClO_4$) = 3.18 Å. In the LiBr crystal and in the gaseous ion pair, respective Li–Br distances are 2.74 and 2.17 Å.[25] The corresponding coordination numbers of Li^+ are 6 and 1. In solution an intermediate Li–Br distance results from an intermediate coordination number. A more precise value is inferred from distances in solid solvates having similar coordination shells. In such a LiCl solvate the Li–Cl distance is 2.35 Å.[6b] Owing to the difference in ionic radii between Cl^- and Br^-, this value leads to r(LiBr) = 2.50 Å.

This good agreement arises probably from a compensation between neglected factors. Solvent molecules of the first coordination shell contribute to the dipole moment of the solute, but do not take part in the orientation polarization of the solvent.[26] If this factor is taken into account calculated dipole moment values must be lowered, and the correction is around 0.5–1 D. On the other hand, dipole moment calculations were achieved using a spherical cavity. This model frequently leads to about 10% discrepancies between the Onsager moments and the true moments (see ref 15, p 187). If the ion pair cavity is a prolate ellipsoid this factor provides a positive correction.

In $LiClO_4$ and $AgClO_4$ ion pairs, interatomic distances can be inferred from crystal structures.[27] For a $LiClO_4$ contact ion pair of C_{3v} symmetry, the result is $r(LiClO_4)$ = 3.45 ± 0.20 Å. The value which was deduced from dipole moment measurements is significantly lower. However, other types of coordination cannot be excluded. The dipole moment of the $AgClO_4$ ion pair is in agreement with the value (10.7 D) determined by Hooper and Kraus in benzene.[17]

In the LiNCS ion pair infrared data have shown that lithium is bound to nitrogen.[28] Di Sipio[29] has achieved a theoretical calculation of the atom charges in SCN^-. As indicated by resonant formulas, the carbon atom is neutral. The charges on sulfur and nitrogen atoms are both equal to −0.5 e. The selected values of polarizabilities[22] and interatomic distances[6c,30] are: $\alpha(SCN^-) = 6.8$ Å^3; α(C≡N) = 2.8

Å^3; α(S) = 4.0 Å^3; Li–N = 2.05 Å; C≡N = 1.25 Å; C–S = 1.60 Å. The ratio $\alpha_\parallel/\alpha_\perp = 2.5$ is taken from analogous linear compounds.[31] Two models were considered for the calculation of μ: a linear ion pair and an angular ion pair with LiNC = 120°. Respective values of μ are 12.3 and 10.7 D. In both cases the agreement is satisfactory with the experimental dipole moment.

In the gaseous state and in inert matrices alkali halide dimers are known to be symmetrical quadrupoles.[32] However, in solution, the observed polarization is far from being negligible. For Li_2Br_2, the calculation made from δ_2 gives an apparent dipole moment of 3 D. A similar behavior has been observed by Pohl and coworkers[33] in carboxylic acid dimers. In both cases the atomic polarization is high, owing to low frequency modes, and there may exist some amounts of open dimers and other polymers. In a recent paper Ting Po I and Grunwald[34] have studied the dimerization of LiCl in octanoic acid by dielectric measurements. Their conclusions are in agreement with ours.

References and Notes

(1) R. C. Miller and P. Kusch, *J. Chem. Phys.*, **25**, 860 (1956); J. Berkowitz and W. A. Chupka, *ibid.*, **29**, 653 (1958).
(2) See, for example, S. Petrucci, "Ionic Interactions", Vol. I, Academic Press, New York, N.Y., 1971.
(3) C. E. Strong and C. A. Kraus, *J. Am. Chem. Soc.*, **72**, 166 (1950); H. S. Young and C. A. Kraus, *ibid.*, **73**, 4732 (1951); K. Ekelin and L. Gunnar Sillén, *Acta Chem. Scand.*, **7**, 987 (1953).
(4) P. Bonnet and M. Chabanel, *C. R. Acad. Sci.*, **257**, 1280 (1963).
(5) K. Bauge and J. W. Smith, *J. Chem. Soc.*, 4244 (1964); M. Davies and G. Johansson, *Acta Chem. Scand.*, **18**, 1171 (1964).
(6) (a) F. Durant, Y. Gobillon, P. Piret, and M. Van Meerssche, *Bull. Soc. Chim. Belg.*, **75**, 52 (1966); (b) F. Durant and M. Griffé, *ibid.*, **77**, 557 (1968); (c) F. Durant, P. Piret, and M. Van Meerssche, *Acta Crystallogr.*, **22**, 52 (1967).
(7) Beilstein Handbuch der Organischen Chemie, Band III, Springer Verlag, Vierte Auflage, 1961, p 44.
(8) J. L. Glimois, D. Paoli, and M. Chabanel, *C. R. Acad. Sci., Ser. C*, **277**, 125 (1973).
(9) F. M. Batson and C. A. Kraus, *J. Am. Chem. Soc.*, **56**, 2017 (1934).
(10) P. Boule, Thesis, Nancy, France, *1970*, p 51.
(11) M. Chabanel, *J. Chim. Phys.*, **63**, 1143 (1966).
(12) M. Chabanel, C. Ménard, and G. Guihéneuf, *C. R. Acad. Sci., Ser. C*, **272**, 253 (1971).
(13) J. Barriol and A. Weissbecker, *C. R. Acad. Sci.*, **259**, 2831 (1964).
(14) V. I. Minkin, O. A. Osipov, and Yu. A. Zhdanov, "Dipole Moments in Organic Chemistry", Plenum Press, New York, N.Y., 1970, p 30; O. A. Osipov, *Zh. Fiz. Khim.*, **31**, 1542 (1957).
(15) C. J. F. Bottcher, "Theory of Electric Polarization", Vol. I, Elsevier, Amsterdam, 1973, p 180.
(16) N. E. Hill, W. E. Vaughan, A. H. Price, and M. Davies, "Dielectric Properties and Molecular Behaviour", Van Nostrand-Reinhold, London, 1969, p 245.
(17) G. S. Hooper and C. A. Kraus, *J. Am. Chem. Soc.*, **56**, 2265 (1934).
(18) See, for example, J. F. Hinton and E. S. Amis, *Chem. Rev.*, **71**, 627 (1971).
(19) M. K. Wong and A. I. Popov, *J. Inorg. Nucl. Chem.*, **34**, 3615 (1972).
(20) V. Gutmann, "Coordination Chemistry in Non-Aqueous Solutions", Springer-Verlag, Wien, 1968, p 23.
(21) A. S. Kertes and G. Markovits, *J. Phys. Chem.*, **72**, 4202 (1968).
(22) E. S. Rittner, *J. Chem. Phys.*, **19**, 1030 (1951).
(23) S. S. Batsanov, "Refractometry and Chemical Structure", Consultants Bureau, New York, N.Y., 1961, p 61.
(24) J. R. Tessmann, A. H. Kahn, and W. Shockley, *Phys. Rev.*, **92**, 890 (1953).
(25) A. Honig, M. Mandel, M. L. Stitch, and C. H. Townes, *Phys. Rev.*, **96**, 629 (1954).
(26) E. Glueckauf, *Trans. Faraday Soc.*, 60, 1637 (1964).
(27) R. W. G. Wyckoff, "Crystal Structures", Vol. III, Interscience, New York, N.Y., 1965, p 680.
(28) C. Ménard, B. Wojtkowiak, and M. Chabanel, *Bull. Soc. Chim. Belg.*, **81**, 241 (1972).
(29) L. Di Sipio, L. Oleari, and G. de Michelis, *Coord. Chem. Rev.*, **1**, 7 (1966).
(30) A. C. Hazell, *J. Chem. Soc.*, 5745 (1963).
(31) C. P. Smyth, "Dielectric Behavior and Structure", McGraw-Hill, New York, N.Y., 1955, p 415.
(32) S. H. Bauer, T. Ino, and R. F. Porter, *J. Chem. Phys.*, **33**, 685 (1960); M. Freiberg, A. Ron, and O. Schnepp, *J. Phys. Chem.*, **72**, 3526 (1968).
(33) H. A. Pohl, M. E. Hobbs, and P. M. Gross, *J. Chem. Phys.*, **9**, 408 (1941).
(34) Ting-Po I and E. Grunwald, *J. Am. Chem. Soc.*, **96**, 2387 (1974). This paper was published after our manuscript was submitted for publication.

Osmotic Height and the Calculation of Molecular Weights[1]

George S. Kell* and Edward Whalley*

Division of Chemistry, National Research Council of Canada, Ottawa, Canada K1A OR9

(Received November 5, 1974)

Publication costs assisted by the National Research Council of Canada

A simpler method than the usual one of calculating molecular weights from osmotic measurements is proposed. The osmotic height h, that is, the head of solution above solvent, is divided by the weight fraction w and extrapolated to zero weight fraction. This is equivalent to the more usual method in which the osmotic height is converted to the osmotic pressure by multiplying by the density ρ of the solution and the gravitational field g, and dividing this product by the volume concentration $w\rho$. In the proposed method h/w is plotted; in the conventional one $gh\rho/w\rho$ is plotted.

It is usual in determining molecular weights by osmometry to measure the head h of solution above the solvent, convert the head to the osmotic pressure $\pi = gh\rho$, where g is the intensity of the gravitational field and ρ is the density of solvent or solution, to divide this pressure by the volume concentration $c = w\rho$, where w is the weight fraction of solute, and to plot the quotient $gh\rho/w\rho$ against the concentration. This note points out that such a procedure is unnecessarily complicated, that the osmotic pressure need not be calculated, and that a plot of h/w (or better of $h(1 - w)/w$) against the concentration is all that is required. This procedure has the additional advantage that it is clear that the density and molecular weight of the solvent need not be known, and the difficulties in principle of defining the mo-

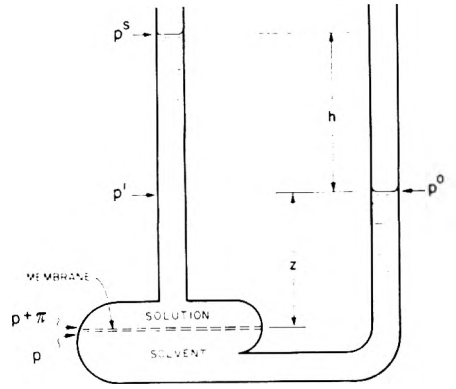

Figure 1. A schematic osmometer, showing the pressures and dimensions referred to in the text.

lecular weight of an associating solvent are seen to be irrelevant. The results of the two methods must, of course, be identical.

Consider the osmotic system for the determination of molecular weights illustrated in Figure 1. The system is in a gravitational (or centrifugal) field, and the solute is involatile and unable to pass the membrane. At equilibrium, the chemical potential of the solvent, including gravitational effects, is everywhere constant. In particular, the values at the two free surfaces are equal, and hence

$$\mu^0(p^0) + \phi^0 = \mu^s(p^s, c_h) + \phi^s \tag{1}$$

where $\mu^0(p^0)$ is the molar chemical potential of pure solvent at zero gravitational potential and with pressure p^0 at the surface. $\mu^s(p^s, c_h)$ is that of solvent at the surface of the solution where the pressure is p^s and the solute concentration is c_h, and ϕ^0 and ϕ^s are the molar gravitational potentials of the solvent at the surfaces of the solvent and solution, respectively. Hence, if the gravitational field intensity is constant

$$\mu^0(p^0) - \mu^s(p^s, c_h) = \phi^s - \phi^0 = gM_1h \tag{2}$$

where M_1 is the molecular weight of the solvent.

This is a remarkable equation whose importance, so far as we know, has not previously been pointed out, although it was given by Chang.[2] It shows that, at equilibrium in the gravitational field, the head h of solution above the surface of the solvent depends only on the differences of chemical potential of the solvent at the two surfaces. In particular, this height is independent of the densities of the solvent and solution, and of the location of the membrane relative to the two surfaces. We propose to call this height the *osmotic height*. Dividing both sides of eq 2 by M_1 shows that the same osmotic height is obtained for the same difference of chemical potential per unit mass of solvent whatever the solvent, whether, for example, it has a low density such as liquid helium, a high density such as liquid platinum, or is highly associated such as liquid water.

This explicit relation between osmotic head and the difference of chemical potentials contrasts with the implicit relation between the osmotic pressure and a somewhat similar difference of chemical potentials

$$\mu^0(p) - \mu^s(p, c_m) = \int_p^{p+\pi} v_1(p, c_m)\, dp = \pi\langle v_1\rangle_{p,p+\pi} \tag{3}$$

where $\mu^0(p)$ and $\mu^s(p, c_m)$ are the chemical potentials at zero gravitational potential of the solvent in pure solvent and solution, respectively, at the indicated pressure and concentration, p and $p + \pi$ are the pressures on the solvent and solution sides of the membrane, π is the osmotic pressure, c_m the concentration of solute in the solution at the level of the membrane, v_1 the partial molar volume of the solvent in the solution, and the brackets $\langle\rangle$ denote the average value of the argument over the pressure range indicated on the lower right-hand side. The concentration c_m is not in general equal to c_h because of the sedimentation equilibrium in the gravitational field. Equation 3 is readily derived by equating the chemical potentials of the solvent on both sides of the membrane, and is the basis for the usual osmometric determination of molecular weights.

In normal osmometric practice the pressure at the surfaces is atmospheric pressure or the vapor pressure, and capillary effects are small and equal in the two limbs, so that $p^0 \sim p^s \sim 0$; pressure can then be dropped as an argument on the left-hand side of eq 2 and 3. Equation 3 is usually approximated by

$$\mu^0 - \mu^s(c) = gh\rho \tag{3a}$$

where ρ is the density of either solvent or solution, which are taken as equal, and the compressibility of the liquid is taken as zero.

On dropping the pressure as an argument, eq 2 becomes

$$-RT \ln a_1(c_h) = gM_1h \tag{4}$$

where a_1 is the activity of the solvent in the solution. If the solution is ideal, eq 4 can be written in terms of the weight fraction w of the solute and the number average molecular weight M_2 of the solute

$$\frac{RT}{gM_1} \ln\left(1 + \frac{w}{1-w}\frac{M_1}{M_2}\right) = h \tag{5}$$

which on expansion gives

$$M_2^{-1} = (g/RT) \lim_{w \to 0} [h(1-w)/w] \tag{6}$$

or

$$M_2^{-1} = (g/RT) \lim_{w \to 0} (h/w) \tag{7}$$

Equations 6 and 7 show that the molecular weight of the solvent plays no part in the determination of the solute molecular weight by osmometry, so the difficulty of defining it, as for an associating solvent, is unimportant.

Sedimentation equilibrium is not reached during a normal osmotic experiment, and may not be attainable because of convection caused by thermal fluctuations. It is perhaps obvious that, because of the limit condition, eq 6 and 7 are correct even when the concentration is uniform, but a direct argument is easily given. When the concentration is uniform, and not in sedimentation equilibrium, the osmotic height is no longer invariant but depends on the position of the membrane, denoted by z in Figure 1, and the nonequilibrium osmotic height h' does not in general equal h. Equilibrium is not complete, but that given by eq 3 holds across the membrane.

If $p^0 = p^s = 0$ and π is expressed in terms of the pressures generated by the hydrostatic columns, then eq 3 becomes

$$-RT \ln a_1(p, c) = \langle v_1(c) \rangle_{p, p+\pi} \left\{ \frac{h'}{\langle \bar{v}^s \rangle_{0, p'}} + \left(\frac{1}{\langle \bar{v}^s \rangle_{p', p+\pi}} - \frac{1}{\langle \bar{v}^0 \rangle_{0, p}} \right) z \right\} g \quad (8)$$

where $\bar{v}^0$ and $\bar{v}^s$ are the specific volumes of the solvent and solution. If pressures p and π are small enough that the pressure dependence of the volumes in eq 8 may be neglected, and if the solution is ideal so that

$$\bar{v}^s = \bar{v}_1 + w(\bar{v}_2 - \bar{v}_1)$$

and

$$v_1/M_1 = \bar{v}_1 = \bar{v}^0$$

then eq 8 becomes

$$\frac{RT}{gM_1} \ln \left(1 + \frac{w}{1 - w} \frac{M_1}{M_2} \right) = \frac{h' + \beta z w}{1 - \beta w} \quad (9)$$

where

$$\beta = (\bar{v}_1 - \bar{v}_2)/\bar{v}_1$$

Hence, eq 6 and 7 are exact if h is replaced by h', either for the limit of low concentration ($w \to 0$) or for ideal solutions at any concentration if the partial specific volumes of solvent and solute are equal ($\beta = 0$) so that sedimentation does not occur. Under either condition the term involving z vanishes, and the right-hand side of eq 9 becomes equal to h of eq 5. As the extrapolation is always to the limit $w \to 0$, eq 6 and 7 are valid for determining M_2 when h' is used instead of h, and if β is small $h' \approx h$ at finite concentrations.

As was mentioned in the first paragraph, the use of eq 3a is equivalent to plotting $gh\rho/w\rho$ against concentration, while the use of eq 7 requires h/w to be plotted. Since it is h and w that are usually measured directly, any conversion of h to π and w to c is therefore quite unnecessary.

The osmotic height can be used in the same way as the osmotic pressure to investigate the nonideality of the solution. Equation 9 can be expanded as a power series in w, and deviations of the coefficients from those predicted by eq 9 measure the interactions of the solute molecules. It is common practice to represent π/c as a power series in c:[3]

$$\pi/c = (\pi/c)_{c=0}(1 + \Gamma_1 c + \Gamma_2 c^2 + \ldots) \quad (10)$$

Since π is usually obtained by multiplying the osmotic height by the density of the solution and by the gravitational field, and c is the weight fraction w multiplied by the density of the solution

$$(\pi/c)/(\pi/c)_{c=0} = (h/w)/(h/w)_{w=0}$$

The coefficients Γ of eq 10 therefore remain unchanged when π/c is replaced by the more directly measured quantity h/w.[3]

References and Notes

(1) NRCC No. 14643.
(2) C.-M. Chang, *Am. J. Phys.*, **40**, 769 (1972).
(3) P. J. Flory, "Principles of Polymer Chemistry", Cornell University Press, Ithaca, N.Y., 1953, p 532.

Densities and Apparent Molal Volumes of Some Aqueous Rare Earth Solutions at 25°. III. Rare Earth Nitrates

F. H. Spedding,* L. E. Shiers, M. A. Brown, J. L. Baker, L. Guitlerrez, L. S. McDowell, and A. Habenschuss

Ames Laboratory—USAEC and Department of Chemistry, Iowa State University, Ames, Iowa 50010 *(Received December 9, 1974)*

Publication costs assisted by Ames Laboratory

The densities of aqueous solutions of $La(NO_3)_3$, $Pr(NO_3)_3$, $Nd(NO_3)_3$, $Sm(NO_3)_3$, $Gd(NO_3)_3$, $Tb(NO_3)_3$, $Dy(NO_3)_3$, $Ho(NO_3)_3$, $Er(NO_3)_3$, $Yb(NO_3)_3$, and $Lu(NO_3)_3$ were determined from approximately 0.03 *m* to saturation at 25° with an accuracy of $\pm 3 \times 10^{-5}$ g/ml by a pycnometric method. The densities are represented with empirical equations. The apparent molal volumes were fitted to semiempirical equations and partial molal volumes were calculated. The partial molal volume data for the nitrate solutions are compared to the rare earth chloride and perchlorate data. The two-series effect in the partial molal volumes of the rare earth nitrates at infinite dilution, attributed to a decrease in the inner-sphere water coordination of the cation, disappears by 0.5 *m*. Above this concentration, the partial molal volumes of the rare earth nitrates generally decrease from $La(NO_3)_3$ to $Lu(NO_3)_3$. These results are interpreted in terms of inner-sphere nitrate complex formation.

Introduction

A two-series effect in the partial molal volumes of the rare earth chlorides, perchlorates, and nitrates at infinite dilution was found to be consistent with a change in inner-sphere water coordination of the cation in the middle of the rare earth series.[1,2] Although the trends for the chlorides and perchlorates were somewhat modified with increasing concentration, due to anion–cation interaction, the persistence of the two-series effect to high concentrations indicated that neither the chloride nor the perchlorate ions penetrate the inner hydration sphere of the rare earth ion.[3,4] Since there is evidence that the nitrate ion tends to

TABLE I: Densities and Apparent Molal Volumes of Some Aqueous Rare Earth Nitrate Solutions at 25°

m	d, g/ml	$10^5\Delta d$	ϕ_V, ml/mol	$\Delta\phi_V$
	$La(NO_3)_3$ M_2 = 324.9202 g/mol			
0.041384	1.00831	−4	52.28	1.27
0.076359	1.01763	−3	54.02	0.71
0.093896	1.02221	4	55.25	−0.04
0.15991	1.03952	3	56.49	0.13
0.24983	1.06271	−1	57.81	0.28
0.35981	1.09041	0	59.39	0.15
0.48912	1.12222	−2	60.87	0.12
0.63972	1.15821	−1	62.42	0.04
1.0003	1.24030	(−20)[a]	65.35	0.09
1.3323	1.31046	5	67.93	−0.15
1.6345	1.37109	(−40)	69.60	0.09
1.9598	1.43159	−0	71.64	−0.08
2.0915	1.45524	−8	72.30	−0.04
2.5231	1.52826	4	74.45	−0.03
2.8925	1.58625	1	76.05	0.02
3.2133	1.63317	(24)	77.38	−0.01
3.6055	1.68736	3	78.77	0.05
3.9997	1.73800	−5	80.05	0.05
4.4561	1.79233	2	81.42	−0.01
4.6100 satd	1.80979	(−1)	81.84	−0.03
	$Pr(NO_3)_3$ M_2 = 326.9224 g/mol			
0.020024	1.00259	1	50.72	−1.41
0.044787	1.00933	2	52.07	−1.15
0.084666	1.02017	−5	52.32	0.27
0.10226	1.02476	7	54.08	−0.92
0.25606	1.06523	−2	56.31	0.20
0.50826	1.12872	−3	59.49	0.28
0.77666	1.19281	5	62.17	0.11
1.0259	1.24952	−0	64.12	0.09
1.3353	1.31616	−1	66.30	0.01
1.6482	1.37960	−3	68.25	−0.04
1.9796	1.44263	5	70.14	−0.10
2.2873	1.49782	−5	71.67	−0.07
2.6134	1.55269	3	73.22	−0.08
2.9405	1.60455	−3	74.62	−0.03
3.2453	1.65002	0	75.84	−0.01
3.5734	1.69625	−1	77.05	0.03
3.9246	1.74270	6	78.26	0.04
4.2189	1.77958	−0	79.18	0.06
4.5344	1.81703	−0	80.11	0.05
4.9102	1.85918	−6	81.13	0.01
5.2340[b]	1.89335	3	81.96	−0.07
	$Nd(NO_3)_3$ M_2 = 330.2547 g/mol			
0.020682	1.00287	−1	49.24	0.21
0.040148	1.00825	0	50.75	0.04
0.060371	1.01380	1	51.74	0.04
0.079755	1.01910	0	52.32	0.20
0.099336	1.02444	−2	52.70	0.45
0.10235	1.02512	(12)	54.10	−0.86
0.16385	1.04177	0	54.41	0.35
0.25617	1.06617	1	56.04	0.37
0.36966	1.09556	0	57.55	0.37
0.50312	1.12929	0	59.06	0.31
0.61514	1.15694	1	60.16	0.24
0.83422	1.20937	−2	62.03	0.14
1.0319	1.25481	−2	63.56	0.04
1.2503	1.30302	1	65.11	−0.07
1.4910	1.35389	0	66.65	−0.13
1.7550	1.40699	3	68.23	−0.17
2.0330	1.46013	−1	69.73	−0.15

TABLE I *(Continued)*

m	d, g/ml	$10^5 \Delta d$	ϕ_V, ml/mol	$\Delta\phi_V$
2.3452	1.51650	−3	71.30	−0.11
2.6621	1.57036	−2	72.77	−0.05
3.0361	1.62988	3	74.37	0.02
3.3940	1.68314	2	75.76	0.09
3.5944	1.71151	−3	76.49	0.13
4.1440	1.78409	0	78.35	0.15
4.6184 satd	1.83999	(132)	80.00	−0.15
	$Sm(NO_3)_3$ M_2 = 336.4147 g/mol			
0.010260	1.00002	−1	48.84	0.02
0.022290	1.00341	2	51.33	−1.29
0.050090	1.01124	2	52.26	−0.58
0.078260	1.01914	−2	52.67	0.11
0.10059	1.02531	1	53.57	−0.12
0.25117	1.06635	−1	56.08	0.21
0.49468	1.13028	0	58.70	0.21
0.75200	1.19485	1	60.80	0.13
1.0107	1.25684	−3	62.57	0.08
1.2834	1.31894	5	64.36	−0.06
1.5943	1.38612	−2	66.14	−0.07
1.8961	1.44759	−1	67.78	−0.09
2.1973	1.50550	1	69.31	−0.09
2.4808	1.55715	−5	70.63	−0.04
2.8069	1.61307	4	72.11	−0.02
3.1028	1.66100	4	73.33	0.03
3.3953	1.70592	−2	74.47	0.08
3.7033	1.75063	−3	75.59	0.10
4.1149	1.80654	1	77.01	0.08
4.2800 satd	1.82668	(119)	77.74	−0.15
	$Gd(NO_3)_3$ M_2 = 343.2647 g/mol			
0.022166	1.00354	0	50.70	−0.31
0.041290	1.00906	1	51.75	−0.41
0.062050	1.01503	1	52.31	−0.23
0.082054	1.02075	1	52.82	−0.19
0.10384	1.02695	1	53.30	−0.16
0.15321	1.04092	−1	54.05	0.02
0.20684	1.05593	−1	54.83	0.04
0.29466	1.08019	−0	55.89	0.03
0.40924	1.11130	0	56.99	0.04
0.59908	1.16152	1	58.51	0.06
0.79553	1.21178	1	59.90	0.04
1.0108	1.26478	(13)	61.39	−0.08
1.2150	1.31345	0	62.52	0.00
1.5064	1.37969	−2	64.17	−0.01
1.7330	1.42876	0	65.40	−0.03
2.0006	1.48413	0	66.77	−0.04
2.3960	1.56102	1	68.68	−0.02
2.8318	1.63940	0	70.62	0.01
3.2985	1.71649	−1	72.54	0.04
3.5492	1.75495	(21)	73.57	0.00
3.9377	1.81159	0	74.97	0.03
4.3766 satd	1.87056	(−0)	76.50	−0.03
	$Tb(NO_3)_3$ M_2 = 344.9401 g/mol			
0.016848	1.00203	1	50.06	0.01
0.094733	1.02455	3	52.79	−0.16
0.15741	1.04249	−5	53.33	0.37
0.23503	1.06425	2	54.77	−0.09
0.35715	1.09803	1	55.96	−0.05
0.46609	1.12777	(−17)	56.49	0.34
0.67485	1.18274	−2	58.35	0.04
0.86019	1.23003	−1	59.61	0.03
1.0453	1.27569	4	60.84	−0.03

TABLE I *(Continuea)*

m	d, g/ml	$10^5\Delta d$	ϕ_V, ml/mol	$\Delta\phi_V$
1.2095	1.31507	−5	61.79	0.01
1.5350	1.38944	3	63.75	−0.07
1.7525	1.43674	2	64.96	−0.08
2.0198	1.49230	−1	66.36	−0.07
2.3845	1.56372	−4	68.17	−0.06
2.7500	1.6 3108	(−59)	69.72	0.12
3.1932	1.70557	6	71.77	−0.01
3.6250	1.77312	−2	73.45	0.04
3.9249	1.81689	−2	74.55	0.03
4.3234	1.87134	1	75.95	−0.04
4.5395 satd	1.89989	(−67)	76.57	−0.00
	$Dy(NO_3)_3$ M_2 = 348.5147 g/mol			
0.051710	1.01235	0	51.67	−0.54
0.086310	1.02248	−1	52.16	−0.15
0.10187	1.02698	1	52.67	−0.34
0.12316	1.03319	−2	52.69	0.02
0.15918	1.04352	4	53.56	−0.31
0.20836	1.05767	−3	53.75	0.13
0.24924	1.06923	2	54.40	−0.07
0.35903	1.10004	2	55.35	0.04
0.40587	1.11305	−2	55.64	0.14
0.49183	1.13657	−0	56.36	0.10
0.64211	1.17689	0	57.49	0.07
0.65455	1.18018	0	57.58	0.07
0.81134	1.22108	−1	58.65	0.05
0.89451	1.24228	1	59.23	0.01
1.2055	1.31893	1	61.22	−0.05
1.4951	1.38650	−0	62.95	−0.07
1.7927	1.45223	0	64.64	−0.08
2.0997	1.51632	−2	66.27	−0.05
2.3790	1.57145	−0	67.69	−0.03
2.6907	1.62963	1	69.18	0.00
2.9627	1.67766	4	70.41	0.02
3.2857	1.73169	−3	71.77	0.05
3.5855	1.77898	−4	72.96	0.05
3.8724	1.82176	5	74.06	0.01
4.1729	1.86442	−1	75.12	−0.04
4.7382 satd	1.94038	(−165)	76.71	−0.01
	$Ho(NO_3)_3$ M_2 = 350.9450 g/mol			
0.048979	1.01173	5	50.32	−0.66
0.080570	1.02115	−2	50.23	0.25
0.10262	1.02763	−0	50.94	−0.00
0.25260	1.07113	−2	53.14	−0.09
0.51386	1.14431	−0	55.56	−0.05
0.74507	1.20646	−0	57.27	0.02
1.0038	1.27307	3	59.06	0.02
1.2960	1.34472	−1	60.92	0.05
1.8958	1.48003	−2	64.49	0.01
2.2048	1.54388	4	66.20	−0.03
2.5060	1.60274	−5	67.73	−0.01
2.7897	1.65503	1	69.12	−0.02
3.1053	1.71004	4	70.57	−0.02
3.4038	1.75923	−1	71.84	0.01
4.0116	1.85130	−2	74.21	0.03
3.7089	1.80669	2	73.07	0.02
4.3767	1.90195	−6	75.50	0.02
4.5945	1.93047	7	76.25	−0.03
4.8080	1.95759	−2	76.92	−0.05
5.0184 satd	1.98420	(−98)	77.44	0.03
	$Er(NO_3)_3$ M_2 = 353.2747 g/mol			
0.052290	1.01292	0	48.79	0.49

TABLE I *(Continued)*

m	d, g/ml	$10^5\Delta d$	ϕ_V, ml/mol	$\Delta\phi_V$
0.077123	1.02037	−1	49.37	0.48
0.094973	1.02566	3	50.15	0.04
0.25759	1.07343	−1	52.16	0.15
0.51021	1.14512	−2	54.37	0.20
0.78850	1.22061	0	56.48	0.17
1.0604	1.29090	2	58.38	0.13
1.3576	1.36390	−1	60.33	0.08
1.6795	1.43842	6	62.37	−0.02
2.0131	1.51118	−8	64.28	−0.02
2.3210	1.57437	(−25)	65.94	−0.01
2.6532	1.63805	1	67.75	−0.10
2.9771	1.69660	2	69.33	−0.09
3.3041	1.75219	−2	70.81	−0.05
3.6440	1.80635	4	72.27	−0.02
3.9871	1.85775	−0	73.62	0.03
4.3986	1.91524	−4	75.15	0.08
4.9790	1.98919	1	77.13	0.09
5.1718	2.01209	0	77.75	0.08
5.4348 satd	2.04058	(145)	78.76	−0.15
	$Yb(NO_3)_3$ M_2 = 359.0547 g/mol			
0.010910	1.00050	1	44.46	1.25
0.039933	1.00953	2	45.88	1.12
0.089004	1.02460	5	47.74	0.37
0.15961	1.04610	1	48.76	0.40
0.26098	1.07652	−3	49.93	0.36
0.49754	1.14559	−6	52.09	0.25
0.68938	1.19964	1	53.64	0.15
0.83623	1.23989	4	54.71	0.13
1.0147	1.28755	−1	55.88	0.17
1.2110	1.33823	−3	57.18	0.16
1.4608	1.40004	5	58.85	0.07
1.6868	1.45364	0	60.26	0.05
1.9627	1.51586	10	61.98	−0.04
2.2492	1.57735	−12	63.59	−0.01
2.5522	1.63841	−1	65.32	−0.08
2.8990	1.70411	−2	67.16	−0.09
3.2261	1.76216	−8	68.78	−0.08
3.5764	1.82019	2	70.45	−0.08
3.9936	1.88439	15	72.29	−0.07
4.4452	1.94868	4	74.08	−0.00
4.8152	1.99758	−9	75.42	0.06
5.3065	2.05754	−4	77.10	0.09
5.7613	2.10868	0	78.51	0.09
6.2791	2.16234	2	79.97	0.03
6.6500 satd	2.19776	(27)	80.98	−0.10
	$Lu(NO_3)_3$ M_2 = 360.9847 g/mol			
0.021459	1.00383	3	45.24	0.04
0.052078	1.01337	4	46.60	−0.17
0.078303	1.02151	2	47.03	0.05
0.10185	1.02876	3	47.63	−0.08
0.12013	1.03437	2	47.99	−0.11
0.25639	1.07572	−6	49.59	0.05
0.48636	1.14344	−5	51.74	0.02
0.70229	1.20483	−3	53.36	0.06
1.0174	1.29055	4	55.54	0.08
1.2251	1.34456	7	56.91	0.08
1.5888	1.43444	2	59.19	0.09
1.9073	1.50823	−1	61.13	0.05
2.1106	1.55302	−4	62.33	0.03
2.4492	1.62374	−5	64.28	−0.01
2.7150	1.67603	−4	65.74	−0.04

TABLE I *(Continued)*

m	d, g/ml	$10^5\Delta d$	ϕ_V, ml/mol	$\Delta\phi_V$
3.0163	1.73202	1	67.33	−0.07
3.4854	1.81286	3	69.64	−0.07
3.7220	1.85092	2	70.73	−0.06
4.0163	1.89585	5	72.02	−0.05
4.5152	1.96658	2	74.05	0.00
5.0094	2.03055	−4	75.88	0.05
5.6401	2.10440	−4	77.97	0.09
6.3225	2.17579	3	79.97	0.03
6.8219 satd	2.22337	(−12)	81.27	−0.06

[a] Values in parentheses were not used in the density fits. [b] Supersaturated.

TABLE II: Density Parameters for Eq 1

Salt	$10A_1$	10^2A_2	10^3A_3	10^2A_4	10^3A_5	10^4A_6	10^5SD
$La(NO_3)_3$	2.747493	−1.93018	−4.51778	−1.322959	5.96254	−7.00355	4
$Pr(NO_3)_3$	2.786812	−2.10643	−1.40986	−1.537933	6.65676	−7.98862	4
$Nd(NO_3)_3$	2.835182	−2.71580	9.87898	−2.442123	9.94105	−12.57370	2
$Sm(NO_3)_3$	2.886956	−2.68440	13.04655	−2.673596	10.31408	−12.42615	3
$Gd(NO_3)_3$	2.949410	−2.33233	10.23393	−2.520501	9.76290	−11.87491	1
$Tb(NO_3)_3$	2.982229	−3.03733	26.15436	−4.015640	15.86346	−20.95752	4
$Dy(NO_3)_3$	2.991086	−1.56604	1.40196	−2.023884	7.97219	−8.83279	2
$Ho(NO_3)_3$	3.058792	−3.00625	25.39529	−3.920141	14.90377	−18.45284	4
$Er(NO_3)_3$	3.084099	−2.68772	21.89112	−3.757400	14.47797	−18.01240	4
$Yb(NO_3)_3$	3.182972	−3.51355	33.83783	−4.421273	15.60378	−17.88538	6
$Lu(NO_3)_3$	3.204885	−3.58907	35.31524	−4.475129	15.47975	−17.35439	4

TABLE III: ϕ_V Parameters for Eq 3

Salt	ϕ_V^0	B_2	B_3	B_4	B_5	SD
$La(NO_3)_3$	49.497	−17.403	−5.220	18.477	−7.330	0.22
$Pr(NO_3)_3$	45.525	15.482	−65.255	56.107	−15.246	0.21
$Nd(NO_3)_3$	45.457	27.180	−97.854	84.128	−22.952	0.22
$Sm(NO_3)_3$	45.997	27.391	−104.372	91.026	−24.877	0.18
$Gd(NO_3)_3$	47.127	−4.039	−42.069	46.741	−13.931	0.10
$Tb(NO_3)_3$	47.376	−12.694	−29.531	41.411	−13.449	0.10
$Dy(NO_3)_3$	46.816	−6.137	−47.864	57.938	−18.258	0.11
$Ho(NO_3)_3$	45.769	−20.549	−11.691	28.348	−10.234	0.08
$Er(NO_3)_3$	45.680	−30.869	8.102	14.579	−6.797	0.13
$Yb(NO_3)_3$	43.753	−29.340	2.345	20.032	−8.256	0.18
$Lu(NO_3)_3$	42.509	−21.146	−11.930	28.660	−10.003	0.07

form inner-sphere complexes with rare earth ions,[5-22] it was of interest to examine the partial molal volume trends in these solutions at higher concentrations. If the nitrate ions penetrate the inner hydration sphere of the rare earth cations, substantial changes in the two-series effect should occur with increasing concentration.

Experimental Section

The densities were determined with 20-ml Sprengel-Ostwald pycnometers used in the previous work.[3,4] The volumes of the pycnometers were calibrated to ±0.0002 ml with conductivity water at 25.000 ± 0.005°. The density of water used was 0.9970751 g/ml.[23]

Stock solutions of the stoichiometric salts were prepared from the oxides and nitric acid by the method described previously.[2] The dilutions were made by weight from the stock solutions and conductivity water. The stock and saturated solutions were analyzed by both EDTA[1] and sulfate[2] methods. For the sulfate analysis, the nitrates were first converted to the chloride with HCl before the additions of H_2SO_4. The analyses agreed to ±0.1% in terms of the molality.

Calculations and Results

Densities. The experimental densities and molal concentrations are listed in Table I. The error in the density measurement for the nitrate solutions is $\pm 3 \times 10^{-5}$ g/ml. The absolute errors in the densities due to the 0.1% uncertainty in the concentration of the stock solution (and saturated solution) ranges from $\pm 1 \times 10^{-5}$ g/ml at 0.02 m to ±(150 to 200) $\times 10^{-5}$ g/ml at saturation. However, the internal consistency of the concentrations of the dilutions made by

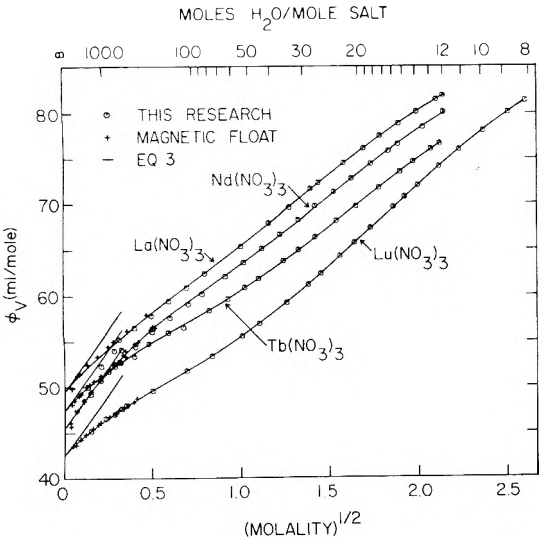

Figure 1. Apparent molal volumes of some aqueous rare earth nitrate solutions at 25°.

weight from the stock solution (excluding the saturated solution) contributes less than $\pm 5 \times 10^{-5}$ g/ml to the error in the density over the whole concentration range. To preserve this internal consistency in the densities, they were fitted to empirical equations of the form

$$d - d^0 = A_1 m + A_2 m^{3/2} + A_3 m^2 + A_4 m^{5/2} + A_5 m^3 + A_6 m^{7/2} \quad (1)$$

generally within $\pm 4 \times 10^{-5}$ g/ml. Since the saturated solutions were analyzed separately, they were not included in these fits. The density of water, d^0, was fixed at 0.9970751 g/ml. The highest concentration for $Pr(NO_3)_3$ is a supersaturated solution; no determination of the saturated value was made for this salt. The parameters in eq 1 and the standard deviations of the fits are given in Table II. The deviations, Δd, of the experimental densities from eq 1 are given in Table I. The experimental and extrapolated densities at saturation agree within the expected error due to the absolute analysis uncertainty for each salt.

Apparent and Partial Molal Volumes. The apparent molal volumes were calculated from

$$\phi_V = \frac{1000(d^0 - d)}{m d d^0} + \frac{M_2}{d} \quad (2)$$

where the symbols have their usual meanings.[3] The experimental apparent molal volumes are listed in Table I, and the results for La, Nd, Tb, and $Lu(NO_3)_3$ are shown in Figure 1. The agreement with the dilute data determined by a magnetic float method[1,2] is excellent. The agreement for the other nitrate solutions is similar. The ϕ_V's were fitted to a Redlich–Meyer type equation[24]

$$\phi_V = \phi_V^0 + S_V \sqrt{d^0} m^{1/2} + B_2 m^{3/4} + B_3 m + B_4 m^{5/4} + B_5 m^{3/2} \quad (3)$$

where S_V (= 27.45) is the Debye–Hückel limiting slope for 3:1 salts and ϕ_V^0, B_2, B_3, ... are empirical constants. In these least-squares fits the dilute, magnetic float data[1,2] were included to constrain the ϕ_V trends at low concentrations. The saturated ϕ_V values were also included.

As shown by Spedding, Cullen, and Habenschuss,[1] the nitrates from La to Gd exhibit positive deviations from the limiting law in dilute solutions. The value of including the theoretical limiting slope in eq 3 for the rare earth nitrate solutions from La to Gd is therefore debatable. However, the theoretical limiting slope was included in eq 3 for all the nitrates since the limiting law is adequately approached for the heavy nitrates, and eq 3 is consistent with the data treatment of the chlorides[3] and perchlorates.[4] Furthermore, the main interest in this paper concerns the more concentrated regions, and eq 3 is adequate in constraining the data at the dilute end of the pycnometric measurements for all the solutions studied. Of course, if the accurate behavior in the dilute region is required, the papers on the magnetic float data[1,2] should be consulted.

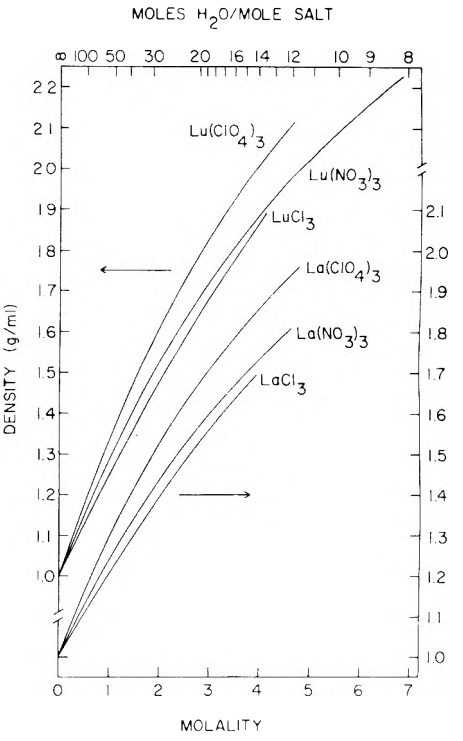

Figure 2. The densities of some rare earth chloride, perchlorate, and nitrate solutions at 25°.

The parameters in eq 3 and the standard deviations of the fits are given in Table III. The deviations, $\Delta\phi_V$, from eq 3 are listed in Table I. The absolute errors in the ϕ_V's are substantially the same as in the chloride and perchlorate measurements, ranging from ±0.2 ml/mol in dilute solutions to ±0.1 ml/mol at saturation.

The partial molal volumes were calculated from

$$\bar{V}_2 = \phi_V + m\left(\frac{\partial \phi_V}{\partial m}\right)_{T,P,n_1} \quad (4)$$

and

$$\bar{V}_1 = \bar{V}_1^0 - \frac{M_1 m^2}{1000}\left(\frac{\partial \phi_V}{\partial m}\right)_{T,P,n_1} \quad (5)$$

where M_1 = 18.0154 g/mol, and $\bar{V}_1^0 = M_1/d^0$.

Discussion

The densities of the rare earth nitrate solutions increase monotonically from La to Lu at any given concentration, in agreement with the expected trend from the atomic weights of the cations. The same order is observed in the densities of the rare earth chloride[3] and perchlorate[4] se-

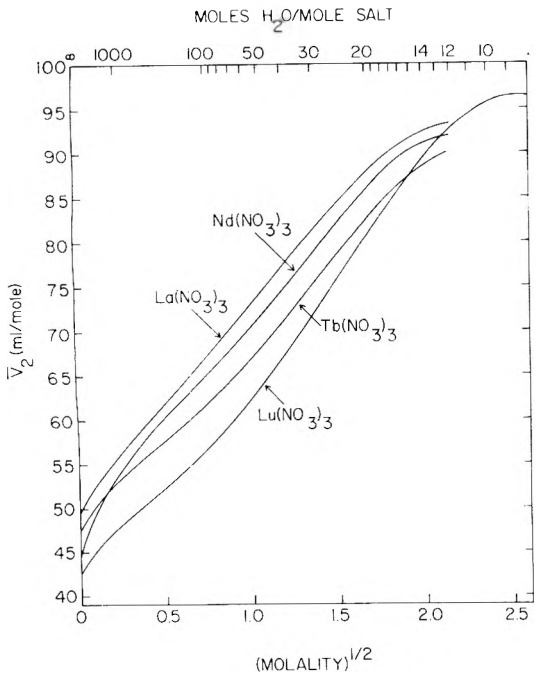

Figure 3. Partial molal volumes of the solute of some rare earth nitrate solutions at 25°.

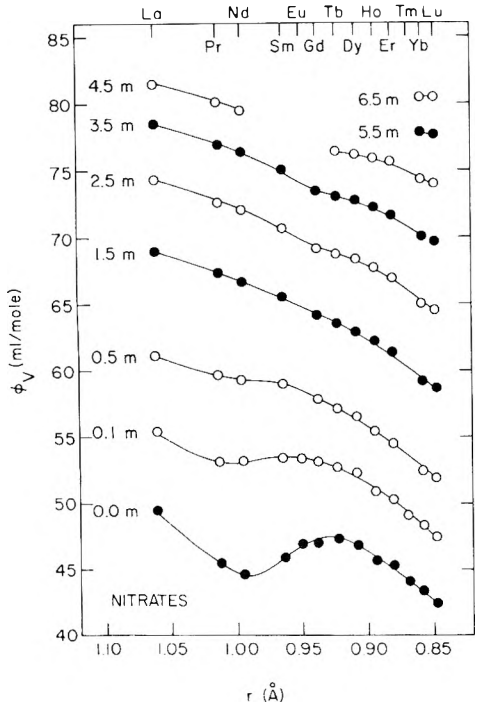

Figure 4. Apparent molal volumes of some aqueous rare earth nitrate solutions at 25°. Values at 0 *m* are taken from ref 1 and 2.

ries.[25] The densities for the three lanthanum and lutetium solutions are compared in Figure 2. The same order occurs for the rest of the rare earth cations[25] and is consistent with the order expected from the anion molecular weights.

The apparent molal volumes of La, Nd, Tb, and Lu nitrates shown in Figure 1 should be compared to similar plots for the chlorides[3] and the perchlorates.[4] At infinite dilution the trends in the ϕ_V^0 ($= \bar{V}_2^0$) are the same in the nitrates as in the chlorides and perchlorates. However, with

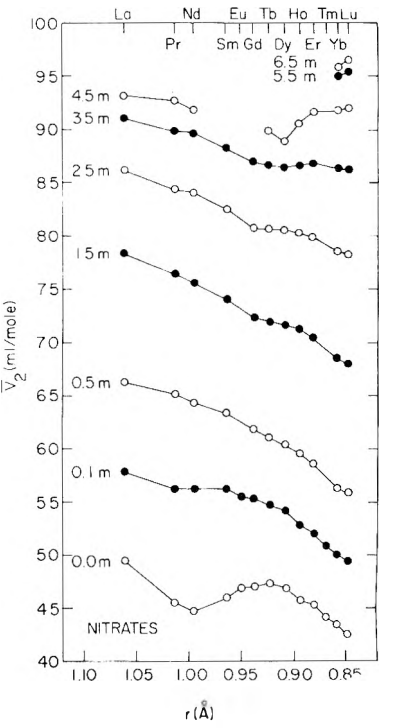

Figure 5. Partial molal volumes of the solute of some aqueous rare earth nitrate solutions at 25°. Values at 0 *m* are taken from ref 1 and 2.

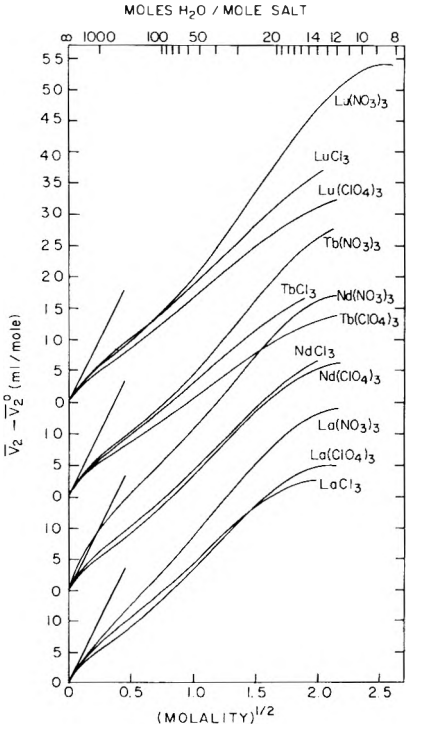

Figure 6. Relative partial molal volumes of the solute for some rare earth chloride, perchlorate, and nitrate solutions at 25°.

increasing concentration the ϕ_V of the nitrate, chloride, and perchlorate series behave differently. For example, the ϕ_V for neodymium and terbium chloride do not cross, while the ϕ_V for neodymium and terbium perchlorate cross at 2.6 *m*. In the nitrates, this crossing occurs at 0.06 *m* (Figure 1). Similar differences occur in the concentration dependence of $\bar{V}_2$, shown for the nitrates in Figure 3.

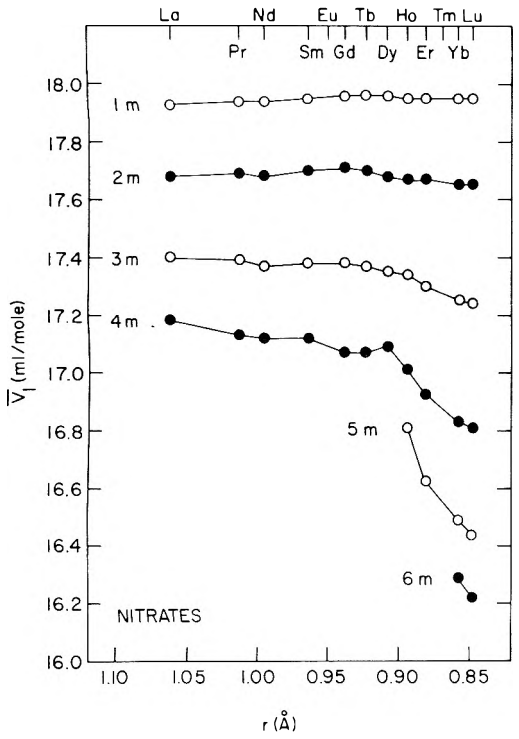

Figure 7. Partial molal volume of the solvent in some rare earth nitrate solutions at 25°.

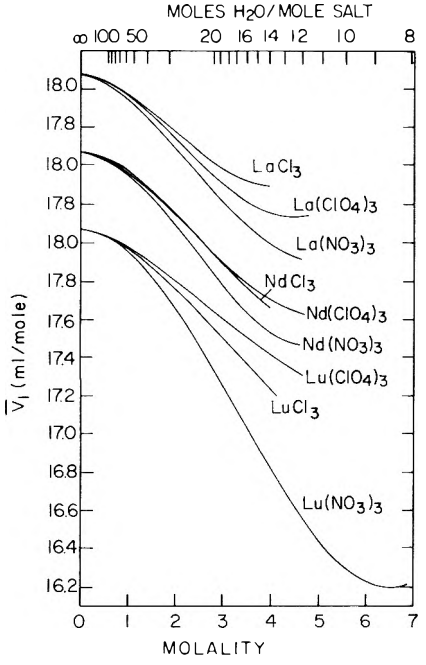

Figure 8. Partial molal volume of the solvent in some rare earth chloride, perchlorate, and nitrate solutions at 25°.

The implication of these differences are most clearly shown in the ϕ_V and $\bar{V}_2$ across the rare earth series presented in Figures 4 and 5 for the nitrates. These should be compared with similar plots for the chlorides[3] and perchlorates.[4] It is apparent that the two-series effect is present at infinite dilution for the three anion series. Since this two-series effect is attributed to a change in inner-sphere cation hydration,[2] and all the salts are 100% ionized at infinite dilution, the $\bar{V}_2^0$ trends should be identical, except for an anion shift. This is indeed found to be the case.[1]

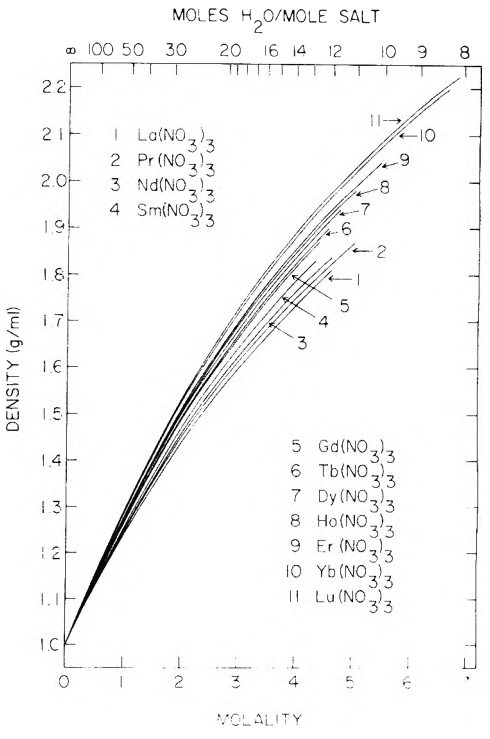

Figure 9. The densities of some rare earth nitrate solutions at 25°.

Although modified somewhat with increasing concentration, the persistence of this two-series effect up to at least 3.5 *m* in the chlorides[3] and perchlorates[4] indicated that the hydration change is operative in the chlorides and perchlorates up to high concentrations, and neither the chloride nor the perchlorate ions penetrate the inner hydration sphere of the cations. In contrast, the two-series effect in the nitrates (Figure 5) is greatly modified by 0.1 *m* and disappears altogether by 0.5 *m*. Since the two-series effect arises from cation inner-sphere water coordination, its disappearance is consistent with the formation of appreciable amounts of inner-sphere ion pairs, where one or more cation inner-sphere waters of hydration are displaced by the nitrate ion(s).

Millero et al.[26,27] have shown that positive deviations (or smaller than expected negative deviations) from the Debye–Hückel limiting slope can be accounted for by ion pair formation (inner and/or outer sphere), since the ΔV of complex formation is positive.[26-34] These conclusions are consistent with the dilute ϕ_V data reported for the nitrates by Spedding et al.[1,2] They found positive deviations in ϕ_V from the limiting law for the light rare earth nitrates, which became more pronounced from La to Nd, decreased to Tb where they became negative deviations, and remained so to Lu. This trend agrees very well with a maximum in the reported stability constants for rare earth nitrate ion pair formation at ionic strengths of one[7,16] and four,[5,6] and with the minimum in the rare earth nitrate conductances below 0.9 *m*.[35] The maximum in the measured stability constants occurs in the region near Sm, and the heavy rare earth nitrates have lower stability constants than the light rare earths.

Excepting the reversal between Nd and Tb, the overall decrease in $\bar{V}_2^0$ at infinite dilution across the rare earth nitrate series is due to the increasing electrostriction of the waters of hydration as the surface charge density on the

rare earth cation increases from La to Lu. The decrease in $\bar{V}_2$ across the series at higher concentration, where inner-sphere nitrate complexes form, is due to either or both of the following. First, we would expect the increasing surface charge density from La to Lu to now act on both the waters of hydration and the inner- and outer-sphere nitrate ions, and their increasing electrostriction would result in a decrease in $\bar{V}_2$ across the rare earth series. Second, the conductance data[35] on the rare earth nitrate solutions indicate that at higher concentrations (>0.9 *m*) the amount of nitrate complex formation decreases from La to Lu. Since ΔV of complex formation is positive,[26-34] this would also result in a decrease in $\bar{V}_2$ across the rare earth series. Obviously, these two effects cannot be separated, and it is likely that both contribute to the decrease in $\bar{V}_2$ from La to Lu.

Just as the decrease in the size of the rare earth ion gives rise to a decrease in inner-sphere water coordination at infinite dilution, similar coordination changes are possible at higher concentration. The larger "kinks" in $\bar{V}_2$ across the series at higher concentrations may be due to such coordination changes. Since the possible coordination changes involve not only the number of water ligands, but also the number and kind (mono- or bidentate) of nitrate ligands, the nature of these coordination changes cannot be unraveled from the volume data.

In Figure 6 we compare the concentration dependence of $\bar{V}_2-\bar{V}_2^0$ for lanthanum, neodymium, gadolinium, and lutetium chlorides, perchlorates, and nitrates. With few exceptions, the perchlorates have the lowest concentration dependence while the nitrates rise most rapidly. Similar curves for the other cations show transitional behavior to those in Figure 6.[25] The partial molal volumes of the water in the rare earth nitrate solutions, $\bar{V}_1$, are shown in Figure 7 at constant molality. The trends reflect the increasing electrostriction and/or the decrease in nitrate complex formation, as well as the absence of the two-series effect, prominent in the $\bar{V}_1$ of the chlorides[3] and perchlorates.[4] The concentration dependence of the $\bar{V}_1$ for the three anions is shown in Figure 8 for the La, Nd, and Lu salts.[25] The chlorides and perchlorates reverse their order between La and Nd. From Sm on, the anion order is the same as in Lu.

Acknowledgment. The authors wish to thank the Ames Laboratory Rare Earth Separation Group for furnishing the oxides. They are also indebted to Dr. J. A. Rard for many helpful discussions.

References and Notes

(1) F. H. Spedding, P. F. Cullen, and A. Habenschuss, *J. Phys. Chem.*, **78**, 1106 (1974).
(2) F. H. Spedding, M. J. Pikal, and B. O. Ayers, *J. Phys. Chem.*, **70**, 2440 (1966).
(3) F. H. Spedding, V. W. Saeger, K. A. Gray, P. K. Boneau, M. A. Brown, C. W. DeKock, J. L. Baker, L. E. Shiers, H. O. Weber, and A. Habenschuss, *J. Chem. Eng. Data*, **20**, 72 (1975).
(4) F. H. Spedding, L. E. Shiers, M. A. Brown, J. L. Derer, D. L. Swanson, and A. Habenschuss, *J. Chem. Eng. Data*, **20**, 81 (1975).
(5) A. Angnostopoulos, P. O. Sakellaridis, *J. Inorg. Nucl. Chem.*, **32**, 1740 (1970).
(6) N. A. Coward, and R. W. Kiser, *J. Phys. Chem.*, **70**, 213 (1966).
(7) D. F. Peppard, G. W. Mason, and I. Hucher, *J. Inorg. Nucl. Chem.*, **24**, 881 (1962).
(8) Y. Marcus and I. Abrahamer, *J. Inorg. Nucl. Chem.*, **22**, 141 (1961).
(9) D. L. Nelson and D. E. Irish, *J. Chem. Phys.*, **54**, 4479 (1971).
(10) J. Knoeck, *Anal. Chem.*, **41**, 2069 (1969).
(11) K. Nakamura and K. Kawamura, *Bull. Chem. Soc. Jpn.*, **44**, 330 (1971).
(12) J. Reuben and D. Fiat, *J. Chem. Phys.*, **51**, 4909 (1969).
(13) I. Abrahamer and Y. Marcus, *Inorg. Chem.*, **6**, 2103 (1967).
(14) H. B. Silber, N. Scheinin, G. Atkinson, and J. Grecsek, *J. Chem. Soc., Faraday Trans. 2*, **68**, 1200 (1972).
(15) R. Garnsey and D. W. Ebdon, *J. Am. Chem. Soc.*, **91**, 50 (1969).
(16) G. R. Choppin and W. F. Strazik, *J. Inorg. Chem.*, **4**, 1250 (1965).
(17) K. Bukietynska and G. R. Choppin, *J. Chem. Phys.*, **52**, 2875 (1970).
(18) G. R. Choppin, D. E. Henrie, and K. Buijs, *Inorg. Chem.*, **5**, 1743 (1966).
(19) B. M. L. Bansal, S. K. Patil, and H. D. Sharma, *J. Inorg. Nucl. Chem.*, **26**, 993 (1963).
(20) I. Abrahamer and Y. Marcus, *J. Inorg. Nucl. Chem.*, **30**, 1563 (1968).
(21) F. H. Spedding and S. Jaffe, *J. Am. Chem. Soc.*, **76**, 884 (1954).
(22) R. E. Hester and R. A. Plane, *Inorg. Chem.*, **3**, 769 (1964).
(23) L. W. Tilton and J. K. Taylor, *J. Res. Natl. Bur. Stand.*, **18**, 205 (1937).
(24) O. Redlich and D. Meyer, *Chem. Rev.*, **64**, 221 (1964).
(25) A complete set of figures can be obtained from the authors.
(26) W. L. Masterton, H. Welles, J. H. Knox, and F. J. Millero, *J. Solution Chem.*, **3**, 91 (1974).
(27) F. J. Millero and W. L. Masterton, *J. Phys. Chem.*, **78**, 1287 (1974).
(28) R. E. Lindstrom and H. E. Wirth, *J. Phys. Chem.*, **73**, 218 (1969).
(29) C. F. Hale and F. H. Spedding, *J. Phys. Chem.*, **76**, 2925 (1972).
(30) F. H. Fisher, *J. Phys. Chem.*, **66**, 1607 (1962).
(31) F. H. Fisher and D. F. Davis, *J. Phys. Chem.*, **71**, 819 (1967).
(32) F. H. Fisher and D. F. Davis, *J. Phys. Chem.*, **69**, 2595 (1965).
(33) S. D. Hamann, P. J. Pearce, and W. Strauss, *J. Phys. Chem.*, **68**, 375 (1964).
(34) T. G. Spiro, A. Revesz, and J. Lee, *J. Am. Chem. Soc.*, **90** 4000 (1968).
(35) J. A. Rard and F. H. Spedding, *J. Phys. Chem.*, **79**, 257 (1975).

An Isochoric Technique for Studying Desorption of Gases from Solids. Preliminary Results on the Water–Bayerite System

I. Y. Wei and Arnulf J. Maeland*

Department of Chemistry, Worcester Polytechnic Institute, Worcester, Massachusetts 01609 *(Received July 16, 1974; Revised Manuscript Received December 30, 1974)*

Publication costs assisted by The Aluminum Association and The American Electroplaters' Society, Incorporated

A method for studying adsorption or desorption phenomena in which the volume and the total amount of adsorbent and adsorbate are kept constant is discussed. The usefulness of this isochoric method is illustrated in the study of the desorption of water from bayerite.

Introduction

Adsorption in a given system is a function of pressure and temperature only and may be described in terms of an empirical adsorption equation

$$X = f(P, T) \quad (1)$$

where X is the amount of gas adsorbed (adsorbate) per unit quantity of solid (adsorbent), P is the equilibrium pressure, and T is the absolute temperature. A common experimental approach to adsorption studies is to determine the amount of gas adsorbed as a function of pressure at constant temperature. The resulting plots are referred to as *isotherms* $X = f_T(P)$.[1,2] One may also keep the pressure constant and determine the amount of gas adsorbed as a function of temperature, or the variation in equilibrium pressure with respect to temperature for a constant amount of gas adsorbed may be determined. In the former case we obtain *isobars*, $X = f_P(T)$, and in the latter case isosteres, $p = f_x(T)$.[1,2] By far the most common method is that of adsorption isotherms.

Under certain conditions we have found that another method, in which the volume and total amount of adsorbent and adsorbate are kept constant, is a convenient and informative procedure. Since this method of study is based on constant volume we shall refer to it as an isochoric adsorption or desorption method. We will describe this method in details and illustrate its usefulness by studying the desorption of water from bayerite.

Experimental Section

The apparatus used in our study was constructed from Pyrex glass and is shown in Figure 1. Referring to Figure 1 the following identifications can be made: A is the sample container with a side arm for introducing the sample, B is a safety device to prevent mercury from being sucked into the sample compartment by accident, C is a capillary tube, D is a mercury reservoir, and E is a stopcock connecting the apparatus to a vacuum line which is equipped with a manometer, a McLeod gauge, and a container for the adsorbate.

The working volume of the apparatus, A plus B, was determined to be 37.8 ± 0.2 ml by filling with water. To start a run approximately 1 g of bayerite, which had been accurately weighed after degassing overnight at 160° under high vacuum, was placed in the bottom of sample tube A through the side arm. The degassing temperature was chosen to be high enough to remove adsorbed water, but not high enough to permit transformation to η-alumina. Our bayerite sample was given to us by Dr. R. C. Spooner of Alcan and contained the following impurities: Fe_2O, 0.005%; SiO_2, 0.15%; TiO_2, 0.001%; V_2O_5, 0.002%; CaO, 0.20%; and Na_2O, 0.81% (Suppliers Analysis). After sealing off the side arm the sample was degassed at 160° under high vacuum for 3 hr. The dead space was determined by filling with helium of known pressure and volume; first the entire apparatus was filled with the mercury in D, and next the apparatus was refilled this time with mercury in the capillary tube C. The sample was then exposed at room temperature for several hours to vapor from previously degassed, distilled water. The amount of water adsorbed can be varied either by controlling the time of exposure to the water vapor or by controlled pumping after prolonged exposure. Mercury from reservoir D was next poured into capillary tube C by tipping the apparatus. The entire apparatus was then placed in a thermostatted oil bath controlled to ±0.01° by a Sargent Hook Model Ed circulating unit. After equilibrium was reached, the pressure of the desorbed gas was measured by adjusting the pressure in the vacuum line until the mercury in the two arms of the capillary tube C was at the same level (zero level); the pressure was read from the manometer attached to the vacuum line. Correction for partial vapor pressure of mercury at the particular temperature of the measurement can be made, although this correction is negligible in the temperature range of this study. The total amount of water adsorbed was determined by heating to 160° and trapping the desorbed vapor in liquid nitrogen and weighing. A new sample was used for each run (which required from 1 to 2 weeks) in order to avoid complications from hysteresis.

Results and Discussion

The simple apparatus, shown in Figure 1, has a pressure range from a few millimeter mercury to perhaps 2–3 atm and may be used in a temperature range up to several hundred degrees provided that a suitable inert and nonvolatile liquid column is used for levelling. Since the total apparatus is in a themostatted bath, it is very useful and convenient for studying volatile materials. For example, if the vapor pressure of the adsorbate is larger than its partial vapor pressure at room temperature, condensation is avoided in this set-up because the entire apparatus is submerged in the thermostatted bath. Once the system is charged, a run through the whole temperature range of interest can be done without tedious adding or removing the adsorbate

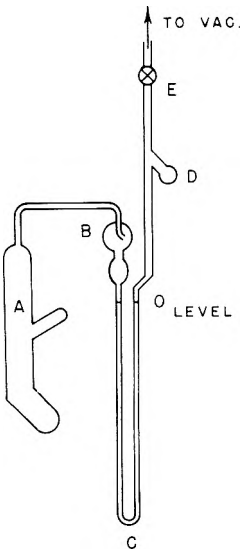

Figure 1. Isochoric desorption apparatus.

which is required in many of the other methods. Furthermore, if a fairly large amount of solid is used and the dead space in A and B is comparatively small, the change of the ratio of adsorbent to adsorbate due to the change of pressure is negligible. Under these circumstances, the apparatus can be used for an isosteric study.

A typical desorption study is shown in Figure 2 where log P is plotted against $1/T$. The initial ratios of adsorbate to adsorbent for runs A through K were 129.6, 50.0, 46.5, 46.1, 44.5, 43.1, 42.7, 42.0, 41.4, 40.6, and 36.1 mg of water/1000.0 mg of bayerite. The heat of desorption may be calculated from the Clausius–Clapeyron equation[1,2]

$$\log P_2 - \log P_1 = \frac{qT_1T_2}{2.30R(T_2 - T_1)} \qquad (2)$$

where R is the gas constant and q is the heat of desorption. It is assumed that the heat of desorption is constant over the temperature range T_1 to T_2, and that the composition remains unchanged, i.e., isosteric conditions. One generally distinguishes two types of adsorption, physical adsorption and chemisorption. The heat of chemisorption is much higher than that of physical adsorption. Physical adsorption may roughly be categorized as multilayer, monolayer, and porous adsorption. The heat of desorption increases in the same order, but the heat of desorption from capillary condensation in pores is much higher than the other two. From a plot of an isochoric study, one may perhaps see the desorption progressing from multilayer to monolayer to porous desorption in a set of runs. For example, it can be seen from Figure 2 that for run A where excess water is condensed on the solid (multilayer) the resulting plot is a straight line from which the heat of desorption can be obtained by the use of eq 2. The heat of desorption determined from A is 10.0 kcal/mol which is pretty close to the value of the heat of vaporization of water, 9.72 kcal/mol at 100°, as one might have expected. Run B shows a straight line between points a and f followed by a less steep portion and then the curve turns up beyond d. Since the plot for run B from a to f is a straight line with the same slope as that of run A, one might conclude that the desorption from a to f is due to multilayer desorption. After f one might be observing monolayer desorption followed by desorption from capillary condensation in pores. For other runs, C to

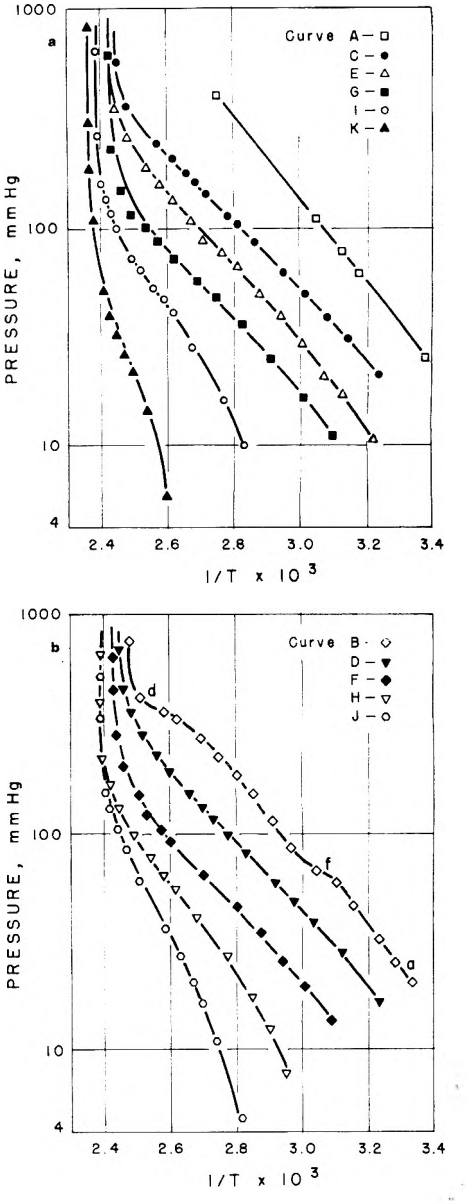

Figure 2. Isochoric desorption of water from bayerite: A, 129.6 mg; B, 50.0 mg; C, 46.5 mg; D, 46.1 mg; E, 44.5 mg; F, 43.1 mg; G, 42.7 mg; H, 42.0 mg; I, 41.4 mg; J, 40.6 mg; K, 36.1 mg of H_2O/1000.0 mg of bayerite.

K, there is no multilayer which is not unexpected because the initial amounts of adsorbate are less than that of run B at point f.

One might expect to obtain the surface area of the adsorbent by determining the amount of monolayer desorption which is possible provided that the various stages of the desorption are distinguishable. This may be done by choosing a suitable ratio for dead volume, adsorbate, and adsorbent. On one hand the dead volume may be chosen to be comparatively large so that complete surface desorption takes place at low temperature and low pressure. As the temperature is raised, the desorption plot may show a flat portion indicating that the desorption from the surface has been completed while the desorption from capillary condensation in pores has not begun. With further increase in temperature a sharp increase in pressure due to the desorption from capillary condensation in pores is expected. Under these conditions we may distinguish between the desorp-

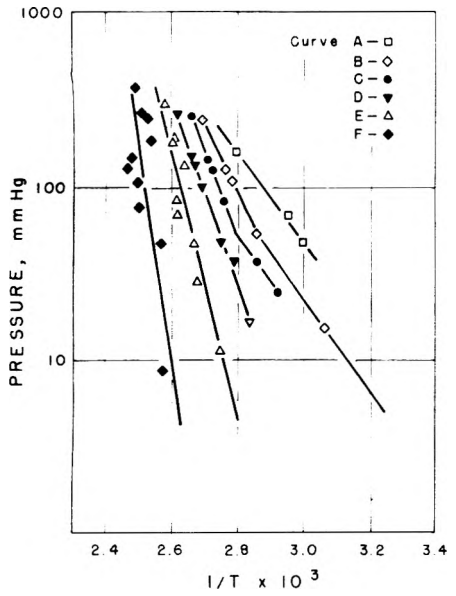

Figure 3. Isosteres in the desorption of water from bayerite: A, 44.3 mg; B, 42.5 mg; C, 41.9 mg; D, 41.3 mg; E, 40.3 mg; F, 39.0 mg H_2O/1000 mg of bayerite.

tion from surface and pores, but not between monolayer and multilayer desorption. On the other hand, the dead volume may be chosen to be comparatively very small and isosteric desorption may be studied. However, between these two extremes one expects to see clearly the changes for all stages of desorption. The comparative ratio of the dead volume and the volume of the adsorbate to be used is of course dependent on the adsorbility of the adsorbent.

If the volume, the pressure, and the initial amount of adsorbate are known, the amount of adsorbate left at any point of observation can be calculated from

$$W_g = \frac{PV}{RT} M \tag{3}$$

and

$$W_t = W_s + W_g \tag{4}$$

where W_g and W_s are the weights of adsorbate in gaseous and solid phase respectively, W_t is the total weight of adsorbate, and M is the molecular weight of adsorbate. The assumption of ideal gas behavior of water is valid in our experiment. Calculations using the semiempirical Berthelot's equation,[3] which is quite accurate for a medium range of pressures, showed that the error introduced into our calculations by assuming ideal gas law behavior was less than 1%.

Since eq 2 is valid only for a system with constant compositions of adsorbate and adsorbent, heats of desorption for monolayers and from capillary condensation in pores may be obtained by connecting the points for all runs which have the same composition. The slopes of the resulting curves give the heats of desorption at a certain composition. The procedure is as follows. If a specific ratio of adsorbate to adsorbent is chosen, the weight of adsorbate in the gaseous phase, W_g, for each isochoric run can be calculated from eq 3 and 4. Under these isosteric conditions eq 3 can be written

$$P/T = W_g R/MV = \text{constant} \tag{5}$$

By selecting different values of T a set of values for P can be calculated. If the temperature and the corresponding calculated pressures are both matched with experimental values in Figure 2, P and T are determined. Thus a plot of isosteres as well as isosteric heats of desorption can be obtained from our isochoric study. Such isosteric plots of desorption (log P vs. $1/T$) with the following ratio of water to bayerite are shown in Figure 3: A, 44.3; B, 42.5; C, 41.9; D, 41.3; E, 40.3; and F, 39.0 mg of water/1000.0 mg of bayerite. The isosteric heats of desorption calculated with a least-squares fit from Figure 3 and eq 2 are: A, 12.3; B, 11.8 and 20.1; C, 12.0 and 24.5; D, 23.2; E, 39.7; and F, 51.3 kcal/mol. The isosteric heats of desorption for A and for the low temperature portions of B and C are 12.3, 11.8, and 12.0 kcal/mol, respectively, which are indeed the same value within experimental error. These values are 2.1 to 2.6 kcal/mol higher than the heat of vaporization of water at 100° and are believed to be due to monolayer desorption. The isosteric heats of desorption for D and the high temperature portions of B and C range from 20.1 to 24.5 kcal/mol. These are probably due to desorption from capillary condensation in pores with different pore size. The heat of desorption from capillary condensation in pores is determined by the pore size and the surface tension of the adsorbate; the larger the pores are the smaller the isosteric heat and vice versa. Also the temperature range for desorption from capillary condensation in pores depends on the distribution of the pore size: the larger the pore size distribution, the larger the temperature range of desorption and vice versa. For E and F the calculated isosteric heats are 39.7 and 51.3 kcal/mol, respectively. These heats are in the range of chemisorption and are accordingly ascribed to structurally adjacent hydroxyl groups combining to lose water. Support for this view may be found in NMR studies. At room temperature the NMR spectrum for bayerite containing adsorbed water consists of a narrow line superimposed on a very broad line. The narrow line is due to adsorbed water and the broad line is due to structural hydroxyl groups. With moderate heating and evacuating the narrow line disappears, as might be expected. However, the broad line also loses intensity, indicating loss of hydroxyl groups. If one operates in a closed system, the conversion of structural hydroxyl groups to adsorbed water may be observed by heating gently to approximately 130°. The broad line decreases in intensity while the narrow line increases.

Isotherms can easily be constructed from an isochoric study by simply picking up a particular temperature and reading the pressures for all the runs at this temperature.

Acknowledgment. This work was supported by a grant from the Aluminum Association and The American Electroplates' Society, Inc. Use of laboratory facilities at Tufts University is gratefully acknowledged (Professor B. M. Fung).

References and Notes

(1) S. Brunauer, "The Adsorption of Gases and Vapors, Vol. 1, Physical Adsorption", Princeton University Press, Princeton, N.J., 1943.
(2) S. J. Gregg and K. S. W. Sing, "Adsorption, Surface Area and Porosity", Academic Press, London, 1967.
(3) J. R. Partington, "An Advanced Treatise on Physical Chemistry, Vol. 1, Fundamental Principles, The Properties of Gases", Longmans, Green and Co., London, 1947, p 706.

Electron Oscillation Effects in the Vibrational Spectra of Tetracyanoquinodimethane Ion Radical Salts

George R. Anderson*

Department of Chemistry, University of Minnesota, Minneapolis, Minnesota 55455

and J. Paul Devlin

Department of Chemistry, Oklahoma State University, Stillwater, Oklahoma 74074 *(Received January 31, 1975)*

Publication costs assisted by the National Science Foundation

Polarized infrared reflection spectra of crystalline potassium tetracyanoquinodimethane (KTCNQ) are presented and vibrational assignments are discussed. Five bands in the 700–2500-cm^{-1} spectral range are reported to originate from totally symmetric (A_g) molecular vibrations of the $TCNQ^-$ anion, based on their intense out-of-plane polarization. A vibronically based charge oscillation, that has previously been recognized for charge-transfer complexes and certain TCNE salts, is thought to be the principal cause for the breakdown of the vibrational selection rules. These results seem to necessitate a drastic reassignment of the vibrational spectrum of this and possibly other radical anion salts.

There have been several recent studies of the vibrational spectra of radical anion salts[1–4] particularly of tetracyanoethylene[2] (TCNE) and tetracyanoquinodimethane (TCNQ).[3,4] The Raman spectra of these strongly colored compounds have, in each case, been marked by the resonant nature of the scattering. This character has been well demonstrated in a wavelength-dependent study of the scattering from TCNQ salts.[4] Although the Raman spectra have, in all cases, been for polycrystalline samples, the additional data provided by the wavelength dependence of the scattering, as related to the positions of the electronic absorption bands, have made possible a reliable assignment of the Raman bands.

The assignment of the infrared spectra of radical salts in general, and TCNQ salts in particular, is a subject of some disagreement. Through a comparison of the infrared and Raman spectra of M^+TCNE^- salts and a qualitative application of the Ferguson–Matsen–Friederich–Person (FMFP) electron oscillation theory for charge-transfer systems,[5] Hinkel and Devlin showed that each of the dominant features in the $TCNE^-$ infrared spectrum is based on the A_g (infrared inactive) modes of the parent molecule.[2] This implies an infrared activation of these modes through a vibronic interaction mechanism that has been referred to as an "electron oscillation". The key characteristic of such an activation is that the transition dipole is along a coordinate joining donor (M^+) and acceptor ($TCNE^-$) species regardless of the direction of the atomic displacements for the mode. The M^+TCNE^- infrared assignment seems firmly established. However, the published infrared data for the TCNQ slats have been interpreted with little regard for the possible (dominant) role of this electron oscillation mechanism.[3,6,7] Thus, each of the strong infrared features has been assigned to a B_{1u}, B_{2u}, or B_{3u} $TCNQ^-$ mode, and Girlando et al. have stated that there is no evidence that vibronic effects are important.[3]

Since the $TCNQ^-$ infrared assignments have been employed in subsequent normal coordinate analyses and the computed force constants have been used to argue for the effect of the radical electron on the bonding in the TCNQ anion,[3,6] the validity of the assumption that vibronic effects are unimportant needs examination (particularly in view of the earlier speculation that the dominance of vibronic effects in the infrared spectra of radical anion salts is likely a general phenomenon[2]).

Considering the crystal structure for K^+TCNQ^-, the anions are stacked approximately plane-to-plane in parallel columns along the needle (a) axis of the crystal.[8,9] The $TCNQ^-$ planes are inclined about 10° from normal to the a axis. Alternating spacings between neighboring TCNQ molecules down the stack suggest that not all intermolecular interactions are equivalent and that pair-wise interactions (of dimers) may be important from a spectroscopic point of view. Indeed, the near-ir electronic transition in KTCNQ at ca. 10,000 cm^{-1} is by all evidence a dimer-type charge transfer band and polarized parallel to the a axis.[8] Thus, it is a simple matter to design an infrared experiment to determine the importance of the electron-oscillation mechanism. The infrared active fundamental modes for neutral TCNQ in the 900–4000-cm^{-1} range are in-plane in nature so that, ignoring any vibronic effects, the transition dipole for these modes should be perpendicular to the crystallographic a axis. On the other hand, the strong interactions of the anion species with each other and with the neighboring cations are out of the molecular planes so any vibronically based electron oscillation should have an out-of-plane character. Thus, the determination of the transition dipole directions by polarized infrared measurements on single crystals of K^+TCNQ^- should immediately indicate the role that vibronic effects play in the $TCNQ^-$ salt spectra and either affirm the suggested vibrational assignments[3,6,7] or necessitate a radically different interpretation.

Actually the requisite infrared measurements and interpretation were made and reported several years ago,[10] but not in the open literature, so a brief review of the results and their implication is in order. Because of the optical density of the salts, the single crystal infrared polarization study was made by reflection, rather than absorption, but the resultant curves, Figure 1, are conclusive in their import. These spectra show that the transition moments for the intense bands 2, 3, 6, 8, 10, and 11 are parallel to the needle axis. Of these, only band 10, for the C–H out-of-

* Address correspondence to Bowdoin College, Brunswick, Maine 04011.

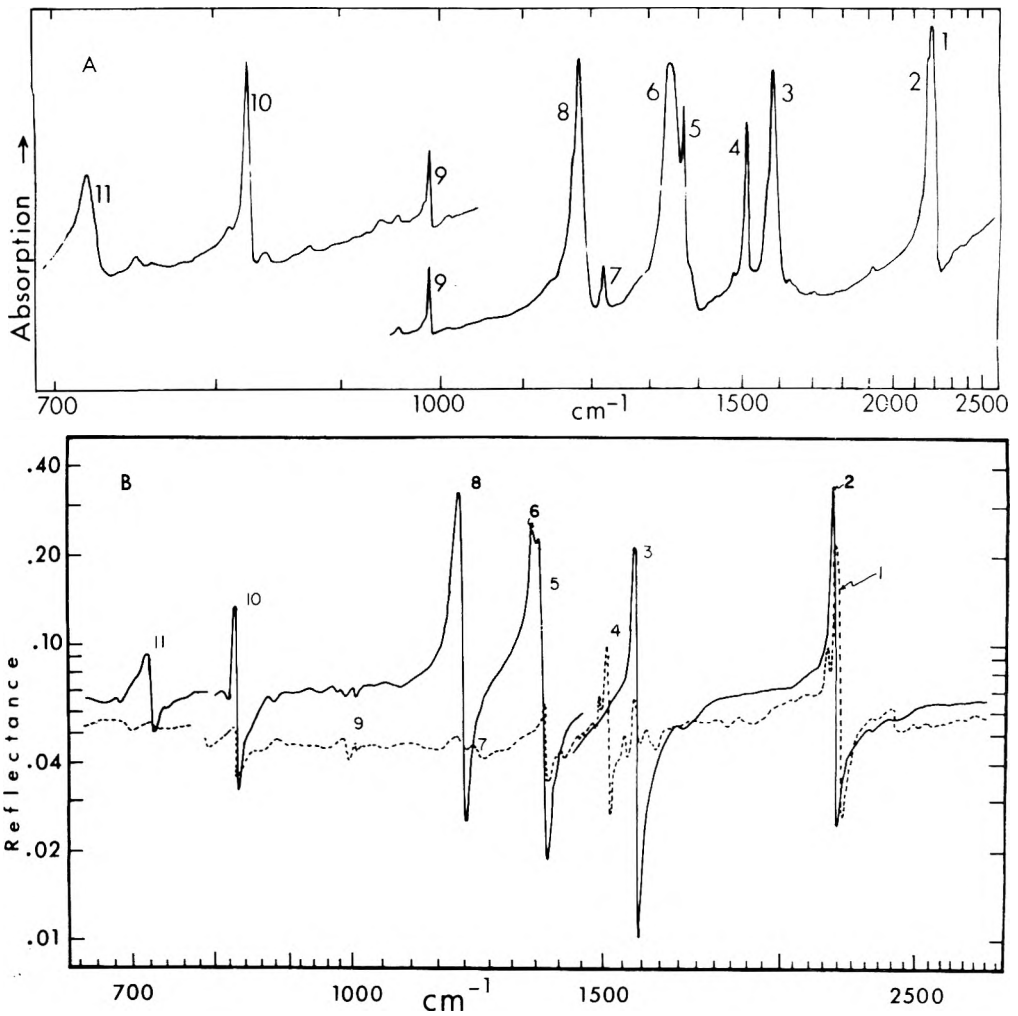

Figure 1. Infrared spectra of crystalline KTCNQ ion-radical salt: (A) absorption spectrum using the KBr pellet technique; (B) room temperature polarized reflection spectra at near-normal incidence where the solid line refers to ir polarization with the **E** vector parallel to the *a* crystallographic (stacking) axis while the broken line refers to polarization perpendicular to this axis and approximately parallel to the molecular planes.

plane mode, would normally have such a polarization. The other five bands, which dominate the $TCNQ^-$ infrared spectrum, cannot result from normal infrared active in-plane modes. The latter, however, are likely sources for bands 1, 4, 5, and 9 which have the expected polarization. The data show that at least five planar modes are accompanied by a strong charge oscillation perpendicular to the direction of atomic motion but in the direction of strong intermolecule interactions. This is characteristic of the FMFP charge oscillation for charge-transfer systems.[5] Since the FMFP activation mechanism is normally strongest for the totally symmetric (A_g) modes,[11] the results are most simply interpreted by assigning features 2, 3, 6, 8, and 11 to A_g modes of the isolated $TCNQ^-$ ion. The instrument used to record the near-normal incident reflection spectra has been described previously.[12] The KTCNQ crystals (needles) were grown from CH_3CN solution. The reflectance surface was composed of six oriented crystals in a mosaic rectangle, 2.0 × 0.63 mm dimensions. Reflection studies at 77° and 4.2°K show no appreciable changes in polarization or band intensities.

The basis for ignoring vibronic effects in previous M^+TCNQ^- studies was the lack of coincidence between infrared and Raman band positions.[3] A comparison of the features of Figure 1 with the published Raman spectra[3,4] show that only the infrared bands at 825 and 1512 cm^{-1} have no Raman counterpart within 40 cm^{-1}. The 825-cm^{-1} feature is for the C–H out-of-plane mode while Figure 1 shows that the 1512-cm^{-1} band results from normal in-plane infrared activity, so neither feature should have an intense Raman counterpart. The small (less than 40 cm^{-1}) difference between the infrared features 2, 3, 6, 7, and 11 and their Raman counterparts, though large for factor-group splittings, are smaller than the factor-group splittings reported for KTCNE[2] and similar in magnitude to such splittings reported for the KTCNQ Raman spectrum.[4] The point is that, since there are eight $TCNQ^-$ units per unit cell,[9] each $TCNQ^-$ fundamental is the basis for eight factor-group components. The Raman active components based on the A_g molecular anion modes will have a somewhat different frequency than the infrared components based on the same molecular modes.

It seems unnecessary to tabulate a new K^+TCNQ^- vibrational assignment since the outgrowth of this analysis is simply stated: the intense infrared bands at 2175, 1583, 1343, 1183, and 719 cm^{-1} should be attributed to molecular anion A_g modes (ν_2, ν_3, ν_4, ν_5, and ν_7, respectively) rather than as previously assigned.[3,6] We would also like to point out the noticeably greater line width of these absorption bands. Compared with bands 1, 4, 5, and 9, these electron-oscillation modes are found to be 2–3 times broader than their simple molecular counterparts. The origin of this

added line width is not clearly understood. Other lower frequency modes, not within the range of this study, have similarly been assigned incorrectly. Since the infrared absorption and polarized reflection data for Cs_2TCNQ_3 are similar to that for KTCNQ, the interpretation here is presumed to extend to that salt as well. In fact these results, combined with those for M^+TCNE^- salts,[2] strongly suggest that vibronic effects must be routinely considered in analyzing the vibrational spectra of radical anion salts. If either ion pairing or dimerization is likely, this view must be extended to solutions of ion radical salts. Only in the absence of strong association with a second species are such FMFP-type activations of symmetric modes improbable.

Acknowledgment. We wish to acknowledge the Central Research Department, E. I. du Pont de Nemours and Company, where the experimental work was carried out by one of the authors (G.R.A.). Also, we wish to acknowledge the help of Dr. G.J. Sloan in growing crystals for this study and of Dr. C.J. Fritchie for his work and discussions on the crystal structure of KTCNQ. Dr. R.E. Merrifield is acknowledged for his long-term interest and useful discussions regarding the TCNQ salts.

References and Notes

(1) P. C. Li, J. P. Devlin, and H. A. Pohl, *J. Phys. Chem.*, **76**, 1026 (1972).
(2) J. J. Hinkel and J. P. Devlin, *J. Chem. Phys.*, **58**, 4750 (1973).
(3) A. Girlando, R. Bozio, and C. Pecile, *Chem. Phys. Lett.*, **25**, 409 (1974).
(4) C. Chi and E. R. Nixon, *Spectrochim. Acta*, in press.
(5) H. B. Friedrich and W. B. Person, *J. Chem. Phys.*, **44**, 2161 (1966); E. E. Ferguson and F. A. Matson, *ibid.* **29**, 105 (1958). NOTE ADDED IN PROOF: One reviewer cited an omission of important recent references in ref 5. These are: R. S. Mulliken and W. B. Person, "Molecular Complexes", Wiley, New York, N.Y., 1969; W. B. Person, in "Spectroscopy and Structure in Molecular Complexes", J. Yarwood, Ed., Plenum Press, London, 1973, Chapter 1.
(6) M. G. Kaplunov, T. P. Panova, E. B. Yagubskii, and Y. G. Borod'ko, *Zh. Strukt. Khim.*, **13**, 440 (1972).
(7) A. Girlando, L. Morelli, and C. Pecile, *Chem. Phys Lett.*, **22**, 553 (1973).
(8) G. R. Anderson and C. J. Fritchie, Jr., Paper 111, Second National Meeting of the Society of Applied Spectroscopy, San Diego, Calif., 1963.
(9) R. P. Shibaeva and L. O. Atovmyan, *Zh. Strukt. Khim.*, **13**, 546 (1972).
(10) G. R. Anderson and R. L. McNeely, Paper R5, Symposium on Molecular Structure and Spectroscopy, Ohio State University, June 1963.
(11) E. E. Ferguson, *J. Chim. Phys.*, **61**, 257 (1964).
(12) G. R. Anderson, *J. Chem. Phys.*, **47**, 3853 (1967).

Inductive Effects and Franck–Condon Shifts in the Visible Spectra of Substituted Chromate Ions

Douglas C. McCain

Department of Chemistry, University of Southern Mississippi, Hattiesburg, Mississippi 39401 *(Received October 9, 1974)*

Publication costs assisted by the University of Southern Mississippi

Ligand shifts in the visible range absorption spectra of substituted chromate ions, CrO_3L^{n-}, support a postulated donor–acceptor interaction between the ligand and CrO_3. A good correlation is found between Taft's inductive substituent coefficient, σ_I, and the energy of the charge transfer band origin. Poor correlations between σ_I and absorption maxima are explained in terms of the Franck–Condon effect.

Introduction

One of the first steps in a chromate oxidation involves formation of a substituted chromate ion,[1] CrO_3L^{n-}, where the ligand L^{n-} may be an organic[2] or an inorganic[3] Lewis base. Especially noteworthy are the chromate esters, $CrO_3(OR)^-$, well known as intermediates in the oxidation of alcohols.[4,5] Other chromates which have been shown to participate in oxidation reactions include[3,6,7] CrO_3Cl^- and $CrO_3(SCN)^-$.

Substituted chromates typically display three distinct bands in their visible and near-ultraviolet spectra.[5] Figure 1 shows a weak band at about 450 nm and the edge of a very strong, broad band which extends beyond 300 nm. The intervening band has been identified[5,8,9] with oxygen-to-chromium charge transfer. It exhibits a partially resolved vibrational progression due to excitation of a symmetric stretching mode in the CrO_3 group. Such spectra are often seen during chromate oxidations and have been used to identify reaction intermediates. This study examines the effects of various ligands on charge transfer spectra. Aprotic solvents were chosen for optimum resolution; vibrational structure is often unresolved in water solutions.

Experimental Section

Reagent grade chemicals were used without further purification. Tetra-*n*-butylammonium salts were prepared from $[(n\text{-}Bu)_4N]ClO_4$ and KBr or KSCN. Traces of perchlorate in the product present no problem because ClO_4^- is not expected to form a stable complex with CrO_3. Tetraphenylarsonium salts were made in a similar way from NH_4F, KBr, and KSCN. Solutions containing the tertiary butoxide ion, $(Ot\text{-}Bu)^-$, were obtained by adding K(Ot-Bu) to a solution of $[(n\text{-}Bu)_4N]ClO_4$. Hexakis(methylisonitrile)iron(II) hydroxide was made from $[Fe(CNCH_3)_6](HSO_4)_2$ and $Ba(OH)_2$. $[Fe(CNCH_3)_6](HSO_4)_2$ and $[Fe(CNCH_3)_6]Cl_2$ were prepared by a standard method.[10]

The solvents used in this study were benzene, chlorobenzene, and dichloromethane; all were dried over Na_2SO_4.

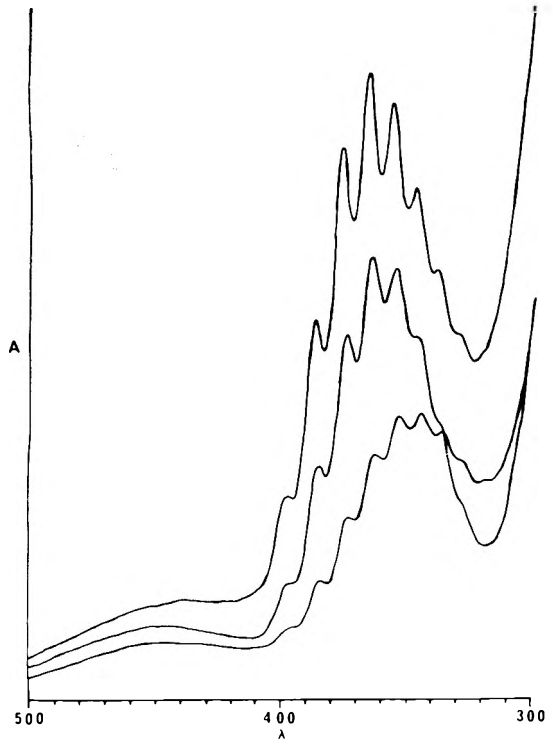

Figure 1. Absorption spectra of CrO_3Br^- (upper curve), CrO_3Cl^- (middle), and CrO_3F^- (lower curve crossing at 330 nm) in chlorobenzene with absorbance, *A*, in arbitrary units, vs. wavelength, λ, in nanometers.

Spectroscopic grade benzene was used as well as an ultrapure product from the James Hinton Co.; no difference was found between results for the two grades. CrO_3 is not detectably soluble in the dry solvents, but solutions are obtained with added water; these exhibit broad featureless spectra, presumably of H_2CrO_4. Water impurities in salts or solvents could affect CrO_3L^{n-} spectra in several ways. Acting as an acid, water could protonate a substituted chromate ion; however, this is unlikely to interfere with the observation of vibrational bands because it can only contribute a broad background signal. Only ions with full C_{3v} symmetry display the well-resolved vibrational structure associated with a Cr–O symmetric stretch. Water could also compete for ligand sites with other Lewis bases or salts; however, in the presence of excess salt, equilibrium should not favor water. Most of the substituted chromate ions discussed here can be formed even in water solution.[11]

Chromate solutions were prepared for study by first dissolving the salt or Lewis base in solvent; then a small portion (several milligrams) of dry CrO_3 was added to about 5 ml of the solution. Caution is advisable at this point; the mixture is potentially explosive. A few seconds of stirring was sufficient to dissolve some CrO_3 and color the solution, which was then decanted into a sample cell and examined on a Cary 17 spectrometer. Properly prepared samples are not dangerous since they contain so little dissolved CrO_3 and no solid residue. Concentrations of salt or Lewis base ranging from 10^{-4} to 10^{-2} *m* all gave satisfactory results; over this range chromate spectra appear to be independent of base concentration. Successful results for the ions and bases reported here depend in large part on a great excess in substrate concentration over that of residual water and CrO_3L^{n-}. Stoichiometric solutions are typically unstable. For this reason it was impractical to measure extinction coefficients.

A number of chloride salts are soluble in organic solvents. In chlorobenzene and dichloromethane solutions these salts dissolve CrO_3 to give spectra which can be identified as the well-known CrO_3Cl^- ion.[6] Essentially identical results are obtained with solutions of $[(n\text{-}Bu)_4N]Cl$, $[(CH_3)_4N]Cl$, $[(CH_3)_3NCH_2CH_2OCOCH_3]Cl$ (acetylcholine chloride), $[(C_6H_5)_4As]Cl$, and $[Fe(CNCH_3)_6]Cl_2$. Deliberate additions of water (ca. 10^{-2} *m*) leave the spectrum unchanged. Some of the salts are insufficiently soluble in benzene and only $[(C_6H_5)_4As]Cl$ was used in that solvent. Similar results for other anions confirm a total lack of spectral dependence on the cation. F^- and $(Ot\text{-}Bu)^-$ are more sensitive to water, however.

Salts containing the hydroxide ion are particularly difficult to dissolve in aprotic solvents. $HCrO_4^-$ was formed by dissolving CrO_3 in dry solutions containing $[Fe(CNCH_3)_6](OH)_2$, or by adding hydric solvent to a solution containing $CrO_3(Ot\text{-}Bu)^-$. $HCrO_4^-$ was distinguished from H_2CrO_4 by its spectrum; H_2CrO_4 does not show resolved vibrational structure.

Pure liquid DMSO and DMF both dissolve CrO_3 directly to give unstable (sometimes explosive!) solutions. A 1–3% by volume mixture of these liquids with solvent was used in this study. Chromate complexes are easily formed but even dilute solutions become turbid and decompose in a few minutes. There can be no assurance that the DMSO or DMF spectrum showing vibrational structure results from direct addition of the Lewis base and not one of its decomposition products. Because of even faster decomposition and other problems, useful spectra were not obtained for a number of ketones and alcohols which were tried, as well as for salts containing the thiosulfate, cyanide, cyanate, azide, and methoxide ions, some of which may be unable to compete as ligands with the residual water.

Results and Discussion

Typical absorption spectra are shown in Figure 1. Vibrational assignments were made after careful examination of the region just above 400 nm. In favorable cases, traces of the first hot band (the $1 \rightarrow 0$ band) were seen with positions and intensity ratios consistent with those expected for thermal excitation of the symmetric stretching mode in the CrO_3 group. In the ground state these frequencies are[1] 911 cm^{-1} for CrO_3F^- and 907 cm^{-1} for CrO_3Cl^-. With this information it is clear that the vibrational progression below 400 nm fits the series $0 \rightarrow 0$, $0 \rightarrow 1$, $0 \rightarrow 2$, . . . , $0 \rightarrow n$.

Table I presents some data obtained for the CrO_3Br^- ion. Measured frequencies are accurate to about four significant figures, the uncertainties being due to spectrometer calibration errors (±0.1 nm) and natural line widths. Spectrometer resolution was not a limiting factor. Results from the three solvents are very similar, but frequencies corresponding to the same vibrational transition increase in the order benzene < chlorobenzene < dichloromethane. This effect, too small to be accurately measured, was also observed in the other substituted chromates. It is presumably related to solvent polarity. The average vibrational spacing $\bar{\nu}_{vib}$, for the first five intervals ($0 \rightarrow 0$ to $0 \rightarrow 5$ transitions) in all three solvents is 768 cm^{-1}, and the average $0 \rightarrow 0$ transition energy, $\bar{\nu}_{00}$, for all three solvents is 25,100 cm^{-1} (to four significant figures).

Similar results for other chromates are found in Table II. Data from the three solvents were averaged and only the first five vibrational spacings were used. In addition, an ab-

TABLE I: Measured Center Frequencies and Vibrational Spacings (in cm^{-1}) for the CrO_3Br^- Ion in Three Solvents

Assignment	$[(C_6H_5)_4As]$-CrO_3Br in benzene	$[(n\text{-}Bu)_4N]$-CrO_3Br in C_6H_5Cl	$[(n\text{-}Bu)_4N]$-CrO_3Br in CH_2Cl_2
0 → 0	25,088	25,101	25,114
	760	782	790
0 → 1	25,848	25,883	25,904
	783	748	768
0 → 2	26,631	26,631	26,672
	757	793	776
0 → 3	27,388	27,424	27,448
	780	749	750
0 → 4	28,168	28,173	28,198
	770	754	766
0 → 5	28,938	28,927	28,964
		769	784
0 → 6		29,696	29,748
		789	765
0 → 7		30,485	30,513

TABLE II: Absorption Frequencies and Vibrational Spacings of Various Substituted Chromate Ions, CrO_3L^{n-}, in Three Solvents[a]

L^{n-}	$\bar{\nu}_{max} \pm 150$ cm^{-1}	$\bar{\nu}_{00} \pm 50$ cm^{-1}	$\bar{\nu}_{vib} \pm 20$ cm^{-1}
F^-	28,500	25,230	737
Cl^-	27,800	25,150	741
Br^-	27,700	25,100	768
I^-	27,200		
SCN^-	27,100	25,000	764
OH^-	26,700	24,520	769
H_2O	25,000		
$(CH_3)_2SO$	27,100	24,800	741
$(CH_3)_2NCHO$		24,840	733
$t\text{-}C_4H_9O^-$	27,000	24,760	725
CH_3COO^-	27,500		
$(CH_3CO)_2O$	26,100		
$(CH_3)_2CO$	24,700		
CH_3CN	27,400		
C_6H_5CN	25,600		
C_5H_5N	23,500		

[a] Results from benzene, chlorobenzene, and dichloromethane were averaged.

sorption maximum, $\bar{\nu}_{max}$, was estimated by drawing an envelope over the spectrum to determine the frequency at which maximum absorption would occur if vibrational structure were unresolved. Such a $\bar{\nu}_{max}$ probably corresponds to the $\bar{\nu}_{max}$ measured in solvents in which these ions show no resolved structure.

Variations of the ligand on CrO_3L^{n-} are known[5,7,12] to cause small shifts in the charge transfer absorption band. Several types of interaction can be postulated which allow a ligand to alter the charge transfer energy. A good electron donor, such as OH^-, might function as an additional electron source for charge transfer, supplementing donation from the oxygens and lowering $\bar{\nu}_{00}$ or $\bar{\nu}_{max}$ compared to a poor donor such as F^-. Alternatively, a good electron acceptor, such as F^-, might decrease electron density near the chromium and facilitate charge transfer from the oxygens, lowering $\bar{\nu}_{00}$ or $\bar{\nu}_{max}$ compared to a poor acceptor such as OH^-. Experimental results in Table II favor the first of these interpretations. If spectral shifts depend only, or primarily, on ligand donor–acceptor properties, we should expect a linear correlation between $\bar{\nu}_{00}$ or $\bar{\nu}_{max}$ and σ_I, Taft's inductive substituent constant.[13,14] σ_I is related to the well-known[13] Hammett σ constants; it is a numerical parameter which correlates with a ligand's inductive (i.e., donor–acceptor) qualities.

Various tables of σ_I values have been proposed[15] based on such diverse measurements as the ionization constants

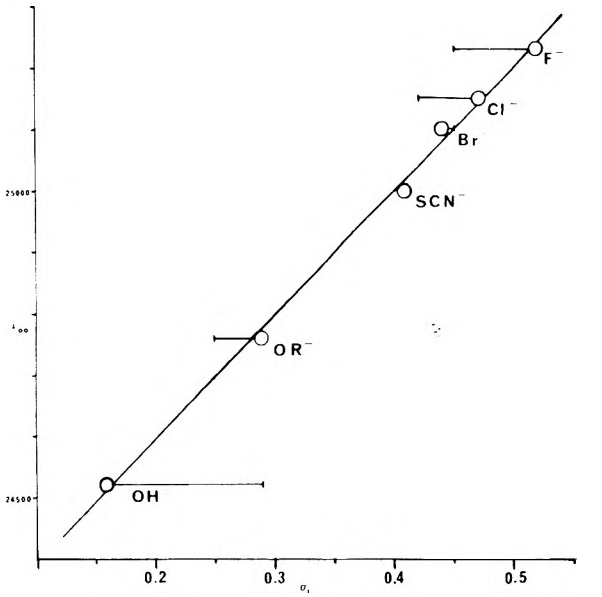

Figure 2. Charge transfer band origin, $\bar{\nu}_{00}$, in cm^{-1} vs. the inductive substituent coefficient, σ_I. Circles represent σ_I values obtained from NMR data and the slope is a least-squares fit to these points. Horizontal bars indicate the maximum range of σ_I as determined by other methods. OR^- is the tertiary butoxide ion.

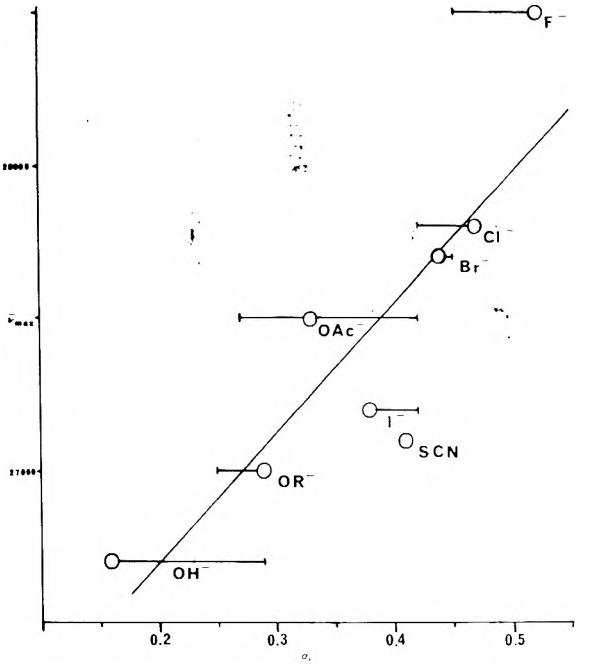

Figure 3. Charge transfer band maximum, $\bar{\nu}_{max}$, in cm^{-1} vs. σ_I. Similar to Figure 2. OAc^- is the acetate ion.

of aliphatic and aromatic acids, reaction rates, NMR chemical shifts,[16] and others. Values of σ_I obtained from NMR studies (circles in Figure 2) show a better correlation with $\bar{\nu}_{00}$ than do any other data, the maximum range of which is indicated by horizontal bars. I have also computed σ_I from the NMR data of Parshall[17] who measured the ^{19}F chemical shifts of *trans-m*-$FC_6H_4Pt(PC_2H_5)_2X$, finding chemical shifts (vs. fluorobenzene) of 1.97 and 1.56 ppm for X = Br (σ_I = 0.44) and X = I (σ_I = 0.38), respectively. From a shift of 1.75 ppm, linear interpolation gives σ_I = 0.41 for X = SCN^- (probably N bonded[17]). It is uncertain whether SCN^- bonds to Cr(VI) through sulfur or nitrogen.[3] Opinion seems to favor S bonding; if so, this value of σ_I may be inappropriate. Parshall's data also gives σ_I = 0.47 for X = Cl^- (2.13 ppm shift). σ_I for tertiary butoxide has apparently not been measured, but it can reasonably be estimated to be equal to that[16] of OCH_3^- (σ_I = 0.29) since the σ_I values of the *t*-butyl and methyl groups themselves are so similar.

Figure 2 shows a plot of $\bar{\nu}_{00}$ vs. σ_I. The linear correlation which is observed supports the proposition that donor–acceptor interactions are responsible for the $\bar{\nu}_{00}$ shift. Figure 3 shows a similar plot of $\bar{\nu}_{max}$ vs. σ_I. Evidently there is some correlation, but the data do not describe a straight line within experimental error. The reason they do not is easily found. A look at Figure 1 will show that $\bar{\nu}_{max}$ in CrO_3Br^- and CrO_3Cl^- occurs near $\bar{\nu}_{03}$, while in CrO_3F^- the peak is near $\bar{\nu}_{05}$. This is a manifestation of the Franck–Condon principle which states that electronic rearrangement takes place much faster than nuclear rearrangement, so that the most probable transitions are "vertical", and, therefore, that the transition moment is always proportional to the overlap between ground and excited vibrational wave functions.[18] $\bar{\nu}_{max}$ would occur at $\bar{\nu}_{00}$ if bonds were the same lengths in both ground and excited electronic states. The CrO_3 ground state symmetric stretching frequencies are[1] 911 cm^{-1} in CrO_3F^- and 907 cm^{-1} in CrO_3Cl^-, while both are significantly lower (Table II) in the excited state. Therefore, excited state bonds are weaker and probably longer. In order for $\bar{\nu}_{max}$ to occur at higher vibrational levels in CrO_3F^-, it is necessary for the F^- substituent either to weaken the upper state Cr–O bonds or to strengthen the lower state Cr–O bonds relative to Cl^- and other ligands. Vibrational frequencies in the upper state (Table II) show considerable experimental scatter but a general trend toward higher frequencies seems to be associated with a lower σ_I value. If CrO_3Cl^- has a higher $\bar{\nu}_{vib}$ than CrO_3F^-, even though its reduced mass is greater, then excited state bonds are indeed weaker in CrO_3F^- than in CrO_3Cl^-. Ground state Cr–O force constants are known[19] to be slightly greater in CrO_3F^- than in CrO_3Cl^-.

Thus it is clear why $\bar{\nu}_{00}$ fits a straight line plot while $\bar{\nu}_{max}$ does not. $\bar{\nu}_{max}$ has two independent inputs of inductive effect, a direct frequency shift, as in $\bar{\nu}_{00}$, but also a Franck–Condon shift. This example illustrates a danger in using $\bar{\nu}_{max}$ data to study correlations. For the correlations to be linear it is necessary that Franck–Condon shifts be either small or constant.

Acknowledgment. I wish to acknowledge support for this project from the Faculty Research Council of the University of Southern Mississippi.

References and Notes

(1) W. P. Griffith, *Coord. Chem. Rev.*, **5**, 459 (1970).
(2) K. B. Wiberg, "Oxidation in Organic Chemistry", Part A, Academic Press, New York, 1965, pp 69–184.
(3) J. K. Beattie and G. P. Haight, Jr., *Prog. Inorg. Chem.*, **17**, 93–145 (1972).
(4) K. B. Wiberg and H. Shafer, *J. Am. Chem. Soc.*, **91**, 927, 933 (1969).
(5) U. Klaning and M. C. R. Symons, *J. Chem. Soc.*, 3204 (1961).
(6) M. Cohen and F. H. Westheimer, *J. Am. Chem. Soc.*, **74**, 4387 (1952).
(7) K. A. Muirhead and G. P. Haight, Jr., *Inorg. Chem.*, **12**, 1116 (1973); *J. Am. Chem. Soc.*, **94**, 3006 (1972).
(8) L. H. Helmholz, H. Brennan, and M. Wolfsberg, *J. Chem. Phys.*, **23**, 853 (1955).
(9) C. J. Ballhausen and H. B. Gray, *ACS Monogr.*, **No. 168**, 3–83 (1971).
(10) L. Malatesta, *Prog. Inorg. Chem.* **1**, 283–379 (1959).
(11) F. A. Cotton and G. Wilkinson, "Advanced Inorganic Chemistry", 2nd ed, Interscience, New York, N.Y., 1966, p 828.
(12) D. G. Lee and R. Stewart, *J. Am. Chem. Soc.*, **86**, 3051 (1964).
(13) L. P. Hammett, "Physical Organic Chemistry", 2nd ed. McGraw-Hill, New York, N.Y., 1970.
(14) R. W. Taft, Jr., *J. Am. Chem. Soc.*, **75**, 4231 (1953); R. W. Taft, Jr., and I. C. Lewis, *ibid.*, **80**, 2436 (1958).
(15) C. D. Ritchie and W. F. Sager, *Prog. Phys. Org. Chem.*, **2**, 232 (1964).
(16) R. W. Taft, Jr., *J. Phys. Chem.*, **64**, 1805 (1960); R. W. Taft, Jr., E. Price, I. R. Fox, I. C. Lewis, K. K. Anderson, and G. T. Davis, *J. Am. Chem. Soc.*, **85**, 709 (1963).
(17) G. W. Parshall, *J. Am. Chem. Soc.*, **86**, 5367 (1964); **88**, 704 (1966).
(18) D. S. McClure and P. J. Stephens, *ACS Monogr.*, **No. 168**, 84–133 (1971).
(19) A. Mueller and G. Nagarajan, *Z. Anorg. Allg. Chem.*, **347**, 87 (1968).

Electron Spin Resonance Oxygen Broadening

M. J. Povich

Chemical Processes Branch, General Electric Corporate Research & Development, Schenectady, New York 12501
(Received September 16, 1974; Revised Manuscript Received February 28, 1975)

Publication costs assisted by the General Electric Research & Development Center

The effect of dissolved oxygen on the ESR line width (W) of dilute nitroxide free-radical (NFR) solutions is investigated. When dilute NFR solutions are saturated with air, oxygen appears to be responsible for the major contribution to W. The oxygen broadening is found to be linear with respect to temperature (T), but independent of solvent viscosity (η). This is in contrast to the Stokes–Einstein diffusion equation which predicts a linear relationship between W and T/η. The ESR data of other workers which departed from a linear W vs. T/η relationship were analyzed and were also found to be linear in T alone. The departures of ESR data from the Stokes–Einstein diffusion equation may have many possible explanations. The potential application of oxygen broadening to the measurement of oxygen concentrations and diffusion coefficients is noted.

Introduction

Many notes have appeared in the literature to point out the importance of removing oxygen from solutions of free radicals prior to recording their ESR spectrum. Methods of removal include purging with nitrogen and vacuum degasification. The effect of oxygen is to produce a broadening of the ESR spectrum which interferes with accurate measurements of natural ESR line widths.

Oxygen broadening is brought about by the magnetic interaction upon oxygen–radical collisions. This interaction is said to be the exchange integral, J, which has been described elsewhere.[1] Because of the exchange interaction, such broadening of ESR spectra is commonly referred to as exchange broadening. Exchange broadening may occur via radical–radical collisions or oxygen–radical collisions.

Pake and Tuttle[2] first described exchange broadening in terms of the radical–radical encounter rate, ν

$$W = K\nu p + R \tag{1}$$

where W is the ESR line width in gauss, K a proportionality constant, ν the radical–radical encounter rate in sec^{-1}, p the probability that exchange will occur upon radical–radical encounter ($0 \leq p \leq 1$), and R represents contributions to the ESR line width independent of ν. Frequently R is associated with the static radical–radical (dipole–dipole) broadening as $\nu \to 0$.

Pake and Tuttle related the encounter rate, ν, to the solvent viscosity (η, poise) and temperature (T, °K) of the solvent through the Stokes–Einstein relation to obtain

$$\nu = Z(N_r/N_s)(k/\pi b\lambda^2)(T/\eta) \tag{2}$$

where Z is the average number of new neighbors encountered by a radical molecule during a jump of length λ, N_r and N_s are the number of radical and solvent molecules per cc, respectively, b is the effective hydrodynamic radius of the radical, and k is Boltzmann's constant.

As seen from eq 1 and 2, if p is constant, a plot of W vs. T/η should yield a straight line. Several workers[3-5] have investigated exchange broadening and have found regions of N_r and T/η that agree with eq 1 and 2.

However, others[1,4] have found that when T/η is greater than about 5000 (°K poise^{-1}) W levels off to a constant value. An example of this nonlinear type of W vs. T/η behavior is illustrated in Figure 1. This leveling off of W has been attributed to a decrease in the probability of exchange, p, as T/η increases. Edelstein, Kwok, and Maki[1] assumed that p was a function of J and the encounter time, τ, to obtain

$$p = 1 - e^{-J\tau} \tag{3}$$

The encounter time, τ, was approximated by the reciprocal of the jumping frequency

$$\tau = (\pi b\lambda^2/k)(\eta/T) \tag{4}$$

In the limit as $J\tau \to 0$, $p \to J\tau$, and $W \to [KZ(N_r/N_s)J + R]$ which is independent of T/η.

Plachy and Kivelson[4] reexamined some of the work of Edelstein et al.[1] correcting for spin rotation, the temperature dependence of concentration, overlapping lines, proton hyperfine effects, and the temperature dependence of λ. They also employ a different form of p as derived by Johnson.[6]

The corrections added by Plachy and Kivelson represent a refinement to the original work of Edelstein, Kwok, and Maki. However, the qualitative relationship between the corrected line widths and T/η are approximately the same, W leveling off with increasing values of T/η.

Departures from the linear W vs. T/η have been observed in both oxygen-free and oxygen-containing free-radical solutions. Edelstein et al.[1] investigated exchange broadening of di-*tert*-butyl nitroxide (DTBN) in solutions of methylcyclohexane. In the absence of oxygen, methylcyclohexane–DTBN solutions exhibited a linear W vs. $1/\eta$ relationship. The temperature was held constant (293°K) while the pressure was varied to alter η. However, in the presence of oxygen, the line width was found to deviate from a linear W vs. $1/\eta$ behavior.

Edelstein et al.[1] also studied oxygen-free solutions of DTBN in *n*-pentane and in propane. In both cases deviations occurred from linear W vs. T/η behavior. Thus, the observed deviations are not limited to oxygen containing solutions.

This paper attempts to further investigate the phenomenon of oxygen broadening. The method of study involves

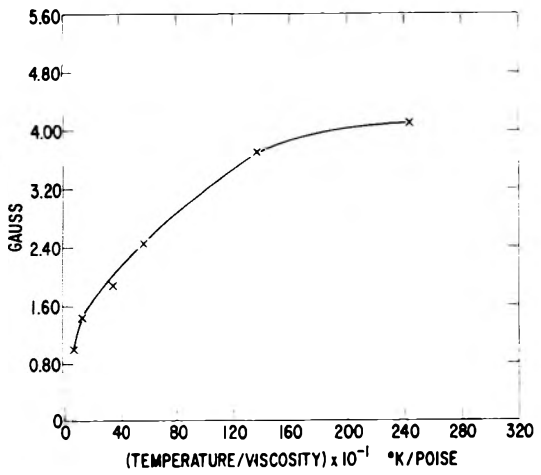

Figure 1. W vs. T/η for 3.7×10^{-4} M TMP in air-saturated 100 cSt silicone fluid SF-96(100).

measuring the line width of air-saturated nitroxide free-radical solutions prepared from different solvents that vary considerably in viscosity. Surprisingly, the viscosity does not affect the line width of the solutions. Moreover, the air-saturated solutions exhibit a markedly similar and linear W vs. T behavior.

Experimental Section

ESR spectra were obtained using a Jeol Co. Model JES ME-X ESR spectrometer with X-band microwave unit, 100-kHz modulation, and TE_{011} cylindrical cavity. Temperature was varied using a Joel Co. variable-temperature controller which incorporates a copper–constantan thermocouple located at the nitrogen inlet to an all quartz cavity dewar. The temperature controller was calibrated against a separate copper–constantan thermocouple and potentiometer.

The magnitude of the 100-kHz modulation was maintained at less than 20% of the measured line width. Lower magnitudes of modulation did not change the measured line width. The magnetic field sweep was calibrated against a 13.0-G hyperfine coupling for Fermi's salt (0.001 M) dissolved in aqueous K_2CO_3. The accuracy of the line width measurements is ±0.1 G.

The nitroxide free radical 2,2,6,6-tetramethylpiperidinooxy (TMP), illustrated in Figure 2, was purchased from Eastman Organic Chemicals (catalog no. 10992). The concentration of TMP in all solutions was 3.7×10^{-4} M. Organic solvents were reagent grade. The silicone fluids were General Electric Silicone Fluids SF-96(100), SF-96(500), and SF-96(1000), the values in parentheses being the fluid viscosity in centistokes at 25°. The temperature dependence of the viscosity for the silicone fluids was obtained from the Silicone Products Department, General Electric Co. Physical data pertaining to silicone fluids were also obtained from McGregor[7] and General Electric Company.[8] The solubility of air in the silicone fluids is 0.168–0.190 cc/cc.[7]

All solutions were contained in standard NMR sample tubes which were sealed with plastic caps.

Results and Discussion

Figure 2 presents the spectra of TMP in air-saturated SF-96(100) at various temperatures. Comparison with Figure 3 illustrates the effect of removing dissolved oxygen on

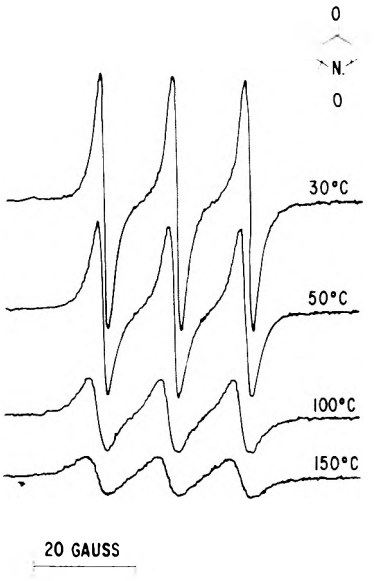

Figure 2. ESR spectra of 3.7×10^{-4} M TMP in air-saturated silicone fluid SF-96(100) at various temperatures. Instrument gain was held constant to illustrate the decrease in signal height accompanying oxygen broadening.

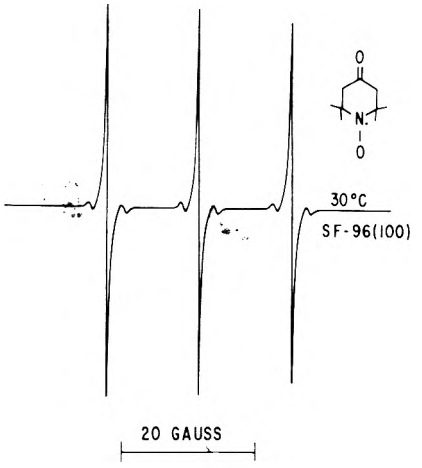

Figure 3. ESR spectrum of 3.7×10^{-4} M TMP in nitrogen purged silicone fluid SF-96(100) at 30°.

the spectrum at 30°. Oxygen appears to be responsible for the major contribution to the line width.

Figure 4 plots the line width W against the absolute temperature T. For air-saturated solutions there appears to be a linear relationship between W and T. Moreover, the line width does not appear to depend upon the solvent viscosity. The viscosity of SF-96(1000) is 10 times greater than SF-96(100), and approximately 1000 times greater than dodecane or benzene. Yet, the measured line width in these solutions do not vary by more than 0.5 G above experimental error. The solubility of oxygen in silicone fluid is not strongly dependent upon its viscosity and is similar in magnitude to the solubility of oxygen in hydrocarbon solvents. Therefore, minor variations in oxygen solubility could not offset the much greater differences in viscosity.

Figure 4 also plots the line width of a solution of TMP in dodecane that was partially purged with nitrogen. If the low temperature point is excluded, a linear W vs. T relationship is exhibited. While the validity of excluding the low-temperature data point may be questioned, it is inter-

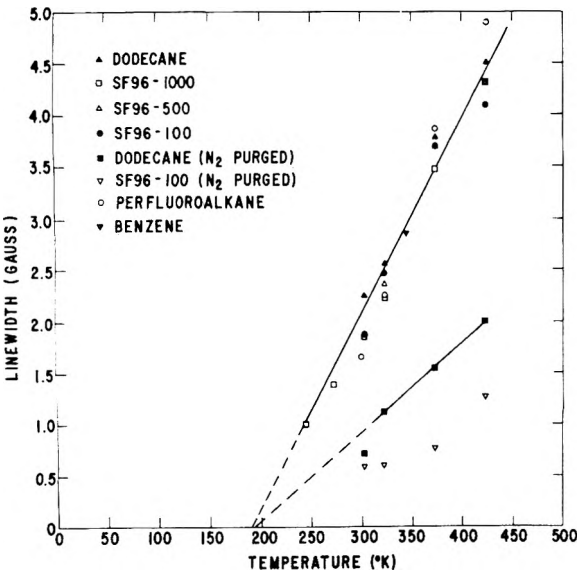

Figure 4. Peak-to-peak line width (W) of the first-derivative ESR spectrum of 3.7×10^{-4} M TMP in various solvents plotted against temperature.

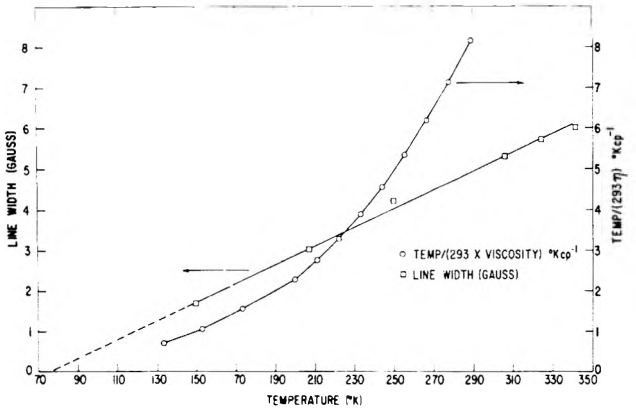

Figure 5. Circles plot $T/293\eta$ (°K/cP) against temperature for propane. These data were constructed via ref 11 and 12. From Figure 1a of ref 1 (W vs. $T/293\eta$) and the $T/293\eta$ vs. T data above, the line width (W) of di-*tert*-butyl nitroxide (DTBN) in propane was plotted as a function of temperature. The larger values of $T/293\eta$ are not shown to reduce the vert cal size of the figure.

esting to note that the extrapolated portion intercepts the T axis at approximately the same temperature as the extrapolated air-saturated data.

One solution of TMP in SF-96(100) was purged with nitrogen for several hours. The line width data for this solution are also included in Figure 4. Considering the low concentration of TMP (3.7×10^{-4} M) and the high viscosity of the SF-96(100) solvent, it is surprising to find W increasing with temperature. For example, it has been shown that dilute nitroxide free-radical solutions (1×10^{-3} M or less) do not exhibit (exchange) broadening of line widths up to T/η values of 30,000 (°K poise^{-1}).[9] For comparison, the 423°K point for SF-96(100) on Figure 4 represents a 3.7×10^{-4} M solution of TMP at $T/\eta = 2438$°K P^{-1}.

While no explanation is readily apparent, one possibility is that the nitrogen used to purge the SF-96(100) was contaminated with oxygen, and that subsequent oxygen–DTBN exchange is responsible for the increase in line width. The solubility of oxygen in silicone is twice as great

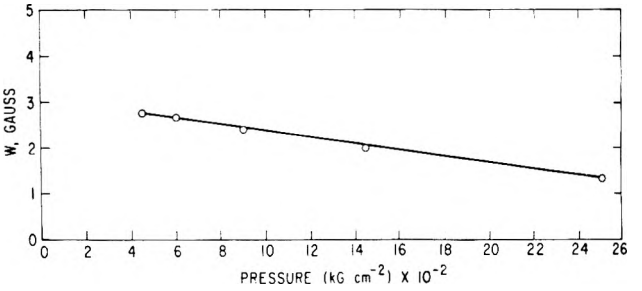

Figure 6. W vs. P plot constructed from Figure 2b of ref 1. W is the line width difference between oxygen containing and deoxygenated solutions of DTBN in methylcyclohexane. The concentration of DTBN is 0.012 M.

as the solubility of nitrogen.[10] Therefore, oxygen could have been concentrated by the silicone fluid.

It is apparent, however, that the line width of air-saturated TMP solutions appears to depend on temperature in a linear fashion. It is further apparent that the line width does not depend strongly upon the viscosity of the solvent. It might be suggested that this behavior is peculiar to air-saturated TMP solutions. It will therefore be interesting to examine the W vs. T/η data of Edelstein et al.[1] for DTBN in degassed propane. With a considerable amount of back calculating via the propane viscosity references[11,12] cited by Edelstein et al., the W vs. T/η data were converted to W vs. T. The results of this conversion are presented in Figure 5, which plots both T/η vs. T and W vs. T. The fit to a straight line of the W vs. T data is relatively good, and extrapolates ($W \rightarrow 0$) to just below the melting point of propane (mp = 83°K).

Assuming that the broadening mechanism involves collisions between magnetic species, an obvious question emerges from the preceding results: is the encounter frequency linear in T or T/η? If linear in T, what type of diffusion model will account for the observed results? The answers to such questions are beyond the scope of this paper, however, it may be enlightening to review the viscosity dependence of reactions in solution.

The linearity in T/η was predicted by the Stokes–Einstein equation for the diffusion coefficient. The diffusion coefficient is more generally expressed as[13]

$$D = kT/\mu \tag{5}$$

where μ is the mobility of the particle under consideration. The mobility of spherical particles in fluid media is given by the Stokes formula

$$\mu = 1/6\pi\eta r$$

which is derived on the basis of a continuous fluid and is a good approximation for not too small values of r. The Stokes formula also applies to molecules that are strongly solvated. In the case of oxygen dissolved in organic liquids the validity of the Stokes formula may be in question. For example, the diffusion coefficient for oxygen in solid silicone rubber is the same order of magnitude as in silicone fluids ($5–16 \times 10^{-5}$ cm^2 sec^{-1}).[10]

Moelwyn-Hughes[14] points out that bimolecular reaction rate constants in solution frequently have the same rate constant as in the gaseous phase. One example cited[15] is the conversion of para-hydrogen into ortho-hydrogen, which is catalyzed by substances having a magnetic moment, i.e., oxygen. The catalytic coefficient of oxygen in the gaseous phase is 9.16 compared to 10.5 (M^{-1} sec^{-1}) in

aqueous solution. Moreover, Moelwyn-Hughes[16] frequently finds a direct, rather than inverse, dependence of bimolecular reaction rates on solvent viscosity.

The foregoing discussion focused on the effect of temperature (and viscosity) on the ESR linewidth, W. However, as mentioned earlier, Edelstein et al.[1] changed the viscosity isothermally by varying the pressure P. In air-saturated DTBN–methylcyclohexane solutions they found that the contribution to W from oxygen alone deviated from the linear W vs. $1/\eta$ behavior. From the data and references cited by Edelstein et al., W vs. P data were calculated and are presented in Figure 6 and show a relatively good linear relationship. No explanation is readily apparent.

In view of the many departures from the Stokes–Einstein collision model, the procedure of adjusting the probability of exchange to fit experimental ESR data may be counterproductive. The phenomenon of ESR exchange broadening may be considered to be a useful tool in the study of solution kinetics, as well as in the study of magnetic interactions. Perhaps the kinetics is in need of adjustment instead of the probability of exchange.

Further experimental work is needed before an adequate model for the line broadening effects can be developed. It is noteworthy, however, that the effect of oxygen on the ESR spectrum of free radicals may be useful in determining the concentration and diffusion coefficient of oxygen in various media.[17]

References and Notes

(1) N. Edelstein, A. Kwok, and A. H. Maki, *J. Chem. Phys.*, **41**, 3473 (1964).
(2) G. E. Pake and T. R. Tuttle, *Phys. Rev. Lett.*, **3**, 423 (1959).
(3) M. T. Jones, *J. Chem. Phys.*, **38**, 2892 (1963).
(4) W. Plachy and D. Kivelson, *J. Chem. Phys.*, **47**, 3312 (1967).
(5) M. J. Povich and J. A. Mann, *J. Phys. Chem.*, **77**, 3020 (1973).
(6) C. S. Johnson, *Mol. Phys.*, **12**, 25 (1967).
(7) R. R. McGregor, "Silicones and Their Uses", McGraw-Hill, New York, N.Y., 1954.
(8) Silicones: Technical Data Book S-90, General Electric Company, Silicone Products Department, Waterford, N.Y.
(9) M. J. Povich, Thesis, University of Hawaii, Honolulu, Hawaii, 1972.
(10) W. L. Robb, General Electric Co. Report No. 65-C-031, Schenectady, N.Y., 1965.
(11) M. W. Lipkin, J. A. Davison, and S. S. Kurtz, *Ind. Eng. Chem.*, **34**, 976 (1942).
(12) B. H. Sage and W. N. Lacey, *Ind. Eng. Chem.*, **30**, 829 (1938).
(13) W. Jost, "Diffusion in Solids, Liquids, Bases", Academic Press, New York, N.Y., 1960.
(14) E. A. Moelwyn-Hughes, "The Kinetics of Reactions in Solution", Oxford University Press, London, 1947, p 243.
(15) Reference 14, p 241.
(16) Reference 14, p 246.
(17) M. J. Povich, *Anal. Chem.*, in press.

Use of the CNDO Method in Spectroscopy. XIII. The Direct Calculation of Self-Consistent Triplet Excited States of Organic Molecules

H. M. Chang, H. H. Jaffé,* and C. A. Masmanidis

Department of Chemistry, University of Cincinnati, Cincinnati, Ohio 45221

(Received September 4, 1974)

A method is reported for the self-consistent calculation of several lower triplet states of organic molecules, based on the CNDO/S formalism. A refinement consisting of combining SCF and CI calculations to obtain extrapolated triplet energies is presented. It is proposed that the lower of SCF or VO/CI results provides an upper limit, the extrapolated values a lower limit to the true triplet energies. This assertion is tested with a number of carbonyl and aromatic heterocyclic compounds. Some detailed analyses of the behavior of orbital energies in series of triplet states are presented.

For many years theoretical chemists have attempted to calculate the electronic spectra of organic molecules by making the most elaborate calculation practical on the ground state and then calculating excited states using the virtual orbital approximation. Beginning with the monumental work of Pariser and Parr[2] it has been customary and been recognized to be essential to include limited configuration interaction to obtain the energies and wave functions of excited states. A very large body of literature exists today on the calculation of the electronic spectra of a wide variety of molecules by this general methodology.[3] Only in very small molecules has it been found practical to make a direct self-consistent field calculation of excited states; a number of factors have contributed to our unwillingness to attempt similar calculations of excited states of large molecules. One of these is the fact that the transition energy between two states, if the states are calculated directly, must come from the comparison of the total energies of the two states of the molecule. Since these are very large numbers, as Coulson has pointed out many years ago, calculation of the transition energy in this way resembles the method of weighing the captain of a ship by weighing the ship with the captain on the bridge and after he has left the ship. Another deterrent has been that a direct SCF calculation of excited states does require a separate quantum chemical calculation with its involved costs for *each* state of the molecule.

On the other hand, the virtual orbital procedure used has a number of disadvantages. In the first place it requires that the calculations of the excited states remain at the same geometry as that used for the ground state or alternately that a ground state calculation followed by a config-

uration interaction calculation be made for each geometry for which an excited state energy is desired. The second major objection is that wave functions for excited states calculated by the virtual orbital approximation, followed by configuration interaction, are not self-consistent; consequently, many of the theorems applicable to self-consistent wave functions cannot be applied to such cases.[4] Thus, it is now becoming evident that there is much to be gained from having self-consistent wave functions.

We have undertaken the job of developing programs for direct self-consistent calculation of excited states of large molecules by the standard semi-empirical methods used for virtual orbital calculations. As an initial effort in this direction, we have programmed the calculation of self-consistent doublet and triplet *states* of molecules using the CNDO/S formalism. These types of *states* were chosen because, in both bases, the wave function of at least one spin component can be expressed as a single Slater determinant.

Basically, two methods are available for the calculation of open-shell states: the unrestricted Hartree–Fock technique originated by Pople and Nesbet[5] and the restricted Hartree–Fock formalism introduced by Roothaan.[6] The former of these techniques has the well-known shortcoming that it does not yield eigenfunctions of S^2. Since spectroscopists, particularly in dealing with molecules of light atoms, are completely tied to discussing compounds in terms of their multiplicities and to regard them in terms of multiplicity manifolds, we have felt that this shortcoming made use of the unrestricted Hartree–Fock method undesirable. True, it is possible after the calculation is completed to use annihilation operators to isolate essentially pure eigen functions of S^2. Unfortunately, however, this procedure at the same time destroys the self-consistency and, therefore, loses much of its gain. An analytical annihilation prior to the SCF calculation would answer all problems, but cannot practically be achieved. Consequently, we have chosen the Roothaan restricted Hartree–Fock SCF procedure and applied to it all the simplifications of the zero differential overlap (ZDO) approximation and of the CNDO/S method.[7] Given these decisions no truly new theoretical developments are necessary. The matrix elements over the HF operator are well defined and all fundamental problems in the theory are well known. Thus, the problem becomes essentially one of coding and of overcoming possible computational problems.

The present paper deals with a description of the method developed, and will give some typical examples of its application to triplet states; comparisons both with experimental results and with the VO method will be reported. Application to doublet states is discussed in a companion paper.[8] In the process of developing this SCF calculation of excited states, certain computational problems arose. These have been treated in detail elsewhere,[9] and will be dealt with here only to the extent required to understand the calculations reported.

Finally, we have found that a combination of the results of VO–CI and SCF calculations appear to lead to an even better estimate of triplet energies then either method alone, and we shall discuss this combined "extrapolation" method.

In the process of these calculations we have observed a very interesting behavior of the orbital energies, and we shall discuss the correlation of orbital energies between a closed-shell ground state and open-shell triplet states. We will further extend this discussion to doublet ground and excited states of the corresponding molecular anions and cations.

Computational

The computations were performed by a perfectly straightforward application of the Roothaan restricted Hartree–Fock open-shell method.[6] The matrix elements were evaluated according to the rules of the ZDO approximation in the CNDO/S form.[7] Expressions for the matrix elements of doublet states are given in the following paper[8] and expressions for the matrix elements of triplet states are perfectly analogous.

Certain computational problems arise. The first one is connected with the use of the molecular aufbau principle. During successive iterations we frequently observe crossing of energy levels, that is, that orbitals of different symmetry do not always occur in the same order. A naïve application of the molecular aufbau principle when such crossing occurs leads to setting up the Fock equation in one iteration for a configuration different from that of the previous one. Such a calculation obviously cannot properly converge. To overcome this problem, we have introduced a determination[10] of the symmetry of each orbital at each iteration and are specifying the configuration desired in terms of the occupation numbers of orbitals for each symmetry species separately. By applying an aufbau principle to the individual symmetry species the problem of crossing of orbitals of different symmetry is immediately overcome.

Unfortunately, this procedure introduced a new complication. The accumulation of rounding error frequently, particularly for higher excited states, leads to a loss of symmetry. To overcome the difficulty we have introduced a resymmetrization at each iteration of the calculation. We have demonstrated that this resymmetrization does not affect the outcome or the precision of the calculation except that it permits us to retain the needed symmetry in our orbitals.[9]

For some of the higher excited states we find that we occasionally run into serious convergence problems. The calculation, rather than converging to a single value of the energy, oscillates between two values which have been shown to correspond to density matrices which concentrate the charge alternately on one part of the molecule and another. We have introduced a number of techniques, in particular averaging of density matrices of successive iterations and introduction of specially designed initial density matrices as starting point for the iteration, to overcome these problems. We have failed to provide a recipe which is universally successful but have, so far, by a combination of these techniques been able to find conditions which allowed convergence to be obtained in every case attempted.

The techniques introduced and their exact effects are discussed in detail elsewhere.[9]

Results and Discussion

Comparison of Self-Consistent and Virtual Orbital Approximations. As a test of the method of calculating self-consistent excited state wave functions, we have calculated all monoexcited triplet states of pyridine accessible to the method. This includes all those states for which each of the two singly occupied orbitals lies between the highest doubly occupied and the lowest virtual orbital of its particular symmetry species. The results of these calculations are given in Table I, where we compare the energy obtained by the virtual orbital and SCF approximations.

TABLE I: Triplet States of Pyridine[a]

	State	VO E, eV	VO Purity	Nature	SCF E, eV	Extrpn E, eV	Exptl[b] E, eV
1	1^3A_1	3.70	0.88	$a_2 \longrightarrow a_2^*$	4.05	3.61	3.70
2	1^3B_2	4.07	0.99	$a_2 \longrightarrow b_1^*$	3.92	3.89	3.87–4.01
3	1^3B_1	4.53	0.93	$a_1(n) \longrightarrow b_1^*$	4.27	3.86	
4	2^3A_1	4.73	0.89	$b_1 \longrightarrow b_1^*$	4.50	4.51	
5	2^3B_2	5.65	0.93	$b_1 \longrightarrow a_2^*$	5.51	5.47	
6	1^3A_2	5.74	0.99	$a_1(n) \longrightarrow a_2^*$	5.25	5.18	
7	3^3B_2	6.43	0.88	$a_2 \longrightarrow b_1^*$ (a)			
8	3^3A_1	7.10	0.84	$b_1 \longrightarrow b_1^*$ (a)			
9	2^3A_2	7.25	0.98	$b_2 \longrightarrow b_1^*$	7.21	7.09	
10	2^3B_1	7.66	0.68 0.56	$b_2 \longrightarrow a_2^*$ $a_1(n) \longrightarrow b_1^*$ (a)	7.68	7.56	
11	3^3B_1	7.81	0.72 0.51	$b_2 \longrightarrow a_2^*$ $a_1(n) \longrightarrow b_1^*$ (a)		7.70	
12	3^3A_2	8.53	0.98	$a_2 \longrightarrow a_1^*$	8.42	8.30	
14	4^3B_1	8.99	0.93	$a_2 \longrightarrow b_2^*$	9.06	8.85	
16	6^3B_1	9.81	0.91	$b_1 \longrightarrow a_1^*$	9.33	9.39	
20	5^3A_1	10.21	0.90	$a_1(n) \longrightarrow a_1^*$	9.45	9.39	
22	6^3A_2	10.46	0.77	$b_1 \longrightarrow b_2^*$	10.39	10.32	
24	5^3B_2	10.64	0.97	$a_1(n) \longrightarrow b_2^*$	9.99	9.91	
30	6^3B_2	11.87	0.99	$b_2 \longrightarrow a_1^*$	11.53	11.52	
36	7^3A_1	12.61	0.99	$b_2 \longrightarrow b_2^*$	12.50	12.50	

[a] b_1 and a_2 orbitals are π orbitals, a_1 and b_2 orbitals are σ. The only occupied a_1 orbital is the "n" orbital. (Orbitals marked (a) are not the lowest orbital of the symmetry species indicated. [b] S. Japar and D. A. Ramsay, *J. Chem. Phys.*, 58, 5832 (1973); cf. also references cited there.

It appears that pyridine was a reasonably fortunate choice for this comparison. First, of the twelve lowest triplet states, nine are accessible to the self-consistent calculation. Of the sixteen states calculated to self-consistency, only two correspond to VO states which are configurationally highly impure, and only two or three others contain, again in the VO method, even important admixtures of other configurations. In most of the states, the coefficient of the highest configuration, the *purity*, lies well above 0.90.

A number of observations immediately present themselves. $\pi \rightarrow \pi^*$ transitions, i.e., transitions between a_2 and b_1 orbitals in any combination, give rather similar results by the two methods. When configurationally sufficiently pure, such as state 2 (cf. Table I), the SCF energy is *slightly*, but only slightly, lower than the VO energy. When the states are not quite pure it is not unusual, such as in state 1, for the SCF energy to appear higher than the VO value, which must be ascribed to lowering of the latter by configuration interaction. The configurationally pure $n \rightarrow \pi^*$ state, state 6, provides a SCF energy 0.5 V below the VO energy. We suggest that in the self-consistent calculation we are including the singlet–triplet separation which cannot be included in the VO calculation, where an $n \rightarrow \pi^*$ triplet of necessity is degenerate with the corresponding singlet. The lowering of the other, lower $n \rightarrow \pi^*$ state, state 3, is significantly less, only about 0.25 V. The configurational purity in the VO calculation is somewhat less, and thus the self-consistent state may still be estimated a little too high, but we believe certainly not by more than, and probably considerably less than 0.25 V. The two B_1 states, 10 and 11, are very close in energy. The self-consistent calculation which gives only the $b_2 \rightarrow a_2$ transition, a $\pi \rightarrow \sigma^*$ transition, falls right into the same order of magnitude. Other $\sigma \rightarrow \pi^*$ and $\pi \rightarrow \sigma^*$ transitions seem generally to be calculated in fairly close agreement by the two methods.

We believe we can conclude from these data that the lower of the SCF and VO energies, particularly for the lowest state of any given symmetry, is an upper limit to the true energy. If the state is configurationally reasonably pure, it can probably be accepted as the best energy obtainable. If the state is configurationally impure, both may be assumed to be overestimates.

We have also made calculations for the pyridine anion radical and the pyridine cation radical, cf. Table II. We have again calculated all singly excited states which are accessible to the method, i.e., all those states in which the lone electron occupies an orbital above the highest doubly occupied and below the lowest virtual orbital of its symmetry species. In each case there are seven states that can be so described of which one, of course, is the ground state. Again, the pyridine situation is fortunate in that, of the lowest eight doublet states of the anion radical, six are accessible to our calculation, of the lowest seven states of the cation radical, five are accessible to SCF calculation, and further, the majority of these states are configurationally reasonably pure. The $\pi \rightarrow \pi^*$ states in the radical, again show very similar energy in the two methods; e.g. the A_2 state of the anion, state 2, and similarly, the A_2 state of the cation, state 7. SCF energies of the $n \rightarrow \pi^*$ states are systematically significantly lower by the SCF calculation as compared to the VO method. The other states again are equal or very nearly equal with the trend being that the self-consistent calculation gives somewhat lower energies and probably provide a slightly better upper bound.

It must be recognized, of course, that in the doublet states the virtual orbital calculations are based on the self-consistent doublet ground state, while in the triplet states,

TABLE II: Doublet States of the Pyridine Anion and Cation Radical

	State	VO E, eV	VO f	VO Purity	VO Nature	SCF E, eV	Extrp E, eV	Exptl *b*	Exptl *c*	Exptl *d*	Exptl *d*	Exptl *d*
					Anion Radical[a]							
1	1^2B_1	0.0	0.0	0.99	—	0.0	0.0	0.0	0.0	0.0	0.0	0.0
2	1^2A_2	0.51	0.0005	0.98	$b_1 \longrightarrow a_2^*$	0.53	0.54					
3	2^2B_1	2.39	0.10	0.90	$b_1 \longrightarrow b_1^*$			2.17			2.21	2.46
4	1^2A_1	4.47	0.004	0.98	$b_1 \longrightarrow a_1^*$	4.24	4.27		3.70	3.88	3.44–3.65	
5	2^2A_1	4.53	0.001	0.92	$a_1(n) \longrightarrow b_1$	4.14	3.92					
6	2^2A_2	5.04	0.18	0.94	$a_2 \longrightarrow b_1$	4.95	5.05					
7	1^2B_2	5.14	0.0	0.96	$b_1 \longrightarrow b_2^*$	5.12	5.10		5.08			
8	3^2B_1	5.17	0.07	0.70	$b_1 \longrightarrow b_1$							
20	5^2B_2	8.01	0.0	1.00	$b_2 \longrightarrow b_1$	7.71	7.71					
					Cation Radical							
1	1^2A_2	0.0	0.0	0.99	—	0.0	0.0					
2	1^2A_1	1.40	0.0	0.98	$a_2(n) \longrightarrow a_2$	0.77	0.81					
3	1^2B_1	1.45	0.006	0.99	$b_1 \longrightarrow a_2$	1.13	1.28					
4	1^2B_2	3.31	0.0	0.99	$b_2 \longrightarrow a_2$	3.15	3.31					
5	2^2B_1	4.32	0.001	0.70	$a_2 \longrightarrow b_1^*$							
6	2^2B_2	4.69	0.0	0.81	$a_1(n) \longrightarrow b_1^*$							
7	2^2A_2	4.91	0.17	0.91	$a_2 \longrightarrow a_2^*$	4.95	4.87					
26	$^2A_1$	9.02	0.0	0.96	$a_2 \longrightarrow a_1^*$	8.86	8.94					
28	$^2B_2$	9.28	0.0004	0.90	$a_2 \longrightarrow b_2^*$	9.32	9.28					

[a] See footnote to Table I. [b] K. Kuwater, T. Ogawa, and K. Hirota, *Bull. Chem. Soc. Jpn.*, 34, 291 (1961). [c] J. W. Dodd, F. J. Hopton, and N. S. Hush, *Proc. Chem. Soc.*, 61 (1962). [d] K. Kalyanraman, C. N. R. Rao, and M. V. George, *J. Chem. Soc. B*, 2406 (1971).

the virtual orbitals are calculated on the basis of a self-consistent singlet ground state. We have not so far made a CI calculation based on a self-consistent lowest triplet state by CI and, thus, do not know how such calculations might come out. One might expect them to be intermediate between the two cases.

We have made similar calculations for a number of other molecules, e.g., the diazines and formaldehyde, and find our general conclusions and patterns confirmed. In the interest of brevity, we shall not report all these detailed calculations. A similar set of calculations on naphthalene was less successful because here most states are configurationally much less pure. This will probably be general in alternant hydrocarbons, and is related to the remnants of the pairing theorem.[1]

The Extrapolation Method. It is generally believed that configuration interaction corrects principally for correlation effects.[11] On the other hand, we have shown above that the SCF calculation corrects the VO results primarily for the singlet–triplet splitting in n–π^* states. If we now make the (admittedly drastic) assumption that the CI and self-consistency corrections are truly *independent*, we can apply them as separate corrections, giving an *extrapolated* energy value. Thus, if the state $^3\Psi_j$ is given by

$$^3\Psi_j = \sum_i C_{ij}{}^{\mu\nu'} T_i$$

and has energy E_j^0, and if the VO and SCF calculations for a state of configuration $^{\mu\nu'}T_i$ give energies ϵ_i^0 and ϵ_i, respectively, the extrapolation yields:

$$E_j = E_j^0 - \sum_i C_{ij}{}^2(\epsilon_i^0 - \epsilon_1)$$

Whenever ϵ_i could not be calculated independently, we have assumed $\epsilon_i = \epsilon_i^0$.

The results from the extrapolation method are included in Tables I and II. It is seen that they always operate in the expected direction; when purity is high, the corrections are minimal; when the purity is low, the corrections become large, and it seems probable that, in such cases, the assumption of independence breaks down and energies may be seriously *underestimated*.

Molecular Orbital Energies. In the process of obtaining the data referred to in the preceding section to check the results of SCF calculations of excited triplets of neutral molecules and of doublet states of molecular ions, we have observed some regularities. To further investigate these, we have made the calculations for all singly excited triplets accessible to the SCF method for a number of molecules and for all singly excited doublet states for the corresponding molecular anions and cations accessible to the SCF method. We have performed these calculations for formaldehyde, ethylene, fulvene, pyridine, the three isomeric diazines, naphthalene, azulene, and quinoxaline (1,4-diazanaphthalene). The regularities observed in these series seem extremely striking, although some possibly could have been anticipated. We have drawn correlation diagrams for all of these cases, and a typical such correlation diagram for pyridine is shown in Figure 1. A number of observations follow immediately from even a cursory examination of these diagrams and have been verified by careful statistical work on the data obtained.

The first observation to appear is the fact the *range* of energies covered by the molecular orbitals is constant or almost constant to within a few tenths of an electron volt for the entire series from the doublet to the anion to the doublets of the cation through the triplets of the neutral molecule for any given compound, even though the absolute energies for the anions, cations, and neutrals differ significantly. What is even more surprising is the fact that the

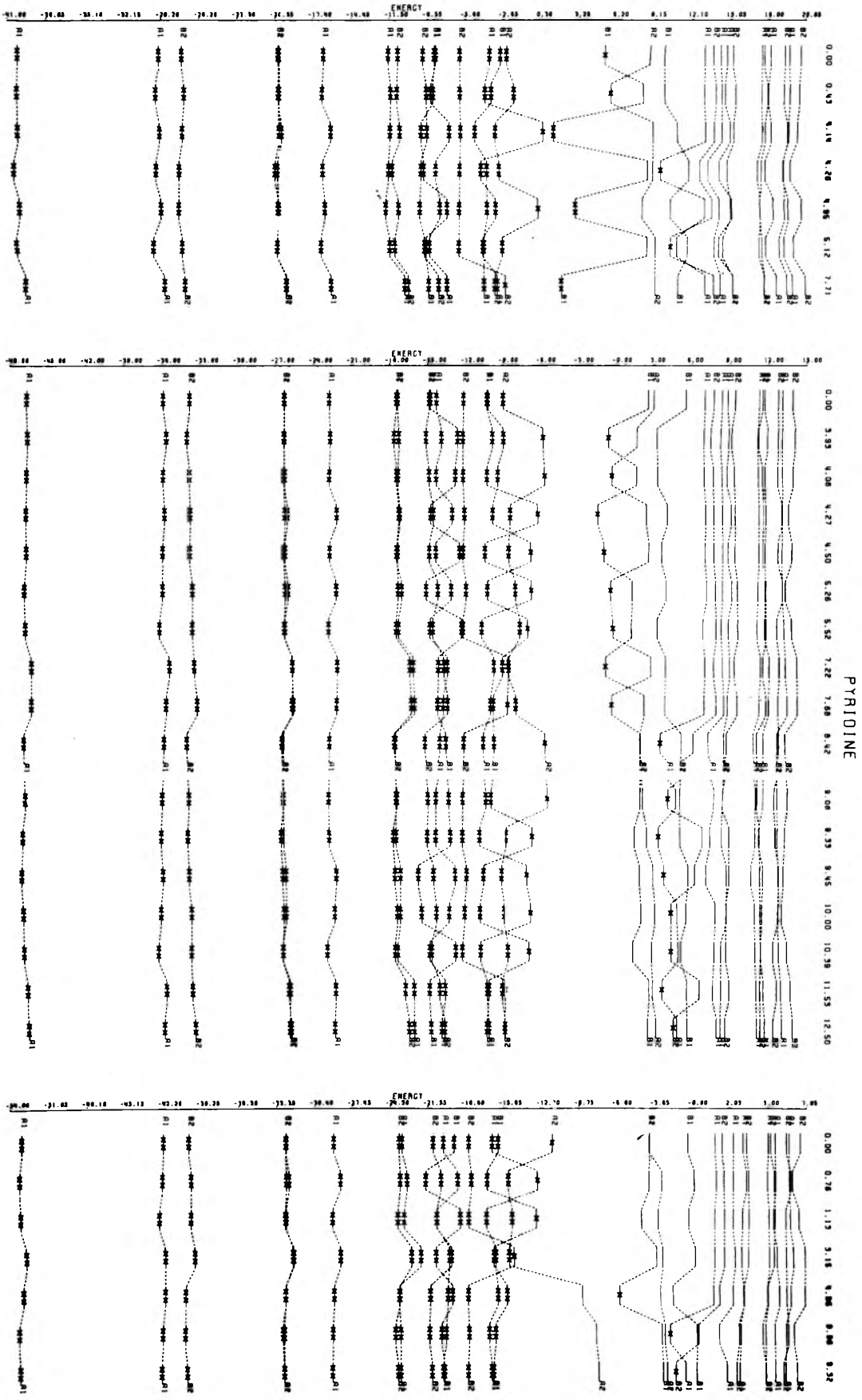

Figure 1. Correlation diagrams for the triplet states (center) of pyridine and the doublet states of its anion (left) and cation (right).

TABLE III: Ranges of Orbital Energies in the Triplet States of Neutral Molecules and the Doublet States of the Corresponding Molecular Cations and Anions[a]

	Anion			Neutral			Cation		
Compound	Lower limit	Upper limit	Range	Lower limit	Upper limit	Range	Lower limit	Upper limit	Range
Naphthalene	−42.13	16.26	58.39	−47.43	11.19	58.61	−52.42	5.81	58.23
Azulene	−44.01	17.10	61.11	−49.09	12.49	61.57	−54.14	6.97	61.11
Pyrazine	−41.15	18.00	59.15	−47.84	11.25	59.10	−54.21	4.53	58.74
Pyrimidine	−41.29	18.17	59.45	−47.97	11.65	59.62	−54.27	4.75	59.02
Pyridazine	−41.09	18.63	59.72	−47.83	11.93	59.76	−54.28	5.17	59.44
Pyridine	−40.64	17.91	58.55	−47.16	11.35	58.51	−53.39	4.87	58.27
Formaldehyde	−37.52	24.73	62.25	−48.26	14.88	63.14	−57.89	5.10	62.99
Quinoxaline	−47.23	18.52	65.75	−52.96	13.34	66.30	−58.43	7.77	66.20
Fulvene	−40.65	17.31	57.96	−46.69	11.35	58.03	−52.94	5.15	58.09
Ethylene	−28.63	19.09	47.72	−36.88	10.56	47.45	−45.18	2.08	47.26

[a] All singly excited states accessible to the SCF method are included.

range of energy is quite constant over the whole range of compounds studied, and Table III gives a summary of these ranges. This observation might possibly have been predicted on the basis of results of simple π electron MO calculations in which, while the ranges vary, they approach a limit as molecules get larger and larger. In the cases dealt with here, the number of orbitals is always quite large, beginning with 10 to 12 for formaldehyde and ethylene and going to 48 in naphthalene and azulene, and apparently we are approaching this limit.

The next observation we have made is that the energies of the lower doubly occupied orbitals are quite constant and are quite widely separated, that a rather large gap exists generally between the highest occupied, and the lowest unoccupied orbitals in the ground states which narrows in the excited states and sometimes even leads to an overlap. Still, there remains a gap between the family of orbitals that were doubly occupied and those that were virtual in the ground state. The virtual orbitals are much more closely spaced, and present an appearance resembling the band encountered in solids.

The third observation that was extremely striking was the change in orbital energy when one electron is removed from a doubly occupied orbital or one is added into a virtual orbital. This change is invariably of the order of 3 eV with the energy increasing (i.e, the negative energy decreasing) when an electron is removed from a doubly occupied orbital and a shift in the opposite direction when a lone electron is added to a virtual orbital. The constancy of this effect was so striking that we have carried out a statistical analysis of these shifts. In the series of compounds studied, which, of course, introduces a bias by its choice, we have found for 657 such shifts an average of 3.18 ± 0.02 eV. We have performed an analysis of variance of the moves of orbital energy and have found the most significant factor to be compound size; thus, the mean changes from 2.7 ± 0.2 in naphthalene at one extreme to 3.77 ± 0.5 in ethylene and 4.3 ± 0.2 in formaldehyde at the other. We are unable to give a rationale for this amazing constancy. We feel that it is connected with the appearance of certain J and K integrals in the calculation of the orbital energies, but no attempt to relate them with the pertinent J's and K's calculated and extracted from our program has been successful. The analysis of variance has further revealed that the effect of point group is highly significant. This, however, may well be an artifact because in the D_{2h} molecules we deal with many more states than in the C_{2v} molecules and the number of states is not well balanced between the different point groups. The next most significant effect lies in the σ or π nature of the orbital which gains or loses the electron. Since all molecules were planar, this classification is possible in all. Much to our surprise, however, the effect is slightly although significantly smaller in π orbitals than in σ orbitals. The only compound in which this generalization is violated is formaldehyde in which apparently we encounter other complicating factors. On the other hand, the analysis of variance indicates that the effects of removal of an electron from a doubly occupied orbital and of addition to a virtual one are indistinguishable in magnitude, though, of course, opposite in sign.

Certain doubly occupied orbitals of the ground state of the neutral molecule appear as virtual orbitals in excited states of the cation; similarly certain virtual orbitals of the neutral molecule appear as doubly occupied in some excited states of the anion. The change in energy of these orbitals has similarly been analyzed. Much to our surprise the energies obtained in this study, normalized to a change/electron added or removed, were very similar to those obtained in the triplet states. For a total of 77 such changes the overall average was 3.34 ± 0.08 eV/electron, less than 0.2 V greater than for the single electron changes. The effect of size is again very clear, in naphthalene the average is 2.64 ± 0.08 V, at the other extreme in ethylene it is 4.19 ± 0.18 V and in formaldehyde 4.98 ± 0.24 V. Table IV contains a summary of these results.

In the triplet states the removal and addition of an electron from a doubly occupied and virtual orbital always occur in coupled pairs. Although we have seen above that the values for a change of energy by addition or removal of a single electron was amazingly constant, we seemed to observe that the coupled pairs always went parallel. A regression analysis of the 243 such pairs shows a correlation coefficient of 0.93 between all of them. When further broken down the 76 pairs where both electrons were σ and the 51 pairs where both electrons were π electrons were correlated with the amazingly high correlation coefficients of 0.97 each, while the case where one orbital was a σ orbital, the other, a π orbital, was slightly less well correlated with a coefficient of 0.89 for 116 pairs. These extremely high and highly significant correlation coefficients gain in impor-

TABLE IV: A Summary of the Effect on Orbital Energy of Removal of One or Two Electrons from a Doubly Occupied, or Addition to a Virtual Orbital

	Single change		Double change[c]	
Compound	N[a]	Mean[b]	N[a]	Mean[b]
a. All Changes by Compounds				
Naphthalene	158	2.70 ± 0.02	14	2.64 ± 0.08
Azulene	46	2.86 ± 0.04	6	2.72 ± 0.09
Quinoxaline	46	3.06 ± 0.05	6	3.18 ± 0.17
Pyrazine	125	3.20 ± 0.03	13	3.27 ± 0.11
Pyrimidine	46	3.27 ± 0.04	6	3.25 ± 0.15
Pyridazine	46	3.36 ± 0.06	6	3.61 ± 0.15
Pyridine	46	3.26 ± 0.04	6	3.28 ± 0.15
Fulvene	46	3.24 ± 0.04	6	3.31 ± 0.14
Ethylene	70	3.77 ± 0.05	10	4.19 ± 0.18
Formaldehyde	28	4.28 ± 0.20	4	4.98 ± 0.24
Class				
b. All Compounds by Classes				
σ	369	3.26 ± 0.03		
π	288	3.07 ± 0.03		
Anions	85	3.27 ± 0.08		
Triplets	486	3.16 ± 0.02		
Cations	86	3.19 ± 0.08		
Removal	328	3.19 ± 0.03	38	3.30 ± 0.12
Addition	329	3.16 ± 0.03	39	3.39 ± 0.12
All	657	3.18 ± 0.02	77	3.34 ± 0.08

Source	DF[e]	SS[f]	MS[g]	F[g]
c. Analysis of Variance Results				
Total	656	186.11		
$\sigma - \pi$ difference	1	5.37	5.37	44.36**
Charge type	2	1.05	0.53	4.34*
Removal–addition differences	1	0.11	0.11	0.89
Compounds	9	101.79	11.31	93.48**
Point groups	1	5.65	5.65	46.68**
Size	2	91.01	45.50	376.09**
Remainder	643	77.80	0.12	

[a] Number of calculations in mean. [b] The mean ± its standard deviation. [c] Normalized per electron. [e] Degrees of freedom. [f] Sum of squares. [g] The variance ratio, F; a single asterisk indicates significance at the 95% m, a double asterisk at the 99% level.

tance when it is recognized that the total variations among the numbers is extremely small. At present we are unable to explain these observations.

We have also attempted to analyze the shifting of the orbitals not involved directly in the electronic transitions from the correlation diagrams of which Figure 1 is an example. The first observation is fairly simple. The lower doubly occupied orbitals and the higher virtual orbitals are relatively unaffected. They remain reasonably constant throughout the entire correlation diagram. In order to then better examine some of the orbitals within the area where larger changes occur, we have enlarged the scale in Figure 2 to show, in a correlation diagram for azulene, only those orbitals which are involved in significant shifts, orbitals 12 to 31 in this case. There are no unambiguous patterns immediately apparent. We have attempted an analysis to see whether we could detect any patterns by a statistical survey. We first examined orbitals which changed in energy by more than 1 eV in going from one state to another and found that these, with rare exception, transformed in the same irreducible representation or at least belonged to the same σ–π classification as the orbital gaining or losing an electron, and varied in the same direction. It also appeared as if such major shifts in energy were more common in the π than in the σ manifold. However the arbitrary cut-off of a shift by 1 eV seems questionably and so we analyzed the movement of all orbitals with the gain and loss of an electron in other orbitals. Here the results were not as clear-cut. When an electron is promoted or ionized out of a π orbital, it appears clear that other π electrons change more rapidly in energy than do σ orbitals. This is essentially independent of whether the electron is promoted into a π orbital or a σ orbital or is ionized. When an electron is lost by a σ orbital, however, there is no clear-cut distinguishability between the changes in σ and π orbitals. It may be that this is due to a compensation, that while the π orbitals are more polarizable, therefore, may change energy more easily, the σ orbitals are inherently more deeply affected by a change in another σ orbital. On the other hand, the apparent greater polarizability of the π electrons may well be an artifact: all the π electrons lie near the middle of the scale of orbital energies, while the σ electrons include the whole range, including the lowest and highest, which are particularly insensitive to the changes in states we induce.

We believe that the observations we are reporting here are of a general nature. The set of compounds we have chosen as a base contains alternants and nonalternants, hydrocarbons, azahydrocarbons, and one carbonyl compound. It may be that differences from these generalizations may have to be formulated if the range of types of compounds are extended very far, but it seems that over the types of compounds which we would commonly examine in the uv spectroscopic investigations these generalizations will hold widely.

Comparison with Experimental Results. The methods described in this paper were tested by a series of calculations on carbonyl compounds and aromatic heterocycles. Of particular interest are compounds where there is some doubt about the nature of the lowest triplet state, particularly whether it has n $\rightarrow \pi^*$ or $\pi \rightarrow \pi^*$ character.

Table V reports the results on a series of representative carbonyl compounds. The result for formaldehyde[12] and acetone[13] are excellent. In the two isomeric acroleins, the SCF results are in excellent agreement with experiment[14] and this appears to be a case where the extrapolation method seriously underestimates the triplet energy. No direct experimental results are available for formic acid. Although McGlynn[15] has argued for a lowest $\pi \rightarrow \pi^*$ triplet (though admittedly on circumstantial grounds) our results suggest that the n $\rightarrow \pi^*$ triplet is lowest, consistent with recent experiments by Ng and Bell[16] from whose singlet energies one may extrapolate to the triplet states.

In some of the aromatic carbonyl compounds the extrapolation method seems to lead to an underestimate of the triplet energies, which is not surprising in view of the usually very low configurational purity of the states; in many cases the leading configuration contributes less than 50% to the state. Thus, in benzaldehyde and 4-hydroxyacetophenone the n $\rightarrow \pi^*$ triplet energies are seriously underestimated by extrapolation. In the latter compound extrapolation brings the $\pi \rightarrow \pi^*$ triplet near the observed value,

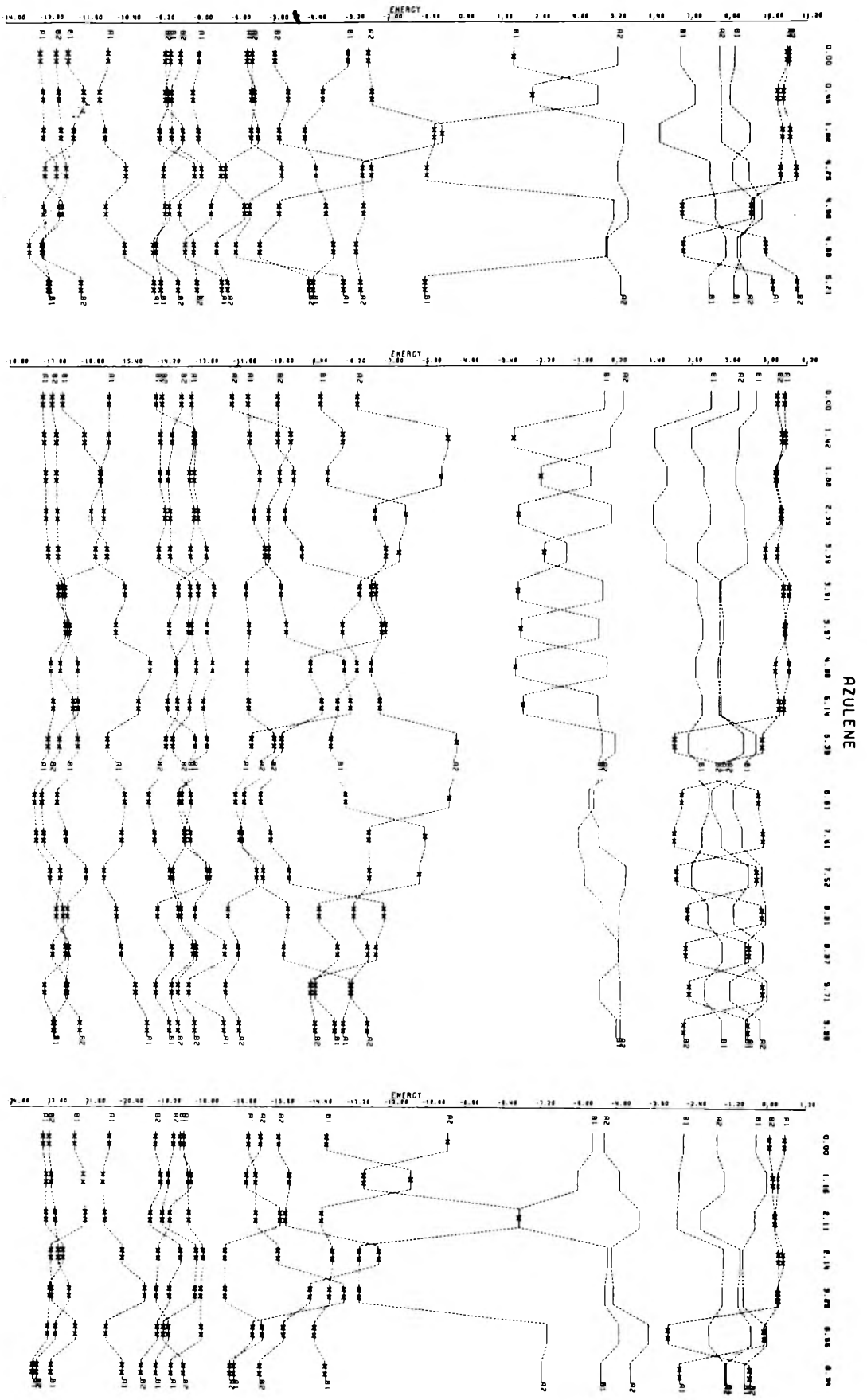

Figure 2. Correlation diagrams for the triplet states (center) of azulene and the doublet states of its anion (left) and cation (right). Only orbitals 12 through 31 are shown.

TABLE V: The Lowest n–π^* and $\pi \rightarrow \pi^*$ Triplet States in Some Carbonyl Compounds (All Energies in eV)

	n–π^* states						$\pi \rightarrow \pi^*$ states					
Compound	Exptl[a]	SCF	VO	P[b]	Extrpn[c]	Sym	Exptl[a]	SCF	VO	P[b]	Extrpn[c]	Sym
Formaldehyde	3.12[d]	3.32	3.79	1.00	3.24	A_2		6.52	6.64	1.00	6.52	A_1
Acetone	3.31[e]	3.39	3.94	0.99	3.22	A_2		6.13	6.32	0.98	5.87	A_1
cis-Acrolein	3.05[f]	3.10	3.60	0.83	(2.39)	A''		(4.39)	4.30	0.94	3.92	A'
trans-Acrolein	3.01[f]	3.07	3.56	0.82	(2.55)	A''		4.43	4.34	0.94	3.93	A'
cis-Methyl vinyl ketone		3.10	3.67	0.79	2.48	A''		3.53	3.48	0.96	3.14	A'
Formic ketone acid		4.09	4.82	1.00	4.06	A''		5.98	6.18	0.98	5.82	A'
	3.17[g,h]											
Benzaldehyde		3.05	3.68	0.71	(2.43)	A''	3.28[h]	(3.71)	3.63	0.72	3.37	A'
	3.29[h]											
Acetophenone	3.20	3.07	3.74	0.71	3.03	A''	3.28[h]	3.84	3.67	0.72	3.49	A'
4-Hydroxyacetophenone		3.10	3.76	0.70	(2.52)	A''	3.14[h]	3.46	3.48	0.85	3.13	A'
Benzoquinone	2.30[i]	(4.02)	3.22	0.82	2.79	A_u		(4.16)	3.44	0.86	3.16	B_{1u}
		(3.75)	3.14	0.87	2.87	B_{1g}		(3.92)	3.45	0.85	3.23	B_{3g}
Benzoic acid		3.85	4.65	0.68	3.53	A''	3.37	(3.82)	3.74	0.67	3.35	A'

[a] Experimental. [b] The purity, i.e., the coefficient of the leading configuration. [c] Extrapolated. [d] Reference 12. [e] Reference 13. [f] Reference 14. [g] J. W. Sidman, *Chem. Rev.*, 58, 689 (1958). [h] Reference 18. [i] Y. Kanda, R. Shimada, H. Shimada, H. Kaseda, and T. Matumura, Preprints of Tokyo Sympsoium (IUPAC) on Molecular Structure and Spectra, Tokyo, Japan, 1962, p 304, as quoted by S. P. McGlynn, T. Azumi, and M. Kinoshita, "Molecular Spectroscopy of the Triplet State," Prentice Hall, New York, N.Y., 1969, p 244. [j] D. S. McClure, *J. Chem. Phys.*, 17, 905 (1949).

TABLE VI: The Lowest Triplet States of Some Hydrocarbons and Heterocycles

	n–π^*						$\pi \rightarrow \pi^*$					
Compound	Exptl[a]	SCF	VO	P[b]	Extrpn[c]	Sym	Exptl[a]	SCF	VO	P[b]	Extrpn[c]	Sym
							3.70[d]	(4.05)	3.70	0.77	3.61	A_1
Pyridine	(3.87)[d]	4.27	4.53	0.87	3.86	B_1	3.87	3.92	4.07	0.98	3.89	B_2
Pyrazine	3.23[e]–3.33	(3.62)	3.39	0.97	3.29	B_{3u}		3.26	3.40	0.85	3.26	B_{1u}
Pyrimidine	3.50[f]–3.59	4.52	4.51	0.97	4.21	B_1		(4.15)	4.06	0.88	3.76	A_1
Pyridazine	3.08[g]–2.82	3.39	3.38	0.93	2.96	B_1		(4.04)	3.61	0.72	3.46	B_2
							3.49[h]	3.90	3.70	0.92	3.57	A_1
2,6-Lutidine		4.31	4.71	0.93	3.94	B_1		3.69	3.88	0.99	3.67	B_2
							3.35[h]	3.68	3.80	0.74	3.55	
3-Cyanopyridine		4.11	4.53	0.81	3.72	A''						A'
								3.66	3.83	0.97	3.44	B_2
4-Cyanopyridine	3.31[h]	3.94	4.33	0.89	3.42	B_1		(3.88)	3.79	0.82	3.50	A_1
Quinoline		3.83	4.25	0.79	3.20	A''	2.71[i]	2.77	2.81	0.86	2.25	A'
Isoquinoline		3.48	3.99	0.85	2.99	A''	2.65	2.72	2.71	0.95	2.43	A'
Cinnoline		3.05	3.25	0.70	2.59	A''	2.41[k]	2.62	2.60	0.79	2.22	A'
Quinazoline		3.66	4.08	0.88	3.20	A''	2.73[l]	3.41	3.42	0.90	3.06	A'
Quinoxaline		2.98	2.74	0.85	2.27	B_1	2.63[m]	3.38	3.58	0.86	2.98	B_2
		3.54	3.54	0.94	3.26	A_2		3.72	3.88	0.97	3.62	A_1
Phthalazine		3.91	3.96	0.81	3.17	B_1	2.85[n]	(2.98)	2.85	0.95	2.58	B_2
								3.49	3.48	0.93	3.15	A_1

[a]–[c] See Table V. [d] Reference 19. [e] References 21 and 22. [f] References 21 and 23. [g] References 21 and 24. [h] Reference 25. [i] Reference 26. [k] References 27 and 29. [l] References 26 and 27. [m] Reference 28. [n] References 29 and 30.

but we still favor the assignment of n $\rightarrow \pi^*$ character to the observed state.[17,18]

It appears from Table V that the SCF method provides good estimates of the lowest n $\rightarrow \pi^*$ triplets, to within less than 0.2 eV; for the $\pi \rightarrow \pi^*$ triplets, as far as they are known, the extrapolation method provides excellent estimates, to less than 0.1 eV.

The aromatic azines present a particularly interesting problem in that the lowest n $\rightarrow \pi$ and $\pi \rightarrow \pi^*$ triplets are very close in energy. Table VI presents the results of some calculations on these compounds. There seems to be little doubt that the first triplet in pyridine has $\pi \rightarrow \pi^*$ character.[19,20] In the three monocyclic diazines, the consensus of opinion places the n $\rightarrow \pi^*$ triplet below the $\pi \rightarrow \pi^*$ state.[21-23] In pyradizine our calculations agree well with experiment, in pyrazine we calculate the lowest n $\rightarrow \pi^*$ and $\pi \rightarrow \pi^*$ states essentially degenerate: in pyrimidine, however, our calculation seems seriously at variance with experiment.

A particularly interesting study concerns three substituted pyridines,[25] where, by appropriate choice of substituents, the order of states could be reversed. For the lutidine and the 3-cyano compound, our calculations, by any of the methods, give the lowest state correctly as $\pi \rightarrow \pi^*$, and for

the 4-cyano derivatives, although the extrapolation method predicts the correct order, the difference between the lowest three states are too small to be significant. All values agree reasonably with the experimental ones.

In the azanaphthalenes, quinoline, and isoquinoline, our calculations predict correctly the $\pi \rightarrow \pi^*$ state to be lowest,[26,27] and the experimental values lie between SCF and extrapolated calculations. In the diazanaphthalenes, also, the calculations appear to give reasonable results,[26,30] although the experimental situation seems far from clear.[29]

Discussion and Conclusions

We believe to have demonstrated that the methodology we propose holds promise to be useful in the prediction and interpretation of triplet spectra. A number of circumstances make more stringent tests difficult at this time. First, the reliable experimental material is relatively scarce, and almost always provides information about only one state (the lowest), although, in principle, information about higher states ought to be available from singlet–triplet absorption. Most of the experimental material comes from low temperature studies so that medium effects, which we cannot currently include in the calculations, may be important. Further, frequently there is little or no information about the equilibrium geometry of the molecules, even in the ground state, much less about the triplet; and we have frequently encountered molecules in which the results have been quite sensitive to geometry.

In spite of these difficulties we believe that we can say that the triplet states will generally lie between the lower of the VO or SCF calculation and the extrapolated value.

A further test of the method will depend on its ability to predict transitions within the triplet manifold. We are currently working on this problem, and preliminary results are encouraging.

Acknowledgments. We wish to acknowledge the courteous service of the Southwestern Ohio Regional Computer Center, which made this study possible.

References and Notes

(1) For previous papers in this series see R. L. Ellis and H. H. Jaffé, *J. Mol. Spectrosc.*, **50**, 474 (1974).
(2) R. Pariser and R. G. Parr, *J. Chem. Phys.*, **21**, 466, 767 (1953).
(3) R. Daudel and C. Sandorfy, "Semiempirical Wave-mechanical Calculations on Polyatomic Molecules", Yale University Press, New Haven, Conn., 1971.
(4) R. Constanciel, *Theor. Chem. Acta*, **26**, 249 (1972).
(5) J. A. Pople and R. N. Nesbet, *J. Chem. Phys.*, **22**, 571 (1954).
(6) C. C. J. Roothaan, *Rev. Mod. Phys.*, **32**, 179 (1960).
(7) J. Del Bene and H. H. Jaffé, *J. Chem. Phys.*, **48m** 1807, 4050 (1968); **49**, 1221 (1968); R. L. Ellis, G. Kuehnlenz, and H. H. Jaffé, *Theor. Chim. Acta*, **26**, 131 (1972).
(8) H. M. Chang, H. H. Jaffé, and C. A. Masmanidis, *J. Phys. Chem.*, following paper.
(9) H. H. Jaffé, H. M. Chang, and C. A. Masmanidis, *J. Comput. Phys.*, **14**, 180 (1974).
(10) H. H. Jaffé and R. L. Ellis, *J. Comput. Phys.*, **16**, 20 (1974).
(11) G. R. Taylor and R. G. Parr, *Proc. Natl. Acad. Sci.*, **38**, 154 (1952).
(12) J. C. D. Brand, *J. Chem. Soc.*, 858 (1956).
(13) W. D. Chandler and L. Goodman, *J. Mol. Spectrosc.*, **36**, 141 (1970).
(14) E. J. Bair, W. Goetz, and D. A. Ramsay, *Can. J. Phys.*, **49**, 2710 (1971); D. A. Hauer and D. A. Dows, *J. Mol. Spectrosoc.*, **34**, 296 (1970).
(15) L. W. Johnson, H. J. Maria, and S. P. McGlynn, *J. Chem. Phys.*, **54**, 3823 (1971).
(16) T. L. Ng and S. Bell, *J. Mol. Spectrosc.*, **50**, 166 (1974).
(17) H. M. Chang and H. H. Jaffé, *Chem. Phys. Lett.*, **23**, 146 (1973).
(18) D. R. Kearns and W. A. Case, *J. Am. Chem. Soc.*, **88**, 5087 (1966).
(19) S. Japar and D. A. Ramsay, *J. Chem. Phys.*, **58**, 5832 (1973).
(20) H. H. Jaffé, C. A. Masmanidis, H. M. Chang, and R. L. Ellis, *J. Chem. Phys.*, **60**, 1696 (1974).
(21) M. A. El-Sayed, *J. Chem. Phys.*, **36**, 573 (1962).
(22) K. K. Innes and L. E. Giddings, *Discuss. Faraday Soc.*, **35**, 192 (1963).
(23) V. G. Krishna and L. Goodman, *J. Chem. Phys.*, **36**, 2217 (1962).
(24) K. K. Innes, W. C. Tincher, and E. F. Pearson, *J. Mol. Spectrosc.*, **46**, 14 (1970).
(25) R. L. Hoover and M. Kasha, *J. Am. Chem. Soc.*, **91**, 6508 (1969).
(26) M. A. El-Sayed, *J. Chem. Phys.*, **38**, 2834 (1963); S. M. Ziegler and M. A. El-Sayed, *ibid.*, **52**, 3257 (1970).
(27) R. Miller and F. Dorr, *Z. Elecktrochem.*, **63**, 1150 (1959).
(28) F. Dorr, H. Gropper, and N. Mika, *Ber. Bunsenges. Phys. Chem.*, **67**, 54 (1963).
(29) J. A. Stikeleather, *Chem. Phys. Lett.*, **24**, 253 (1974).
(30) E. C. Lim and J. Stanislaus, *J. Chem. Phys.*, **53**, 2096 (1970).

Use of the CNDO Method in Spectroscopy. XIV. Electronic Spectra of Free Radicals and Free Radical Ions[1,2]

H. M. Chang, H. H. Jaffe,* and C. A. Masmanidis

Department of Chemistry, University of Cincinnati, Cincinnati, Ohio 45221 *(Received September 4, 1974)*

The CNDO/S method is extended to the calculations of doublet states. The ground state of doublets is calculated by the restricted Hartree–Fock SCF method of Roothaan, and the higher states are obtained either by the virtual orbital approximation and refined by configuration interaction or directly calculated by a SCF method. The calculated spectra by the open-shell CNDO/S method for a series of radicals and radical ions are in reasonable agreement with the experimental data.

Most early attempts at calculation of electronic spectra of free radicals are based on the restricted Hartree–Fock (RHF) method of Longuet-Higgins and Pople.[3] However, in this method the interaction between the unpaired electron and those represented by the doubly occupied orbitals is neglected. The Roothaan RHF method,[4] on the other hand, does not suffer from this neglect. We have used the Roothaan RHF formalism, coupled with the approxima-

tions implicit in the CNDO/S scheme for closed-shell systems,[5] to develop a method for the calculation of electronic spectra of molecules with doublet ground states.

The method, perfectly analogous to the CNDO/S closed-shell calculation, uses semiempirical values for most integrals, calculates the wave function of the ground state, and develops excited configurations using the virtual orbitals of the ground state. It then invokes limited configuration interaction with singly excited configurations to obtain excited state energies, and transition moments and polarizations for the transitions. This method will be referred to as the VO method. Full use is made of the zero-differential-overlap (ZDO) approximation inherent in all CNDO calculations. Although treatment of quartet states by the method employed is perfectly feasible, we have not bothered with such calculations since we know of no experimental results for quartet states.

We have simultaneously developed a second method for calculation of excited doublet states. This method depends on the direct SCF calculation of the state in question. It involves all the same approximations, but does not use any configuration interaction. Thus, it provides self-consistent wave functions and their energies. When states are configurationally reasonably pure, the direct SCF method probably provides a better approximation to the true energy than the VO–CI method, but where configurational mixing is severe, results are likely not to be reliable. The direct SCF method has been described in detail elsewhere,[6] and is quite analogous to the corresponding method applied to triplet states, which is described in a companion paper.[1] In what follows, we shall compare results obtained by both methods.

To demonstrate the validity and usefulness of these methods, we have performed calculations on a reasonable number of molecules with doublet ground states (free radicals and radical ions). We first studied the benzyl radical, the spectrum of which has been widely investigated, and its isoelectronic analogs, the phenoxy and anilino radicals. We have then extended the study to the well-known spectra of the polycyclic hydrocarbon anion radicals, and the much less studied cation analogs. Finally, we have studied a series of radical ions derived from cyano- and nitrobenzene, pyridine, and *p*-benzosemiquinone.

The crucial point of any semiempirical quantum mechanical study is the choice of the semiempirical parameters. Two types of such parameters should be distinguished: on the one hand, those which are systematically chosen, usually from atomic spectroscopic data (such as the Γ_{rr}) or approximated by more or less well-justified interpolation methods or general formulas; on the other hand, those which are freely and numerically *adjustable*. The degree of validity of a method depends to a large extent on the relation of the number of adjustable parameters to the number of experimental observables which are reproduced with reasonable accuracy.

In the method which we are presenting here, *no new* parameters have been adjusted *numerically; all adjustable parameters*, the β_r^0 and κ, *as well as all systematic parameters were carried over unchanged from the closed-shell CNDO/S method*. The only *arbitrary* decision required lay in the choice of the approximation formula used for the two-center electron repulsion integrals, Γ_{rs}. The closed-shell CNDO/S methods used for these integrals, were the Mataga–Nishimoto approximation[7] when calculating singlet states, and the Pariser–Parr interpolation method[8] when calculating triplet states. As will be shown below, the latter is the approximation of choice for doublet states also.

Methods of Calculation

Systems with one unpaired electron in the ground state can be represented by a single configuration wave function consisting of a single Slater determinant. There are three types of configurations corresponding formally to one-electron excitation: the ground and the four types of excited configurations denoted as G, A, B, and C in Chart I. Configurations of type G, A, and B give rise to doublet states only, while configurations of type C give rise to a quartet and *two* doublets, C_α and C_β. The corresponding wave functions for the doublet states are

$$^2\Psi_G = (2m-1)!^{-1/2}|\psi_1\bar{\psi}_1\cdots\psi_{m-1}\bar{\psi}_{m-1}\psi_m|$$

$$^2\Psi_A = (2m-1)!^{-1/2}|\psi_1\bar{\psi}_1\cdots\psi_i\bar{\psi}_m\cdots\psi_{m-1}\bar{\psi}_{m-1}\psi_m|$$

$$^2\Psi_B = (2m-1)!^{-1/2}|\psi_1\bar{\psi}_1\cdots\psi_i\bar{\psi}_i\cdots\psi_{m-1}\bar{\psi}_{m-1}\psi_x|$$

$$^2\Psi_{C_\alpha} = (2m-1)!^{-1/2}\frac{1}{\sqrt{2}}(|\psi_1\bar{\psi}_1\cdots\psi_i\bar{\psi}_x\cdots\psi_{m-1}\bar{\psi}_{m-1}\psi_m| + |\psi_1\bar{\psi}_1\cdots\psi_x\bar{\psi}_i\cdots\psi_{m-1}\bar{\psi}_{m-1}\psi_m|)$$

$$^2\Psi_{C_\beta} = (2m-1)!^{-1/2}\frac{1}{\sqrt{6}}(|\psi_1\bar{\psi}_1\cdots\psi_i\bar{\psi}_x\cdots\psi_{m-1}\bar{\psi}_{m-1}\psi_m| - |\psi_1\bar{\psi}_1\cdots\psi_x\bar{\psi}_i\cdots\psi_{m-1}\psi_{m-1}\psi_m| + 2|\psi_1\bar{\psi}_1\cdots\psi_i\bar{\psi}_m\cdots\psi_{m-1}\psi_{m-1}\psi_x|)$$

The molecular orbitals in the LCAO form are given by

$$\psi_\mu = \sum_\rho c_{\mu\rho}\phi_\rho$$

where ϕ_ρ are valence atomic orbitals. The LCAO coefficients are obtained by solution of the pseudo-eigenvalue problem

$$\sum_\sigma (F_{\rho\sigma} - \delta_{\rho\sigma}\epsilon)c_{i\sigma} = 0$$

where the matrix elements of Hartree–Fock's operators are given by

$$F_{\rho\rho} = -\frac{1}{2}(I_A + A_A) - \left(Z_A - \frac{1}{2} + \frac{1}{2}\sum_k C_{k\rho}2 + \frac{3}{2}\sum_m C_{m\rho}^2\right)\Gamma_{AA} + \sum_\lambda\left(\sum_k C_{k\lambda}^2 + \frac{1}{2}\Sigma C_{mx}^2\right)\Gamma_{AB\text{-}B\neq A}\Sigma Z_B\Gamma_{AB} + 2\sum_x\left(\sum_k C_{k\rho}C_{k\lambda} + \frac{1}{2}\sum_m C_{m\rho}C_{m\lambda}\right)\sum_m C_{m\rho}C_{m\lambda}\Gamma_{AB}$$

$$F_{\rho\sigma} = \frac{1}{2}\left(\beta_A^0 + \beta_B^0\right)S_{\rho\sigma} - \frac{1}{2}\left(\sum_k C_{k\rho}C_{k\sigma} + \frac{3}{2}\sum_m C_{m\rho}C_{m\sigma}\right)\Gamma_{AB} + \sum_\lambda\left(\sum_k C_{k\rho}C_{k\lambda} + \frac{1}{2}\sum_m C_{m\rho}C_{m\lambda}\right)\sum_m C_{m\rho}C_{m\lambda}\Gamma_{CB} + \left(\sum_k C_{k\lambda}C_{k\sigma} + \frac{1}{2}\sum_m C_{m\lambda}C_{m\sigma}\right)\sum_m C_{m\sigma}C_{m\lambda}\Gamma_{AC}$$

and I_A is the valence state ionization potential of atom A, A_A is the electron affinity of atom A, Z_A is the Slater effective nuclear charge of atom A, Γ_{AB} is the two center elec-

Chart I

	G	A	B	C
y	———	———	———	———
x	———	———	—X—	—X—
m	—X—	–X–X–	———	—X—
j	–X–X–	–X–X–	–X–X–	—X—
i	–X–X–	—X—	–X–X–	–X–X–

tron repulsion integral on atoms A and B, β_A^0 is the adjustable parameter depending only on the nature of atom A (see Table I for the numerical values assigned these parameters). $S_{\mu m} = S_{\mu m}^{\sigma} + \kappa S_{\rho\sigma}^{\pi}$, and $S_{\rho\sigma}^{\sigma}$ and $S_{\rho\sigma}^{\pi}$ are, respectively, the σ and the π components of the overlap integral; κ is a parameter which is suggested by Del Bene and Jaffé.[5] The electronic energy of the ground configuration is given by

$$E = \sum_k (H_k + \epsilon_k) + \frac{1}{2}(H_m + \epsilon_m) - \sum_k K_{km} - \frac{1}{4} K_{mm}$$

where the ϵ's are the "orbital energies".

The single determinant wave functions Ψ_I were improved by configuration interaction, as in the closed-shell CNDO/S method.[5] The excitation energies for the configuration are obtained according to the formulas given by Felton et al.[9] and by Zahradnik and Čársky.[10] The matrix elements between doublets states are evaluated according formulas given by the latter authors.[10]

Results and Discussion

We present below, in a series of tables, the results obtained for a variety of molecules. In these tables we list all states calculated by the VO method below 6.0 eV. Wherever possible, calculations by the SCF method are also given. Where these results are lower than the VO results, they probably present a better approximation to the true energy of the state in question. Unfortunately, the configurational purity (as measured by the CI coefficient of the leading configuration) is often so low, that the SCF method does not give better results than the VO method. As we have seen previously for triplets, the SCF method is particularly useful for states involving transitions of electrons between σ and π orbitals, and this observation is reconfirmed here. Unfortunately, such transitions do not appear to have been observed in radical spectra because of their low intensity.

The Benzyl Isoelectronic Series. As a first test of the method we have examined the isoelectronic series based on the benzyl radical: benzyl (1) $C_6H_5CH_2$·, anilino (2), C_5H_5NH·, and phenoxy (3), C_6H_5O·. The exocyclic C–C distance in 1 was taken as 1.44 Å according to Schug and Phillips.[11] 2 was assumed to transform in point group C_s with a C–N bond length of 1.44 Å and a CNH angle of 120°. In consideration of the relation between bond lengths and bond orders, we have taken 1.40 Å for the CO bond in 3. For the two-center electron repulsion integrals, we have tried both the Pariser–Parr interpolation method[8] and Mataga–Nishimoto approximation.[7] The calculations were performed with 50 configurations.

The results of these calculations are compared with experimental values in Tables II–IV. The experimental results for 1 are taken from the work of Porter,[12] Leach,[13] and Albrecht[14] and their respective coworkers, all of which are in good agreement. The symmetry of the first excited state of benzyl has been controversial until it was recently resolved in favor of A_2 by Leach et al.,[13] and confirmed by Albrecht et al.[14b] The latter authors also corrected the symmetries of the higher excited states. The results for the other two radicals also come from Porter's laboratory.[12]

TABLE I: CNDO/S Parameters[a]

Element	β^a	$\Gamma_{AA}{}^b$	UUSO[c]	UUPO[c]
H	12.0	12.85	14.35	
Li		2.98	6.21	4.10
Be		5.35	13.10	6.87
B	5.0	8.10	20.61	8.74
C	17.5	10.93	29.92	11.61
N	26.0	11.88	40.97	16.96
O	45.0	15.13	54.51	21.93
F	50.0	17.36	56.96	24.36

[a] β is the empirical parameter for the atom A. [b] Γ_{AA} is the difference between ionization potential (IP) and electron affinity (EA) for the valence electron in atom A. [c] UUSO and UUPO are the sum of the IP and EA for the s and p orbital electron, respectively. [d] All values are in electron volts.

The calculated results for these three radicals agree well with the experimental values. For the seven bands found, results with Pariser–Parr (PP) Γ's agree to an average of 0.14 eV, those obtained with Mataga–Nishimoto (MN) Γ's to an average deviation of 0.21 eV. Furthermore, the results for the benzyl radical with the PP integrals are clearly superior (average deviation 0.03 eV) to those obtained with the MN integrals (average deviation 0.11 eV), and in this molecule we have without a doubt the best experimental work and the best knowledge of the geometry. Our symmetry assignment of the lowest state of benzyl of A_2 also agrees with the latest experimental finding, although not too much importance should be attached to this result in the light of the minimal energy difference between the B_1 and A_2 states. Calculations for benzyl by Hinchliffe et al.[15] and by Schug and Phillips[11] do not fit the experimental data as well.

Since the Pariser–Parr interpolation for Γ_{rs} gave significantly better results in the calculations of the benzyl, anilino, and phenoxy radicals, this approximation was used in the remaining calculations.

Hydrocarbon Radical Ions. The spectra of the naphthalene, antracene, phenanthrene, tetracene, and pyrene radical anions, and of the anthracene, tetracene, and pyrene radical cations were calculated. The geometries of the radical anions and cations were assumed to be same as those of the corresponding parent neutral molecules which were taken from crystallographic data in the literature.

The calculated results of this work in Tables V–VIII and Figures 1–8 show that in the cases of radical anions, our results are in good agreement with the experimental data[16] and better than those of other available calculations.[17-20] If we can trust our guesses as to what is vibronic structure, and our assignments, we have, for the three compounds of Tables V–VII, 11 bands with an average deviation of 0.17 eV.

The situation in the radical cations is greatly complicated by the fact that the experimental results, particularly for the anthracene and pyrene radical cations,[21] differ widely with the conditions used. It would appear, however, that anthracene definitely has transitions near 1.76 and 2.83 eV, and probably near 3.49 and 3.91 eV. The assignment of a correspondence to calculated transitions seems too uncertain to attempt. The situation in pyrene is no bet-

TABLE II: Observed and Calculated Spectra of Benzyl Radical (All Energies in eV)

Exptl[a] energy (ref 12–14)	SCF[b,c] energy	VO PP[b] energy	VO f[d]	VO Sym[e] type	VO Purity[f]	VO MN[g] energy	Lit. Ref 15 Energy	Lit. Ref 15 f[d]	Lit. Ref 11 Energy	Lit. Ref 11 f[d]
0	0	0		B_1	0.99	0	0		0	
2.73	M	2.77	0.002	A_2	M	2.62	2.69	0.002	3.08	0
	–	2.78	0.005	B_1	M	2.49	3.43	0.002	2.66	0.004
3.88	M	3.85	0.04	A_2	M	4.02	4.05	0.39	4.74	0.06
	–	4.38	0.04	B_1(C)	0.81	4.01			4.41	0
4.77	–	4.80	0.20	B_1(C)	M	4.86	4.72	1.23	5.43	0.22
	–	5.48	0.0005	A_2(C)	M	5.25	5.30	0.28		
	–	5.75	0.005	B_1(B)	0.66	5.27				
	5.75	5.78	0.001	A_1(A)[h]	0.85					

[a] No intensities are available. [b] Using Pariser-Parr integrals. [c] M indicates that no clear leading configuration could be found. A dash indicates states inaccessible to SCF calculation. [d] Oscillator strength. [e] The type (in parentheses) refers to the classification given in the text. [f] The coefficient of the leading configuration. [g] Using Mataga-Nishimoto integrals. [h] $\sigma \rightarrow \pi^*$ (or $n \rightarrow \pi^*$) transition.

TABLE III: Observed and Calculated Spectra of Phenoxy Radical

Exptl[a] energy (ref 12)	SCF[b,c] energy	VO PP[b] energy	VO f[d]	VO Sym type[e]	VO Purity[f]	VO MN[g] energy	Lit. (ref 11) Energy	Lit. (ref 11) f[d]
0	0	0		A_1	0.99	0	0	
	0.16	0.66	0	B_1(A)	0.88	0.35		
	2.21	2.34	0.003	A_2(A)	0.83	2.36	2.46	0
3.09	M	3.22	0.02	B_2	M	2.64	3.43	0.04
3.94	(3.88)	3.81	0.10	A_2(B)	0.79	3.82	4.16	0.63
	M	4.73	0.30	B_2	M	4.12	4.71	0.22
	–	4.88	0.19	B_2(C)	0.75	4.95	5.13	0.06
	–	5.06	0.0003	A_1(B)	0.87			
	–	5.22	0	B_1(A)	0.76			

[a–h] All energies in eV. For footnotes *a–h* cf. Table II.

TABLE IV: Observed and Calculated Spectra of the Anilino Radical ($C_6H_5NH\cdot$)

Exptl[a] energy (ref 12)	SCF[b,c] energy	VO PP[b] energy	VO f[d]	VO Sym type[e]	VO Purity[f]	VO MN[g] energy	Lit. (ref 11) Energy	Lit. (ref 11) f[d]
0	0	0		A''	0.99	0	0	
	1.71	2.13	0.002	A'(A)[h]	0.90	2.52		
	–	2.74	0.001	A''(A)	0.70	2.56		
3.09	–	2.85	0.008	A''	M	2.71	2.83	0.007
	–	3.80	0.04	A''(B)	0.64	3.96	3.50	0.02
4.01	–	4.36	0.16	A''	M	4.02	4.27	0.47
	–	4.58	0.12	A''(C)	0.77	5.03	4.72	0.53
	–	5.48	0.001	A''(C)	0.66	5.11		
	–	5.63	0	A'(A)[h]	0.80			
	–	5.74	0.0009	A''	M			

[a–h] All energies in eV. For footnotes *a–h*, cf. Table II.

ter. However, the tetracene cation radical appears to present a cleaner picture; five bands seem discernible in the spectrum, and might well correspond to the first six calculated transitions (cf. Figure 8). At this point we cannot say more about the radical cations; whether the failure to better reproduce the spectra is due to uncertainties in the geometries, in the strong solvent or anion interaction or whether the method actually fails is not known.

Our calculations on the hydrocarbon radical ions agree with those of Hoijtink et al.[21] in predicting that most low-energy bands are due to transitions from the singly occupied orbital to the virtual orbitals or from the doubly occupied orbital to the singly occupied one, i.e., involve upper states of B or A type.

TABLE V: Observed and Calculated Spectra of Naphthalene Anion Radical

Exptl[a] (ref 16)		SCF[b,c]	VO			
Energy	$10^{-4}\epsilon$[i]	energy	Energy	f[d]	Sym[e] type	Purity[f]
0		0	0		B_{2g}	0.99
		0.36	0.69	0	B_{1g}(B)	0.98
1.49	0.26	(1.51)	1.42	0.14	B_{3u}(B)	0.96
1.64	0.28					
		(2.58)	2.19	0.08	A_u(B)	0.91
		—	3.36	0	B_{1g}(B)	0.89
3.60	0.29					
3.84	1.27	(4.22)	3.90	0.23	A_u(A)	0.85
3.97	0.70					
		4.23	4.75	0	B_{2u}(B)[j]	1.00
4.22	1.70	(4.78)	4.65	0.26	B_{3u}(A)	0.76
4.34	1.05					
		5.11	5.51	0	B_{2g}(B)[j]	1.00
		5.35	5.69	0	A_g(B)[j]	0.99
		(6.20)	5.51	0	B_{1g}(A)	0.76
		—	5.78	0.14	A_u(C)	0.75
		M	5.79	0	B_{2g}	M
		—	5.90	0	B_{1g}(C)	0.94
			5.91	0	B_{2g}	0.68
			5.93	0	B_{2u}(B)[j]	1.00

[a-h] All energies in eV. For footnotes a–h, cf. Table II. [i] (Extinction coefficient)10^{-4}. [j] $\pi \rightarrow \sigma^*$ transition.

TABLE VI: Observed and Calculated Spectra of the Anthracene Anion Radical

Exptl[a] (ref 16)		SCF[b,c]	VO			
Energy	$10^{-4}\epsilon$[i]	energy	Energy	f[d]	Sym[e] type	Purity[f]
0		0	0		B_{3u}	0.99
		1.16	1.43	0	A_u(B)	0.96
1.70	0.89	(1.79)	1.63	0.24	B_{2g}(B)	0.95
2.11	0.51	M	2.27	0	B_{1g}	M
		—	2.49	0	B_{3u}(B)	0.94
3.16	0.56					
3.38	2.43	M	3.24	0.35	B_{1g}	M
3.50	1.38					
		—	3.90	0	A_u(B)	0.73
		M	3.97	0.05	B_{1g}	M
3.81	3.84	(4.09)	3.98	0.27	B_{2g}(A)	0.68
		—	4.69	0	A_u(C)	0.82
4.71	7.6	—	4.86	0.55	B_{2g}(C)	0.69
		5.02	5.40	0	B_{2u}(B)[j]	0.90
		M	5.13	0	A_u	M
		—	5.32	0.006	B_{1g}(C)	0.76
		M	5.43	0	B_{3u}	M
		M	5.62	0	B_{3u}	M
		M	5.70	0.0001	B_{1g}	M
		—	5.94	0.19	B_{2g}(C)	0.68

[a-h] All energies in eV. For footnotes a–h, cf. Table II. [i] (Extinction coefficient)10^{-4}. [j] $\pi \rightarrow \sigma^*$ transition.

Calculations for *trans*-butadiene radical anion and cation are reported and compared with experimental values[22,23] in Table VIII. As frequently found with CNDO/S calculations, results on small molecules are far from satisfactory. The results for the radical cation, as for the other hydrocarbon radical cations, seriously overestimate all

TABLE VII: Observed and Calculated Spectra of Phenanthrene Anion Radical

Exptl[a] (ref 16)		SCF[b,c]	VO			
Energy	$10^{-4}\epsilon$[i]	energy	Energy	f[d]	Sym[e] type	Purity[f]
0		0	0		A_2	0.99
0.72	0.01					
1.15	0.24	(1.28)	1.23	0.003	B_2(B)	0.85
1.31	0.26					
1.90	0.11	—	1.96	0.06	B_2(B)	0.85
2.73	0.92		2.43	0.09	A_2(B)	0.87
2.99	0.90	2.43	2.48	0.44	B_2(A)	0.92
3.14	0.70		2.56	0.01	A_2(B)	0.84
		—	3.72	0.03	A_2(C)	0.74
		—	3.93	0	B_2(B)	0.64
		—	4.46	0.12	A_2(A)	0.63
		—	4.69	0	B_2	M
		—	4.77	0.01	B_1[j]	M
		—	4.91	0	A_2	M
		—	5.19	0.003	B_2	M
		5.22	5.55	0	B_1(A)[j]	1.00
		—	5.25	0.14	A_2(B)	0.67
		—	5.44	0.01	B_2	M
		—	5.53	0.27	A_2(A)	0.61

[a-h] All energies in eV. For footnotes a–h, cf. Table II. [i] (Extinction coefficient)10^{-4}. [j] $\pi \rightarrow \sigma^*$ transitions.

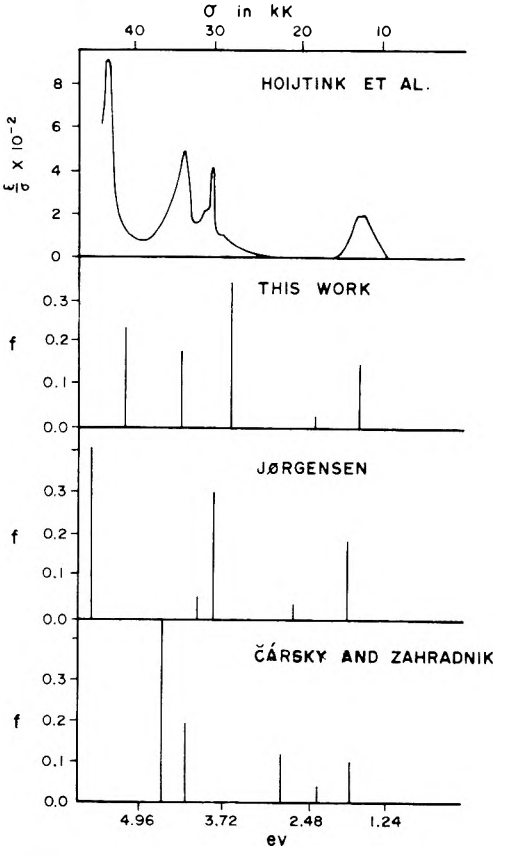

Figure 1. Comparison of observed and calculated spectra of the naphthalene radical anion.

TABLE VIII: Observed and Calculated Spectra of *trans*-Butadiene Anion and Cation Radicals

Exptl[a] (ref 23)		SCF[b,c]	VO				Lit. (ref 22)	
Energy	OD[i]	energy	Energy	f[d]	Sym type	Purity[e]	Energy	f[d]
			Anion					
0		0	0		A_u	0.99	0	
2.18	0.30	(2.12)	2.00	0.09	B_g(B)	0.95	2.03	0.04
3.19	1.40	(4.40)	4.13	0.59	B_g(A)	0.89	3.29	0.56
		4.31	4.31	0	B_u(B)[j]	0.95	4.34	0
		(5.70)	5.11	0.04	A_g(B)[j]	0.91	4.85	0.04
		—	5.84	0	B_u(B)[j]	0.91		
		—	5.89	0	A_u(A)	0.80	5.52	0
			Cation					
0		0	0		B_g	0.99		
2.16	0.45							
3.22	1.15	(3.22)	2.94	0.04	A_u(A)	0.83		
		4.02	4.01	0	A_g(A)[h]	0.98		
		(4.41)	4.33	0.75	A_u(B)	0.77		
		—	4.94	0	A_g(A)[h]	0.99		
		—	5.26	0	B_g(B)	0.91		
		—	5.46	0.0002	B_u(A)[h]	0.94		

[a-h] All energies in eV. For footnotes *a-h*, cf. Table II. [i] Optical density. [j] $\pi \rightarrow \sigma^*$ transition.

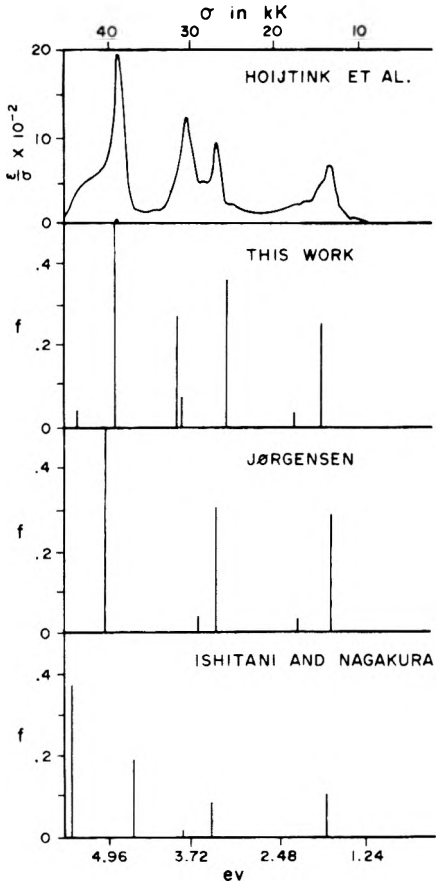

Figure 2. Comparison of observed and calculated spectra of the anthracene radical anion.

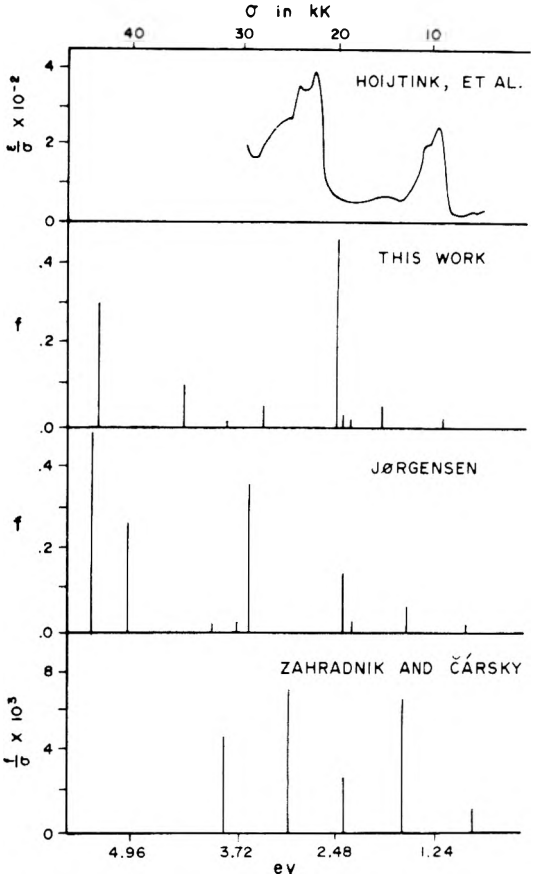

Figure 3. Comparison of observed and calculated spectra of the phenanthrene radical anion.

transition energies. For the anion, the lowest state is not badly reproduced.

Radical Anions of Benzonitrile and Analogs. The spectra of the radical anions of benzonitrile, C_6H_5CN (4), phthalonitrile, *o*-$C_6H_4(CN)_2$ (5), isophthalonitrile, *m*-$C_6H_4(CN)_2$ (6), terephthalonitrile, *p*-$C_6H_4(CN)_2$ (7), and pyromellitonitrile, *sym*-$C_6H_2(CN)_4$ (8), were calculated. In this calculation, we used the same geometries as Ishitani and Nagakura.[19]

Our calculations, Table IX, result in B_2 symmetry for the

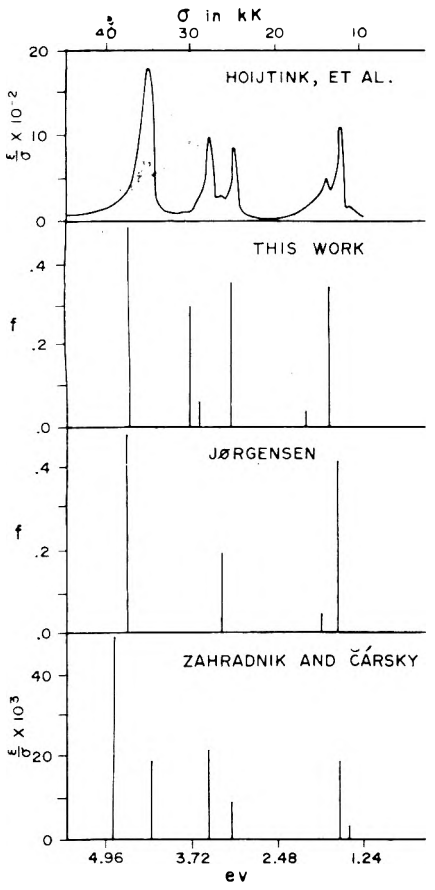

Figure 4. Comparison of observed and calculated spectra of the tetracene radical anion.

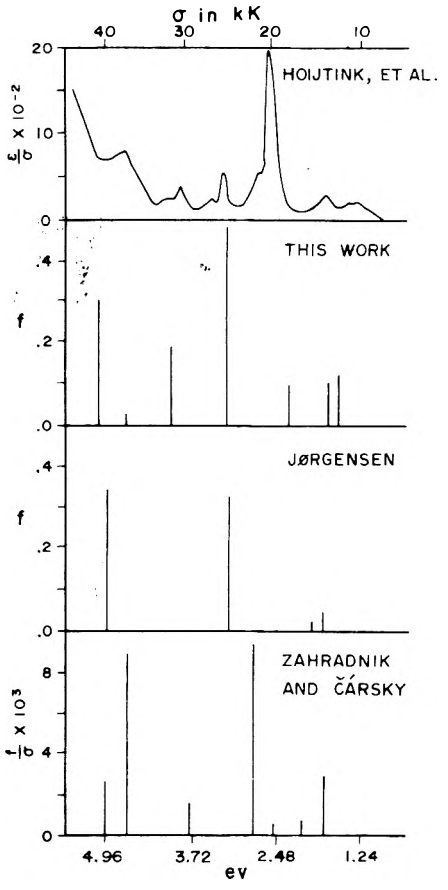

Figure 5. Comparison of observed and calculated spectra of the pyrene radical anion.

ground state of the benzonitrile radical anion, in contrast to the A symmetry assigned by Ishitani and Nagakura.[19] The lowest calculated band in this compound at 0.38 eV falls clearly in the infrared region and is of very low intensity; it is unlikely that it would have been observed. The next transition, observed at 1.65 eV, is calculated by the VO methods at about 2.2 eV, in excellent agreement with the calculation of the Japanese authors. However, a charge transfer transition, calculated by the VO method at 2.65 eV, is brought down to 1.88 eV by a SCF calculation. We would like to propose that the otherwise unexplained 1.65-eV observed band corresponds to this charge transfer transition. This assignment implies that the strongest observed band at 2.53 eV must be assigned to the B_2 (B) state at 2.21 eV, which is also the most intense calculated transition in that region. The 3.26-eV observed band agrees well with the transition calculated at 3.17 eV. Three more strong bands at 4.55, 4.92, and 6.06 eV are predicted in this calculation.

The spectra of phthalo- and isophthalonitrile anion radicals, Tables X and XI, show a very similar pattern: a first band of very low intensity is calculated in the infrared but not observed; an observed band not far from 1.5 eV does not appear in the calculation; thereafter the agreement appears more reasonable. The results of the Japanese authors[19] are very similar, except that the agreement for the higher energy states is less satisfactory.

In terephthalo- and pyromellitonitrile anion radicals we again encounter the low-energy (infrared) band, cf. Tables XII and XIII. In all these compounds this transition is strictly localized in the benzene ring, and corresponds to a

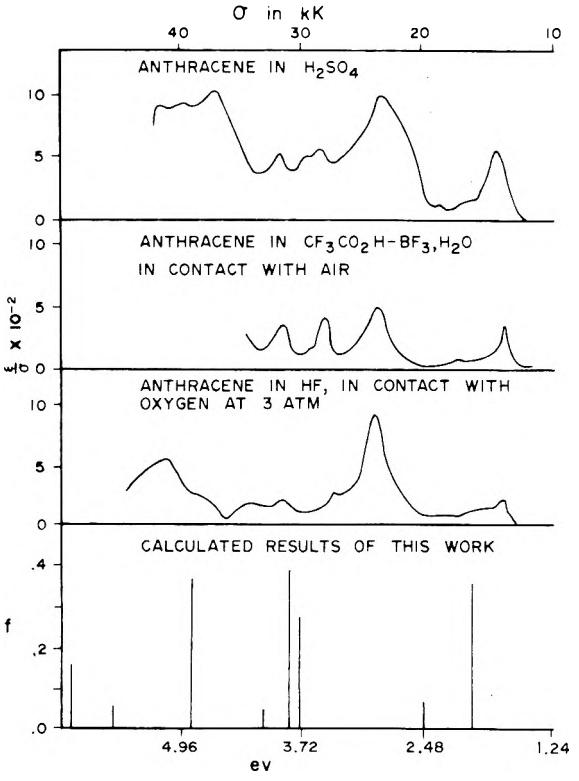

Figure 6. Comparison of observed and calculated spectra of the anthracene radical cation.

TABLE IX: Observed and Calculated Spectra of Benzonitrile Anion Radical

Exptl[a] (ref 19)		SCF[b,c]	VO				Lit. (ref 19)	
Energy	OD[i]	energy	Energy	f[d]	Sym type	Purity[e]	Energy	f[d]
0		0	0		B_2	0.99	0	
		0.38	0.60	0.001	$A_2(B)$	0.99	0.71	0.002
1.65	0.10	1.88	2.65	0	$B_1(B)$[g]	0.95		
2.53	0.50	—	2.22	0.14	$B_2(B)$	0.86	2.23	0.22
3.26	0.33	—	3.25	0.05	$B_2(B)$	0.87	3.47	0.009
		4.02	4.35	0.006	$A_1(B)$[j]	0.95		
		—	4.58	0.28	$B_2(A)$	0.84		
		(5.06)	4.95	0.13	$A_2(A)$	0.82		
		—	5.27	0.03	$A_1(B)$[j]	0.93		
		—	5.32	0	$B_1(B)$[j]	0.95		
		—	5.68	0.04	$A_2(C)$	0.75		
		—	6.06	0.19	$B_2(C)$	0.84		

[a-h] All energies in eV. For footnotes *a-h*, cf. Table II. [i] Optical density. [j] $\pi \rightarrow \sigma^*$ transition. [k] Charge transfer transition.

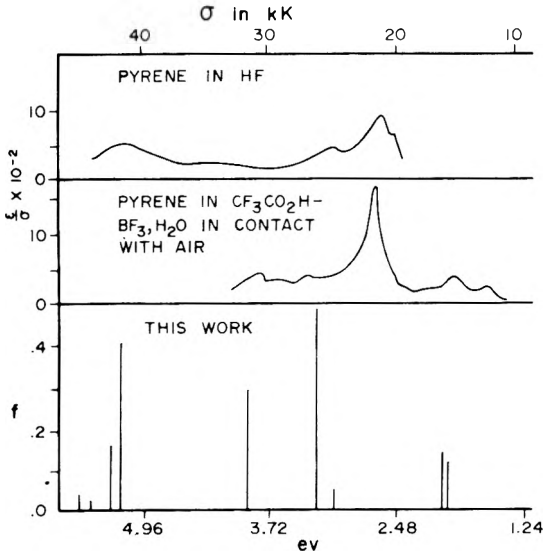

Figure 7. Comparison of observed and calculated spectra of the pyrene radical cation.

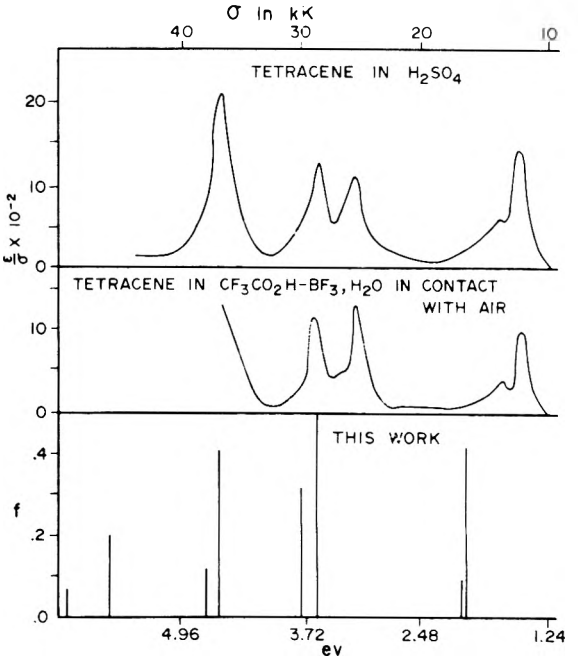

Figure 8. Comparison of observed and calculated spectra of the tetracene radical cation.

transition between a pair of orbitals which are degenerate in benzene, but are split by the perturbation due to the substitution, which destroys the sixfold symmetry. For **7** our calculations agree quite well with experiment (although the pattern of intensities is not satisfactory); for the tetrasubstituted compound the agreement, particularly for the lower energy bands, is much less satisfactory.

We would like to propose that, in all the cyano-substituted benzenes, there exists a charge-transfer state near 1.5 eV. In the monosubstituted compound the calculation allowed this assignment rather clearly. We believe that the unexplained bands in **5** and **6** correspond to A_1 and B_1 states, calculated over 1 eV too high because of the extreme sensitivity of charge transfer transitions to geometry, medium effects, etc. We further believe that corresponding states are also present in **7** and **8** (B_{3g} or B_{1u} for **7**, B_{2u} for **8**) but are not observed because they are more strongly forbidden in the molecules of higher symmetry (D_{2h}).

A strong band at about 6 eV is predicted in every cyanobenzene radical anion in this calculation. In each case this transition, which needs experimental confirmation, is localized in the benzene ring. This band corresponds to a transition observed in most benzene derivatives, although usually at somewhat higher energies. A corresponding transition is calculated in benzyl at 6.66 eV (*f* 0.21), in anilino at 6.61 eV (*f* 0.18), and in phenoxy at 6.64 eV (*f* 0.05). In benzosemiquinone, to be discussed below, a corresponding band occurs at 6.06 eV (*f* 0.52). The upper states of all these transitions are configurationally very impure, but in each case the leading term is a C type state of similar orbital origin.

We have attempted to unravel the highly confused experimental situation in the nitrobenzene radical anion[24-30] and its reduction products, nitrosobenzene radical anion[19,29] and azobenzene radical anion.[31] The almost complete lack of consistency in the experimental results makes an analysis difficult, and we are unable to shed any light on this confused question.

Radical Anions of Heterocyclic Compounds. Pyridine

TABLE X: Observed and Calculated Spectra of Phthalonitrile Anion Radical

Exptl[a] (ref 19)		SCF[b,c]	VO				Lit. (ref 19)	
Energy	OD[i]	energy	Energy	f[d]	Sym type	Purity[e]	Energy	f[d]
0		0	0		A_2	0.91	0	
		0.36	0.54	0.003	$B_2(B)$	0.97	0.62	0.02
1.24	0.10							
2.18	0.75							
2.36	0.70	–	2.41	0.12	$A_2(B)$	0.86	2.46	0.12
		2.42	3.00	0	$A_1(B)^{j,k}$	0.98		
		2.97	3.63	0.002	$B_1(B)^{j,k}$	0.97		
3.65	0.48	–	3.62	0.05	$B_2(B)^k$	0.96		
		–	3.95	0.11	$A_2(B)$	0.89	2.84	0.05
		–	4.35	0.01	$B_1(B)^j$	0.93		
		(4.58)	4.46	0.22	$B_2(A)$	0.88	4.39	0.07
		–	4.88	0.20	$A_2(A)$	0.75		
		–	5.52	0	$A_1(C)^j$	0.93		
		–	5.62	0.02	$B_1(B)^j$	0.92		
		–	5.67	0.04	$B_2(B)$	0.88		
		–	6.02	0.25	$A_2(C)$	0.72		

[a-g] All energies in eV. For footnotes *a-g*, cf. Table II. [i] Optical density. [j] $\pi \rightarrow \sigma^*$ transition. [k] Charge transfer transition.

TABLE XI: Observed and Calculated Spectra of Isophthalonitrile Anion Radical

Exptl[a] (ref 19)		SCF[b,c]	VO				Lit. (ref 19)	
Energy	OD[i]	energy	Energy	f[d]	Sym type	Purity[e]	Energy	f[d]
0		0	0		A_2	0.99	0	
1.65		0.20	0.43	0.002	$B_2(B)$	0.90	0.35	0.004
2.18	0.42	–	2.08	0.14	$B_2(B)$	0.83	1.97	0.18
		2.77	3.30	0	$A_1(B)^{j,k}$	0.96		
		2.94	3.31	0.001	$B_1(B)^{j,k}$	0.95		
3.54	0.35	–	3.77	0.02	$A_2(B)^k$	0.94	3.18	0.05
		–	4.17	0.09	$B_2(B)^k$	0.90	4.18	0.04
		–	4.44	0	$A_1(B)^j$	0.98		
		–	4.61	0.21	$A_2(A)$	0.80	4.66	0.11
4.96	0.80							
		(5.03)	4.87	0.16	$B_2(A)$	0.70		
		–	5.27	0.04	$B_1(B)^j$	0.95		
		–	5.52	0	$A_1(B)^j$	0.96		
		–	5.57	0.07	$A_2(C)$	0.75		
		–	5.98	0.32	$B_2(C)$	0.63		

[a-h] All energies in eV. For footnotes *a-h*, cf. Table II. [i] Optical density. [j] $\pi \rightarrow \sigma^*$ transition. [k] Charge transfer transition.

Radical Anion. Kuwata et al.[32] have reported that the pyridine radical anion, prepared by the reduction of pyridine with sodium in tetrahydrofuran, absorbed at 17,500 cm^{-1} (2.17 eV). Dodd and coworkers[33] found that the pyridine radical anion produced by the same method gave absorption bands at 29,850 cm^{-1} (3.70 eV, ϵ 2000) and 40,980 cm^{-1} (5.08 eV, ϵ 3340). Rao et al.[34] observed that pyridine radical anion generated by alkali metal reduction of pyridine in tetrahydrofuran showed an absorption(s) at 320 nm (3.88 eV) with lithium reduction, at 340–360 (3.65–3.44 eV) and 560 nm (2.21 eV) with sodium reduction, or at 340 (3.65 eV) and 505 nm (2.46 eV) with potassium reduction. In this work, the calculated strong bands at 2.39 and 5.04 eV in Table XIV match the experimental data very well. The bands at 4.14 and 4.26 eV are $n \rightarrow \pi^*$ and $\pi \rightarrow \sigma^*$ transitions, and hence might well be expected to be particularly sensitive to the environment.

The experimental situation in the radical anions of the other azines and in the radical cations of pyridine and the azines is too confused to permit any reasonable interpretation of calculated results; hence we do not present such results here.

p-Benzosemiquinone Anion Radical. In a very recent paper, Fukuzumi et al.[35] have reported the spectrum of *p*-benzosemiquinone anion radical (**9**), $p\text{-}OC_6H_4O^-$. Previous π-electron calculations on this compound[36] are in good agreement with the new experimental data; the geometry used was a self-consistent geometry based on a bond length–bond order correlation. We have calculated the spectrum of **9** assuming that the geometry is that of a benzene ring with C–O distances of 1.36 Å (compared to the self-consistent value of Haruda[36] of 1.16 Å). Our results, given in Table XV, also agree well with the experimental values; the high-intensity B_{3u} (B) state is better represent-

TABLE XII: Observed and Calculated Spectra of Terephthalonitrile Anion Radical

Exptl[a] (ref 19)		SCF[b,c]	VO				Lit. (ref 19)	
Energy	OD[i]	energy	Energy	f[d]	Sym type	Purity[e]	Energy	f[d]
0		0	0		B_{3u}	0.99	0	
		0.54	0.77	0	A_u(B)	0.99		
2.48	0.25	(2.54)	2.13	0.18	B_{1g}(B)	0.89	1.88	0.39
		2.95	3.22	0	B_{1g}(B)[k]	0.96		
		3.09	3.38	0	B_{1u}(B)[k]	0.96		
3.65	1.80	–	3.81	0.10	B_{1g}(B)	0.88	4.02	0.22
		–	4.00	0	B_{3u}(B)[k]	0.97		
4.38	2.00	(4.56)	4.41	0.42	B_{1g}(A)	0.88	4.35	
		4.44	4.59	0	B_{2u}(B)[j]	0.99		
		(4.83)	4.75	0.15	B_{2g}(A)	0.89		
		5.15	5.23	0.03	A_g(B)[j]	0.98		
		–	5.62	0.02	B_{2g}(C)	0.75		
		–	5.76	0	B_{3g}(B)[j]	0.98		
		–	6.06	0.23	B_{2g}(C)	0.85		

[a–h] All energies in eV. For footnotes *a–h*, cf. Table II. [i] Optical density. [j] $\pi \rightarrow \sigma^*$ transition. [k] Charge transfer transition.

TABLE XIII: Observed and Calculated Spectra of Pyromellitonitrile Anion Radical

Exptl[a] (ref 19)		SCF[b,c]					Lit. (ref 19)	
Energy	OD[i]	energy	Energy	f[d]	Sym type	Purity[e]	Energy	f[d]
0		0	0		A_u	0.99	0	
		0.55	0.64	0	B_{3u}(B)	0.97		
2.68	0.48	(2.53)	2.15	0.17	B_{2g}(B)	0.90	1.94	0.34
3.31	0.45							
		3.50	3.77	0	A_g(B)[j,k]	0.98		
3.49	0.44							
		3.69	4.13	0	B_{2u}(B)[j,k]	0.98		
		4.07	4.52	0.25	B_{1g}(B)[k]	0.89		
		4.14	4.55	0	B_{1u}(B)[k]	0.97		
4.44	1.40	4.20	4.57	0.01	B_{3g}(B)[j,k]	0.97	4.41	0.30
		(4.38)	4.27	0.10	B_{1g}(A)	0.81	3.38	0.06
		–	4.59	0	B_{3u}(B)[k]	0.98		
4.78	1.00	(4.76)	4.67	0.46	B_{2g}(A)	0.79	4.59	0.01
		–	4.73	0	B_{1u}(B)[j,k]	0.99		
		–	4.87	0	A_u(B)	0.99		
		–	5.04	0.09	B_{1g}(B)[j]	0.87		
		–	5.57	0.03	B_{1g}(C)	0.87		
		–	5.71	0.02	B_{3g}(A)[j]	0.92		
		–	5.92	0	A_g(C)[j]	0.97		
		–	5.94	0.27	B_{2g}(C)	0.69		

[a–h] All energies in eV. For footnotes *a–h*, cf. Table II. [i] Optical density. [j] $\pi \rightarrow \sigma^*$ transition. [k] Charge transfer transition.

ed than by the older calculations, and the intensity pattern fits the experiments much better.

Molecules with Degenerate Doublet Ground States. Some very special problems arise in molecules which have degenerate doublet ground states. A typical example is the molecular ion of *s*-triazine. In the neutral molecule the highest occupied molecular orbital is doubly degenerate, having largely nitrogen n character. Consequently, a proper description of the ground state of the molecular cation would be a linear combination of two determinants. Unfortunately, we cannot currently handle the calculation of such a state, since our method is restricted to states described by a single Slater determinant. As a result we treat the molecule as if it had the symmetry of the highest non-degenerate subgroup of the molecular point group, in this case C_{2v}. Proceeding in this fashion, we obtain a ground state of A_1 symmetry for the molecular ion; in the VO calculation this splits the degeneracy widely, in *s*-triazine by almost 1 eV; in the SCF calculation, however, the two components are split by less than 0.1 eV, i.e., of the order of our estimated uncertainty, cf. Table XVI. Similarly, the next two doublets of *s*-triazine, which are excited by about 0.5 V in SCF calculations and nearly degenerate there, are split by almost 1 V in the VO calculation. The situation becomes even more confused in higher excited states where B type states can be derived as monoexcited from either of the degenerate pair of ground states. Many of these are, of course, inaccessible to the VO calculation as monoexcited states;

TABLE XIV: Observed and Calculated Spectra of Pyridine Anion Radical

Exptl[c] energy			SCF[b,c] energy	VO			
Ref 32	Ref 33	Ref 34		Energy	f[d]	Sym type[e]	Purity[f]
0	0	0	0	0		B_2	0.99
			0.43	0.51	0.0005	$A_2(B)$	0.99
		2.21					
2.17		2.46	—	2.39	0.10	$B_2(B)$	0.90
	3.34	3.44	4.14	4.53	0.001	$A_1(A)$[h]	0.92
	3.70	3.88	4.26	4.51	0.002	$A_1(B)$[i]	0.98
	5.08	5.05	4.95	5.04	0.18	$A_2(A)$	0.94
			5.12	5.19	0	$B_1(B)$	0.97
			—	5.17	0.07	B_2	M
			—	5.47	0	$B_1(C)$	0.87

[a-h] All energies in eV. For footnotes a-h, cf. Table II. [i] $\pi \rightarrow \sigma^*$ transition.

TABLE XV: Observed and Calculated Spectra of *p*-Benzosemiquinone Anion Radical

Exptl (ref 35)		SCF[b,c] energy	VO				Lit. (ref 36)	
Energy	f		Energy	f[d]	Sym type[e]	Purity[f]	Energy	f[d]
0		0	0		B_{2g}	0.99	0	
		(2.61)	2.10	0	$B_{3g}(A)$[n]	0.89		
		(2.47)	2.13	0	$B_{2u}(A)$	0.91		
2.88	0.06	2.70	3.01	0.16	$A_u(B)$	0.99	2.96	0.03
		2.88	2.95	0	$B_{1g}(A)$	0.96		
3.34	0.03	(3.51)	2.89	0.13	$B_{3u}(A)$	0.82	3.48	0.11
3.93	0.35	4.20	4.24	0.44	$B_{3u}(B)$	0.74	4.46	0.69
		—	4.79	0	$B_{2g}(B)$	0.74		
		—	5.71	0	$B_{2u}(C)$[h]	0.76		
		5.73	5.93	0	$A_g(A)$[h]	0.98		
		—	5.75	0	$B_{3g}(C)$[h]	0.75		
		—	5.79	0	$B_{1u}(C)$[h]	0.87		
		—	6.06	0.52	$B_{3u}(C)$	0.75		

[a-h] All energies in eV. For footnotes a-h, cf. Table II.

TABLE XVI: Lowest Excited States of *s*-Triazine and *s*-Trifluorotriazine[a]

Compd	State	Type[b]	SCF	VO
$C_3H_3N_3$	E′	n	0.0	0.0; 0.97
	E″	π	0.51	0.57; 1.43
$C_3F_3N_3$	E″	π	0.0	0.0; 1.14
	E′	n	0.13	0.11; 1.23

[a] All energies in electron volts. [b] Nature of the unpaired electron.

they would appear there as doubly excited states. On the other hand, in these types of molecules, the profusion of C type states is great, and these cannot currently be handled by an SCF calculation.

The situation is even worse in trifluoro-*s*-triazine. In the ground state of the neutral molecule we have two pairs of degenerate orbitals, one of n character, the other of π character, in close proximity, cf. Table XVI. Upon ionization in the molecular ion this leads to four states which differ only within the error of the calculation, that is within about 0.1 eV. In the VO calculation these four states are split by over 1 V and actually the degenerate pairs are split, one member of each being close to one member of the other set. Thus, in these cases, VO calculations seem to be all but useless. Whether the self-consistent states we obtain are good approximation to what should be two-determinant states, we cannot at this point ascertain, although we believe that the splitting obtained from the interaction of the determinants is not going to be large and thus the self-consistent energies are probably pretty good approximations to the true energies. Unfortunately, of course, the SCF calculations are only capable of providing us with A type states, relative to the degenerate ground states, and with B type states; the profusion of C type states is large and we do not feel that we have any meaningful information about these at this time. Thus, the molecules with degenerate doublet ground states may be considered as an unsolved problem.

Conclusions

The CNDO/S open shell method as applied to the calculation of spectra of free radicals and radical ions appears to us to show considerable promise. The tests reported here suffer from a lack of adequate experimental material and of good intensity determination. Equally, little is known of the geometry of the radicals studied, which contributes a further area of uncertainty. Overall, however, the calculated spectra seem to fit the experimental material quite well, almost invariably better than previous theoretical studies.

In at least two cases we propose significant new assign-

ments: the charge transfer transition in benzonitrile anion radical at 1.88 eV, and the n → π^* and $\pi \rightarrow \sigma^*$ transitions in pyridine anion radical. Many of the other assignments made, by implication in the tables, may also be new. Thus we believe that this method is capable of contributing considerable new information in the assignments and interpretation of spectra of radicals.

A further application of the method presented is to a calculation and interpretation of photoelectron spectra. Work along these lines is in progress in this laboratory, and preliminary results have been presented elsewhere.[37]

Acknowledgment. The authors wish to thank the Southwestern Ohio Regional Computer Center for providing the computer time necessary for this work.

References and Notes

(1) For the previous paper in this series see H. M. Chang, H. H. Jaffé, and C. A. Masmanidis, *J. Phys. Chem.*, preceding paper.
(2) A preliminary report on this work has appeared in H. M. Chang and H. H. Jaffé, *Chem. Phys. Lett.*, **23**, 146 (1973).
(3) H. C. Longuet-Higgins and J. A. Pople, *Proc. Phys. Soc.*, **68**, 591 (1955).
(4) C. C. J. Roothaan, *Rev. Mod. Phys.*, **32**, 179 (1960).
(5) J. Del Bene and H. H. Jaffé, *J. Chem. Phys.*, **48**, 1807, 4050 (1968); **49**, 1221 (1968); **50**, 1126 (1969).
(6) H. M. Jaffé, H. M. Chang, and C. A. Masmanidis, *J. Comput. Phys.*, **14**, 180 (1974).
(7) K. Nishimoto and N. Mataga, *Z. Phys. Chem. (Frankfurt am Main)* **12**, (1957); **13**, 140 (1957).
(8) R. Pariser and R. G. Parr, *J. Chem. Phys.*, **21**, 767 (1953).
(9) J. Fajer, B. H. J. Bielski, and R. H. Felton, *J. Phys. Chem.*, **72**, 1281 (1968).
(10) R. Zahradnik and P. Čársky, *J. Phys. Chem.*, **74**, 1235 (1970).
(11) J. C. Schug and D. H. Phillips, *J. Chem. Phys.*, **49**, 3734 (1968).
(12) G. Porter and E. Strachan, *Spectrochim. Acta*, **12**, 299 (1958); E. J. Land and G. Porter, *Trans. Faraday Soc.*, **67**, 2027 (1963); G. Porter and M. I. Savadatti, *Spectrochim. Acta*, **22**, 803 (1966).
(13) L. Grajcar and S. Leach, *J. Chim. Phys.*, **61**, 1523 (1964); C. Cossart-Magos and S. Leach, *J. Chem. Phys.*, **56**, 1534 (1972).
(14) (a) P. M. Johnson and A. C. Albrecht, *J. Chem. Phys.*, **48**, 851 (1968); (b) D. M. Friedrich and A. C. Albrecht, *ibid.*, **58**, 4766 (1973).
(15) A. Hinchliffe, R. E. Stainbank, and M. A. Ali, *Theor. Chim. Acta*, **5**, 95 (1966).
(16) P. Balk, G. J. Hoijtink, and J. W. H. Schreurs, *Recl. Trav. Chim. Pays-Bas*, **76**, 813 (1957).
(17) A. Hinchliffe, J. N. Murrel, and N. Trinajstic, *Trans. Faraday Soc.*, **62**, 1362 (1966).
(18) R. Zahradnik and P. Čársky, *J. Phys. Chem.*, **74**, 1240 (1970).
(19) A. Ishitani and S. Nagakura, *Theor. Chem. Acta*, **4**, 236 (1966).
(20) P. Jorgensen, *J. Chem. Phys.*, **57**, 4884 (1972).
(21) (a) W. I. Aalbersberg, G. J. Hoijtink, E. L. Mackor, and W. P. Weijland, *J. Chem. Soc.*, 3049 (1959); (b) G. J. Hoijtink, N. H. Velthorst, and P. J. Zandstra, *Mol. Phys.*, **3**, 533 (1960).
(22) T. Shida and W. H. Hamill, *J. Am. Chem. Soc.*, **88**, 5371 (1966).
(23) B. Badger and B. Brocklehurst, *Trans. Faraday Soc.*, **65**, 2576 (1969).
(24) W. Kemula and R. Sioda, *Nature (London)*, **197**, 588 (1963).
(25) A. Ishitani, K. Kuwata, H. Tsubomura, and S. Nagakura, *Bull. Chem. Soc. Jpn.*, **36**, 1357 (1963).
(26) B. Kastening, *Electrochim. Acta*, **2**, 241 (1964).
(27) J. G. Chambers and R. N. Adams, *Mol. Phys.*, **9**, 413 (1965).
(28) J. M. Gross and J. D. Barnes, *Chem. Commun.*, **50** (1968).
(29) V. Kalyanaraman, C. N. R. Rao, and M. V. George, *Tetrahedron Lett.*, 4889 (1969).
(30) T. Shida and S. Iwata, *J. Phys. Chem.*, **75**, 2591 (1971).
(31) V. Kalyanaraman, S. S. Dua, C. N. R. Rao, and M. V. George, *Tetrahedron Lett.*, 235 (1968).
(32) K. Kuwata, T. Ogawa, and K. Hirota, *Bull. Chem. Soc. Jpn.* **34**, 291 (1961).
(33) J. W. Dodd, F. J. Hopton, and N. S. Hush, *Proc. Chem. Soc.*, 61 (1962).
(34) V. Kalyanaraman, C. N. R. Rao, and M. V. George, *J. Chem. Soc. B*, 2406 (1971).
(35) S. Fukuzumi, Y. Ono, and T. Keii, *Bull. Chem. Soc. Jpn.* **46**, 3353 (1973).
(36) Y. Harada, *Mol. Phys.*, **8**, 273 (1964).
(37) R. L. Ellis, H. H. Jaffé, and C. A. Masmanidis, *J. Am. Chem. Soc.*, **96**, 2623 (1974).

Inhomogeneously Broadened Line Shapes and Information Content of Calculated Paramagnetic Resonance Spectra of Biological Molecules Containing High-Spin Iron(III)

R. E. Coffman

Department of Chemistry, University of Iowa, Iowa City, Iowa 52242 *(Received December 23, 1974)*

A general expression for the rigid lattice EPR (electron paramagnetic resonance) line shape for spin 5/2 Fe(III) is presented. The paramagnetic resonance absorption function $\chi''(\omega,B)$ for single crystals and powders is considered using a generalized spin-hamiltonian and multiple convolution integrals for the inhomogeneously broadened line shapes. Numerically calculated EPR line shapes are presented for field swept and frequency swept experiments for a randomly oriented sample of molecules (metmyoglobin) with axial symmetry and zero-field splitting parameter "D" = 10.7 cm^{-1}. The information content as defined for a continuous probability distribution is used to calculate the relative information content of the calculated line shapes. A hybrid experiment with least-squares computer simulation and numerical fitting of data to a common theoretical basis is proposed as the optimum experiment design, yielding maximum information for randomly oriented spin 5/2 systems with large zero-field splitting.

Introduction

The paramagnetic resonance spectra of high-spin Fe(III) containing molecules are of considerable interest in inorganic and bioinorganic chemistry, but the quantitative analysis of such EPR spectra is, in the general case, accompanied by a number of theoretical and experimental difficulties which have, so far, not been completely resolved. These difficulties have limited nearly all studies on biological high-spin heme Fe(III) to the $M_s = 1/2 \leftrightarrow -1/2$ transi-

tion which is always observable as a result of time reversal symmetry in a system with an odd number of electrons. The relatively large zero-field splittings (ZFS) between the three Kramer's doublets ($M_s = \pm 1/2, \pm 3/2, \pm 5/2$), which are generally present in these systems, cause rapid relaxation whenever the molecule is able to tumble with respect to the external magnetic field, so that the study of rigid lattice spectra is the rule rather than the exception.[1] Now, if the *entire* spectrum for the rigid lattice case (consisting of $5 + 4 + 3 + 2 + 1 = 15$ transitions of variable relative intensities) could be observed, then one would potentially have a considerably greater amount of information at hand about the electronic ground and excited states of the molecular fragment containing the Fe(III) atom than is normally available from study of the $M_s = \pm 1/2$ doublet. Assuming that such a spectrum (or set of spectra) was available, then one would, in practice, approach the problem of obtaining this information by extracting from the spectrum the parameters of the spin-Hamiltonian and the line shape parameters which give rise to the well-known[2] strong anisotropy of line widths in $S = 5/2$ systems. An important consideration, in respect to this problem, is whether the set of parameters obtained from the spectrum are unique and whether they are determined with suitable precision to be theoretically useful. A necessary (but not sufficient) condition for both uniqueness and precision is that the experimental spectrum be obtained in a form having a maximum amount of structure (resolved "lines"), with each absorption "line" being measured as accurately as possible.

We are often forced by experimental conditions to make EPR measurements on randomly oriented (polycrystalline or "glassy") samples. This invariably leads to some loss of information (overlapping peaks in the resulting spectrum, loss of knowledge of orientation of spin-hamiltonian tensors with respect to the crystallographic unit cell) and greatly complicates the calculations by requiring angular integrations over the unit sphere. In some cases, however, there are advantages, as, for example, being able to obtain greater magnetic dilution than in an undiluted single crystal. Moreover, the peaks in the powder spectrum correspond to the turning points of the single crystal spectrum, not all of which may correspond with principle axis turning points.[3] Thus, if one is able to adjust the ratio of ZFS/transition frequency, then it is possible to modify appreciably the shape and complexity of the resulting absorption spectrum, an effect which we should, in principle, be able to use to great advantage.

The EPR spectra of the $M_s = \pm 1/2$ doublet of high-spin heme Fe(III) have been widely studied. The normally accessible X-band spectra vary from the $g_\parallel = 2$, $g_\perp = 6$ "signature" for axial symmetry to the $g_{iso} = 30/7$ isotropic resonance for rhombic symmetry with many known cases being in between the two extremes. It is also known from studies of proteins containing high-spin heme Fe(III) that conformation changes affect EPR spectrum structure, line widths, and relaxation properties. Ligand hyperfine structure has been resolved by EPR for special cases, and normally unresolved ligand hfs has been resolved by double resonance experiments.[4] In addition, studies on inorganic solids have shown that the EPR line shapes for high-spin Fe(III) systems are largely determined by inhomogeneous broadening, with the effects of single crystal mosaic structure,[5] strain broadening,[6-8] internal electric fields,[9,10] and unresolved ligand hfs[11] being added to the intrinsic line shape. This, in addition to the known complexity of the $S = 5/2$ spin Hamiltonian,[12,13] makes this analysis of line shape at once both potentially highly rewarding and uncommonly complicated.

The Paramagnetic Resonance Absorption Line Shape

The imaginary part of the frequency-dependent susceptibility, which is proportional to the power absorption in a paramagnetic resonance experiment, is readily found to have the following form, under the assumption that both the energy levels $\epsilon_i(B,\Omega)$ and the selection rule matrix elements $\mu_{ij}(B,\Omega)$ vary slowly across any inhomogeneously broadened line shape for each $i \rightarrow j$ transition:[14,15]

$$\chi''(\omega, B;\Omega) = \frac{\pi N_0}{\hbar Z} \sum_{i<j} |\mu_{ij}|^2 (e^{-\epsilon_i/kT} - e^{-\epsilon_j/kT}) G[\omega - \omega_{ij}(B,\Omega)] \quad (1)$$

Here, N_0 = the number of absorbing $S = 5/2$ centers, Z = the partition function for the magnetic energy, and $\epsilon_i = \epsilon_i(B,\Omega)$ is an energy eigenvalue found by diagonalizing the spin Hamiltonian with magnetic field B (gauss) having direction $\Omega = (\theta,\phi)$ with respect to a set of fixed molecular (or laboratory) axes. The radiation-hamiltonian matrix element is μ_{ij}, and $G(\omega - \omega_{ij})$ is the convoluted line shape of the i to j transition resulting from the combined effects of homogeneous broadening and all sources of inhomogeneous broadening. The transition frequencies $\omega_{ij}(B,\Omega)$ are found from the energy eigenvalues for each value of the field B and orientation Ω: $h\omega_{ij} = \epsilon_i - \epsilon_j$, and the selection rule matrix elements are found, in the usual way, as matrix elements of the radiation hamiltonian: $\mu_{ij} = \langle \Psi_i | \mathcal{H}_{rad} | \Psi_j \rangle$ with $\mathcal{H}_{rad}$ being constructed from a Zeeman operator containing the microwave B_1 field.

The line shape function $G[\omega - \omega_{ij}(B,\Omega)]$ peaks at the field and angle dependent transition frequency $\omega_{ij}(B,\Omega)$. Thus, as either the frequency, ω, or field, B, are swept, the summation (eq 1) sweeps through each absorption peak in the frequency or field interval scanned, weighted by the intrinsic intensity and population differences for each transition. The line shape $G(\omega - \omega_{ij})$ is a composite line shape determined by the shape function of each line broadening mechanism which contributes to the total line shape. These shape functions may be classified as either homogeneous or inhomogeneous, depending on whether the broadening mechanism acts in the same way for each molecule in the system, or differently for each.[17] Thus, if $g(\omega - \sigma)$ is the homogeneously broadened line shape, and $h(\sigma - \omega_{ij})$ is the net inhomogeneously broadened line shape, then the composite line shape for the $i \rightarrow j$ transition is found by the convolution of both line shapes

$$G(\omega - \omega_{ij}) = \int d\sigma h(\omega - \omega_{ij}) g(\omega - \sigma) \quad (2)$$

where (assuming four different independent contributions to the inhomogeneous broadening)

$$h(\sigma - \omega_{ij}) = \iiint d\omega' \, d\omega'' \, d\omega''' \, h_1(\omega' - \omega_{ij}) \times h_2(\omega'' - \omega') h_3(\omega''' - \omega'') h_4(\sigma - \omega''') \quad (3)$$

The individual functions h_1, h_2, h_3, and h_4 above represent four of the principle mechanisms of inhomogeneous line broadening: single crystal mosaic structure,[5] strain broadening,[6-8] internal electric fields,[9,10] and long-range magnetic dipolar coupling (unresolved hyperfine structure[11]).

The central problem in the rigid lattice line shape theory is the calculation of a reasonable approximation to the shape functions (eq 2 and eq 3). The simplest model, which incorporates a unique contribution from each inhomo-

geneous process, is to assume that each of the functions h_i in (eq 3) can be represented by a gaussian-type function:

$$h_i(\omega - \omega_0) = \frac{T_{2i}}{\sqrt{2\pi}} e^{-1/2T_{2i}^2(\omega-\omega_0)^2} \quad (4)$$

Then, since the convolution of a gaussian function with another gaussian is also a gaussian function (easily proved by use of standard integral tables[18]), the width of the net inhomogeneous distribution $h(\sigma - \omega_{ij})$ is given by

$$\left(\frac{1}{T_2}\right)_{in}^2 = \sum_i \left(\frac{1}{T_{2i}}\right)^2 \quad (5)$$

this being the manner in which relaxation times add for convoluted gaussian line shapes. We assume the homogeneous line shape to be represented by a normalized, lorentzian line shape function:

$$g(\omega - \sigma) = \frac{T_2'}{\pi} \frac{1}{1 + T_2'^2(\omega - \sigma)^2} \quad (6)$$

The composite line shape function $G(\omega - \omega_{ij})$ is therefore to be found, according to (eq 2), as the convolution of a gaussian with a lorentzian line shape. The calculation of this convolution integral has been considered for a special case ($\omega - \omega_{ij} = 0$, at the center of the line) by Castner[19] and for the general case ($\omega = \omega_{ij} \neq 0$) by Farach and Teitelbaum.[20] A closed expression can be found for the center of the composite line shape, $G(\omega - \omega_{ij})$, but a general expression appears to be expressible only as a slowly convergent series of error functions. A strictly numerical approach to this problem may prove to be suitable for some cases of general evaluation of the integrals of eq 2 and 3.

A method of calculation of the inhomogeneous shape function $h_i(\omega - \omega_{ij})$, valid for any mechanism, has been described by Stoneham.[21] This method, the statistical method, has proved to be a satisfactory approach for all cases of inhomogeneous broadening in solids, which have, so far, been studied in detail. Thus, the functions $h_i(\omega - \omega_{ij})$, are, in principle, calculable once the details of the mechanism coupling the spins to the lattice are specified. It is reasonable to assume that an effective $1/T_{2i}$ can be defined from the true inhomogeneous function h_i, for use in the gaussian approximation of eq 4. An elementary example of a calculation of a strain-broadened $1/T_2$, giving rise to an anisotropic line width different for each transition, will be given in the next section.

The spin hamiltonian, $\mathcal{H}_{SH}$, determines the primary structure of the spectrum through the resonance frequencies $\omega_{ij}(B,\Omega)$. Hence, the choice of a correct spin hamiltonian is of great importance. Now, the spin hamiltonian for high-spin Fe(III) is considerably more complicated than for most other iron group atom paramagnetic states (ionic or chemically bound), with the exception of Mn(II). We may quite generally write $\mathcal{H}_{SH}$ (neglecting hyperfine effects for ^{57}Fe) as the sum of two terms

$$\mathcal{H}_{SH} = \mathcal{H}_Z + \mathcal{H}_{ZFS} \quad (7)$$

where the Zeeman term, $\mathcal{H}_Z$, is field-dependent and the zero-field splitting term, $\mathcal{H}_{ZFS}$, is field independent. The conventional spin hamiltonian is obtained, for Fe(III), in the following manner. First $\mathcal{H}_Z$ is assumed to be of the form

$$\mathcal{H}_Z = \mu_B \mathbf{B} \cdot \boldsymbol{g} \cdot \mathbf{S} \quad (8)$$

where the g tensor is usually assumed to be isotropic. Secondly, the ZFS part of $\mathcal{H}_{SH}$ is assumed to have four principle terms:[13]

$$\mathcal{H}_{ZFS} = D(S_z^2 - 35/12) + E(S_x^2 - S_y^2) + \frac{a}{6}(S_\xi^4 + S_\eta^4 + S_\zeta^4 - 707/16) + (7F/36)(S_z^4 - (95/14)S_z^2 + 81/16) \quad (9)$$

While the conventional spin hamiltonian has been shown to be entirely adequate for several particular cases of well-defined single crystals, giving rise to very narrow EPR lines,[22,23] there are now a number of cases where additional terms in the spin hamiltonian have been found necessary for accurate representation of the centers of all resonance lines arising from the $S = 3/2$ or $5/2$ manifold of states.[23-25]

The fundamental arguments on the general nature of the spin hamiltonian for $S = 5/2$ are group theoretical in nature. A particularly evident way of viewing the general nature of this operator is to regard $\mathcal{H}_{SH}$ as an operator in the Liouville space appropriate to spin 5/2. Since the bra-ket space constructed from the orthonormal, linearly independent set $\{|5/2,M\rangle\}$ is of dimension 6, the corresponding Liouville space of operators which may operate on functions of the spin operators is of dimension $6 \times 6 = 36$. Thus, $\mathcal{H}_{SH}$ contains, in general, 36 terms, far more than the maximum number of terms obtainable from eq 8 and 9. The general form of $\mathcal{H}_{SH}$ follows by expansion in a complete set of irreducible tensor operators $\hat{S}_m^{(k)}$ where $k = 0$, 1, 2, 3, 4, 5, and $m = -k$ to $+k$. (The sum $1 + 3 + 5 + 7 + 9 + 11 = 36$.) By the use of time reversal symmetry, we can separate the terms in this expansion into terms which are field dependent, and others which are field independent. Thus, we find in analogy with eq 8 and 9

$$\mathcal{H}_Z = \sum_{k=1,3,5} \sum_{m=-k}^{+k} (-1)^m Q_m^{(k)}(B) \hat{S}_{-m}^{(k)} \quad (10)$$

and

$$\mathcal{H}_{ZFS} = \sum_{k=2,4} \sum_{m=-k}^{+k} (-1)^m F_m^{(k)} \hat{S}_{-m}^{(k)} \quad (11)$$

(The $k = 0$ term in eq 11 has been dropped, since it yields the identity operator.) The operators $\hat{S}_m^{(k)}$ are closely related to Steven's operator equivalents, but they are here chosen to be complex operators so that they transform under rotations as bases for the irreducible representations of the rotation group. The operator (eq 10) contains the elements of the customary cartesian coordinate Zeeman operator, as well as the additional small field-dependent terms whose cartesian coordinate form is $B_xS_x^3$, $B_yS_y^3$, $B_zS_z^3$, etc.[25] The form of the operator (eq 11), as a general form for the ZFS operator, is well known.[13] Thus, there is no fundamental problem with finding a suitably general spin hamiltonian for the spin 5/2 system, but there is a general lack of empirical knowledge as to when to expect that the additional terms, implicit in the irreducible tensor form of $\mathcal{H}_{SH}$, are to be expected.

An "Indirect" Line Shape Calculation

We have programmed the absorption function of eq 1 so as to calculate and plot a numerical line shape, using relatively simple assumptions concerning the choice of spin hamiltonian and approximations for the total convoluted line shape function $G(\omega - \omega_{ij})$. This type of calculation is properly termed "indirect", since it proceeds via an eigenvalue-eigenvector subprogram. A "direct" calculation, using the ideas of superoperators in Liouville space, would yield the spectrum as a solution to a matrix inversion problem without repeated solution of an eigenproblem. Such methods have been developed mainly for slow-tumbling

line shape problems, and have not yet been applied to time independent problems containing inhomogeneous broadening effects.

The spin hamiltonian used here is the conventional spin hamiltonian, eq 8 and 9, with all quadratic and quartic spin operators quantized in the same (z) direction. An anisotropic convoluted line shape is constructed by assuming that $g(\omega - \sigma)$ of eq 2 may be represented by a gaussian type function with isotropic line width $(1/T_2)$, and a strain-broadening gaussian function is assumed for $h(\omega - \sigma_{ij})$. An expression for $1/T_{2s}$, the (anisotropic) strain-broadened width, is developed in the following phenomenological manner: first, we assume that $h(\omega - \omega_{ij})$ may be represented by a normalized gaussian distribution function:

$$h(\omega - \omega_{ij}) = \frac{T_{2s}}{\sqrt{2\pi}} e^{-1/2T_{2s}^2(\omega - \omega_{ij})^2} \quad (12)$$

Then, we assume that the result of the strain coupling between magnetic spins and lattice strains may be represented, for each spin, by

$$\mathcal{H}_{STR}^{(i)} = D_i' S_z^2 + E_i'(S_x^2 - S_y^2) \quad (13)$$

where we assumed D_i', E_i' to represent the deviation of the actual D, E for spin "i" from the average value for all spins: $D_i' = D_i - \langle D \rangle$, $E_i' = E_i - \langle E \rangle$. It is convenient to introduce the root-mean-square quantities σ_D and σ_E:

$$\sigma_D = \left(\sum_{i=1}^{N} (D_i')^2 / N \right)^{1/2} \quad (14)$$

with σ_E being similarly defined. The strain broadened $1/T_{2s}$ is then evaluated by equating the mean-square value of $\omega - \omega_{ij}$ of eq 12 to the mean-square value of $\Delta\epsilon_{ij}'$ resulting from the strain operator (eq 13):

$$\langle (\omega - \omega_0)^2 \rangle = \langle (\Delta\epsilon_{ij}')^2 \rangle \quad (15)$$

The equality 15 is to be calculated for each $i \rightarrow j$ transition. The resulting expression for $(1/T_{2s})_{ij}$ depends on the validity of two assumptions: the first is that σ_D and σ_E are relatively small, so that the $\Delta\epsilon_{ij}'$ are well represented by first-order perturbation theory. The second is that D_i' and E_i' vary from spin to spin randomly *and* independently. (The latter assumption is arbitrary, but appears to have some justification in experimental useage.[2,6]) It follows directly, that $1/T_{2s}$ is different for each $i \rightarrow j$ transition, and is given by

$$\left(\frac{1}{T_{2s}}\right)_{ij}^2 = \sigma_D^2\{\langle\psi_i|S_z^2|\psi_i\rangle - \langle\psi_j|S_z^2|\psi_j\rangle\}^2 + \sigma_E^2\{\langle\psi_i|S_x^2 - S_y^2|\psi_i\rangle - \langle\psi_j|S_x^2 - S_y^2|\psi_j\rangle\}^2 \quad (16)$$

The overall width of the convoluted line shape $G(\omega - \omega_{ij})$ is then given by (since we have assumed both g and h to be gaussian)

$$\left(\frac{1}{T_2}\right)_{ij}^2 = \left(\frac{1}{T_2}\right)^2 + \left(\frac{1}{T_{2s}}\right)_{ij}^2 \quad (17)$$

which will lead to a strongly anisotropic line width for many transitions, if σ_D and σ_E are much larger than the intrinsic width $1/T_2$. We have verified that anisotropic widths are readily obtained for Fe(III) in single crystal MgO, quite similar to the perturbation theory and experimental results obtained by Feher.[2]

The line width expressions (eq 16 and 17) are readily expressed in matrix language. A quantity $S(\omega,B;\Omega)$, proportional to χ'' of eq 1, was then calculated for each desired value of ω and B and the spin-hamiltonian and line shape parameters. An integration over the angles (Ω) was performed in order to obtain the "powder" spectrum:

$$S(\omega, B) = \int S(\omega, B;\Omega)\, d\Omega \quad (18)$$

Since the symmetry is axial, we take $d\Omega = \frac{1}{2} \sin\theta\, d\theta$. The spherical integrations were then accomplished by the addition of each spectrum for an equally spaced set of angles θ_i uniformly distributed over 90° of arc (pole to equator on the unit sphere), weighted by $\sin\theta_i$. The field-swept spectra were calculated by diagonalizing $\mathcal{H}_{SH}$ at a fixed set of field points (the number of which could be adjusted to minimize interpolation error), and then the field-dependent quantities ω_{ij}, P_{ij}, and $(1/T_2)_{ij}$ were interpolated between these points, to obtain the complete numerical spectrum $S(\omega,B;\Omega)$ for each value of B.

Results

The foregoing analysis is directed toward the development of a quantitative tool for the interpretation of magnetic resonance line shape data in terms of the details of the electric and magnetic interactions of Fe(III) with its molecular environment. As a first application, we have examined some questions concerning uniqueness of solution to the problem of obtaining a satisfactory set of values of spin-hamiltonian and line width parameters from an experimental spectrum and some questions concerning the best choice of experiments. In order to do this conveniently, we have chosen to study the EPR line shape of metmyoglobin, the zero-field splitting parameters of which are known[26,27] to be similar to those of acid methemoglobin, the EPR spectrum of which has recently been measured by Alpert, Couder, Tuchendler, and Thomé[28] at millimeter and submillimeter wavelengths using magnetic fields produced by a superconducting coil. The value of $|D| \approx 10.7$ cm^{-1} which they report is a sufficiently large value of ZFS so as to be representative of other high-spin Fe(III) systems with large ZFS. We use this system, therefore, as a typical system to test for the numerical behavior of the absorption function $S(\omega,B)$.

The calculated values of $S(\omega,B)$ and $dS(\omega,B)/dB$ vs. field are presented in Figures 1–4 for microwave frequencies of 9, 35, 70, 135, 274, and 372 GHz. The parameter values used in these calculations were $g = 2.005$, $a = 120 \times 10^{-4}$ cm^{-1}, $F = 0.0$, $D = 10.7$ cm^{-1}, $\sigma_D = 200 \times 10^{-4}$ cm^{-1}, $\sigma_E = 100 \times 10^{-4}$ cm^{-1}, isotropic line width (converted to the equivalent $1/T_2$) = 1000 G, and $T = 77$°K. While these values are "typical", only the value of D is derived from experiment for this representative system. The relatively broad intrinsic line width has been set to this value to make convergence of the angular integrations easier, and to facilitate the display of the accompanying calculated line shapes.

The calculated spectra of Figures 1–4 show a number of interesting and significant features. The general shift toward higher field values as ω (klystron) increases is expected, as is the observation that the derivative spectrum is generally quite insensitive to broad absorption lines. Thus, at 9 GHz the broad absorption line at 140 kG is completely lacking in the derivative spectrum, although the sharper lower field lines are quite prominent. A significant finding is that as ω increases, the structure of the powder spectrum also increases. At 9 GHz the field-swept spectrum exhibits only 3–4 absorption maxima (the detail below 3 kG is not well resolved on this scale, and would require a smaller line width to simulate an experimental spectrum than used in these calculations), but at 372 GHz one can easily discern

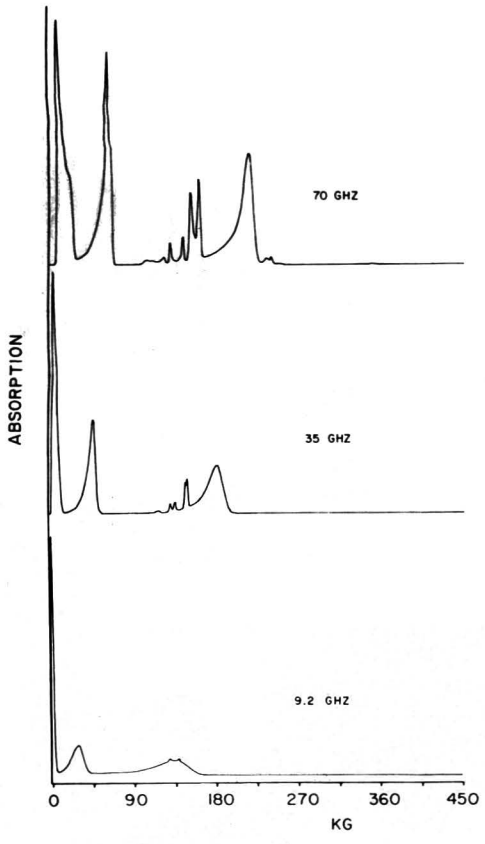

Figure 1. Spherically averaged absorption function (arbitrary units) vs. magnetic field, *B* (kilogauss). Spin-hamiltonian and line width parameter values as quoted in text. Microwave frequencies 9.2, 35, and 70 GHz.

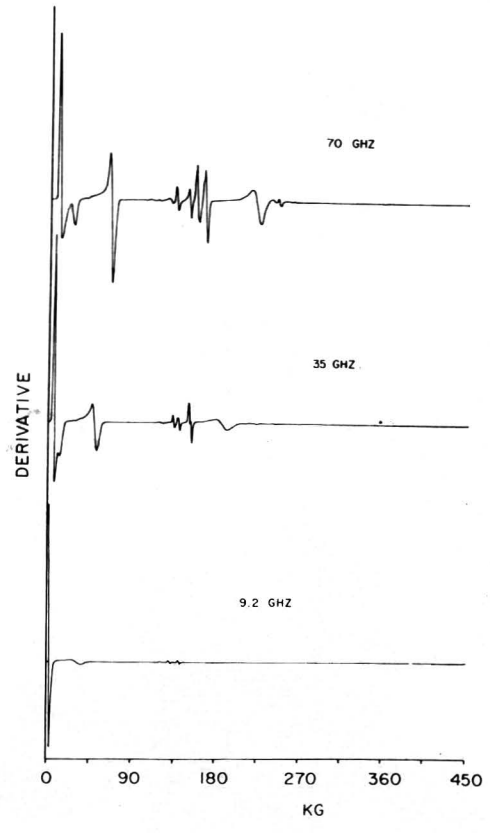

Figure 3. The derivative of the absorption function of Figure 1 vs. field.

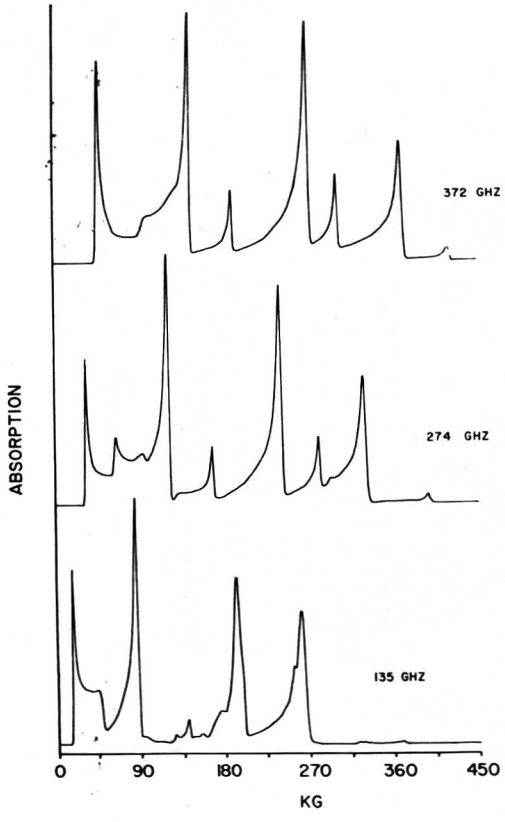

Figure 2. Spherically averaged absorption function (arbitrary units) vs. magnetic field. Microwave frequencies 135, 274, 372 GHz.

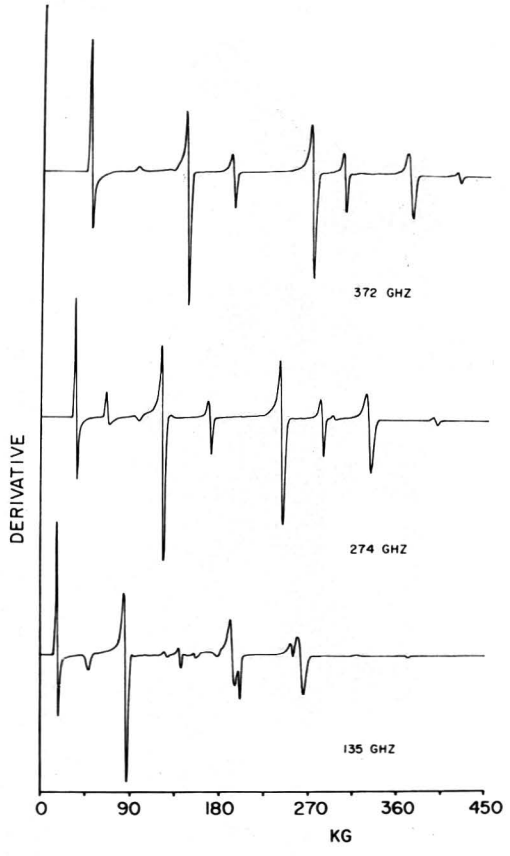

Figure 4. The derivative of the absorption function of Figure 2 vs. field.

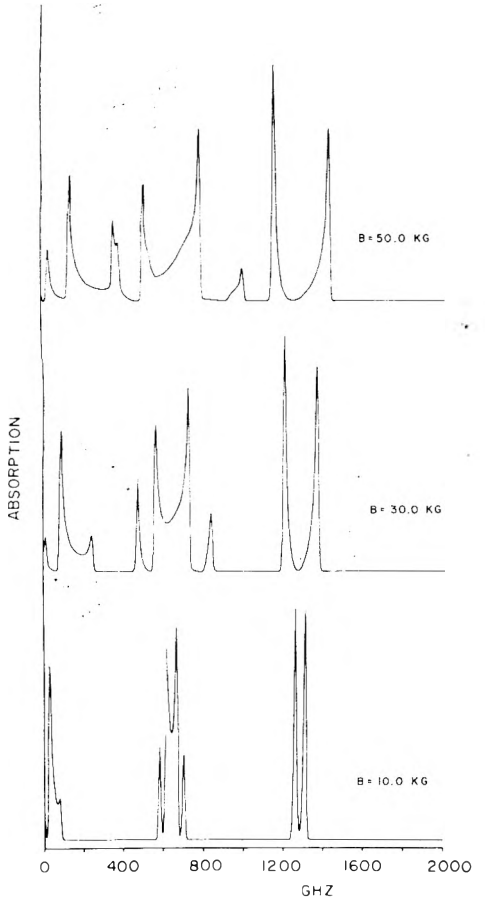

Figure 5. Calculated values of the absorption function, $S(\omega,B)$, vs. frequency (GHz) for fixed values of the magnetic field: B = 10, 30, and 50 kG.

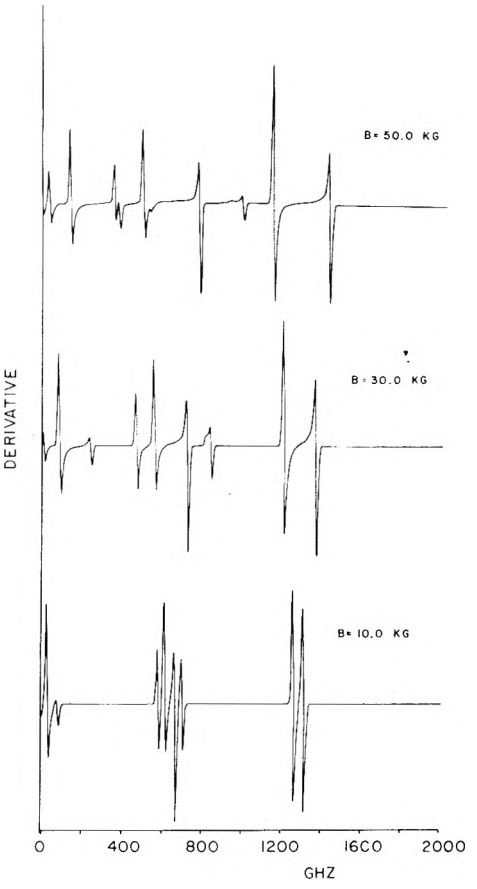

Figure 6. The derivative, with respect to frequency, of the absorption function of Figure 5.

10–11 well-defined turning points in the spectrum. Thus, the higher frequency spectra contain more analyzable information than the lower frequency spectra, and in a sense represents an increase in "resolution".

The maximum magnetic fields required to measure the interesting higher field transitions clearly increase dramatically as the magnitude of the ZFS increases. We decided, accordingly, to calculate $S(\omega,B)$ (and its derivative with respect to frequency) vs. frequency with various fixed values of B. This swept-frequency spectrum is similar to the spectra obtained in the far-infrared experiments of Brackett, Richards, and Caughey.[27] The results for static magnetic fields (B stat) of 10, 30, and 50 kG are given in Figures 5 and 6. In these spectra, the general position of the sets of absorption lines are determined by the ZFS, and the resolution determined by the magnitude of the static magnetic field. Clearly, a resolution comparable to that of the swept-field spectra is obtained for magnetic field strengths of 20–50 kG, values roughly 10% of the maximum values required for the same resolution of all resonance lines in the swept-field (ordinary EPR) experiments.

Spectrum Information Content

Both types of calculated magnetic resonance spectra exhibit an increase in spectral detail as the microwave frequency or magnetic field (for field-swept or frequency-swept cases, respectively) are increased. It is clearly difficult to realize, experimentally, the strengths of the magnetic field required in order to record the highest field EPR line at 374 GHz (ca. 420 kG), while a spectrum of apparently equal complexity is achieved in the swept-frequency experiment at a value of B_0 about 10% of this value. In order to assess the relative value of these (and other) spectra in relation to the spin-hamiltonian and line width parameter problems, we have calculated the information content of each spectrum using a definition of information useful for a continuous probability distribution.[29]

We define the quantity $P(x)$ to be the normalized line shape function $S(\omega,B)$ (eq 18) where x is chosen equal to the variable ω or B. Then, the information of the continuous distribution $P(x)$ is defined as

$$I = -\frac{1}{\ln 2}\int P(x) \ln P(x)\, dx \qquad (19)$$

which is the same, apart from the choice of units, as Shannon's "Entropy of a Continuous Distribution".[30] This definition has the property that the information of a single isotropic gaussian line, e.g., eq 4, is equal to $\ln (2^{1/2}\pi e\sigma)/\ln 2$ (whether integrated over ω or B), which is dependent on $\sigma = 1/T_2$, and has no lower bound. Thus, I is clearly a relative measure of information for a continuous probability distribution. If $P(x)$ is a sum of nonoverlapping gaussians

$$P(x) = N\sum_{i=1}^{n} f_i S_i(x) \qquad (20)$$

where N is a normalization constant, then

$$I(n) \cong \frac{1}{\ln 2}\left\{\langle S_i\rangle - \sum_{i=1}^{n} p_i \ln p_i\right\} \qquad (21)$$

Here, n = the number of lines, and p_i is the relative weight (normalized to one) of each line: $p_i = f_i/N$. Thus, $I(n)$ consists of a continuous part and a discrete part: in the case that *the* relative weights are all the same, the discrete part becomes ln (n)/ln 2, and $I(n)$ therefore clearly increases as the number of lines in the (normalized) spectrum increases.

We postulate, therefore, that the quantity defined by eq 19 is a useful measure of the relative information content (I) of the calculated spectra of Figures 1–6. (Note that the intrinsic line width $\sigma_B \approx h/g\beta BT_2$ in kilogauss units is constant throughout the calculations and is approximately of order of magnitude unity.) The calculated I's for the spectra of the type obtain here are given in Figure 7 plotted vs. microwave frequency or vs. magnetic field. We draw the following conclusions from this figure: (a) the information content of the Kramer's doublet is quite small compared to the whole spectrum, (b) extremely high microwave frequencies and peak values of the magnetic field are required in order to obtain the highest information content swept-field EPR spectra, and (c) the swept-frequency spectra are superior in the information content (i.e., resolution, the number and sharpness of lines), and the highest "resolution" is obtained at what appear to be readily attainable values of magnetic fields using superconducting magnet systems. The calculated I's appear, roughly, to parallel the number of distinctly resolved lines in the absorption spectrum.

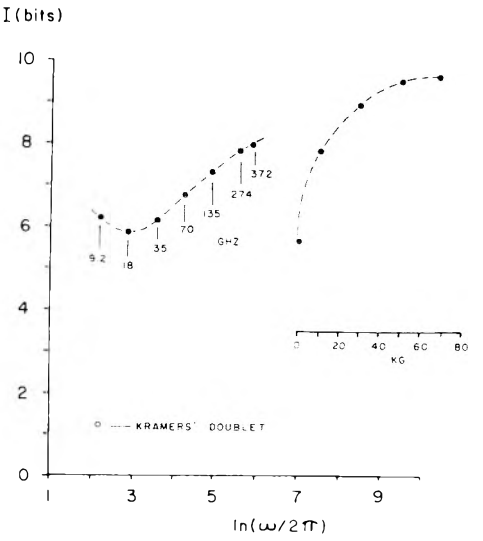

Figure 7. The relative information content, as defined in the text, vs. the natural logarithm of microwave frequency for the field-swept experiments. The inset shows relative information content vs. B (kilogauss) for the swept-frequency experiments.

Conclusions

A general method of attack on the problem of the calculation of rigid lattice magnetic resonance line shapes of high-spin Fe(III) systems has been formulated within the framework of existing theory. Some unsolved problems are the number of necessary terms to be included in the spin hamiltonian for $S = 5/2$ molecules with large values of zero-field splittings, and the evaluation of the necessary consolution integrals determining the total composite line shape of each electronic spin transition. If a satisfactory approximation is found for each of these problems, then the general single crystal or powder line shape numerical problem is completely solvable, using existing algorithms for rapid computation of the necessary integrals, complex matrix diagonalizations, and other matrix operations.

A number of interesting and useful mechanisms contribute to the values of the spin-hamiltonian and line shape parameters, accurate information about which can be obtained only if higher (than currently available) information content spectra can be obtained. The calculations presented here show that the customary X-band EPR spectrum is inherently a low-resolution measurement for $|D| = 10.7$ cm^{-1}, and presumably the resolution (of the entire spectrum) becomes worse as the ZFS increases. The increase in resolution and information content for the swept-field experiment as the microwave frequency is increased is related to the increase in the number of off-principle-axis turning points, an effect which we have previously investigated.[3] An approximate doubling of the number of lines (over the number expected from simple x,y,z principle axis turning points) is observed for the axial case when $|D| \approx \hbar\omega$. Thus, the information content of the powder spectrum for this case is about six times as much as for any single-crystal orientation spectrum. The information obtained by measuring only the Kramer's doublet transitions, for a powder, is about $1/10$ of this maximum. Unfortunately, the maximum magnetic fields necessary to record *all* of the resonance lines in field-swept experiments appears to be beyond the capabilities of present day technology.

In contrast, the resolution of the frequency-swept experiments increases rapidly with magnetic field, yielding equal or higher resolution with large, but experimentally accessible values of the static magnetic field, B_{stat}. The frequency range necessary to encompass all known values of ZFS "D" values[31] is about 0–300 cm^{-1}, and for the case considered here all resonance lines come within the interval 0–60 cm^{-1} for $B_{stat} \leq 70$ kG. This corresponds exactly to the region of the spectrum suited especially to, for example, Fourier transform spectroscopy using a Michelson interferometer, the region 3–400 cm^{-1}.[32] While this particular method for submillimeter wave spectroscopy has a finite resolution (ca. ± 0.05 cm^{-1}), the use of harmonic generation of coherent microwaves for narrow sweep regions[32] can produce local resolution of 10^{-5} cm^{-1}. The region omitted by these methods, 0–3 cm^{-1}, corresponds exactly to the region of absorption in ordinary EPR by the Kramer's doublet $M_s = \pm 1/2$ states. Thus, a method of studying all of the transitions within the spin 5/2 manifold of states is to use a hybrid experiment, using a conventional EPR experiment (at one or more microwave frequencies) for measuring all of the details of the Kramer's doublet, and a submillimeter swept-frequency experiment for measuring the high-frequency transitions at one or more values of B_{stat} sufficiently large to ensure a well-resolved spectrum. The data of both experiments may then be subjected to a least-squares fitting to a single, consistent theoretical model for $\chi''(\omega,B)$ such as outlined here. The resulting spin-hamiltonian and line width and line shape parameters should permit a more exacting and quantitative analysis of the electronic structure and conformation related properties of high spin Fe(III) in macromolecules, and other systems, than is presently possible.

These conclusions are clearly based on the assumption that one is able to measure pure magnetic dipole absorption vs. field or frequency as the case may be. This, unfortunately, is not always a matter of free choice. In the case of the conventional EPR experiment, a high-Q resonant microwave cavity is used to obtain pure magnetic dipole

absorption, the electric-multipole absorption being suppressed by placing the sample on an E-field node. Alpert et al.[28] have demonstrated with a heme protein at 1.5°K that one may obtain essentially pure magnetic dipole absorption in an EPR experiment at 135 GHz (4.5 cm^{-1}) by use of an oversized waveguide transmission technique. With increasing frequency, however, they observed both an increase in nonresonant (but field dependent) absorption, presumably due to protein-bound water, and a steady progression of the magnetic resonance lines to extremely high fields. With the far-infrared magnetic resonance experiment, in contrast, not only are the necessary static magnetic fields considerably smaller, but the ir "window" is larger to begin with. Thus, Brackett et al. found a 3–18 cm^{-1} window for heme proteins, and a 3–50 cm^{-1} window for water-free metal–ligand complexes. Moreover, the calculations presented here (particularly Figures 5 and 6) demonstrate that for given magnitude of ZFS, the effect of increasing B_0 field is to "push" some resonance lines down (in frequency) into the ir window, an extremely useful effect which is opposite to that observed in conventional EPR spectroscopy. The drawback here (in contrast to conventional EPR) is that the true line shape cannot be measured by far-ir spectroscopy. The experimental resolution is finite, in comparison with the true line width, which means that the measured magnetic resonance line shape is a convolution of the true line shape with an instrumental line shape function. Thus, there are clear advantages to each technique, and the optimum approach must be to use both methods and subject them to simultaneous analysis. It is also clear that if these methods are at all useful for the study of high-spin Fe(II) and Fe(III) heme proteins, then they must be even more useful for the study of their synthetic analogs such as the "picket-fence" porphyrins.[33]

Acknowledgments. I wish to thank Professor A. D. Buckingham for his kind hospitality during my stay at University Chemical Laboratory, Cambridge, where part of this work was done. Several conversations with Dr. R.M. Lynden-Bell on irreducible tensor operators were most helpful, as were the remarks by Professor K.W.H. Stevens on the problem of uniqueness of solution. Mr. R.S. Johnson did much of the program development. The generous computing time made available to me by the University of Iowa is gratefully acknowledged. Supported, in part, by Biomedical Sciences Support Grant No. FR-07035, General Research Support Branch, Division of Research Resources, National Institutes of Health.

References and Notes

(1) T. Asakura, G. H. Reed, and J. S. Leigh, Jr., *Biochemistry*, **11**, 334 (1972).
(2) E. R. Feher, *Phys. Rev.*, **136**, A145 (1969).
(3) W. V. Sweeney, D. Coucouvanis, and R. E. Coffman, *J. Chem. Phys.*, **59** 369 (1973).
(4) G. Feher, R. A. Isaacson, and C. P. Scholes, *Ann. N. Y. Acad. Sci.*, **222**, 86 (1973).
(5) D. Shaltiel and W. Low, *Phys. Rev.*, **124**, 1062 (1961).
(6) Y. H. Ya, *Aust. J. Phys.*, **23**, 445 (1970).
(7) C. J. Kirkby and J. S. Thorp, *J. Phys. C*, 913 (1968).
(8) R. F. Wenzel and Y. W. Kim, *Phys. Rev.*, **140**, A1592 (1966).
(9) W. B. Mims and R. Gillen, *Phys. Rev.*, **148**, 438 (1966).
(10) A. B. Roitsin, *Sov. Phys. Usp.* (*Engl. Transl.*), **14**, No. 6, 766 (1972).
(11) C. P. Scholes, *J. Chem. Phys.*, **52**, 4890 (1970).
(12) B. Bleaney and K. W. H. Stevens, *Rep. Prog. Phys.*, **16**, 108 (1953).
(13) A. Abragam and B. Bleaney, "Electron Paramagnetic Resonance of Transition Ions", Clarendon Press, Oxford, 1970.
(14) A. M. Portis, *Phys. Rev.*, **91**, 1071 (1953).
(15) C. P. Slichter, "Principles of Magnetic Resonance", Harper and Row, New York, N.Y., 1963.
(16) T. F. Yen, "Electron Spin Resonance of Metal Complexes", Plenum Press, New York, N.Y., 1969, p 33.
(17) A more exacting definition is given by Stoneham, ref 21.
(18) I. S. Gradshteyn and I. M. Rhyzhik, "Table of Integrals", Academic Press, New York, N.Y., 1965, p 338.
(19) T. G. Castner, Jr., *Phys. Rev.*, **115**, 1506 (1959).
(20) H. A. Farach and H. Teitelbaum, *Can. J. Phys.*, **45**, 2913 (1967).
(21) A. M. Stoneham, *Rev. Mod. Phys.*, **41**, 82 (1969).
(22) H. F. Symmons and G. S. Bogle, *Proc. Phys. Soc., London*, **79**, 468 (1962).
(23) J. R. Thyer, S. M. Quick, and F. Holuj, *Can. J. Phys.*, **45**, 3597 (1967).
(24) F. S. Ham et al., *Phys. Rev. Lett.*, **5**, 468 (1960).
(25) B. Bleaney, *Proc. Phys. Soc.*, **73**, 939 (1959).
(26) M. Kotani, *Ann. N. Y. Acad. Sci.*, **158**, 20 (1969).
(27) G. C. Brackett, P. L. Richards, and W. S. Caughey, *J. Chem. Phys.*, **54**, 4383 (1971).
(28) Y. Alpert, Y. Couder, J. Tuchendler, and H. Thomé, *Biochim. Biophys. Acta*, **322**, 34 (1973).
(29) A. Katz, "Principles of Statistical Mechanics; The Information Theory Approach", W. H. Freeman, San Francisco, Calif., 1967.
(30) C. E. Shannon and W. Weaver, "The Mathematical Theory of Communication", University of Illinois Press, Urbana, Ill., 1964.
(31) W. Low, "Paramagnetic Spectroscopy at Submillimeter Wave Frequencies", in "Submillimeter Waves", J. Fox, Ed., Polytechnic Press, New York, N.Y., 1971.
(32) D. H. Martin, Ed., "Spectroscopic Techniques for Far Infrared, Submillimetre and Millimetre Waves", North-Holland Publishing Co., Amsterdam, 1967.
(33) J. P. Collman, R. R. Gagne, C. A. Reed, W. T. Robinson, and G. A. Rodley, *Proc. Natl. Acad. Sci. U.S.A.*, **71**, 1326 (1974).

COMMUNICATIONS TO THE EDITOR

Exciplex Formation between 2-Aminopyridine and *p*-Nitroaniline

Sir: Interest in exciplex phenomena has been increasing since the initial reports by Leonhardt and Weller[1-3] that fluorescence quenching via charge transfer in the excited state can lead to a new chemical species with its own individual spectral properties. In the course of studying the fluorescence of 2-aminopyridine, 2-AMP, we have observed that *p*-nitroaniline, PNA, is a singlet quencher but more importantly leads to a new fluorescence emission, which we believe to be exciplex emission. The fluorescence of aminopyridines has been characterized in previous reports from this laboratory.[4,5] Excitation of 4×10^{-4} *M* 2-AMP in EPA with 254-nm excitation leads to a fluorescence with a wavelength maximum at 340 nm and a quantum yield of ~0.2. Upon addition of PNA the fluorescence of 2-AMP decreases and leads to a new emission, which is unstructured and shifted to longer wavelengths from the normal molecular fluorescence. *p*-Nitroaniline is nonfluorescent in all solvents studied, when excited with 254- or 366-nm excitation. The fluorescence behavior of 2-AMP in the presence of *p*-nitroaniline is presented in Figure 1, where a new emission is seen to grow in at ~410 nm concomitantly with decreasing 2-AMP fluorescence upon addition of PNA. The reversal in the exciplex emission intensity when comparing spectra (3) and (4) is due to increased absorption of PNA, which leads to fewer excited singlets of 2-AMP available for exciplex formation. The uv absorption spectra of the two molecules exhibit no interaction, so that a ground-state complex can easily be excluded. Since *p*-nitroaniline has a lower lying singlet state than 2-AMP, we have also excited PNA directly with 366 nm, a wavelength which is not absorbed by 2-AMP; however, no exciplex emission is observed. The exciplex emission is also observed in ethyl ether and in acetonitrile solutions with emission wavelength maxima of 396 and 405 nm, respectively. This shift of exciplex emission with solvent is quite normal and indicates a species of strong polar character in the excited-state complex.

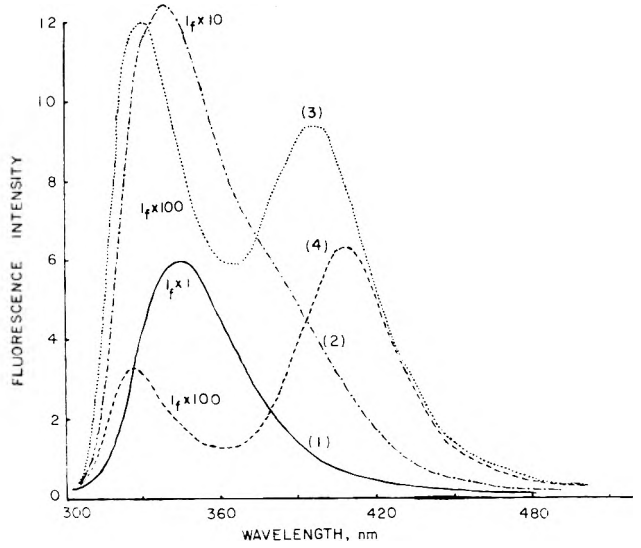

Figure 1. Fluorescence spectra of 4×10^{-4} *M* 2-aminopyridine in EPA at room temperature as a function of added *p*-nitroaniline concentration: (1) no *p*-nitroaniline, (2) 1.4×10^{-4} *M*, (3) 2.9×10^{-4} *M*, and (4) 7.2×10^{-4} *M* (λ_{exc} 254 nm).

It is quite evident that 2-AMP is the electron donor in this new exciplex system and that the ground state rather than the excited singlet state of PNA is involved in the charge-transfer process which results in exciplex formation. The decreasing fluorescence observed for 2-AMP, corrected for the strong PNA absorption in the 250-nm region, and the increasing emission upon addition of PNA indicate that the excited singlet state of 2-AMP is required for exciplex formation. The following scheme indicates the origin of two emissions observed

$$(2\text{-AMP})^{*1} + \text{PNA} \rightleftharpoons [(2\text{-AMP})^{+} \cdots (\text{PNA})^{-}]^{*1}$$
$$\downarrow h\nu_F \qquad\qquad \downarrow h\nu_F'$$

The fluorescence yield of 2-AMP is not affected by degassing; however, the exciplex emission yield is reduced about 15% in air-saturated solutions.

This exciplex system has the interesting property that the electron acceptor, *p*-nitroaniline, is nonfluorescent and thus provides an interesting case of perturbation of a nonfluorescent molecule to produce luminescence. In addition PNA is a bifunctional molecule which possesses an electron donor and acceptor group. The fact that the exciplex emission is also observed in acetonitrile, whereas charge-trans-

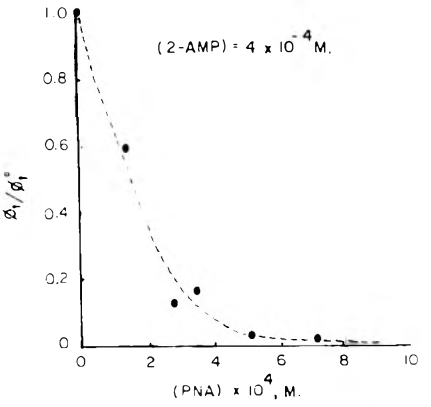

Figure 2. Stern–Volmer plot for the fluorescence quenching of 4×10^{-4} *M* 2-aminopyridine in EPA by *p*-nitroaniline.

fer complexes such as anthracene–diethylamine in the same solvent lead to cation and anion production,[6] indicate that in (2-AMP···PNA)*[1] there is significant resonance interaction which stabilizes the exciplex. The Stern–Volmer fluroescence quenching plot of 2-AMP with *p*-nitroaniline is shown in Figure 2 and the half-concentration value of PNA is seen to be 1.5×10^{-4} *M*. This value is indicative of a relatively stable complex. Fluorescence quenching of the absorbing monomer through exciplex formation gives a nonlinear Stern–Volmer plot, which results from an equilibrium between the monomer and exciplex species. The ordinate in Figure 2 is normalized to the fluorescence yield for a 4×10^{-4} *M* solution of 2-AMP in the absence of PNA, and the values are corrected for the percentage of light absorbed by PNA at 254 nm. Although the large PNA absorption at 254 nm complicated the determination of the exciplex emission yield, we estimate that its fluorescence yield is approximately 1% of the value for 2-AMP or 0.002.

The new exciplex system described here provides a basis for generating many new and novel exciplex systems. Further studies are in progress and will be discussed in a future report.

References and Notes

(1) H. Leonhardt and A. Weller, *Z. Phys. Chem. (Frankfurt am Main)*, **29**, 277 (1961).
(2) H. Leonhardt and A. Weller, "Luminescence of Organic-Inorganic Materials", H. P. Kallmann and G. M. Spruch, Ed., Wiley, New York, N.Y., 1962, p 74.
(3) H. Leonhardt and A. Weller, *Ber. Bunsenges, Phys. Chem.*, **67**, 791 (1963).
(4) A. Weisstuch and A. C. Testa, *J. Phys. Chem.*, **72**, 1982 (1968).
(5) A. C. Testa, A. Weisstuch, and J. Hennessy in "Molecular Luminescence", E. C. Lim, Ed., W. A. Benjamin, New York, N.Y., 1969, p 863.
(6) H. Knibbe, D. Rehm, and A. Weller, *Ber. Bunsenges. Phys. Chem.* **72**, 257 (1968).

Department of Chemistry
St. John's University
Jamaica, New York 11439

J. Wolleben
A. C. Testa*

Received January 8, 1975

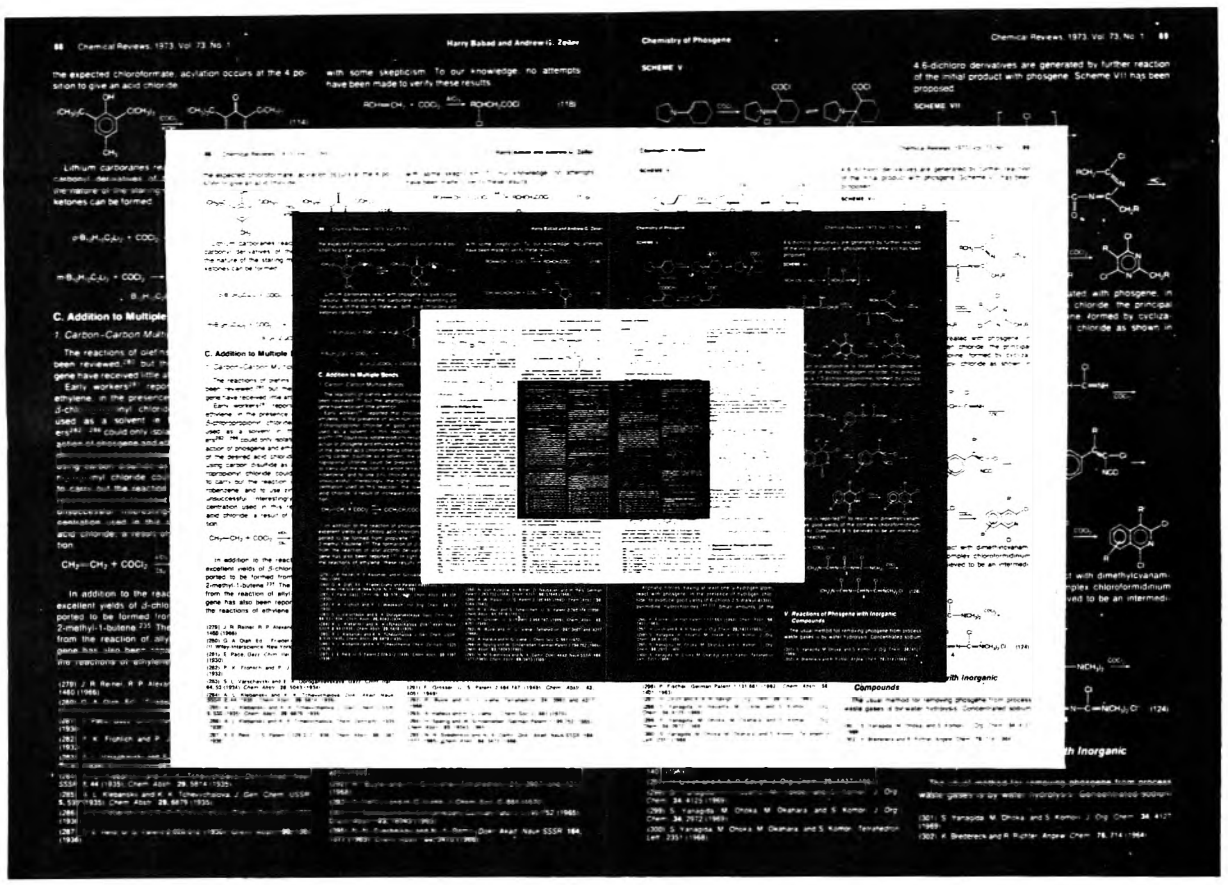

INFORMATION IMPLOSION!

The ACS Journal Microform Program

One of the steps being taken by ACS Publications to reduce new chemical information to manageable proportions is the adoption of microform techniques for storage and publication.

We are using both microfilm and microfiche.

MICROFILM: Most of the ACS periodical publications are now available on **microfilm**, 16 mm or 35 mm, negative or positive, open reel or special cartridge. Back issues—back to Volume 1 for many journals—are available. Subscriptions to current volumes also are available; the **microfilm** is supplied at year's end.

Current subscriptions to **microfilm** editions of journals include a subscription to "hard copy" issues of the journal. **Microfilm** subscriptions are on a lease basis that specifically grants the subscriber a license to make unlimited numbers of photocopies for internal use.

Microfilm editions contain supplementary materials–such as tables, charts, computer printouts, and the like–that are not printed in the regular hard copies. They thus constitute the most complete version of each journal.

MICROFICHE: The supplementary materials which are included at the end of each year in the current microfilm editions of the journals are also available on 105 x 148 mm negative **microfiche** cards.

Journal users can obtain material supplementary to an article, on **microfiche**, soon after publication by following the ordering instructions given at the end of the article.

Microfiche cards containing supplementary material are available on a subscription basis for five journals that have a substantial, continuing volume of such material—these five are Journal of the American Chemical Society, Journal of Organic Chemistry, Journal of Physical Chemistry, Inorganic Chemistry, and Journal of Chemical & Engineering Data. Most, but not necessarily all, issues of these journals have supplementary material. **Microfiche** subscriptions are not available on other ACS publications.

Microfilm edition subscribers receive all **microfiche** cards for the particular journal to which they subscribe and thus do not need to special-order any **microfiche** cards for that journal.

Note: Single issues of journals and entire articles are not available either on microfilm or on microfiche.

To: Special Issues Sales
American Chemical Society
1155 16th St., N.W., Washington, D.C. 20036

Please send me full information on the ACS Journal microform program.

Name _____

Title _____

Address _____

_____